Study of dry sliding wear characteristics of sillimanite reinforced aluminium alloy matrix composites

A Dissertation Submitted
In Partial Fulfillment of the Requirements
for the Degree of

Doctor of Philosophy

Submitted by

Sandeep Sharma
Regd. No. 901508002

Under the guidance of

Dr. Tarun Nanda
Associate Professor,
MED, TIET, Patiala

Dr. O. P. Pandey
Senior Professor,
SPMS, TIET, Patiala

Mechanical Engineering Department
Thapar Institute of Engineering and Technology
(Deemed to be University), Patiala
January, 2021

Dedicated to the
Loving Memory of
My Mother

(Late Smt. Urmila Sharma)

CERTIFICATE

Certified that the work presented in the thesis entitled "**Study of dry sliding wear characteristics of sillimanite reinforced aluminium alloy matrix composites**" being submitted by Mr Sandeep Sharma (Regd. No. 901508002) in fulfilment of the requirements for the award of the degree of 'Doctor of Philosophy' in the Department of Mechanical Engineering, Thapar Institute of Engineering and Technology, Patiala, is an authentic record of the candidate's own work carried out during the period from June 2015 to January 2021 at this institute under my supervision. The matter presented in this dissertation has not been submitted for the award of any other degree in any university.

Dr. Tarun Nanda
Associate Professor,
MED, TIET, Patiala

Dr. O. P. Pandey
Senior Professor,
SPMS, TIET, Patiala

DECLARATION

I hereby certify that the work which is being presented in this thesis, entitled "**Study of dry sliding wear characteristics of sillimanite reinforced aluminium alloy matrix composites**", in the fulfilment of the requirements for the award of degree of 'Doctor of Philosophy' in Mechanical Engineering submitted to the Department of Mechanical Engineering of Thapar Institute of Engineering and Technology (Deemed to be University), Patiala is an authentic record of my own work carried out under the supervision of Dr. Tarun Nanda, Associate Professor, Mechanical Engineering Department, Thapar Institute of Engineering and Technology, Patiala and Dr. O. P. Pandey, Senior Professor, School of Physics and Materials Science, Thapar Institute of Engineering and Technology, Patiala.

The matter presented in this dissertation has not been submitted in part or full to any other university or institute for the award of any degree in India or abroad.

Sandeep Sharma

ACKNOWLEDGEMENT

First of all, I would like to express my gratitude to my supervisors Dr. Tarun Nanda, Associate Professor, Mechanical Engineering Department, Thapar Institute of Engineering and Technology, Patiala and Dr. O. P. Pandey, Senior Professor, School of Physics and Materials Science, Thapar Institute of Engineering and Technology, Patiala for their invaluable guidance, moral support and encouragement during the entire period of this research which cannot adequately be expressed in words in this acknowledgement.

I would like to extend my acknowledgment to my doctoral committee member Dr. J. S. Saini, Dr. Dheeraj Gupta, and Dr. Kulvir Singh for their valuable observations, suggestions, and feedback. I am very much grateful to my friends Raju, Vishal Singh, Rahul Gupta, and Varun Singhal for their help and support.

I would like to thank my seniors Dr. Suresh Kumar Dr. Karanbir Singh and my fellow PhD scholars Rahul Gupta, Daksh Shelly, Vikas Deep Mann who provided a great support during my dissertation writing. A special thanks to Dr. Raju (my roommate and a close friend) who spent every day motivating me to achieve this goal.

I would like to thank my parents, Sh. Rattan Lal Sharma and Late Smt. Urmila Sharma whose consistent love and support motivated me throughout the period of research. I would also like to thank my sister, Ms. Sushma Sharma for her understanding, patience and valuable support which helped me in achieving the goal.

Special thanks to my wife Ms. Neelam Kumari for her understanding and support during the entire period of research program. Special thanks to my daughter Ms. Pragya Sharma who was the source of my motivation.

Above all, I thank Almighty whose blessings have enabled me to accomplish this research work.

Sandeep Sharma

LIST OF PUBLICATIONS

PUBLICATIONS RELATED TO PRESENT WORK:

- *Sandeep Sharma, Tarun Nanda, O.P. Pandey (2018) Effect of particle size on dry sliding wear behaviour of sillimanite reinforced aluminium matrix composites. Ceramics International. 44, 104–114.*

- *Sandeep Sharma, Tarun Nanda, O.P. Pandey (2018) Effect of dual particle size (DPS) on dry sliding wear behaviour of LM30/sillimanite composites. Tribology International. 123, 142–154.*

- *Sandeep Sharma, Tarun Nanda, O.P. Pandey (2018) Effect of elevated temperatures and applied pressure on the tribological properties of LM30/sillimanite aluminium alloy composites. Journal of Composite Materials. 53(11), 1521–1539.*

- *Sandeep Sharma, Rahul Gupta, Tarun Nanda, O.P. Pandey (2021) Influence of two different range of sillimanite particle reinforcement on tribological characteristics of LM30 based composites under elevated temperature conditions. Materials Chemistry and Physics. 258, 123988.*

OTHER PUBLICATIONS:

- *Sandeep Sharma, Suresh Kumar, Tarun Nanda, O.P. Pandey (2019) Effect of heat treatment on the wear behavior of zircon reinforced aluminium matrix composites. Materials Research Express. 6(5), 056535.*

- *Sandeep Sharma, Tarun Nanda, O.P. Pandey (2019) Investigation of T4 and T6 heat treatment on the wear properties of sillimanite reinforced LM30 aluminium alloy composites. Wear. 426, 27–36.*

- *Rahul Gupta, Sandeep Sharma, Tarun Nanda, O.P. Pandey (2019) A comparative study of dry sliding wear behaviour of sillimanite and rutile reinforced LM27 aluminium alloy composites. Materials Research Express. 7(1), 016540.*

- *Rahul Gupta, Sandeep Sharma, Tarun Nanda, O.P. Pandey (2020) Wear studies of hybrid AMCs reinforced with naturally occurring sillimanite and rutile ceramic particles for brake rotor applications. Ceramics International. 46(10B), 16849-16859.*

ABSTRACT

The aim of the present study was to develop light-weight, economical, and high temperature resistant aluminium matrix composites for brake rotor applications. Aluminium matrix composites (AMCs) containing LM30 aluminium alloy as matrix and sillimanite mineral particles as reinforcement were processed using stir casting. Sillimanite particles were taken in three different size range viz. coarse (75–106 μm), medium (32–50 μm), and fine (1–20 μm). Two main categories of AMCs were processed. The first category included single particle size AMCs (SPS) where the matrix material was reinforced with sillimanite particles of one specific size range (coarse, or medium, or fine). The second category included dual particle size AMCs (DPS) where the matrix was reinforced with sillimanite particles of two specific size ranges. For both type of AMCs, the maximum reinforcement level (with uniform distribution of particles with nearly no agglomeration) was 15 wt.% (0–15 wt.%; in step size of 3 wt.%). Further, for DPS composites, a mix of fine and coarse sized particles were reinforced with fine:coarse weight ratio as 1:3, 1:1, or 3:1.

For processing of composites, the base alloy was melted and stirred at 630 rpm for 4–5 minutes at 750 ℃. Pre-heated sillimanite particles (heated to 350 ℃) were added to molten mass at a reduced stirrer speed of 250 rpm. The mixture was stirred at 630 rpm for 10–12 minutes and poured into a cast iron mould. For wear testing, pins of 8 mm diameter were machined as per ASTM G99 standard.

EDS analysis of sillimanite particles showed the constitution as $SiAl_{1.8}O_{6.1}$ which confirmed the purity of sillimanite (Al_2SiO_5). XRD analysis of base alloy showed presence of aluminium, silicon, and aluminium-copper phases. For AMCs, in addition to these phases, sillimanite and aluminium silicate ($Al_2Si_4O_{10}$) phases were also observed. Optical micrographs of base alloy showed presence of eutectic aluminium, eutectic silicon, and large facets of proeutectic (primary) silicon phases. For AMCs, in addition to these phases, sillimanite particles were also observed. Micrographs revealed that sillimanite particles were uniformly distributed in AMCs till 15 wt.% reinforcement. X-ray line profile of AMCs revealed high concentration of silicon phase in the proximity of reinforced particles. Further, X-ray dot mapping showed significant refinement of silicon phase in AMCs compared to base alloy.

High nanohardness values were obtained at the particle-matrix interface of AMCs indicating that the processing methodology was effective. Further, Brinell hardness values of AMCs showed increase with increase in reinforcement level and decrease in particle size. For SPS composites, maximum hardness was obtained for composite reinforced with 15 wt.% of fine sized sillimanite particles. The overall maximum hardness was obtained for 15 wt.% reinforced DPS composite containing large proportion of fine sized particles (fine:coarse ratio of 3:1). The hardness of this DPS composite was comparable (only 4.5% lower) to commercial grade cast iron material used in brake rotor applications.

Wear rate of AMCs under room temperature conditions was significantly lower than the base alloy for any given contact pressure and sliding distance condition. Further, wear rate of AMCs showed a continuous decrease with increase in reinforcement level and decrease in particle size. For SPS composites, maximum reduction in wear rate (55% lesser than base alloy) was obtained for composite reinforced with 15 wt.% of fine sized sillimanite particles. The overall best wear results (59% lesser than the base alloy) were obtained for 15 wt.% reinforced DPS composites containing large proportion of fine sized particles (fine:coarse ratio of 3:1). The maximum wear rate of this DPS composite was comparable (only 8% higher) to cast iron specimen. Mathematical modelling of wear rate showed good agreement with the experimental results. Coefficient of friction (COF) of AMCs were also significantly

lower than the base alloy with maximum reduction of 42% (over the base alloy) achieved for the 15 wt.% DPS composites.

Finally, for room temperature testing conditions, SEM-EDS analysis of wear tracks and wear debris revealed that wear mechanisms causing material loss were mainly dependent on contact pressure and sliding distance. At low contact pressure and smaller sliding distances, abrasive wear mechanism was predominant. However, at higher contact pressure and larger sliding distances, adhesive/delamination wear mainly caused material loss.

Next, the properties of processed AMCs were evaluated under elevated temperature conditions. DTA-TGA analysis revealed that sillimanite particles were thermally stable till 900 ℃. Coefficient of thermal expansion (CTE) values of AMCs were significantly lower than the base alloy. For SPS composites, maximum reduction in CTE value (25% less than base alloy) was obtained for composites reinforced with 15 wt.% of fine sized sillimanite particles. The overall maximum reduction in COF value (28% lower than base alloy) was obtained for 15 wt.% reinforced DPS composite (with fine:coarse ratio of 3:1).

For all elevated temperature conditions (50–300 ℃), sillimanite reinforcement decreased the wear rate of AMCs significantly over the base alloy. At any given elevated temperature, wear rate of AMCs decreased with increase in reinforcement level and decrease in particle size.

The transition from mild-to-severe wear for base alloy was observed at an operating temperature of 150 ℃. Sillimanite reinforcement in AMCs raised the transition temperature to 200 ℃. At this transition temperature of 200 ℃, maximum reduction in wear rate of 80% (over the base alloy) was shown by 15 wt.% DPS composite containing large proportion of fine particles (fine:coarse ratio of 3:1). The mean steady-state-wear rate of this DPS composite at the transition temperature (200 ℃) was even lower (1.5% less) than the cast iron specimen. This DPS composite also showed maximum reduction of 54% in COF value over the base alloy.

The results of XRD analysis of wear track and wear debris of AMCs showed presence of various oxides (Al_2O_3, SiO_2, Fe_2O_3, and FeO etc.), sillimanite particles, and various other phases like aluminium, silicon and aluminium-copper etc. and confirmed the formation of mechanically mixed layer. SEM-EDS analysis of wear track and wear debris at the transition temperature of 200 ℃ indicated that at contact pressure of 0.2 MPa, abrasive wear was predominant whereas at 1 MPa condition, adhesive/delamination wear mainly causing material loss.

The present research showed that the best wear and friction results (both at room temperature and elevated temperature conditions) were observed for 15 wt.% DPS composite containing fine particles in larger proportion (fine:coarse ratio of 3:1). Wear rate and COF values of SPS AMCs at a given reinforcement level decreased with decrease in particle size. However, it was noted that at a given reinforcement level, the wear rate and COF values reduced further for DPS composites containing larger proportion of finer particles (fine:coarse ratio of 3:1). The fine particles provide large interfacial sites for effective load transfer and hence reduced wear rate/COF values whereas the coarse particles carry a major proportion of applied load and shield the finer particles from ploughing action. Further, the wear rate and COF values of 15 wt.% DPS composites with higher concentration of fine particles i.e. fine:coarse in the ratio of 3:1 was almost comparable with grey cast iron specimen. Also, the brake rotors fabricated using composites provide a weight reduction of 60% as compared to cast iron brake rotors. Considering these facts, 15 wt.% DPS composites with higher portion of finer particles can act as a substitute for brake rotor materials in light motor vehicles.

TABLE OF CONTENTS

LIST OF TABLE

LIST OF FIGURES

CHAPTER 1
INTRODUCTION

OVERVIEW

This chapter presents a general introduction of composites. The metal matrix composites, especially the particle reinforced metal matrix composites are described in detail. It also discusses the applications of aluminium matrix composites (AMCs) and various factors affecting the tribological properties of AMCs. The chapter finally discusses the origin of present research work and presents the outline of complete thesis.

1.1 COMPOSITES

Composites are materials systems composed of two or more phases. One of the phases is termed as the matrix which is continuous phase and envelopes the second phase termed as the dispersed phase or reinforcement. The two phases are significantly different in their physical, chemical, and mechanical properties [1]. The unique combination of properties is achieved by varying the shape, size and distribution of reinforcement. The matrix-reinforcement interface bonding also affects the properties of composites [2–4]. Matrix material is selected based on the working conditions, environmental conditions, and applications for which the composites are developed [5]. For structural applications, aluminium or titanium matrix is mostly used. Similarly, cobalt, nickel and its alloys are used as matrix materials for high temperature applications. The discontinuous phase of composites is known as reinforcement. The reinforcement generally has higher stiffness and high hardness compared to the matrix. Addition of reinforcement to the matrix augments the mechanical and tribological properties of the overall composite system [3].

Composites are processed by a combination of metals, non-metals and ceramic materials. This allows fabrication of composites for a variety of applications. In the past decades, composites were used for advanced mechanical applications. Nowadays, the applications of composites have increased exponentially and are not just limited to the fields of automobiles, ships, aircrafts, defence etc. [3,6]. Composites can provide substantial weight reduction over the traditional materials used for different applications [3].

1.2 METAL MATRIX COMPOSITES (MMCs)

Metal matrix composites (MMCs) are composites in which a metal (aluminium, cobalt, nikel, copper, magnesium, titanium, iron etc.) acts as a matrix material. Metals usually have high specific strength, high modulus, good ductility, and good thermal and electrical conductivity. MMCs are in demand for different engineering applications like in automobile sector, defence sector, aerospace sector etc. They provide greater flexibility in altering the mechanical properties needed for engineering applications [2,7,8]. Processing methods for MMCs are of two main types, (i) solid state processes viz. powder blending followed by consolidation (P/M processing), diffusion bonding, vapour deposition and (ii) liquid state processes viz. stir casting, infiltration, spray casting, and in-situ (reactive) processing. Out of these processes, stir casting process is widely used due of its simplicity and flexibility. The process is economical and suitable for mass

production [9–12]. However, to fabricate composites using the stir casting route, homogeneous particle distribution with good wettability is necessary [13,14]. In stir casting process, the distribution of particles is dependent on various parameters viz. wettability, stirring speed, stirring time, processing temperature, blade angle etc. [15–17]. This process is suitable for fabrication of composites with reinforcement volume fraction of less than 30% [18–20].

1.3 PARTICLE REINFORCED ALUMINIUM MATRIX COMPOSITES

The choice of matrix material for composites largely depends on its end application. Metal matrix composites (MMCs) are in demand for a variety of engineering applications. Of these, aluminium matrix composites (AMCs) reinforced with ceramic particles are of great interest in automobile, defence, aerospace, and structural applications [21–25]. Aluminium alloys act as an exceptional matrix for fabrication of AMCs as they have low density, high specific strength, and high corrosion resistance [26,27]. Aluminium alloys also exhibit good mechanical properties but they lack in tribological properties. This limits the use of aluminium alloys for certain engineering applications [28,29]. For enhancement in tribological properties, aluminium alloys are reinforced with (a) synthetic ceramic minerals viz. silicon carbide [30–32], silicon nitride [33,34], boron carbide [35–38], titanium nitride [39] and alumina [40–42] and/or (b) natural ceramic minerals viz. sillimanite [43–45], garnet [46,47], zircon [48–50], and rutile [51,52] etc. Out of these ceramic particles, natural ceramic minerals are cheap and economical for the fabrication of composites. Ceramic particle reinforcement is an economical way of enhancing tribological properties of AMCs [3,53,54]. Various industries use SiC and Al_2O_3 reinforced AMCs for fabrication of pistons, brake rotors, liners of engine valve springs, retainer cams, and lifter bodies to reduce weight and improve wear resistance and strength [55].

1.4 APPLICATIONS OF AMCs

AMCs are a class of newer materials which provide superior tribological properties. Aluminium based composites find applications in automobile, aerospace, marine, and mineral processing industries. AMCs have improved specific strength, good wear resistance, higher thermal conductivity and lower coefficient of thermal expansion [54,56,57]. Table 1.1 presents the applications of AMCs in various automobile components. The wear properties of AMCs are comparable to their conventional counterparts. In addition to this, AMCs also provide significant

weight reduction when compared to conventional materials. The brake rotors fabricated using AMCs are found to be 60% lighter in comparison to rotors made of cast iron, and thus, increase the fuel efficiency [58]. AMCs reduce the weight and also the brake noise. Moreover, AMCs have high thermal conductivity which is greater than that of cast iron. The working temperature of brake rotors can reach till 300 ℃, hence, higher thermal conductivity leads to better heat transfer as compared to cast iron. In connecting rods and pistons, AMCs are basically used to reduce the weight of parts so that fuel efficiency is improved [59].

Table 1.1 Applications of aluminium matrix composites

Part application	Property	Reference	Temperature (℃)
Wrist Pins	Specific stiffness, wear resistance, creep resistance	P. Rohatgi [55], Allison and Cole [59]	120–150
Cylinder Heads and Blocks	Wear resistance, low friction, weight	P. Rohatgi [55], Allison and Cole [59], G. S. Cole and A. M. Sherman[60], Deuis et al. [61], Arslan et al. [62]	200 (max.)
Cylinder Liners	Wear resistance	P. Rohatgi [55], Allison and Cole [59], G. S. Cole and A. M. Sherman [60], Deuis et al. [61], Arslan et al. [62]	200 (max.)
Disk Rotors	Wear resistance, weight	P. Rohatgi [55], Allison and Cole [59], G. S. Cole and A. M. Sherman [60], Deuis et al. [61]	300–450
Pistons	Wear resistance, high strength	P. Rohatgi [55], Allison and Cole [59], G. S. Cole and A. M. Sherman [60], Deuis et al. [61], Arslan et al. [62]	250–300
Connecting Rods	Wear resistance, fatigue strength	P. Rohatgi [55], Allison and Cole [59]	150–180

1.5 FACTORS AFFECTING WEAR BEHAVIOUR OF AMCs

The wear behaviour of AMCs is influenced by a variety of factors viz. microstructure, solidification rate, interface, porosity, distribution of particles, and wettability etc.

a) MICROSTRUCTURE

The microstructure of Al-Si alloys plays an important role in improving the wear characteristics of composites. Aluminium-silicon alloys are broadly classified into three categories viz. hypoeutectic (Si<12.8 wt%), eutectic (Si=12.8 wt%), and hypereutectic (Si>12.8). The microstructure of these three different Al-Si alloys has a lot of variations. Hypereutectic Al-Si alloys have a greater portion of primary silicon phase in the microstructure. This primary silicon

is a hard phase. For this reason, the wear resistance of hypereutectic Al-Si alloys is higher than eutectic and hypoeutectic Al-Si alloys [63,64].

b) SOLIDIFICATION

Solidification is a phase transformation process where the liquid phase transforms to the solid phase. When the temperature of melt drops below the melting point, solidification starts. Solidification process strongly affects the characteristic features of the material. Solidification leads to microstructural changes in the material. Faster solidification leads to development of internal stresses in material. Solidification process controls the microstructure, interfacial reactions, and distribution of various phases in the composites [65,66].

c) INTERFACE

The chemical interaction between matrix and reinforcement of composites is termed as interface adhesion. The reinforcement-matrix interfacial reaction is important for improving the tribological properties of composites. Interfacial hardness is an important parameter which governs the applications of composites. Higher interface hardness is directly related to strong particle-matrix bonding [67,68].

d) POROSITY

Porosity is a measure of voids/empty spaces inside the material developed during casting. Porosity calculations provide an idea about the percentage of void space in the total volume of the material. Porosity considerably affects the performance of the material. Shape and size of void spaces also play an important role in determining the performance of materials. Larger sized voids adversely affect the performance of materials. Thus, for improved tribological properties, porosity in a material should be at the minimum possible level [69,70].

e) DISTRIBUTION OF REINFORCED PHASE

Distribution of reinforced particles plays a vital role in tailoring the tribological properties of composites. Uniform distribution of reinforcement improves the wear characteristics of the composites. Segregation and clustering of reinforced particles is a major concern during casting. Segregation restricts uniform particle distribution in the matrix which leads to a decrement in

properties of composites. Processing route should be optimized in a way that uniform particle distribution is achieved [4,71].

f) WETTABILITY

Wettability is the tendency of one fluid to spread on, or adhere to a solid surface. For superior tribological properties of composites, the reinforced particles must have high wettability with the molten matrix metal. Higher wettability of the reinforced particles with the matrix improves the interfacial bonding and hence improves the tribological properties of composites [13,14][3,14].

1.6 ORIGIN OF THE PRESENT STUDY

Researchers have been investigating the wear characteristics of AMCs for a long period. Attempts have been made to fabricate AMCs using different processing techniques and using different reinforced particles [54,72,81–84,73–80]. Most of the studies on aluminium matrix composites (AMCs) have involved use of pure ceramic particles (silicon carbide [30–32], silicon nitride [33,34], boron carbide [36–38], and alumina [40–42]) as reinforcement. However, it is noted that pure ceramics are expensive and lead to increase in cost of fabricated AMCs which is not desirable for large scale engineering applications of AMCs. To reduce the cost, reinforcement of naturally occurring minerals like sillimanite [43–45], garnet [46,47], zircon [49,50], and rutile [51,52] etc. has been used by various researchers.

India has a large coastline, and is gifted with valuable sea beach minerals. The coastal lines of Kerela, Tamil Nadu, Odisha, and Andhra Pradesh have substantial deposits of sea beach minerals including rutile (TiO_2), garnet, sillimanite ($Al_2O_3.SiO_2$), and zircon ($ZrO_2.SiO_2$) etc. Indian resources constitute about 35% of world's resources of sillimanite, 10% rutile, 10% garnet and 14% zircon [85–88]. Thus, these minerals are cheap, can substitute pure ceramic particles, and reduce the overall cost of processing of composites. These minerals have high thermal shock resistance, high creep resistance, high hardness, high corrosion resistance, high modulus, low coefficient of expansion, and excellent thermal stability. Thus, natural ceramic sands when reinforced with Al-alloys can make them highly attractive materials [43–45,88–90]. Such AMCs can be used as wear-resistant materials in automotive components viz. brake drums, cylinder heads, pistons, and liners etc. [43–45,89,90]. Sillimanite is one example of natural ceramic mineral and is available in abundance in coastal areas of India and is therefore cheaper than other

classes of reinforcements. Sillimanite also has good thermal/chemical stability and provides sound interfacial bonding with Al matrix, and thus, significantly lowers the wear rate [43–45,89,90]. Thus, aluminium alloys when reinforced with sillimanite particles can act as a wear resistant material for variety of engineering applications. Sillimanite reinforced AMCs, thus can act as an economical substitute for commercial materials presently being used in dry sliding wear applications.

In the light of aforesaid discussions, in the present research work, LM30 aluminium alloy matrix composites were processed with sillimanite mineral reinforcement (different particle size and weight percentage) for enhanced wear characteristics.

1.7 OUTLINE OF THE THESIS

The present research developed wear resistant AMCs with sillimanite as reinforcement and LM30 Al-Si alloy as matrix. Sillimanite reinforced AMCs with varying weight percentage (3–15 wt.%; at interval of 3 wt.%) and particle size (1–20 μm; 32–50 μm; and 75–106 μm) were processed using stir casting method. The subject matter corresponding to the present study on microstructure and wear properties has been investigated and organized in six separate chapters. The outline of the chapters is listed as follows:

- **Chapter 1:** The chapter introduces the basic terms involving the present study. This chapter discusses the need for improving the wear characteristics of aluminium based MMCs. The applications and factors affecting the tribological properties have also been discussed. The origin of the present research work has also been discussed.

- **Chapter 2:** The chapter presents a review of literature on wear and friction properties of (i) mineral reinforced AMCs at room temperature (ii) mineral reinforced AMCs at elevated temperatures. The chapter also brings out the main gaps in the existing literature in this field of work.

- **Chapter 3:** The chapter presents design of the present research work. It discusses the formulation of research objectives based on gaps in the existing literature. The chapter clearly establishes the need for the present research. It includes details of materials, processing

methodology, and equipment used for fabrication, testing, and characterization of aluminium silicon based composites reinforced with sillimanite mineral particles.

- **Chapter 4:** This chapter presents the microstructure, X-ray line profile, and X-ray dot mapping of the processed composites. This chapter also presents the results pertaining to hardness, wear and friction analysis of processed AMCs at room temperature. SEM-EDS analysis of the wear tracks and wear debris are also discussed in this chapter.

- **Chapter 5:** This chapter presents the results pertaining to wear and friction analysis of AMCs at elevated temperatures. The chapter also presents the results of thermal strain and coefficient of thermal expansion. Further, DTG-TGA of sillimanite has also been discussed. Next, XRD results of wear tracks and wear debris are discussed. Finally, SEM-EDS analysis of the wear tracks and wear debris are discussed.

- **Chapter 6:** This chapter presents the summary of results and significant findings of the experimental work embodied in this thesis. It also discusses the major conclusions to be drawn from the present research. The scope for possible extension of the present work is also discussed.

As per this outline, a detailed review of literature is presented in the next chapter.

CHAPTER 2
REVIEW OF LITERATURE

OVERVIEW

This chapter presents an extensive literature review on aluminium matrix composites processed for improved wear characteristics. The review is restricted mainly to particle reinforced aluminium matrix composites. The role of different constituents and reinforcements on the wear properties of such composite systems is discussed. Further, the influence of elevated temperatures on the wear behaviour of composites is also discussed. The review is presented in the following main sections:

- Particulate reinforced AMCs at room temperature
- Particulate reinforced AMCs at elevated temperatures
- Sillimanite reinforced aluminium matrix composites

2.1 ALUMINIUM-SILICON ALLOYS

Aluminium-silicon (Al-Si) alloys are widely used in a variety of engineering applications as they possess low density, high specific strength, good castability, high resistance to corrosion, and good wear properties [91,92]. Al-Si alloys with silicon concentration in the range of 4–20 wt.% are generally used for different engineering applications. Based on the weight fraction of silicon, Al-Si alloys are generally classified into three different segments viz. hypoeutectic Al-Si alloys (Si<12.6 wt.%), eutectic Al-Si alloys (Si =12.6 wt.%), and hypereutectic Al-Si alloys (Si>12.6 wt.%). Figure 2.1 presents the aluminium-silicon phase diagram. The only invariant reaction present is the eutectic reaction as presented in Equation 2.1.

$$L \rightarrow \alpha + \beta \qquad \ldots\ldots\ldots\ldots (2.1)$$

Where,

L: liquid phase,

α: predominantly aluminum, and

β: predominantly silicon

The eutectic reaction of Al-Si alloys take place at 577 ℃ with liquid solution phase of 12.6 wt.% silicon. Hypoeutectic Al-Si alloy comprises of proeutectic/primary Al phase and Al-Si eutectic mixture. Hypereutectic Al-Si alloys contain proeutectic/primary Si phase and Al-Si eutectic mixture. Generally, hypereutectic Al-Si alloys are used for a variety of engineering applications due to the presence of primary silicon phase. Hypereutectic silicon in Al-Si alloys provides good castability, good hardness, and good wear resistance [93–95].

2.2 ROLE OF ALLOYING ELEMENTS IN Al-Si ALLOYS

Various alloying elements like Mg, Cu, Ni, Sn, Mn, etc. are added to Al-Si alloys to improve different properties viz. hardness, weldability, strength etc. Each alloying element has a unique role of improving the physical, mechanical, and/or chemical properties of Al-Si alloys. Copper addition to the Al-Si alloy leads to enhancement in strength and hardness of casted aluminum alloys. Copper leads to formation of intermetallic phases like AlCu and Al_2Cu. These are hard and improve the strength of Al-Si alloys [96,97]. Magnesium when combined with silicon leads to development of a phase called Mg_2Si. This phase is hard and provides good corrosion

resistance, good weldability, and high strength [98,99]. Nickel forms an intermetallic compound (Al_3Ni) which improves the hardness, compression, and flexural resistance of Al-Si alloys [100,101]. Tin acts as a lubricating agent when surfaces are in contact with each other and helps to reduce the friction in bearing/bushing applications [101]. Similarly, manganese leads to improvement in tensile strength, corrosion resistance, and low-cycle fatigue resistance of Al- Si alloys [102].

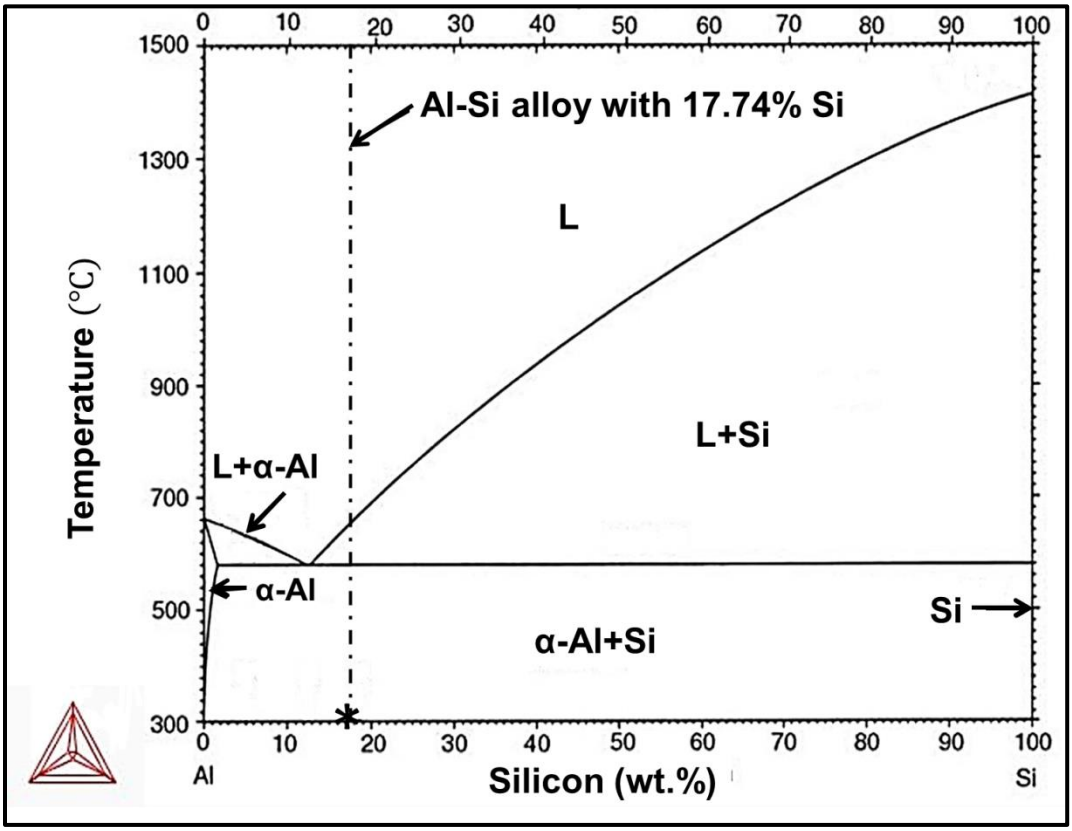

Figure 2.1 Aluminium-silicon phase diagram

2.3 WEAR BEHAVIOR OF PARTICLE REINFORCED AMCs

Hypereutectic Al-Si alloys display good wear resistance characteristics. The distribution of primary silicon phase in the matrix plays a crucial role in improving the wear resistance of hypereutectic Al-Si alloys [63,64]. The wear behaviour of hypereutectic Al-Si alloys is influenced by a variety of factors including the (i) shape, size, and distribution of primary silicon phase in the matrix, (ii) composition, distribution, and geometry of micro-constituents in the

matrix, and (iii) external factors viz. contact pressure, sliding speed, working temperature, counter surface hardness, and operating environment etc. [103–106].

The growth of primary silicon depends upon the nucleation and cooling rate of hypereutectic Al-Si alloys [107]. The wear resistance decreases due to presence of coarse and heterogeneous distribution of primary silicon. [108]. Thus, for improved wear properties, a refined and uniform distribution of primary silicon is desirable [108]. Primary silicon structure can be refined by use of (i) chemical method (addition of elements like Na, P, S etc.), (ii) physical method (using overheating electromagnetic stirring), or (iii) combined method (using elemental/mineral addition followed by overheating and stirring) [108–111].

Reinforcement of ceramic particles plays a vital role in modifying the wear behavior of Al-Si alloys. Thus, it is an important area of research for development of wear resistant and durable materials for engineering applications. The literature review presented here focuses on the dry sliding wear behavior of particle reinforced AMCs. The review of literature presented in this chapter is classified into the following main sections:

- Particle reinforced AMCs at room temperature
- Particle reinforced AMCs at elevated temperatures
- Sillimanite reinforced aluminium matrix composites

2.3.1 PARTICLE REINFORCED AMCs AT ROOM TEMPERATURE

This section provides a summary of the literature pertaining to the wear behavior of particle reinforced AMCs at room temperature.

Sharma [112] in **2001** studied the dry sliding wear behavior of Al6061–garnet particulate AMCs. The composites were fabricated using the stir casting process. Garnet mineral with particle size of 90–150 μm was reinforced to aluminium alloy. The weight percentage of garnet was varied between 4–12 wt.% (at interval of 4 wt.%). The authors observed that wear resistance of garnet reinforced AMCs was superior to that of base alloy. Wear resistance improved with increase in garnet reinforcement level. Further, the author observed that contact pressure, sliding distance, and sliding velocity have a significant effect on the transition in wear mode. Addition of garnet particles postponed the transition point. The average COF of the composites was lower

than base alloy. Formation of mechanical mixed layer (MML) lowered the wear and COF of AMCs.

Ranganath *et al.* [113] in **2001** investigated the wear behaviour of garnet zinc/aluminium MMCs. The composites were processed by stir casting method. Composites with garnet particle size of 30–50 μm were added to ZA-27 aluminium alloy. Garnet wt.% was kept in the range of 2–6 wt.% (at interval of 2 wt.%). The authors observed decrease in wear rate with increasing garnet reinforcement level. However, the wear rate increased with the increase in applied load. AMCs displayed abrasive wear (at low loads) and delamination wear (at high loads). Beyond the critical load, the wear rate increased abruptly. High wear rate region was indicated by large surface damage and large volume of material transfer to the disc. Reinforcement delayed the wear transition to severe wear regime.

Lee *et al.* [114] in **2002** developed a physical model for abrasive wear test of AMCs. The authors observed that the role of reinforcement was critically dependent on relative particle size, depth of plowing, and matrix/reinforcement strength of interface. The model successfully described the variation of reinforcement volume percentage on the abrasive wear rates of AMCs. Model predictions were in complete agreement with the two-body (pin-on-drum) abrasive wear experimental tests.

Velasco *et al.* [115] in **2002** studied the wear behaviour and mechanical properties of AMCs reinforced with (Fe_3Al) particles. AMCs were fabricated using powder metallurgy route. The authors observed that the reinforced intermetallic particles interacted with matrix and absorbed copper. An improvement in mechanical properties of AMCs was noted. The intermetallic reinforcement improved the wear resistance of composites. A three-fold increase in wear resistance was observed for the AMCs (over the base alloy).

Shorowordi *et al.* [116] in **2003** investigated the microstructure and interfacial characteristics of B_4C, SiC, and Al_2O_3 reinforced AMCs fabricated using stir casting process. AMCs with 0–20 vol.% SiC, 0–20 vol.% Al_2O_3, and 0–13 vol.% Al–B_4C were processed. The authors observed that particle distribution of Al–B_4C was better in comparison to Al–SiC and Al–Al_2O_3 AMCs. Interfacial reaction product was found at Al–SiC interface, while no interface reaction was

observed at Al–B_4C and Al–Al_2O_3 interfaces. Two secondary phases observed in Al matrix (away from the interface) in Al–B_4C composites were Al_2O_3 and Al_3BC. From SEM-EDS and fractured surface analysis, Al–B_4C AMCs exhibited superior interfacial bonding as compared to other composite formulations.

Korkut [117] in **2004** investigated the wear characteristics of M_7C_3, SiC, SiFe, Al_2O_3 and SiFe–Al_2O_3 particle reinforced AMCs. The wear rate of AMCs decreased with increase in particle vol.% but was independent of the type of reinforcement. However, the COF of AMCs was not affected by the vol.%, or the type of reinforced particles. Thus, the authors concluded that the reinforcement which was the cheapest could be chosen to reduce the overall cost.

Basavarajappa and Chandramohan [118] in **2005** studied the dry sliding wear characteristics of hybrid metal-matrix AMCs. AMCs were fabricated using the liquid metallurgy route. SiC (10 wt.%; average particle size of 25 μm) and graphite (3 wt.%; average particle size of 45 μm) was added to Al2219 Al alloy. Wear rate of graphite reinforced AMCs was lower compared to SiCp reinforced AMCs and the base alloy. Further, for a given reinforcement type and level, wear rate decreased as the sliding speed increased to the transition speed and load. Further, seizure was observed for base alloy; however, no seizure was observed for Al/SiCp and graphitic reinforced AMCs. Abrasion, delamination, and adhesion wear mechanisms were dominant.

Kumar *et al.* [119] in **2006** investigated the dry sliding wear of garnet reinforced zinc-aluminium alloy MMCs. Composites were fabricated using the stir casting route. ZA27 aluminium alloy was reinforced with garnet (particle size of 50–70 μm; level of 0–20 wt.%; at interval of 5 wt.%). Wear and friction tests were performed. The authors observed that wear resistance increased with garnet reinforcement in aluminium alloy. The dry sliding wear rate of MMCs and base alloy increased with increase in sliding speed and applied load. COF of the MMCs decreased with increase in reinforcement level.

Shorowordi *et al.* [120] in **2006** studied the worn out surface characteristics of Al–B_4C and Al–SiC AMCs under various applied pressures. AMCs were fabricated using stir casting process. The authors observed an increase in surface roughness and wear rate of MMCs with increase in contact pressures in the range of 0.75–3 MPa. At high contact pressures, marginal decrease in

COF of AMCs was observed. COF and wear rate of Al–B_4C composites was lower than Al–SiC composites due to lower hardness and pulling out of SiC. Transfer layer formed on the processed MMCs mainly comprised of the counterbody material and its thickness was directly proportional to the applied pressure.

Aigbodiona and Hassan [121] in **2007** investigated the effects of SiC reinforcement on the tensile behaviour of Al-Si-Fe/SiC AMCs. Addition of 20% SiCp to the alloy increased the yield strength, ultimate tensile strength, and hardness values. A slight increase in apparent porosity of composites with increase in SiC addition was observed. The authors concluded that for optimum service performance; silicon carbide reinforcement level range is 15–20 wt.%, not exceeding beyond 20 wt.%.

Basavarajappa *et al.* [122] in **2007** studied the effect of sliding speed on sub-surface deformation and wear behaviour of hybrid AMCs. AMCs were fabricated using the liquid metallurgy route. Al2219 aluminium alloy was reinforced with 15 wt.% SiC (average particle size of 25 μm) and 3 wt.% graphite. Addition of SiCp reinforcement decreased the wear rate of AMCs. For all sliding speeds, the wear resistance of Al–SiCp–graphite was higher than Al–SiCp AMCs. Based upon bulk hardness, the sub-surface deformation was characterized into three different zones viz. Zone 1 till a depth of 60 μm for the worn surface of both Al–15SiCp and Al–15SiCp–3graphite composite which had high hardness values, Zone 2 till a depth of 60–180 μm for Al–15SiCp and 60–140 μm for Al–15SiCp–3graphite composite which had lower hardness as compared to Zone 1, and Zone 3 where no change in hardness was observed. Microhardness of Al–15SiCp composites just below the wear surface was high. The microhardness decreased with increase in depth. Whereas, for the severe wear region, the microhardness just below the worn surface was lower. The degree of sub-surface deformation of graphite reinforced composite was lower than other composite formulation.

Abdizadeh *et al.* [123] in **2008** studied the effect of processing temperature on $ZrSiO_4$/TiB_2 aluminum composites. AMCs were fabricated using the stir casting process. Authors observed that addition of $ZrSiO_4$ and TiB_2 particles enhanced the hardness and tensile strength of base alloy. This was due to the high strengthening and work-hardening at low strain in AMCs. The best property values for Al-5% $ZrSiO_4$ were achieved for composites casted at 750 °C and for

Al-5% TiB_2 at 950 ℃ as $ZrSiO_4$ has a lower thermal expansion than of TiB_2. Due to lower thermal expansion of TiB_2, higher dislocation density induced around the interface region which degrades the properties. The wettability of TiB_2 with aluminum was better than $ZrSiO_4$. Consequently, a larger fraction of TiB_2 particles can be incorporated in the matrix, and hence, the microhardness and tensile strength of Al-TiB_2 AMCs was higher than Al-$ZrSiO_4$ AMCs.

Singla *et al.* [124] in **2009** investigated the wear behaviour of Al-SiC AMCs processed using the stir casting process. Pure aluminium was reinforced with SiC particles (5–25 wt.%). Authors observed that under dry sliding conditions, for a given applied load, the volume loss increased linearly with increase in sliding distance. The volume loss decreased till 20 wt.% SiC reinforcement level, and beyond this, the volume loss increased. Further, the friction coefficient of composites was observed to be lower than pure aluminium.

Hassan *et al.* [125] in **2009** investigated the wear behavior of SiC reinforced Al-Mg-Cu AMCs processed using the slurry casting route. Addition of SiC particles increased the wear resistance of composites. Further, the volume loss of AMCs increased with increase in sliding distance. Addition of SiC particles significantly improved the wear resistance of Al–4wt.% Mg–Cu alloys. Presence of SiCp led to formation of tribofilm and resulted in three-body abrasion system, and thus, decreasing the COF. The transfer of iron from disc to the pin and vice versa led to formation of mechanical mixed layer (MML) for both Al–Mg–Cu alloys and Al–Mg–Cu/SiC composites.

Kumar *et al.* [126] in **2010** investigated the wear properties of Al 6061-SiC and Al 7075-Al_2O_3 AMCs processed using the stir casting route. The hardness of Al 7075-Al_2O_3 AMCs was superior to Al 6061-SiC AMCs. Hardness of Al6061-SiC and Al7075-Al_2O_3 composites was found to be 60–97 VHN and 80–109 VHN respectively. Wear resistance and mechanical properties of Al 6061-SiC AMCs was found to be superior to Al 7075-Al_2O_3 AMCs.

Rao and Das [127] in **2010** investigated the influence of SiC particles on the sliding wear characteristics of AMCs processed through stir casting route. AA7010, AA7009, and AA2024 aluminum alloys were reinforced with SiC (average particle size of 20–40 μm). SiC reinforced AA7010 alloy showed maximum improvement in wear resistance. Wear track and wear debris

analysis revealed formation of an oxide layer and MML. Authors concluded that AMCs can be used as an exceptional material for high strength and wear resistance applications for structural, aerospace and general engineering applications.

Rao and Das [128] in **2011** studied the effect of various parameters on the wear and friction behavior of as-cast and heat-treated Al–SiCp AMCs. AMCs were processed by the stir casting route. Authors observed uniform distribution and good interface bonding at particle-matrix interface. Some intermetallic phases such as $Mg_2Cu_6Al_5$ and Al_2CuMg were observed at the interface. Hardness increased by 30% on addition of 25 wt.% SiCp to the alloy. Irrespective of the material, the wear rate increased with increase in applied load (0.2–1.4 MPa) and sliding distance (0–5000 m). Particle addition and heat treatment significantly improved the wear resistance of base alloy. Wear debris analysis revealed formation of continuous grooves at low contact pressures. At high contact pressure, deeper grooves with transverse and longitudinal cracks were observed.

Kumar *et al.* [129] in **2012** studied the tribological characteristics of LM13 aluminium alloy composites. Stir casting process was used for fabrication of AMCs. LM13 aluminium alloy was reinforced with zircon, SiC, and zirfloor (particle size of 1–32 μm; weight percentage of 15 wt.%). The authors observed higher improvement in hardness of AMCs with addition of tri-reinforcement particles (TRP) in aluminum as compared to single reinforcement particle (SRP). TRP enhanced the wear resistance as compared to SRP reinforcement particle when mixed in an equal proportion.

Sharma *et al.* [130] in **2012** investigated the influence of particle size on the wear behavior of Al-Si alloy composites. AMCs were fabricated using the stir casting process. LM13 aluminium alloy was reinforced with 15 wt.% zircon and 15 wt.% SiC particles (particle size of coarse 106–125 μm and fine 20–32 μm). Authors observed that the fine size zircon reinforced AMCs exhibited superior wear resistance than coarse size zircon AMCs. Wear resistance of SiC reinforced AMCs was superior to zircon reinforced AMCs.

Rasidhar *et al.* [131] in **2013** studied the properties of Al-ilmenite ($FeTiO_3$) nanocomposites. AMCs were fabricated using the stir casting process. Pure aluminium was reinforced with nano

sized ilmenite ($FeTiO_3$; 1–5 wt.%). The authors observed that tensile strength and hardness of composites improved with increase in ilmenite till 5 wt.%. Maximum improvement in mechanical properties was observed for 5 wt.% ilmenite reinforced AMCs without much effect on the ductility of matrix material.

Baradeswaran and Perumal [36] in **2013** investigated the effect of reinforcement of B_4C particles (5–20 wt.%; at interval of 5 wt.%) on the tribological and mechanical properties of Al-B_4C AMCs. Al 7075-B_4C AMCs were fabricated using the stir casting process. Addition of K_2TiF_6 flux (equal proportion of B_4C particles) increased the wettability and interfacial bonding. Hardness, tensile strength, flexural strength, compressive strength, and wear resistance of AMCs improved with increase in B_4C reinforcement level. The wear resistance of 10 wt.% B_4C AMC was 89% superior to that of base alloy.

Umanath *et al.* [132] in **2013** investigated the wear behaviour of Al6061/SiC/Al_2O_3 hybrid AMCs processed by stir casting route. The mathematical model used by the authors predicted the dry sliding metal to metal contact wear of AMCs with 95% confidence level. All the main factors (volume fraction, applied load, rotational speed, and counter-face hardness) showed a significant effect on wear behaviour of hybrid AMCs. SEM revealed that the wear track of AMCs was much rougher than that of base alloy. This was because of the abrasive wear nature resulting from hard ceramic particles exposed on the surface.

Arora *et al.* [133] in **2014** studied the effect of particle size on the wear behaviour of rutile-reinforced AMCs. AMCs were fabricated using the stir casting route. LM13 aluminium alloy was reinforced with 15 and 20 wt.% rutile particles with particle size range of 106–125 μm and 50–75 μm. The authors observed that the hardness of the composites increased with decrease in particle size and increase in weight percentage. Further, the wear resistance of fine particle reinforced AMCs was superior than the base alloy and coarse particle reinforced AMCs.

Arora *et al.* [134] in **2014** investigated the wear behaviour of rutile reinforced AMCs fabricated using stir casting process. LM13 aluminium alloy was reinforced with rutile (average particle size: 106–125 μm; level: 5 and 10 wt.%). The improvement in wear resistance was observed with increase in rutile wt.% from 5–10 %. Formation of tribo oxide layer (between the

countersurfaces) was observed at low applied loads which depicted the mild wear. At high applied loads, transition in wear rate from mild to severe wear was observed. Severe wear was indicated by removal of material by the fracturing of the tribo-oxide layer followed by material removal in the form of adhesion, oxidation, delamination, and plastic deformation.

Arora *et al.* [52] in **2015** studied the effect of different particle sizes of reinforcement on the wear behaviour of rutile reinforced AMCs. AMCs were fabricated using the stir casting process. LM13 alloy was reinforced with rutile (particle size: 50–75 µm, and 106–125 µm). The authors observed that rutile particle inclusion modified the microstructure and improved the wear resistance of AMCs. DPS composites (containing a mix of both particle sizes) revealed a superior wear resistance than the single particle composites. At a critical load (5 kg), transition from mild-to-severe wear occurred which was evident by extensive surface damage.

Prasad and Bandekar [46] in **2015** studied the mechanical properties of aluminum/garnet/carbon hybrid AMCs fabricated using chill casting method. LM13 alloy was used as matrix whereas garnet and carbon particles were used as reinforcement. Garnet particles were added in the weight percentage of 3–12 wt.%. However, a fixed amount of carbon particles was added i.e. 3 wt.%. The authors reported that the UTS properties of the composite increased as the garnet amount increased up to 9 wt.%, beyond which the decrease in mechanical properties was observed. Out of copper, steel, iron and SiC as chiller, composite with 9 wt.% garnet and 3 wt.% carbon showed better mechanical properties for copper chilling.

Kaushik and Rao [8] in **2016** studied the influence of heat treatment on two body abrasive wear of Al–SiC–Gr hybrid AMCs. AMCs were fabricated using the stir casting process. The authors observed a superior wear resistance for hybrid AMCs as compared to single SiC reinforced AMCs and base alloy. Graphite acted as a self-lubricant which improved the wear resistance of hybrid AMCs due to graphitic film formation. The wear rate increased with increase in applied pressure for both, as cast and T6 condition. At high applied pressures, wear resistance of hybrid AMCs improved by 16.4% and 27% in the as-cast condition and T6 condition respectively.

Viswanatha *et al.* [135] in **2016** studied the hardness and wear properties of A356-SiC_p-Gr AMCs fabricated by stir casting process. A356 alloy was reinforced with SiC (average particle

size: 25 μm; level: 3, 6, 9 wt.%), and graphite particles (average particle size: 44 μm level: 3 wt.%) were used as reinforcement. Microstructure of base alloy and AMCs revealed presence of primary α-phase dendrites. SiC and Gr particles were present at eutectic and interdendritic regions, respectively. With increase in SiC till 9 wt.%, hardness of composite increased. SiC particles acted as load bearing members and prevented the dislocation movement within the matrix. A356-9SiC-3Gr composites showed maximum wear resistance as compared to other AMCs. SEM images of wear tracks revealed that base alloy underwent severe plastic deformation whereas composites suffered mild wear.

Ghasali *et al.* [136] in **2017** fabricated aluminium matrix composites (AMCs) by using different heating methods. Pure aluminium and 1056 aluminium powder were used as matrix materials whereas SiC and TiC particles were used as reinforcements. Composites were processed by adding 15 wt.% of SiC and 7 wt.% of TiC in two different matrix materials i.e. pure aluminium and 1056 aluminium powder. Samples of size 5×5×25 mm^3 were made by applying pressure of 240 MPa on powder mixture of matrix and reinforcement. Further, samples were sintered at 650 ℃ and 750 ℃ for 1 hour. Heating rate of sintering process was varied by using two different furnaces i.e. conventional and microwave furnace. In conventional furnace, composites were heated at a rate of 10 ℃/min whereas in microwave furnace, it was 60 ℃/min. XRD analysis showed presence of aluminium along with crystalline phase of SiC and TiC. Composites formed by 1056 aluminium powder showed higher values of relative density, bending strength and microhardness. SEM revealed the occurrence of uniform particle distribution in both the matrix under conventional and microwave heating methods. Microwave sintering of Al 1056 composites resulted in improved mechanical properties at lower sintering time and energy. The volumetric nature of heating in microwave sintering resulted in higher densities which enhances the properties of composite.

Kaushik and Rao [32] in **2017** studied the effect of applied load on the abrasive wear nature of hybrid Gr/SiC/Al-Mg-Si AMCs. AMCs were fabricated using stir casting route. Al 6082 aluminium alloy was reinforced with 10 wt.% SiC and hybrid (5 wt.% Gr and 5 wt.% SiC) particles. The authors observed an increase in wear groove depth with a rise in applied pressure. Further, the wear groove depth decreased with T6 heat treatment. For the as-cast condition, a maximum reduction in wear depth of 38.1% and 16.2 % (over Al 6082 alloy) was observed for

applied load conditions of 5N and 15N respectively. In T6 condition, the maximum reduction in wear depth (over base alloy) was 25.1% and 27% at applied load of 5N and 15N load respectively. Wear results of Gr/SiC/Al-Mg-Si AMCs were superior to SiC/Al-Mg-Si AMCs. Graphite forms a self-lubricating layer and protects the surface from damage. The authors also noted that the wear rate of AMCs was influenced by the interfacial bonding between reinforcement and matrix. The authors concluded that the stronger interfacial bonding obstructed the plastic flow of matrix, whereas weak interfacial bonding created a cavity in AMCs and led to fracture of reinforcement.

Daniel *et al.* [137] in **2018** studied the wear properties of Al5059 aluminium alloy reinforced with combination of ceramic (i.e. SiC) and solid lubricant (i.e. MoS_2) particles. Particles size used for SiC was 10, 20, and 40 µm. AMCs were fabricated using the compo casting process. Reinforcements were added after mixing the SiC and MoS_2 particles. SiC particles were added in the weight percentage of 5, 10, and 15 wt.% by fixing the amount of MoS_2 to 2 wt.%. The authors observed that weight percentage and particle size of SiC were the main factors accountable for wear of hybrid AMCs. ANOVA predicted that SiC wt.% and particle size have 23.43% and 20.73% influence on wear rate. For COF, maximum influence was observed for operating temperature and SiC content was 39.85% and 34.60% respectively. Maximum decrease in wear rate (wear loss of 0.0045g) and COF (0.228) of composites was observed for 15 wt.% SiC reinforced AMCs with average particle size of 10 µm. Increase in temperature from 50–150 ℃ showed an increase in wear rate of composites.

Kurapati *et al.* [138] in **2018** investigated the influence of various parameters on dry sliding wear properties of hybrid AMCs by using Taguchi technique, ANOVA, and mathematical modelling. AA2024 Al alloy was reinforced with equal proportions of fly ash (FA) and SiC particles in weight fractions of 5, 10 and 15 wt.%. AMCs were fabricated using the stir casting process. Wear tests revealed that addition of FA and SiC in AA2024 resulted in increase of wear resistance. Increase in applied load and sliding distance increased the wear rate of composites. According to Taguchi technique, wear was observed to be affected by applied pressure, sliding time and reinforcement level. ANOVA showed that applied pressure had the most significant effect (43.83%) followed by sliding time (28.47%) and weight percentage (20.10%). Composite with 15 wt.% of reinforcement tested at 45 min sliding time and 0.5 Kgf load showed best results

for wear resistance. SEM image of the composites showed oxide fragments, peeling of layers, particles in the form of debris, delamination, and abrasive grooves.

Pethuraj *et al.* [139] in **2018** studied the effect of solid particle erosion behavior of sillimanite reinforced AMCs. The composites were fabricated using vacuum assisted stir casting process. Pure aluminum was reinforced with sillimanite (particle size: 80 μm; reinforcement level: 5 and 10 wt.%). Hardness, tensile strength, and impact strength of sillimanite reinforced AMCs was better than the base alloy. Erosion tests were carried out using alumina slurry at different velocities (41 m/s, 72 m/s, and 100 m/s) and angle of impingement (45^o, 60^o and 90^o). The erosion rate of matrix material and AMCs increased with increase in velocity and a decrease in impingement angle. Further, the erosion of 10 wt.% sillimanite reinforced AMCs was higher than the pure aluminum. Composite with higher sillimanite content had less particle to particle distance. Hence, during erosion, the impact of erodent resulted in initiation and propagation which causes pulling out and loosen of reinforced particles.

Vadghule *et al.* [140] in **2018** studied the tribological properties of LM26 AMCs fabricated by stir casting technique. LM26 Al-Si alloy was reinforced with SiC (5–15 wt.%). The increase in applied pressure increased the wear rate of AMCs. The rise in SiC wt.% decreased the wear rate of the AMCs. The authors also concluded that sliding velocity played insignificant role in the wear characteristics of AMCs.

Balakumar *et al.* [141] in **2018** studied the hardness and wear characteristics of AMCs processed by stir casting route. Al6061 alloy was reinforced with fly ash, graphite, and copper powder. The authors observed that use of fly ash composites can help to reduce industrial waste. AMCs with 15 wt.% fly ash, 4 wt.% Cu and 4 wt.% graphite provided the best wear properties. The hardness of Al-fly ash/Cu/Gr AMCs increased with rise in fly ash and graphite reinforcement level.

Vinod *et al.* [142] in **2019** processed hybrid AMCs through double stir casting process. Fly ash (FA) (inorganic) and rice husk ash (RHA) (organic) were added to A356 Al alloy. FA and RHA waste materials were successfully reinforced to matrix. Mechanical properties of A356 alloy matrix increased with addition of organic and inorganic particles. Higher hardness values

obtained were a representative of higher interfacial bonding. The best properties were demonstrated by A356/10% FA-10% RHA hybrid composite. The rise in reinforcement from 10 to 12.5 wt.% decreased the interfacial bonding and hardness.

Mishra *et al.* [143] in **2019** investigated the wear behaviour of garnet and flyash (FA) reinforced Al-7075 hybrid AMCs. AMCs were fabricated by the two-step stir casting technique. The steady-state wear rate improved with rise in applied pressure, sliding velocity, and temperature but decreased with rise in sliding distance. The average wear rate of garnet reinforced hybrid AMCs was 8.7% less than that of FA reinforced composites. The oxide layer and MML on the wear track were responsible for improvement in wear resistance.

Çelik and Kilickap [144] in **2019** investigated the hardness and wear behaviour of hybrid (B_4C and SiC) AMCs. Pure aluminium was reinforced with B_4C (4–16 wt.%), SiC (4–8 wt.%), and hybrid (B_4C: SiC in the ratio of 0:12, 0:16, 2:2, 8:4, 4:8, 12:4, and 4:12 respectively) using powder metallurgy method. The authors observed that the increase in the reinforcement ratio improved the hardness of the AMCs. The hardness of 16 wt.% B_4C reinforced AMCs was best amongst all AMCs. Further, the wear resistance of AMCs increased with rise in reinforcement ratio and was maximum for 16 wt.% SiC reinforced AMCs at an applied load and sliding distance of 5 N and 250 m respectively. However, wear rate of all composites decreased with applied pressure and sliding distance.

Lakshmikanthan *et al.* [145] in **2019** studied the mechanical properties and wear behaviour of A357 dual particle sized (DPS) SiC particle reinforced AMCs. AMCs were fabricated by stir casting technique. The hardness of AMCs improved with rise in DPS loading. Maximum hardness, yield strength, and ultimate tensile strength was observed for DPS composites containing 4 wt.% large and 2 wt.% fine sized SiCp. The wear rate of AMCs decreased with rise in SiCp loading. Best wear resistance was also observed for AMCs reinforced with 4 wt.% large and 2 wt.% fine sized SiCp. The wear resistance of AMCs improved with rise in concentration of larger particles in the DPS mixture.

Gecu and Karaaslan [146] in **2020** studied the effect of casting temperature on wear resistance and corrosion resistance of A356/304 stainless steel reinforced AMCs. AMCs were fabricated

using vacuum-assisted melt infiltration casting technique. For casting, the temperature was varied in the range of 630–880 ℃ at interval of 50 ℃. The optimum casting temperature was found to be in the range of 730–780℃. In this range, matrix observed minimum shrinkage cavities. Also, the intermetallics formed at the interface were discontinuous. Two intermetallic phases viz. θ (Fe_4Al_{13}) and η (Fe_2Al_5) were observed. The presence of intermetallic at interface causes the increment in wear resistance of composites. Worn out surface revealed that for the base alloy adhesive wear was dominant whereas, for AMCs abrasive wear was dominant. Till the temperature of 730 ℃, abrasive wear was observed due to the microploughing action. Beyond 730 ℃, microcutting action was observed. For casting temperature till 780 ℃, no dissolution of reinforcement and intermetallic compounds were observed during the corrosion test. However, for casting temperature greater than 780 ℃, a dissolution of reinforcement and intermetallic compounds was observed hence, increase in corrosion of AMCs was noted.

Yadav *et al.* [147] in **2020** compared the high stress abrasive wear behaviour of aluminium piston matrix composites. LM13 alloy and ADC12 alloy were individually reinforced with 7 wt.% SiC and 7 wt.% TiB_2 particles. Addition of TiB_2 and SiC reinforcement to LM13 alloy and ADC12 alloy improved the abrasive wear nature of the AMCs and decreased the crater wear. The authors concluded that the addition of TiB_2 and SiC to LM13 and ADC12 Al alloys is most advantageous in improving the sliding wear resistance of AMCs.

Girish *et al.* [148] in **2020** studied the effect of hot forging on wear characteristics of A6061 aluminium alloy composites. Aluminium alloy was reinforced with SiC particles (particle size 25–30 μm; weight percentage 2, 4, and 6) by using the stir casting method. AMCs were then forged at a temperature of 430 ℃ following the reduction rates of 20%, 40% and 60%. The wear rate of forged composites showed better wear resistance than the non-forged composites. This was attributed to decrease in porosity which enhanced the resistance to crack propagation. Simultaneously, the resistance to debonding of particles during forging also helped in improving the wear resistance of composites. The wear rate increased with the increase in load up to 40% reduction, which later reduced due to severe plastic deformation of the composite.

2.3.2 PARTICLE REINFORCED AMCs AT ELEVATED TEMPERATURES

This section provides a summary of the literature pertaining to the wear behavior of particle reinforced AMCs at elevated temperatures.

Degnan *et al.* [149] in **2001** investigated the wear nature of TiCp-steel matrix reinforced MMCs at elevated temperatures. The authors observed that two wear regimes viz. mild wear regime represented by oxide generation and low wear rates and severe wear represented by metallic contact at rubbing surfaces and high wear rates. At room temperature, wear resistance of base alloy and MMCs decreased with increase in applied pressure. The transition in mild-to-severe wear for the MMCs occurred at higher loads (at room temperature as well as elevated temperature of 250 ℃) as compared to the base alloy. Whereas, for the wear at temperature of 500 ℃, oxidative wear is dominant for both base alloy and composites.

Muratoğlu and Aksoy [150] in **2006** studied the abrasive wear beahviour of Al2124-SiC AMCs at elevated temperatures (20–200 ℃). AMCs were fabricated using powder metallurgy technique. AMCs were also given T6 heat treatment. For all operating temperatures, wear resistance of heat treated composites was higher than non-heat treated AMCs. For heat treated composites, wear rate of AMCs at room temperature was lower than that at elevated temperatures. No significant change in wear rate was noted above the operating temperature of 50 ℃. Higher temperatures led to softening of material and loosening of hard SiCp causing increased wear rate.

Karin ***et al.*** [151] in **2007** investigated the high temperature wear resistance of Ni_3Al-based intermetallic alloys (NAC alloy). Hot isostactic processing (HIP) was used for fabrication of Cr_3C_2 particle reinforced Ni_3Al composites. The wear rate of composites was also compared with cast iron. On comparison of Ni_3Al base alloy with cast iron, authors observed that Ni_3Al-based alloys sustained much higher contact pressures than the conventional wear-resistant cast iron. The Cr_3C_2 particle reinforced Ni_3Al composites further improved the wear resistance as compared to Ni_3Al-based alloys. The addition of Cr_3C_2 particles separated the two sliding surfaces and reduced the adhesion between sliding surfaces.

Lee *et al.* [152] in **2008** studied the high temperature wear behaviour of MAO (micro-arc oxidized) coated A356/20 vol.% SiCp composites. The authors observed that MAO coating with α-aluminium, γ-aluminium, and mullite was successfully obtained which has led to rise in hardness of AMCs. For mild wear regions, wear resistance of MAO coated and an uncoated A356/SiCp composite was similar. Decrease in COF values was observed with increase in applied pressure. This could be attributed to formation of MML on MAO-coated layer. For severe wear regions, MAO-coated AMCs revealed superior wear resistance as compared to uncoated composites.

Natarajan *et al.* [153] in **2009** studied the wear nature of Al 6063/TiB_2 in-situ AMCs at elevated temperatures. Aluminium 6063 alloy was superheated to 850 ℃ and K_2TiF_6 and KBF_4 were added to the molten alloy. The exothermic reaction between the salts led to formation of TiB_2 particles in the base alloy. The authors observed that particles improved the wear resistance of AMCs, both at room as well as elevated temperatures. For temperatures less than 100 ℃, abrasive wear mechanism followed by void nucleation was dominant for material removal. Thereafter, for temperatures till 200 ℃, oxidative wear was dominant. Finally, for temperatures higher than 200 ℃, severe adhesive wear along with crack generation and propagation was dominant.

Kumar *et al.* [154] in **2010** studied the high temperature wear nature of Al-4Cu-TiB_2 in-situ AMCs. The addition of TiB_2 particles decreased the wear resistance and COF of Al-4Cu alloys. The wear rate of Al-4Cu alloys and AMCs increased with rise in applied pressure and temperature. The mild-to-severe transition in wear of Al-4Cu alloy was dependent on the applied pressure and temperature. For a given concentration of TiB_2 particles, wear resistance improved with increase in temperature. Further, for base alloy, adhesion was a dominant wear mechanism. However, for Al-4Cu-TiB_2 AMCs, oxidation and delamination were dominant wear mechanisms.

Jerome *et al.* [155] in **2010** evaluated the mechanical and high temperature wear behaviour of in-situ Al-TiC AMCs. The authors observed that the in-situ Al-TiC AMCs improved the hardness, tensile strength, and wear characteristics over the base alloy. For all the operating temperatures, wear rate of AMCs decreased with rise in amount of reinforcing particles. The

wear rate of AMCs increased linearly with rise in applied pressure at all temperature range. At room temperature, transfer layer mechanism was dominant whereas at elevated temperatures oxidative layer was dominant which reduced the wear rate.

Rajaram *et al.* [156] in **2010** investigated the high temperature wear of Al-Si/graphite composites. AMCs were fabricated using the stir casting technique. The wear resistance of Al-Si-graphite AMCs was superior to Al-Si alloys, both at room and elevated temperatures. Al-Si-graphite composites withstood the temperature of 300 ℃, whereas, for Al-Si alloys maximum operating temperature was 250 ℃. The oxide layer prevented direct metal-to-metal contact of countersurfaces. Wear rate of AMCs was lower than that of base alloy. This was because of a combined effect of oxide layer and graphite glaze layer on the sliding surfaces. For the base alloy, delamination wear mechanism followed partial abrasive wear for temperatures in excess of 100 ℃. For composites, only delamination wear mechanism was observed for operating temperatures in excess of 100 ℃. Oxidative wear mechanism was dominant for temperatures greater than 150 ℃, both for base alloy and composites.

Zhu *et al.* [157] in **2012** investigated the friction and wear behaviour of (Al_3Zr+α-Al_2O_3)/Al AMCs at elevated temperatures. AMCs were fabricated using the PM technique. For the test temperature of 100 ℃, wear rate increased till a sliding velocity of 0.6 m/s and beyond this, the wear rate decreased. For the temperature of 200 ℃, a constant decrease in wear rate was observed for all sliding velocities (0.4–1 m/s; at interval of 0.1 m/s). Further, for the temperature of 200 ℃, applied load of 50 N and sliding velocity of 0.6 m/s, a sudden increase in COF was observed. At 20 N load and 100 ℃ temperature, COF values 0.25, 0.14, and 0.11 was observed for sliding velocities of 0.4, 0.5, and 0.6 m/s, respectively. However, for the sliding velocity of 0.7 m/s, the COF increased to 0.25. Next, with increase in the volume fraction (20–30 vol.%) the wear rate of the composites decreased with rise in temperature.

Zhu *et al.* [158] in **2012** investigated the wear behaviour of Al-ZrO_2-B AMCs at high temperatures. AMCs were fabricated using PM technique. The authors observed that wear rate increased linearly with increase in elevated temperature and applied load. For operating temperature of 100 ℃ and applied load of 20 N, wear resistance of AMCs decreased with the increase in sliding velocity till 0.6 m/s, and beyond this, the wear resistance increased. For

operating temperature of 200 ℃ and applied load of 20 N, an increase in wear resistance was observed for all sliding velocities. Further, the sub-surface deformation increased with increase in B/ZrO_2 molar ratios of 0, 1, and 2.

Kumar *et al.* [159] in **2013** studied the influence of particle size on the wear nature of zircon reinforced AMCs at high temperatures (100–300℃). Stir casting process was used for fabrication of composites. LM13 aluminium alloy was reinforced with zircon. The authors observed that AMCs reinforced with fine sized zircon particles (20–32 μm) exhibited superior wear properties than coarse sized counterparts, at all loads and temperatures. This was because finer is the size of particles, higher is the surface area, and thus, more number of particles exist per unit area. The wear mode transition for both type of AMCs was observed above 200 ℃ for all applied loads. Materials loss during sliding was primarily due to delamination of mechanical mixed layer.

Kumar *et al.* [160] in **2013** investigated the effect of elevated temperatures on dual reinforced particles (DRP) based LM13 aluminum alloy composites. LM13 aluminium alloy was reinforced with SiC and $ZrSiO_4$ particles using stir casting. The authors observed that SiC particles refined the silicon whereas zircon particles improved the interfacial bonding of matrix reinforcement. SiC and $ZrSiO_4$ particles provided the active nucleation sites for silicon nucleation. For all temperatures and applied pressures, the combination of $ZrSiO_4$ and SiC in the weight ratio of 1:3 exhibited best wear resistance. DRP enhanced the wear resistance as compared to single reinforced particles when mixed in a definite ratio. Wear rate of AMCs increased linearly with increase in operating temperature. At higher applied pressures, oxide film and mechanical mixed layer formation protected the countersurfaces from wear.

Rajan *et al.* [161] in **2014** investigated the influence of in-situ TiB_2 particles on the wear characteristics of AA7075/TiB_2 in-situ AMCs. XRD analysis revealed formation of TIB_2 in-situ particles. At a given operating temperature, wear rate of AMCs decreased with increase in TiB_2 content. The transition temperature increased from 180 ℃ (for base alloy) to 210 ℃ (for AMCs). At higher temperature of 240 ℃, TiB_2 particles decreased the sub-surface deformation of AMCs. Abrasive wear was dominant at room temperature, whereas metal flow (delamination) was dominant for elevated temperature.

Arora *et al.* [162] in **2015** studied the influence of contact pressure on the wear behaviour of DPS rutile reinforced AMCs fabricated by stir casting technique. LM13 alloy was reinforced with DPS rutile particles (50–75 μm, and 106–125 μm). The hardness of AMCs improved with increase in rutile weight percentage. For the operating temperature of 150 ℃, a transition in wear nature from mild to severe was observed. Wear track and debris analysis revealed the formation of MML. MML formation reduced the wear rate of AMCs. For operating temperatures in excess of 150 ℃, the mechanical mixed layer got removed and plastic deformation of material occurred, thus, increasing the wear rate.

Kumar *et al.* [163] in **2016** investigated the wear behaviour of Si_3N_4, AlN and ZrB_2 reinforced Al 2618 aluminium alloy in-situ composites at high temperatures. Hardness of composites improved with rise in reinforcement level. Wear rate, specific wear rate, and COF values decreased with increase in reinforcement level. Taguchi method predicted minimum wear rate of 0.000523 mm^3/m for 8 wt.% reinforcement, 200 ℃ temperature, 10 N applied load, 5 m/s sliding velocity and 2000 m sliding distance. ANOVA predicted that particle composition had 63.84% influence on wear rate of AMCs. Sliding distance, temperature, load, and sliding velocity influenced the wear rate by 20.2%, 5.32%, 4.01%, and 3.96% respectively. The wear rate predicted by generic algorithm (0.0016308 mm^3/m) was in close comparison to the experimental results (0.0016458 mm^3/m).

Nemati *et al.* [164] in **2016** studied the mechanical properties and high temperature wear behaviour of $Al_{13}Fe_4$ complex metallic alloys (CMA) nanoparticle (0–10 wt.%) reinforced Al composites. AMCs were fabricated by PM technique. The authors observed that addition of $Al_{13}Fe_4$ CMA nanoparticle improved the mechanical and tribological properties of AMCs. The work-hardening caused by extrusion and the tendency of particles to obstruct the dislocation movement in matrix improved the wear resistance of AMCs. Lowest wear and friction results were observed for 5 wt.% $Al_{13}Fe_4$ CMA nanoparticle reinforced AMCs at an elevated temperature of 250 ℃. Beyond 5 wt.% reinforcement, the wear rate and COF values increased. This was due to clustering and agglomeration effects of $Al_{13}Fe_4$ CMA nanoparticles in the matrix.

Raju *et al.* [165] in **2019** studied the tribological properties of Al-1100-coconut shell ash (CSA) AMCs at high temperatures. Composites were fabricated by stir casting technique. The wear rate of CAS reinforced AMCs improved in comparison with as-cast alloy for rise in applied pressure at elevated temperature. Maximum improvement of 70% in specific strength (over base alloy) was observed for 15 wt.% CSA reinforced AMCs. Density and elongation decreased by 6% and 46% respectively. A minimal change in COF values was observed with increase in contact pressure at room temperature. At elevated temperatures, the COF increased till a contact pressure of 6 N/mm^2, beyond which the formation of oxides reduced the COF of AMCs.

2.3.3 SILLIMANITE REINFORCED ALUMINIUM MATRIX COMPOSITES

The proposed research tends to investigate the hardness and wear characteristics of AMCs reinforced with sillimanite ceramic mineral. An extensive literature review revealed that limited work (only 5 papers till date) is reported on AMCs reinforced with sillimanite. Moreover, this work has been performed by the same research group. The details of this work are as follows:

Singh *et al.* [89] in **2001** prepared and studied the properties of stir cast sillimanite reinforced AMCs. LM6 Al alloy was reinforced with sillimanite (average particle size of 140 μm, and 10 wt.%). Optical microscopy revealed uniform distribution of sillimanite particles and good mechanical bonding with the matrix alloy. Hardness of AMCs improved from 57 to 85 HV. There was decrease in percentage elongation (2.25 to 1.42%) and ultimate tensile strength (132 to 121 MPa) which was in accordance with earlier reported literature for other AMCs. The decrease in UTS and percent elongation was attributed to ineffective load transfer capacity from matrix to the sillimanite particles. Also, the difference in thermal coefficients of matrix and reinforcement resulting in generation of thermal residual stresses could be another reason. The wear was studied against a 25 μm abrasive size disc. Under all sliding distance and applied load conditions, the wear rate of sillimanite based composites was lesser than the base alloy. This was because sillimanite particles prevented the abrasive particles (of the disc) from penetrating into the matrix. This decreased the depth of grooves. The authors claimed that dispersoid sillimanite particles carried a major portion of the load, thereby providing enhanced wear resistance.

Singh *et al.* [43] in **2002** studied the abrasive wear nature of LM6-sillimanite reinforced AMCs. As-received Al-Si (LM6) alloy was reinforced with sillimanite (average particle size of 50–150

μm, and 10 wt. %). AMCs were fabricated by the stir casting technique. Micrographs revealed uniform sillimanite particle distribution in the matrix. Further, the wear rate of the AMCs increased with increase in contact pressure (1, 3, 5, and 7 N) and abrasive size (25, 100, and 200 μm). The wear rate of materials decreased for longer sliding distances. With increase in sliding distance, the abrasive particles get blunt and their cutting efficiency decreases. The work hardening of matrix also increased with higher sliding distance, thus decreasing the wear rate. Further, the wear resistance for finer sized abrasives was superior in comparison to coarser sized abrasives. It was observed that the applied pressure and abrasive size were inversely proportional. Beyond a critical limit, the sillimanite particles were fractured/ fragmented or scooped off from the wear surface of the AMCs, thus causing an increase in wear rate.

Singh *et al.* [44] in **2003** studied the wear behavior of sillimanite reinforced AMCs fabricated by stir casting process. As-received Al-Si (LM6) alloy was reinforced with sillimanite particles (average particle size of 50–150 μm, and 10 wt.%). Factorial design was used for the calculation of regression equation for wear rate. Various parameters like sliding distance, applied load, and abrasive size of the SiC wheel were used for calculation of wear rate regression equation. Wear rate increased with increase in applied load (1–7 N) and abrasive size (25–200 μm) and decreased with increase in sliding distance (0–130 m). However, with higher sliding distance, the wear rate of the AMCs reduced more rapidly in comparison to the base. This was because of blunting of abrasives, which reduced the wear rate of AMCs. Beyond a critical applied load (4 N) and abrasive size (112.5 μm), AMCs showed higher wear rate than the base alloy. The wear rate was significantly dependent on the combination of applied load-abrasive size rather than with the combination of abrasive size-sliding distance or applied load-sliding distance. Regression equation successfully predicted the wear rate of composites within the selected experimental range.

Singh *et al.* [90] in **2003** studied the influence of sillimanite particle reinforcement on the wear behaviour of AMCs fabricated by stir casting technique. As-received Al-Si (LM6) alloy was reinforced with sillimanite particles (average particle size of 50–230 μm, and 10 wt. %). The wear rate of AMCs improved with rise in applied pressure. Wear rate of sillimanite reinforced AMCs was found to be lower than the unreinforced alloy. For all the composites, temperature near matrix surface increased with increase in applied pressure. Higher temperature rise was

observed for unreinforced alloy over the composite. COF values of composite were lesser in comparison with the matrix alloy. Sliding led to significant microstructural changes in the subsurface. It was reported that MML controls the wear nature of composites.

Singh *et al.* [45] in **2006** studied the wear response of sillimanite reinforced AMCs fabricated by stir casting technique. As-received Al-Si (LM6) alloy was reinforced with sillimanite (average particle size of 50–150 μm, and 10%). Wear test was conducted using abrasive particles (of size in the range, 212–300 μm). AMCs displayed better hardness and wear resistance than the matrix alloy. Wear rate decreased with increase in sliding distance. However, after attaining certain values, it remained constant which could be attributed to subsurface hardening. Wear rate of AMCs increased with applied pressures. At low load conditions, material removal was due to rolling of abrasive particles. At high applied pressures, material removal was due to the cutting action of abrasives. Work-hardening of AMCs decreased with rise in applied pressures. Maximum work-hardening was noted upto a critical depth from abraded surface. Next, to the abraded surface, micro cracks with softening of materials was also observed. The work hardening was efficient till a depth of 250 μm from the abraded surface.

2.4 SUMMARY OF THE LITERATURE

- Most of the researchers have worked on fabrication of AMCs using stir casting method. Stir casting has proved to be a very efficient and economical method to fabricate AMCs. Tribological properties achieved by this method have been reported to be quite good.
- Most authors have studied the influence of particle size and reinforcement type on the wear behaviour AMCs. A few authors have studied the influence of dual reinforced particles on the wear characteristics of AMCs. Authors have reported that addition of ceramic particles like rutile, sillimanite, SiC, Al_2O_3, and B_4C etc. as reinforcement in AMCs improves the mechanical properties and wear characteristics of AMCs. This is due to high hardness of ceramic sands. Another reason is better bonding and refinement of microstructure due to difference in coefficient of thermal expansion of matrix and ceramic particles.
- With rise in reinforcement level (ceramic sands), there is improvement in wear characteristics till a certain value. During the wear test, oxide formation and mechanically mixed layer (MML) helped in restricting the wear of composites.

- With rise in applied load, there is a rise in wear of composites though lesser as compared to that of base alloy. Wear mechanism observed in wear test of AMCs include abrasion wear, adhesion wear, delamination wear, and microcutting wear etc.
- Ceramic particle reinforcement improved the tribological properties of AMCs, both at room temperature as well as at elevated temperatures. Addition of ceramic particles increased the working range of AMCs and also delayed the transition of wear from mild-to-severe wear region.

2.5 GAPS IN THE EXISTING LITERATURE

Several authors have worked on the synthesis, characterization, and evaluation of mechanical and tribological properties of aluminium alloy based MMCs with ceramic reinforcement. However, the following limitations are observed after a detailed literature review.

- Many authors have studied the wear characteristics of AMCs reinforced with various ceramic materials. However, limited work has been reported to investigate the mechanical properties (impact strength, high temperature stability, tensile strength etc.) of AMCs. Further, the effect of cooling rate (during solidification) on the mechanical and tribological characteristics has not been investigated.
- Significant work has been done on the fabrication of AMCs using single particle size of reinforcement. Only a few authors have worked on fabrication of AMCs using a combination of two grit size reinforcements in composites.
- Significant work has been done to investigate the wear characteristics of AMCs reinforced with single reinforcement particle viz. SiC, Al_2O_3, $ZrSiO_4$, TiO_2, B_4C etc. However, limited work has been reported to study the effect of dual reinforcement on wear characteristics of AMCs.
- Limited work is available to study the influence of reinforcement type, particle size, and weight fraction of reinforcement on the wear characteristics of AMCs at elevated temperatures.
- Limited work has been reported on AMCs with sillimanite mineral as the reinforcement. In all the studies on sillimanite reinforced AMCs, the matrix material remained the same i.e. LM6 alloy. In these studies, the effect of sillimanite particle size on the resulting properties

was not investigated. In all the investigations, a broad range of sizes (50–150 μm) were considered. Further, the effect of sillimanite reinforcement level on the wear characteristics of AMCs was not investigated. In all the reported studies, the sillimanite weight percentage was kept constant (10 wt.%). Also, to evaluate the influence of temperature on wear characteristics and to observe the transition in wear mode (from mild-to-severe and vice versa), the high temperature wear studies on sillimanite reinforced AMCs have not been conducted.

The next chapter presents the design of the study used in the present research work.

CHAPTER 3
DESIGN OF THE STUDY

OVERVIEW

On the basis of limitations observed in the reviewed literature, this chapter discusses the formation of research objective and key issues. The chapter also discusses the details of materials and methods used in the research work. In addition to this, the details of equipment used for processing, testing, and characterization of AMCs have also been discussed.

3.1 OBJECTIVE

An extensive amount of literature is available on the processing, characterization, and wear testing of AMCs reinforced with ceramic particles. However, in most of the reported work, AMCs are reinforced with synthetic ceramic particles. There has been limited research on the wear behaviour of AMCs reinforced with naturally available ceramic mineral particles. Amongst the few natural ceramic particles investigated, sillimanite mineral is an effective reinforcement to improve the wear performance of AMCs. However, literature review showed that work on sillimanite reinforced AMCs has been conducted by only one research group. The investigations remained restricted to (i) a fixed reinforcement level of 10 wt.% sillimanite and, (ii) a given broad particle size range of 50–150 µm. In order to overcome these limitations of past research, the main objective of the present work was *"to investigate the effect of particle size and weight fraction of sillimanite reinforcement on the microstructure and wear characteristics of aluminium matrix composites"*.

The key issues addressed to meet this objective were as follows:

- To fabricate aluminium matrix composites with sillimanite as the reinforcement and LM30 aluminium alloy as the matrix through stir casting route. Composites with different particle size range of reinforced particles (1–20 µm, 32–50 µm, and 75–106 µm) and weight fractions (0–15 wt.%; at interval of 3 wt.%) of reinforcement were processed.
- To evaluate the microhardness/nanohardness and microstructure of developed composites through different characterization techniques (Brinell hardness testing, optical microscopy, SEM-EDS analysis, XRD etc.) to determine structure-property relationship.
- To analyze the dry sliding wear behaviour of the fabricated AMCs, both at room temperature as well as at elevated temperature conditions (50–300 ℃; at interval of 50 ℃).

3.2 STARTING MATERIALS

As-received LM30 Al-Si alloy was used as the matrix material for fabrication of composites. LM30 Al-Si alloy was procured from Emmes Metals Private Limited, Mumbai, India. Table 3.1 presents the chemical composition of LM30 aluminium-silicon alloy. LM30 Al-Si alloy is used in fabrication of brake rotors, pistons, cylinder liners, piston rings etc.

Table 3.1 Chemical composition of the base material (LM30 alloy)

Constituent elements	Si	Cu	Fe	Mn	Mg	Zn	Cr	Ni	Ti	Ca	Pb	Sn	Sr	Al
Wt. %	17.74	4.10	0.533	0.106	0.523	0.262	0.034	0.023	0.0825	0.018	0.0832	0.031	0.0006	76.4

Sillimanite (Al_2SiO_5), which is a natural ceramic mineral, was used as reinforcement in the processing of composites. Sillimanite mineral was procured from Indian Rare Earths Limited, Mumbai, India. Table 3.2 presents the chemical composition of sillimanite mineral used in the present study. Sillimanite mineral has high hardness, and low coefficient of thermal expansion.

Table 3.2 Chemical composition of sillimanite (Al_2SiO_5)

Composition	Al_2O_3	SiO_2	ZrO_2	TiO_2	Fe_2O_3
Wt. %	58.60	38.54	2.20	0.26	0.40

Further, the automobile grade grey cast iron (SAE-ASTM Grade) was used as the representative commercial material for comparison of wear results with the developed composites. Grey cast iron is used in fabrication of brake rotors of automobiles. Table 3.3 presents the spectroscopy analysis (Foundry-Master UV, Oxford Instruments, UK) of chemical composition of cast iron used for comparison in the present study.

Table 3.3 Chemical composition of automobile grade cast iron

Composition	C	Si	Mg	P	S	Cr	Fe
Wt. %	3.5	1.7	0.7	0.13	0.11	0.14	Balance

Table 3.4 presents the details of physical, mechanical, and thermal properties of the base material (LM30 aluminium alloy), sillimanite particles, and the automobile grade grey cast iron.

Table 3.4 Properties of matrix material, reinforced particles, and commercial material

	Density (g/cm^3)	Shear modulus (GPa)	Elastic modulus (GPa)	Bulk modulus (GPa)	CTE ($\times 10^{-6}$/°C)
LM30 aluminium alloy	2.73	34	88.5	106	24
Sillimanite	3.25	87.8	224.9	170.9	2.1
Grey cast iron	7.8	51.6	90	143	12.5

3.3 MATERIALS AND METHODS

AMCs with sillimanite as reinforcement and LM30 alloy as matrix were processed through the stir casting route. For melting of the LM30 base alloy, a resistance furnace was used. The base material, LM30 alloy (1000–1500 g) was melted in a graphite crucible of 3 kg capacity. The molten alloy was held at 750 ℃ for half an hour. The molten metal was stirred with a graphite stirrer at 630 rpm for 4–5 min. to create the vortex inside the melt. Before charging, the sillimanite sand particles were preheated to a temperature of 350 ℃ to remove moisture and other volatile matter. These preheated sillimanite particles (heated to 350 ℃) were added to the vortex with the help of a funnel kept on the top of the vortex during the stirring of molten metal. After addition of reinforcement to the matrix, molten mass was further stirred for 10–12 min. to get uniform distribution of sillimanite particles. The molten mass was poured into a cast iron mold of dimensions 12×12×4 cm^3 followed by air cooling. Composites containing different weight percentage of sillimanite (0–15 wt.%; at interval of 3 wt.%) and single particle size (SPS) of sillimanite mineral were prepared using this procedure. Sillimanite reinforced AMCs with single particle size (SPS) were classified into three classes (i) fine (containing sillimanite particles with an average particle size in range of 1–20 μm), (ii) medium (average particle size: 32–50 μm) and, (iii) coarse (average particle size: 75–106 μm). Further, AMCs reinforced with a mix of two particle sizes of sillimanite particles (referred here as dual particle size) were also processed. For dual particle size reinforced AMCs, fine (average particle size: 1–20 μm) and coarse sized sillimanite particles (average particle size: 75–106 μm) were taken in weight ratio (fine particles: coarse particles) of 1:3, 1:1, and 3:1 respectively. For dual particle size reinforced AMCs also, the sillimanite weight percentage was the same (0–15 wt.%; at interval of 3 wt.%). From these stir cast composites, specimens were prepared for characterization and wear testing. For microscopy, the samples were prepared by standard metallographic technique. Further, for wear testing, the pins (8 mm diameter) were prepared according to the ASTM G99-05 (2010) standard [166]. The roughness (Ra) value of test pins was maintained in the range of 10–15 μm and measured using Surf test SJ-400, Mitutoyo, Japan. The samples were subjected to wear testing at room temperature for different contact pressures (0.2, 0.4, 0.6, 0.8, and 1 MPa) and at elevated temperatures (100 ℃, 150 ℃, 200 ℃, 250 ℃, and 300 ℃) for different contact pressures (0.2, 0.6, and 1 MPa). The wear test specimens were further subjected to SEM-EDS analysis to determine the structure-property relationship. Figure 3.1 presents the flow chart of methodology

used for processing, characterization, and testing of sillimanite reinforced LM30 alloy based AMCs. Table 3.5 presents the processing parameters used for fabrication of composites. Table 3.6 presents the designation of various SPS and DPS composites processed in the present study.

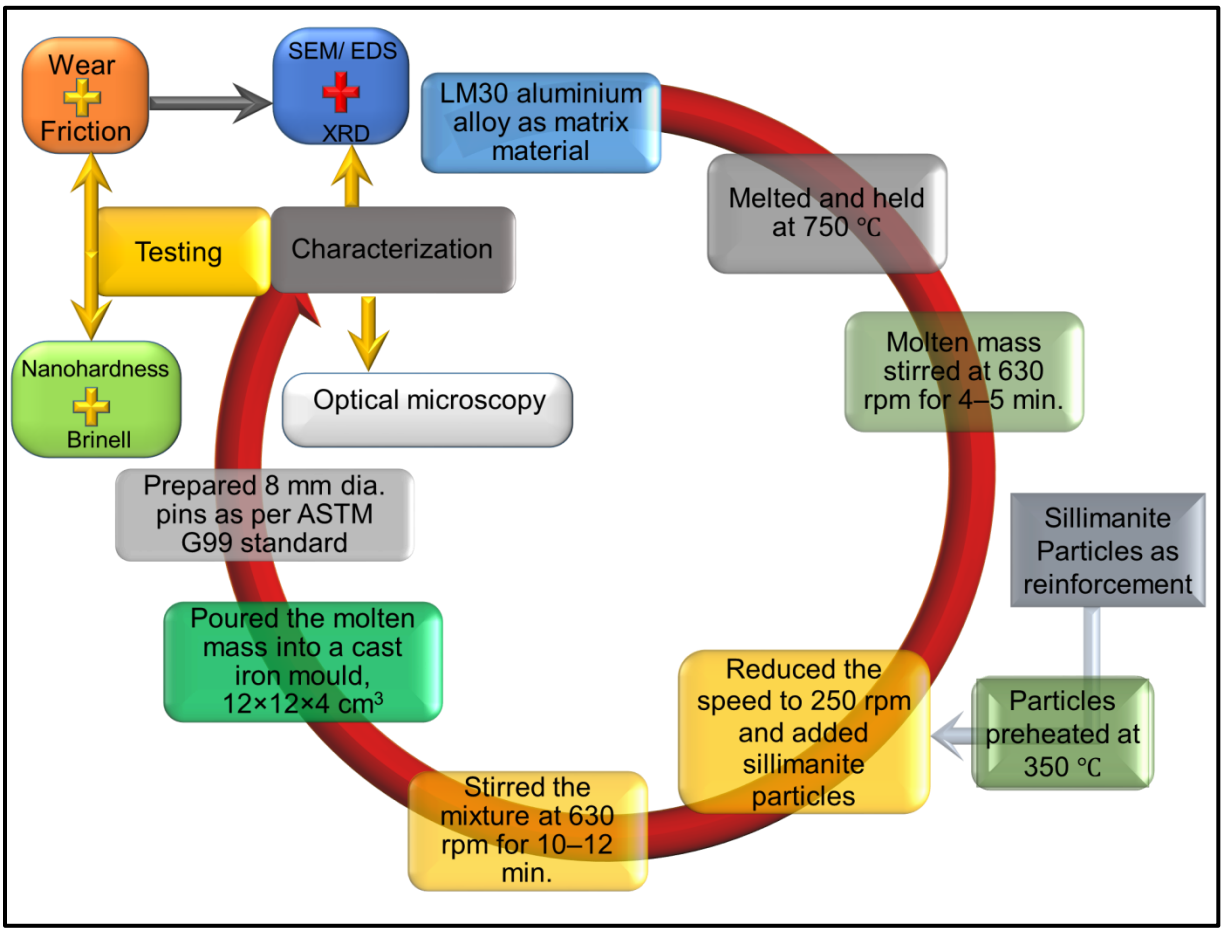

Figure 3.1 Flow chart of methodology used in the present research

Table 3.5 Details of processing parameters

Process parameter	Value/range
Melting and holding temperature	750 ℃
Number of blades on stirrer	3
Stirring time before particle addition	4–5 min
Stirring time after particle addition	10–12 min
Blade angle of the stirrer	45^{o}
Position of stirrer in the molten mass	Up to 2/3 depth in the melt

Table 3.6 Designation used for various AMCs processed in the present work

Weight percentage of sillimanite in AMCs (wt.%)	Designation of single particle size reinforced AMCs with sillimanite particle size as			Designation of dual particle size reinforced AMCs with ratio of fine (1–20 µm): coarse (75–106 µm) sillimanite particle size as		
	Coarse (75–106 µm)	*Medium (32–50 µm)*	*Fine (1–20 µm)*	*1:3*	*1:1*	*3:1*
3.0	3SPS-C	3SPS-M	3SPS-F	3DPS-1	3DPS-2	3DPS-3
6.0	6SPS-C	6SPS-M	6SPS-F	6DPS-1	6DPS-2	6DPS-3
9.0	9SPS-C	9SPS-M	9SPS-F	9DPS-1	9DPS-2	9DPS-3
12.0	12SPS-C	12SPS-M	12SPS-F	12DPS-1	12DPS-2	12DPS-3
15.0	15SPS-C	15SPS-M	15SPS-F	15DPS-1	15DPS-2	15DPS-3
18.0	18SPS-C	18SPS-M	18SPS-F	18DPS-1	18DPS-2	18DPS-3

3.4 MACHINES AND EQUIPMENT

This section provides a brief description of various machines and equipment used in the present study.

a) POWER CUTTING SAW

The as-received LM30 alloy billets (purchased from Emmes Metals Private Limited, Mumbai, India) were 900 mm in length and weighed nearly 8–9 kg. Power cutting saw (Tansi, HMT, Bengaluru, India) was used to cut the billets to appropriate size.

b) BALL MILLING

Sillimanite mineral (purchased from Indian Rare Earths Limited, Mumbai, India) having initial particle size in the range of 200–300 µm was milled using ball milling set-up (PM100, Retsch, Germany) to reduce the particle size. Ball milling reduced the particles to desired sizes (1–20 µm, 32–50 µm, and 75–106 µm). Table 3.7 presents the ball milling parameters used in the present study.

Table 3.7 Ball milling specifications

Aspect/Parameter	Value
Initial sillimanite particle size	200–300 μm
Time period of ball milling	24 hours
Ball milling speed	283 rpm
Ball diameter	12 mm
Ball:powder mass ratio	10:1

c) SIEVE SHAKER

The milled powders were sieved in different size range using a sieve shaker (AS200, Retsch, Germany). The equipment was loaded with 150–200 g of ball milled powder into the top shelf. Sieves of different sizes viz. 125 µm, 106 µm, 75 µm, 50 µm, 32 µm, and 20 µm were used. Sieving was carried out for three hours at an amplitude of 2.5 mm. For the particle size of 1–20 µm, the sillimanite powder that passed through the 20 µm sieve size was selected. For the particle size of 75–106 µm, the particles that passed through the sieve size of 106 µm and were retained by the sieve size of 75 µm were taken.

d) STIR CASTING SET-UP

Stir casting set-up was used to process the composites. The system included an electric resistance furnace and a stirrer control mechanism. The melting of LM30 aluminium alloy was carried out in the electric arc furnace capable of reaching a peak temperature of 1000 ℃. After the melting of the alloy at 750℃, the stirrer mechanism was lowered into the melt and stirring was performed. Table 3.5 presented the process parameters used for stir casting. Figure 3.2 presents the stir casting set-used in the present study.

e) GRINDING

Grinding process was carried out to flatten the surface of wear test pins. A flat pin surface is necessary for wear analysis and also to observe the microstructure of composites. Abrasive papers of different grit sizes 400, 600, 800, 1000, 1500, and 2000 were used. The samples were rubbed on abrasive papers in to-and-fro motion. This induced scratches on the samples in direction of rubbing. When all the scratches were in the direction, the sample was rubbed against the abrasive papers of finer grades in a sequential way so that the new scratches were perpendicular to the previous scratches. Similarly, the process was repeated till the grit paper of 2000. Light pressure was applied on the pin so that overheating of pin surface was avoided and no modification in the microstructure occurred.

Figure 3.2 Stir casting set-up (Courtesy: TIET, Patiala)

f) POLISHING

The samples were now polished using a polishing machine (MetaServ 3000, Buehler Binghamton, New York) to obtain a scratch free mirror finished surface. Polishing was carried out on a soft velvet cloth. Before polishing, the cloth was washed with water and placed on the rotating disc of the machine. The polishing medium (diamond paste) was then spread on the cloth and the sample was held on the rotating disc. Finally, the sample was polished with water to achieve a mirror finish.

g) PRECISION CUTTER

The diamond cutter (Sample Cutter for POD Unit, Ducom Instruments, Bangalore, India) was used to cut samples after wear analysis for SEM analysis. The specimen was mounted on steel vice. The specimen was placed in a position relative to the cutting wheel using a micrometre

screw. The material was cut by lowering the specimen over the cutter using a dead weight mechanism.

3.5 TESTING AND CHARACTERIZATION

This section describes the equipment for testing and characterization of developed composites. The procedures adopted for wear and friction test, nanohardness evaluation, DTA-TGA analysis and dilatometric analysis are described.

3.5.1 *WEAR AND FRICTION TESTING*

Dry sliding wear and friction tests were performed on the wear and friction testing set-up (Wear and Friction Monitor TR-20 CH-400, Ducom Instruments, Bangalore, India) both at room temperature as well as at elevated temperatures (50–300 ℃; at interval of 50 ℃). The tests were performed on cylindrical pins (8 mm diameter; as per ASTM G99-05 (2010) standard) sliding against an EN32 steel disc (bulk hardness: 65 HRC/700 HB and; nanohardness: 8.9±0.48 GPa) at a constant sliding velocity of 1.6 m/s. The LVDT sensor on the pin-on-disc set-up measured the height loss (μm) of the specimen. Further, the total volume loss of the specimen was calculated as the product of height loss and contact area of the pin and disc. The wear rate was then calculated as the ratio of volume loss and sliding distance. The reference material was selected to be cast iron used in brake drums of the automobiles. For the tests, the operating loads were carefully chosen to correctly simulate the different contact pressures applied on the brake drum in actual practice. Pin-on-disc set-up simulated the abrasive nature of wear applied on the brake drums. The maximum contact pressure was kept as 1 MPa; further increase in contact pressure to 1.2 MPa led to seizure of material followed by a loud noise. Further increase in contact pressure to 1.4 MPa led to complete worn out of the matrix material (LM30 alloy) at a sliding distance of 2700 m. When brake drums are used for a long duration, the temperature of brake drum increases and can reach to as high as 300 ℃. Thus, the maximum temperature for wear testing of base alloy/AMCs at elevated temperatures was selected as 300 ℃. The maximum contact pressure for wear analysis at elevated temperatures was selected as 1 MPa. For 1 MPa contact pressure and 300 ℃ operating temperature, the base alloy was completely worn out at 1850 m. Table 3.8 presents the wear testing specifications. Wear rate at any given condition (applied load-sliding distance), the value mentioned is the average of five values. Error bar corresponding to each

expressed value is also shown. Figure 3.3a–b presents the set-up for wear testing along with the control unit. Figure 3.4 a–b presents the EN32 steel disc before and after wear testing.

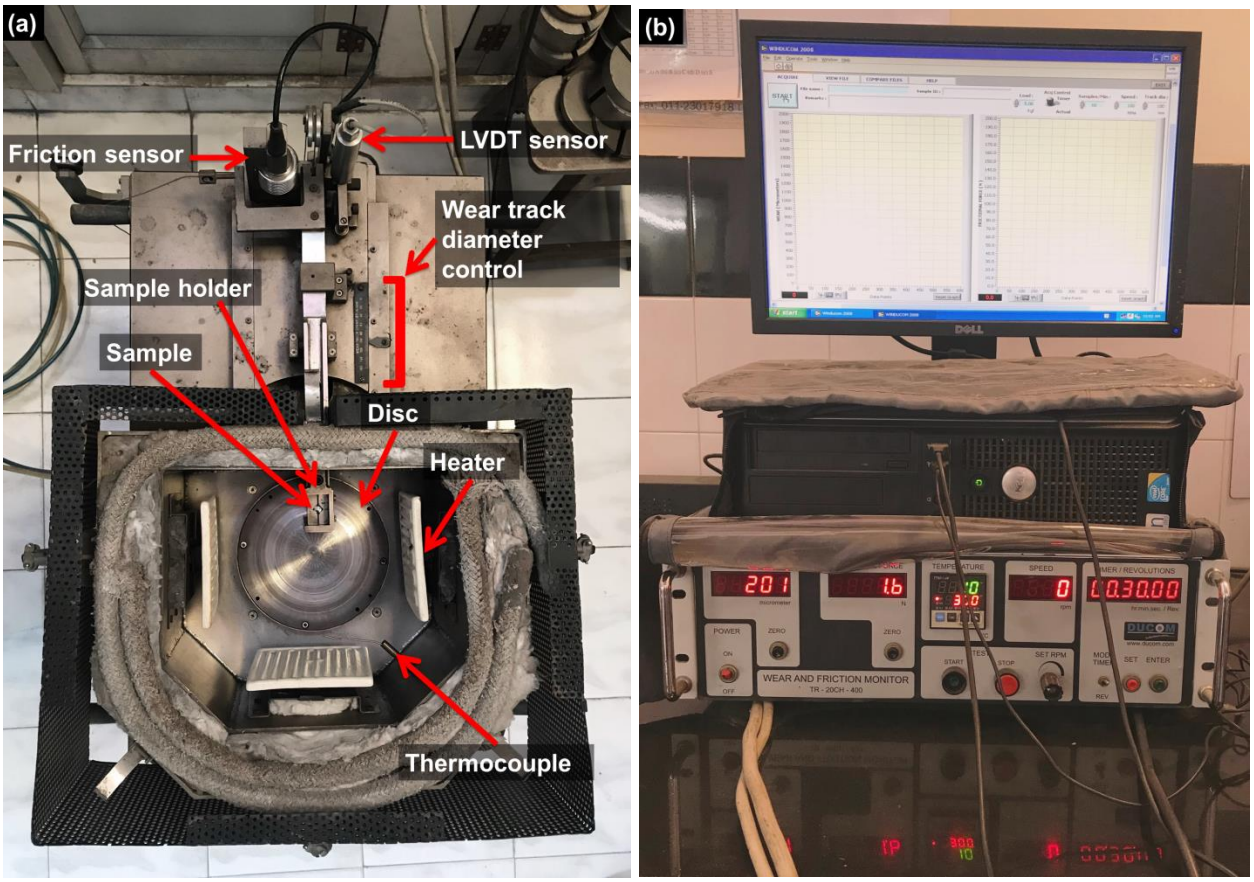

Figure 3.3 Pin-on-disc set-up (a) wear testing machine, and (b) control unit (Courtesy: TIET, Patiala)

Table 3.8 Pin-on-disc wear testing specifications

Aspect/parameter	**Value/range**
Contact pressure for room temperature	0.2, 0.4, 0.6, 0.8 and 1 MPa
Testing temperature	50–300 ℃; at interval of 50 ℃
Contact pressure for elevated temperatures	0.2, 0.6, and 1 MPa
Sliding velocity	1.6 m/s
Pin diameter	8 mm; ASTM G99-05 standard
Maximum sliding distance	3000 m
Sliding countersurface	EN32 die steel disc
Counntersurface hardness	65 HRC/700 HB
Least count of LVDT sensor	0.001 mm
Maximum measuring capacity of LVDT	2.000 mm

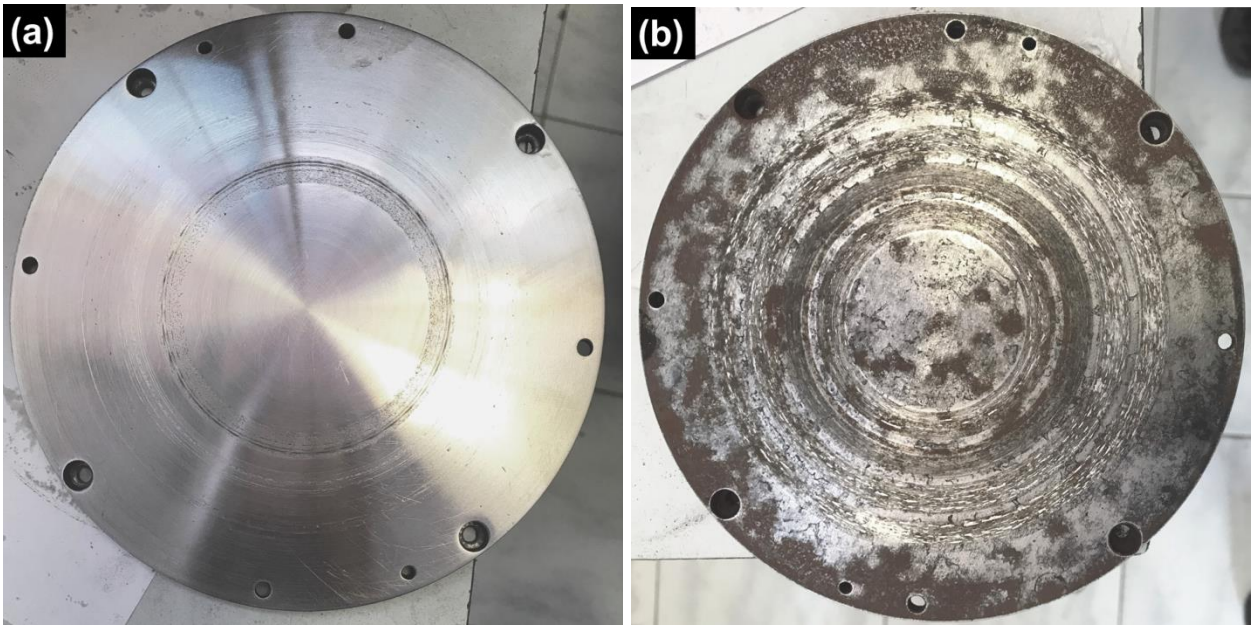

Figure 3.4 Wear disc (a) before wear, and (b) after wear

3.5.2 NANOHARDNESS TESTING

To confirm the presence of different phases in the composites, nanoindentation tests were carried out on Tribo-indenter machine (Make: TI 950 TriboIndenter, Hysitron Inc., United States). Nanoindentation tests were performed at a load of 1mN and for a dwell time of 5 s. All nanoindentation values presented in the present work are average of ten indentations per phase.

3.5.3 DTA-TGA AND DSC ANALYSIS

For high temperature applications, the reinforced particles have to be thermally stable. To determine the thermal stability of sillimanite particles, DTG-TGA set-up (STA 449 F3 Jupiter, NETZSCH, Germany) was used. DTG-TGA and DSC analysis was carried out till a temperature of 900 ℃ (since maximum casting temperature in present research was 750 ℃, a temperature higher than this maximum temperature was selected to evaluate thermal stability of particles).

3.5.4 DILATOMETERIC ANALYSIS

Coefficient of thermal expansion (CTE) determines the behavior of materials at elevated temperatures. Wear and friction testing of specimens was carried out for a temperature range of 50–300 ℃ hence, and so CTE of specimens was calculated till 400 ℃. To observe the behavior

of different composites at high temperatures, CTE was measured using dilatometer (DIL 402 PC, NETZSCH, Germany).

3.5.5 *OPTICAL MICROSCOPY*

Optical microscopy (Eclipse MA-100, Nikon Instruments, Tokyo, Japan) was used to evaluate the distribution of sillimanite particles in the matrix of various AMCs.

3.5.6 SEM-EDS ANALYSIS

SEM (JSM-6510LV, JOEL Ltd., Tokyo, Japan) was used to observe the microstructure of base alloy and various composites. After wear test, SEM was also used to analyze the wear track and wear debris to reveal the underlying wear mechanisms. EDS (Make: INCA 51-ADD 0076, Oxford Instruments, Abingdon, United Kingdom) was used to study the elemental composition of materials present in the micrographs of wear tracks and wear debris. X-ray line profile and X-ray dot mapping of micrographs was also performed to observe the distribution of different phases in various microstructures.

3.5.7 XRD ANALYSIS

XRD analysis (PANalytical X′pert PRO X-ray diffractometer with CuKα radiation of λ =1.54 Å) was used to analyze the various phases formed during the processing of composites. Also, XRD was used to analyze the various phases developed in the wear tracks and wear debris formed during wear testing.

The next chapter presents the results and discussion of various tests and characterization of base alloy/AMCs performed under room temperature conditions.

CHAPTER 4
RESULTS AND DISCUSSION
(Characterization and testing of AMCs at room temperature)

OVERVIEW

This chapter presents the details of microstructure of sillimanite reinforced AMCs developed after casting. The role of microstructure and its influence on wear and friction characteristics obtained after wear testing at room temperature have been explained. The results of nanoindentation have also been discussed. The results of wear test have also been validated by mathematical modeling. Finally, SEM-EDS analysis of wear track and wear debris has been done to predict the different wear mechanisms operative during sliding at different contact pressures.

4.1 EDS ANALYSIS OF SILLIMANITE PARTICLES

Figure 4.1 presents the EDS analysis of sillimanite particles used as reinforcement in the present work. The results of EDS analysis indicated the presence of aluminium, silicon and oxygen. By considering the atomic percentage of elements present, the composition of sillimanite mineral comes out to be $SiAl_{1.8}O_{6.1}$ which is close to Al_2SiO_5 as EDS gives tentative percentage of elements present.

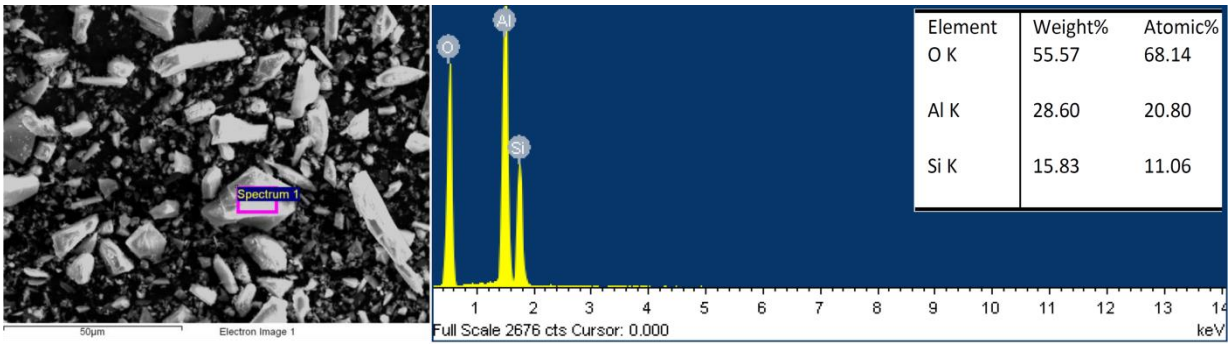

Figure 4.1 EDS analysis of sillimanite particles

4.2 XRD ANALYSIS OF BASE ALLOY AND COMPOSITES

Figure 4.2a–b presents the X-ray diffraction (XRD) patterns of LM30 base alloy and 15SPS-F composite. The peaks of aluminium, silicon, and aluminium-copper (AlCu) phases were observed in the base alloy (Figure 4.2a). AlCu formation was attributed to the presence of copper (4.1 wt.%) in the base alloy. AlCu phase is stronger than the matrix material and its presence lowers the wear rate of matrix [63]. Figure 4.2b presents the peaks of sillimanite along with aluminium, silicon, and AlCu phases in 15SPS-F composite. Apart from these phases, aluminium silicate ($Al_2Si_4O_{10}$) was also observed in the composite. Aluminium silicate formation was attributed to the interfacial reactions of sillimanite and LM30 alloy at the particle-matrix interface during melting and casting.

4.3 MICROSTRUCTURE CHARACTERIZATION

4.3.1 BASE ALLOY

LM30 aluminium alloy is a hypereutectic alloy comprising of Al-Si eutectic mixture and proeutectic (primary) silicon phase (Figure 4.3a). As the alloy solidifies, primary silicon grows

like a faceted structure followed by eutectic solidification. Primary silicon morphology present in the matrix of eutectic was largely of polyhedral shape. The morphology of primary silicon phase considerably depends on solidification parameters viz. freezing rate, temperature gradient in the liquid, and composition of the liquid [107]. The cast structure of hypereutectic Al-Si alloy consisted of coarse and segregated primary silicon phase along with needle-like eutectic silicon (Figure 4.3). Coarse primary silicon leads to large scale reduction in extrudability, machinability, strength, and ductility of the alloy. To achieve better wear resistance from a hypereutectic Al-Si alloy, fine size of primary silicon along with uniform distribution is necessary [107].

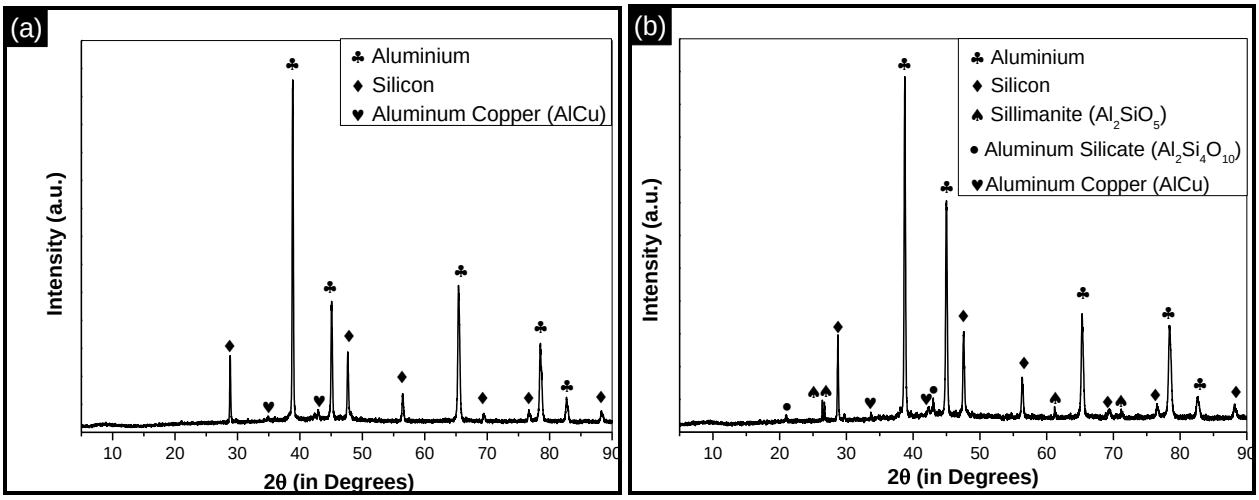

Figure 4.2 XRD patterns of (a) base alloy, and (b) 15SPS-F composite showing presence of different phases

Figure 4.3b shows the distribution of primary silicon and eutectic silicon present in the base alloy. Coarse sized primary silicon is clearly visible throughout the micrograph (Figure 4.3b). Hypereutectic Al-Si alloys have good wear resistant properties. This is because of the presence of primary silicon in these alloys. The distribution of primary silicon plays a crucial role in improving the wear properties. Silicon phase is harder than other phases typically found in aluminium alloy castings. This hard phase is more abrasion resistant, and thus, improves the wear resistance of hypereutectic Al-Si alloys [167]. However, coarse silicon phase is highly brittle, and if it gets segregated, it leads to an increase in wear rate of aluminium alloy. Fine and uniform distribution of primary silicon is necessary for improved wear resistance [107]. Reinforcement of sillimanite particles to hypereutectic Al-Si alloys helps in refining proeutectic silicon [107].

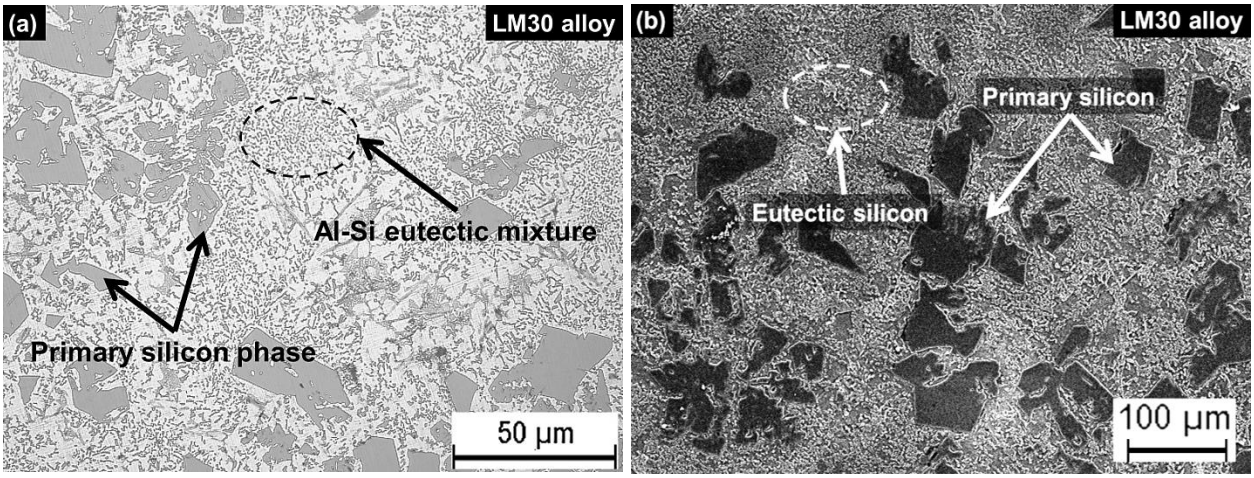

Figure 4.3 Micrograph of the base alloy (a) optical micrograph, and (b) SEM micrograph

Figure 4.4 presents the X-ray line profile of the base alloy. Phases like aluminium, silicon, and copper were observed. The concentration of copper was higher in the vicinity of primary silicon. Copper in Al-Si alloys led to formation of intermetallic elements viz. AlCu and Al_2Cu. These are hard phases and improve the hardness of composites.

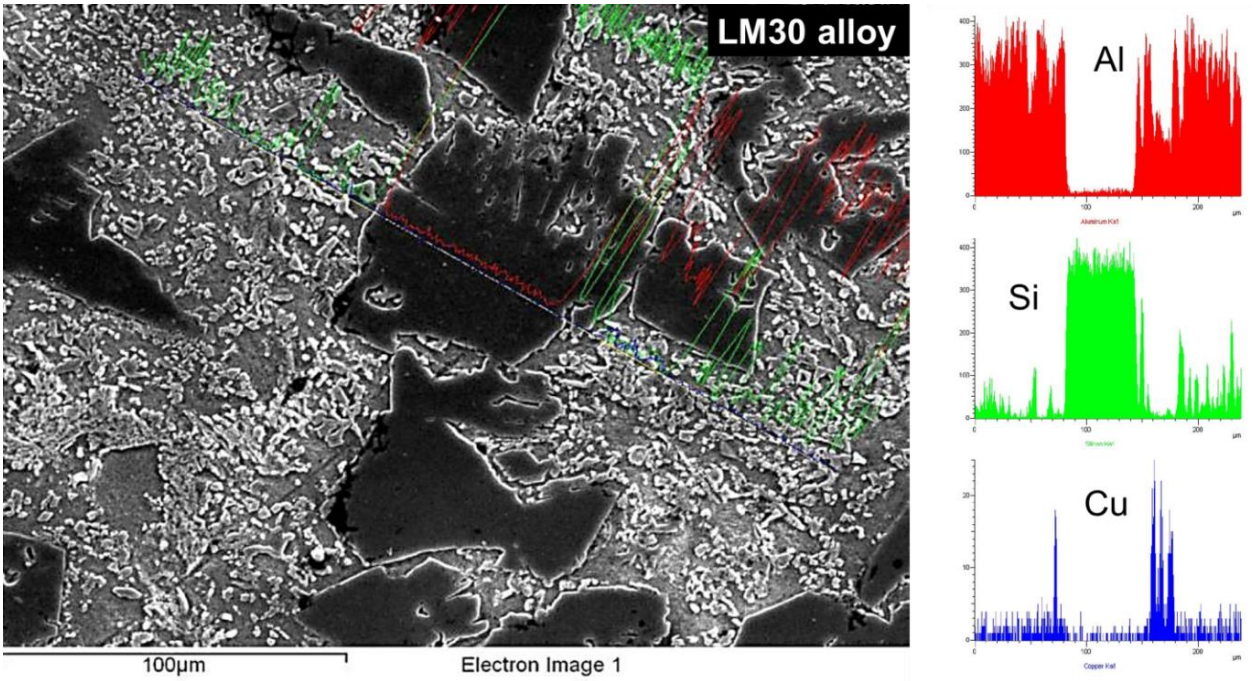

Figure 4.4 Line profile of LM30 base alloy

Figure 4.5 presents the X-ray dot mapping of LM30 base alloy. The presence of aluminium, silicon, copper, and oxygen was noted. Concentration of oxygen in the base alloy was minimal. This inclusion was due to the effect of casting. During casting, some atmospheric oxygen gets dissolved in the alloy. It was observed that silicon in the base alloy was heterogeneously distributed and was coarser in size. Copper was uniformly distributed in the matrix and its concentration was higher in the vicinity of primary silicon.

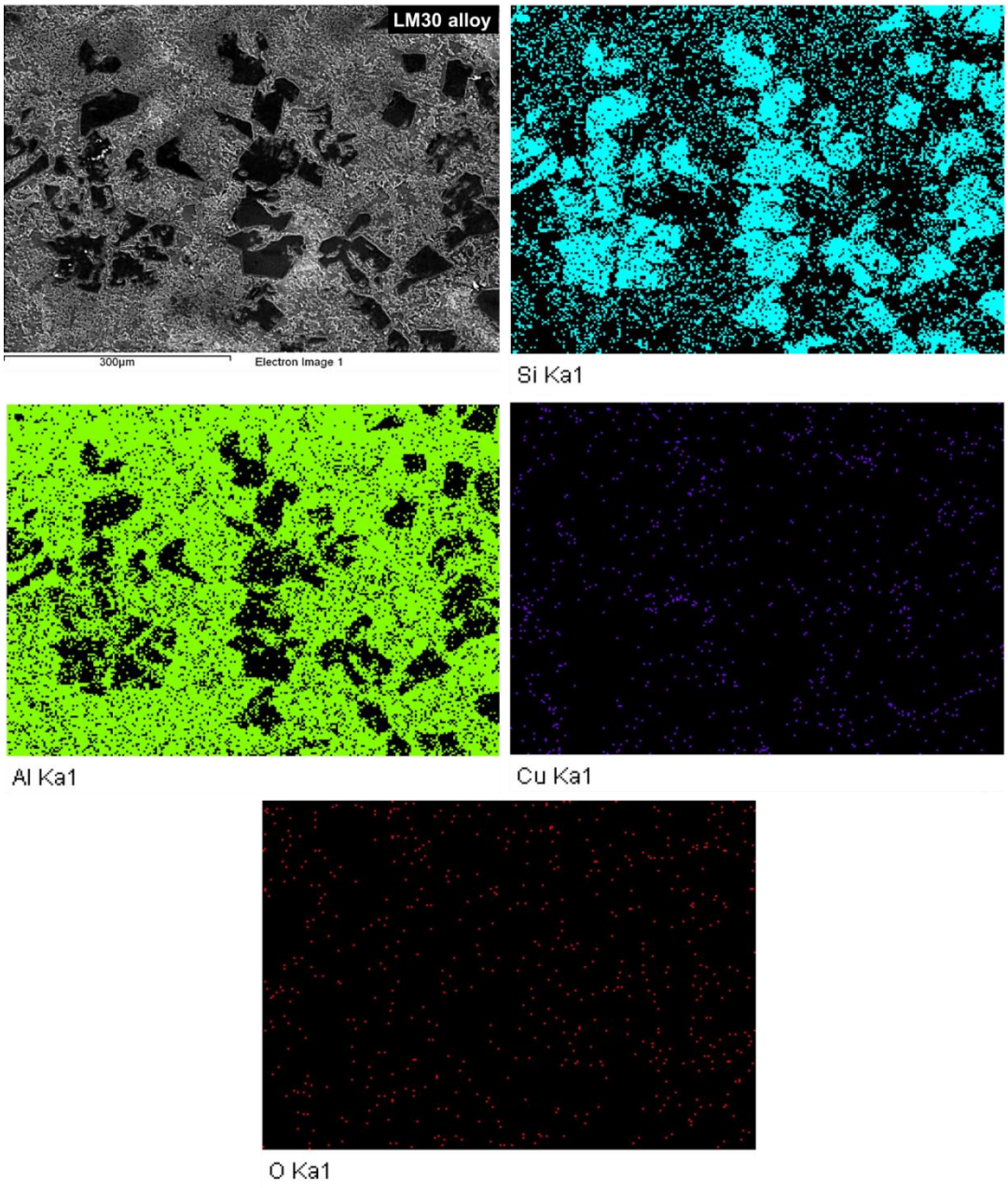

Figure 4.5 X-ray dot mapping of LM30 base alloy

4.3.2 OPTICAL MICROGRAPHS OF VARIOUS COMPOSITES

Figure 4.6a–f presents the optical micrographs of 3SPS-C, 3SPS-M, 3SPS-F, 3DPS-1, 3DPS-2, and 3DPS-3 composites reinforced with 3 wt,% of sillimanite particles in LM30 alloy matrix. Refinement in silicon morphology was observed throughout the microstructure. During solidification, the particles are engulfed in the moving solid interface. For the various composites, no segregation of particles was observed for 3SPS-C, 3SPS-M, 3SPS-F, and 3DPS-1 AMCs.

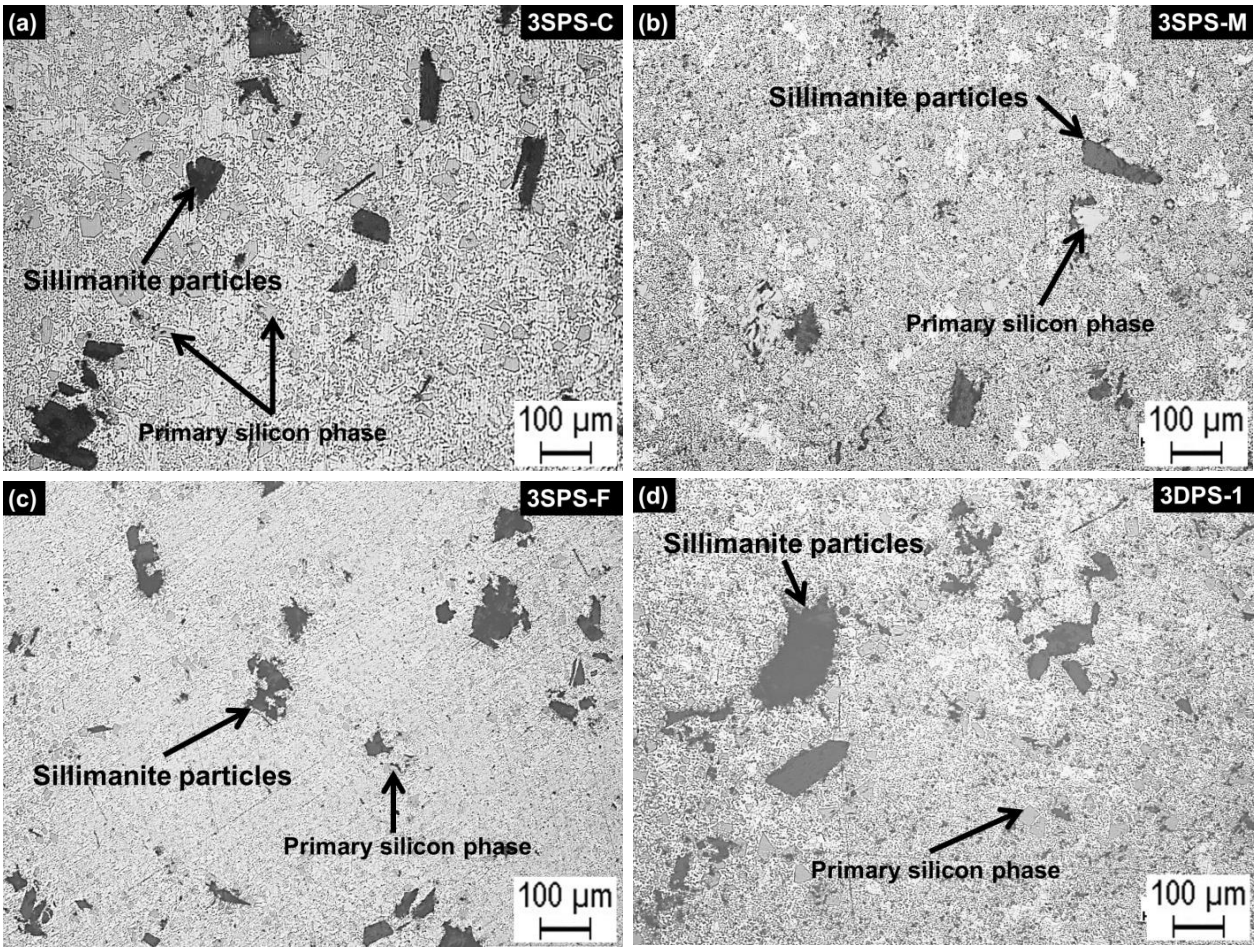

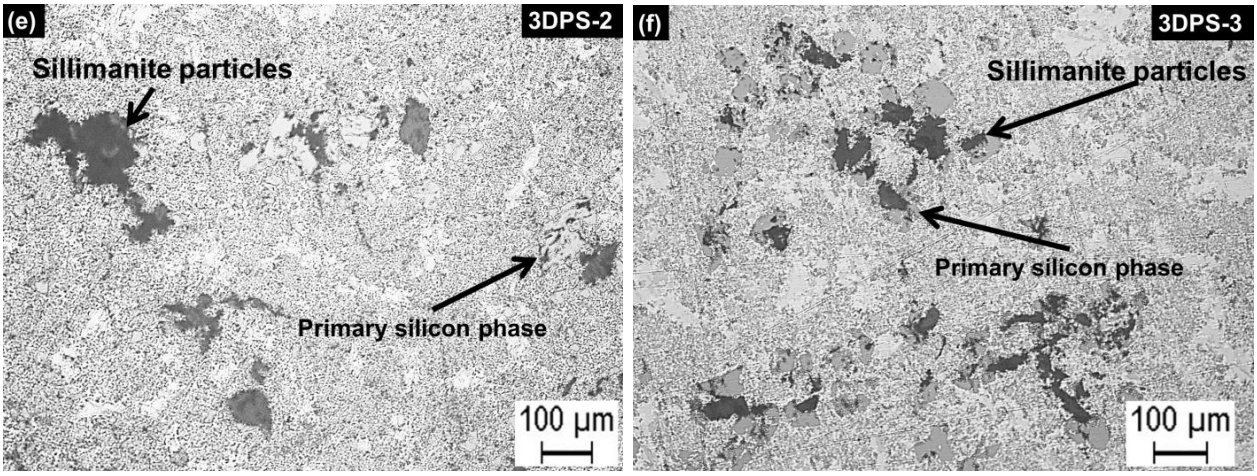

Figure 4.6 Optical micrographs of AMCs (a) 3SPS-C, (b) 3SPS-M, (c) 3SPS-F, (d) 3DPS-1, (e) 3DPS-2, and (f) 3DPS-3

However, segregation was observed for 3DPS-2 and 3DPS-3 AMCs (Figure 4.6e and 4.6f). Segregation leads to loose bonding of particles and reduces the wear characteristics of composites. In general, sillimanite particles were uniformly distributed throughout the matrix. Ceramic particles have a lower thermal conductivity and heat diffusivity than the molten Al alloy. Thus, particles have a slower cooling rate and hence remain at somewhat higher temperature as compared to the molten matrix material. The hotter particles may heat up the liquid in their immediate surroundings leading to a delay in the solidification of molten matrix around it. Thus, addition of particles to the matrix slows down the solidification front and act as nucleation sites for silicon phase [16,168]. The increase in nucleation sites leads to grain refinement. Hence, refinement in, both primary and eutectic silicon was observed.

Figure 4.7a–f presents the optical micrographs of 6SPS-C, 6SPS-M, 6SPS-F, 6DPS-1, 6DPS-2, and 6DPS-3 composites reinforced with 6 wt.% of sillimanite sand particles in the base alloy matrix. Increase in reinforcement (3 to 6 wt.%) increased the refinement of both primary and eutectic silicon. Figure 4.7g–f presents the high magnification micrographs of 6SPS-M and 6DPS-2 composites. These high magnification images clearly show an effective interfacial bonding between the particles and matrix. Interfacial bonding between particles and matrix is a result of physical, chemical, and/or mechanical interactions between the particles and matrix. Thermal stresses generated at the particle-matrix interface further help in strong interfacial bonding. Sound particle–matrix interfacial bonding improves the load transfer capability and delays the onset of particle–matrix de-cohesion [67].

The morphology of primary silicon changed from acicular in the base alloy to globular in the AMCs. Also, the size of primary silicon facets got refined. The presence of particles in the matrix hinders the growth of dendrites, and thus, refines the matrix structure. The dendrites of aluminium grow in a columnar manner if no hindrance is provided [16]. When particles are added to the matrix, the dendrite front grows by pushing the particles forward. However, particle pushing is not a dominant growth mechanism. Thus, particles are assumed as a barrier to the dendritic growth. When a dendrite approaches a particle, it splits/breaks (owing to the role of particle as physical barrier to solute diffusion and mechanical force). Splitting/breaking of dendrites leads to the refinement of grains [16]. In addition to this, the addition of particles lead to heterogeneous nucleation which restricts the spaces between the reinforcements and leads to grain refinement of the matrix [169]. Increase in number of particles increases the possibility of increase in heterogeneous nucleation sites for the matrix resulting in more refined microstructure [170]. The refinement in primary and eutectic silicon leads to improvement of strength and tribological properties [95]. Silicon concentration (both, primary and eutectic silicon) was higher in the proximity of reinforced particles. Moreover, some silicon depleted zones were also observed near the sillimanite particles. This was attributed to the fact that the sillimanite particles have lower thermal conductivity as compared to the matrix material. Thus, the particles remain at a higher temperature as compared to the matrix. The hotter particles heat the molten matrix in their proximity. This causes delay in the solidification in the vicinity of the particles. The temperature of molten metal away from the particles is relatively lower. This leads to the solidification of aluminium matrix away from the particles (where temperature is lower). The growth of aluminium matrix away from the particle leads to enrichment of silicon and other solutes in the proximity of the particles [16]. Thus, higher content of silicon was observed to nucleate in the proximity of the sillimanite particles.

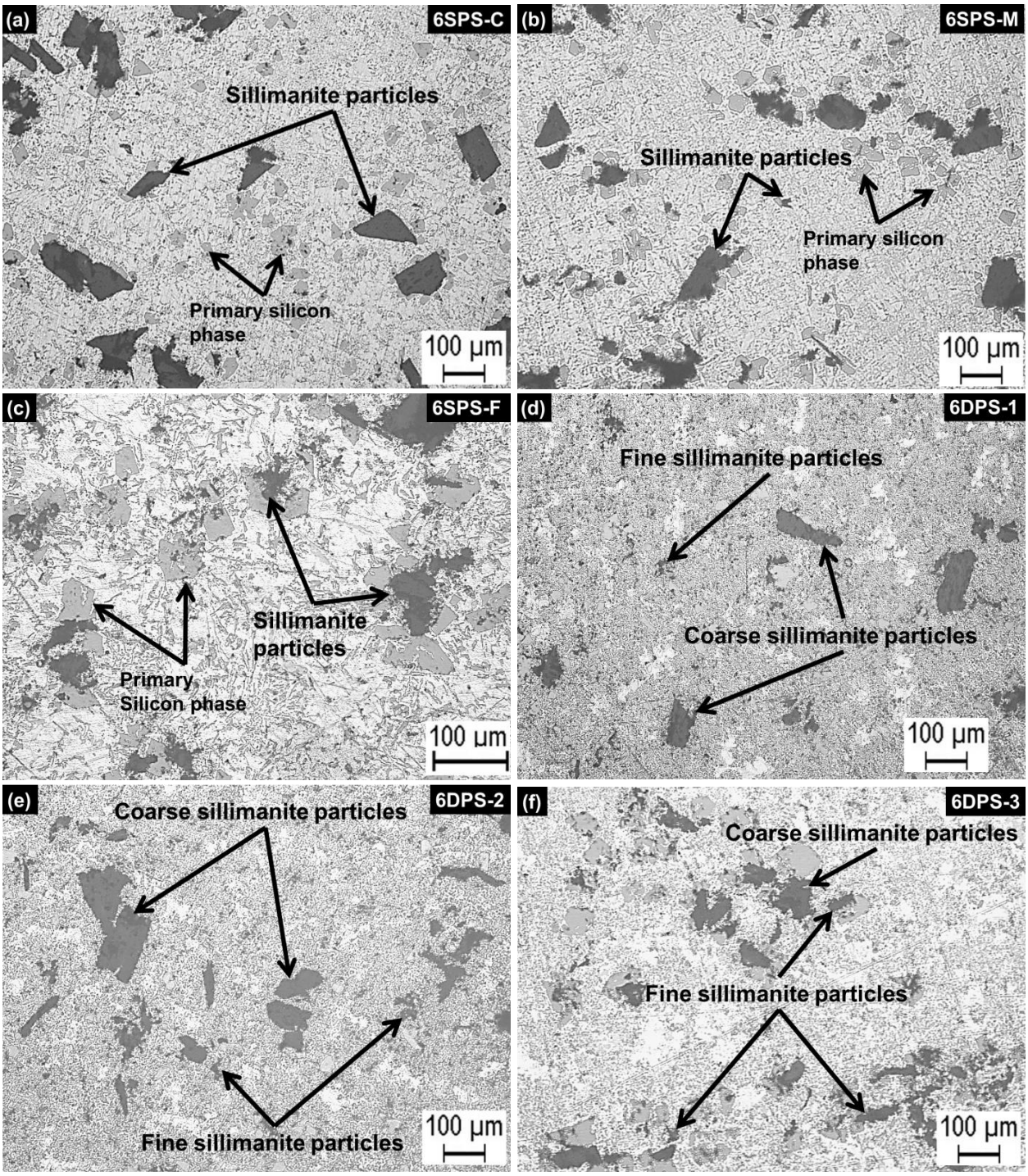
(a)
6SPS-C
Sillimanite particles
Primary silicon phase
100 µm
(b)
6SPS-M
Sillimanite particles
Primary silicon phase
100 µm
(c)
6SPS-F
Sillimanite particles
Primary Silicon phase
100 µm
(d)
6DPS-1
Fine sillimanite particles
Coarse sillimanite particles
100 µm
(e)
6DPS-2
Coarse sillimanite particles
Fine sillimanite particles
100 µm
(f)
6DPS-3
Coarse sillimanite particles
Fine sillimanite particles
100 µm

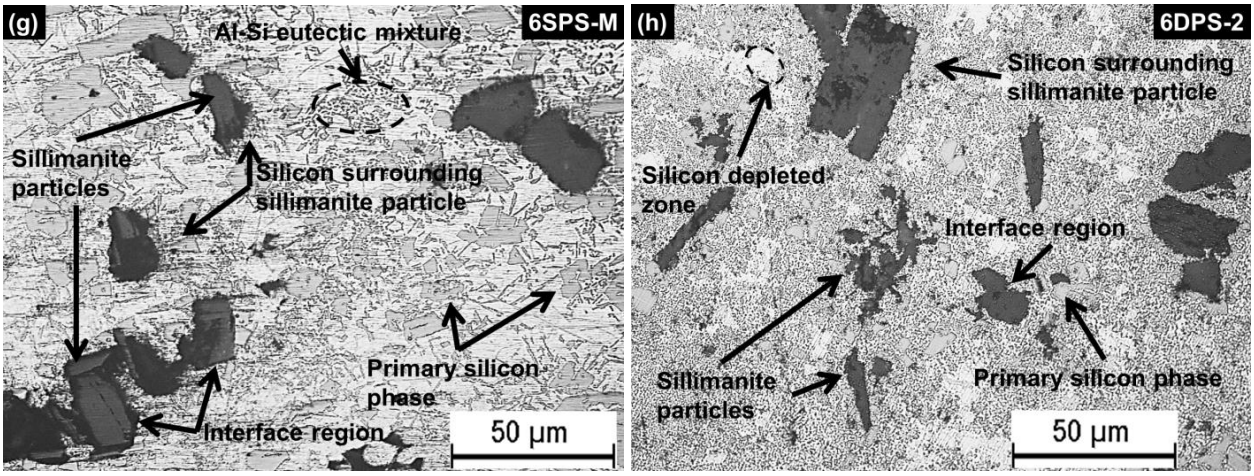

Figure 4.7 Optical micrographs of AMCs (a) 6SPS-C, (b) 6SPS-M, (c) 6SPS-F, (d) 6DPS-1, (e) 6DPS-2, (f) 6DPS-3, (g) 6SPS-M at high magnification, and (h) 6DPS-2 at high magnification

Figure 4.8a–f presents the optical micrographs of 9SPS-C, 9SPS-M, 9SPS-F, 9DPS-1, 9DPS-2, and 9DPS-3 composites reinforced with 9 wt.% of sillimanite sand particles in LM30 alloy matrix. Uniform distribution of sillimanite particles was observed throughout the matrix. However, some particle agglomerations were observed for 9SPS-F, 9DPS-1, 9DPS-2, and 9DPS-3 composites (Figure 4.8c–f). The increase in weight percentage of sillimanite reinforcement increased the refinement of matrix and also increased agglomeration of particles in the matrix. The advancing solidification front pushes the fine particles at faster rate and leads to their agglomeration [160]. The agglomeration of particles increased with increase in concentration of fine particles in dual particle-sized reinforced composites. The primary and eutectic silicon morphology also got refined. The refinement was attributed to particle addition as the temperature difference between the reinforced particles and the melt leads to dendritic fragmentation of the matrix due to stirring action of the stirrer. Further, the presence of ceramic particulates in the melt slows down the velocity of solidification front, causing delay in solidification. As the solidification time increases, more nuclei form leading to grain refinement [171].

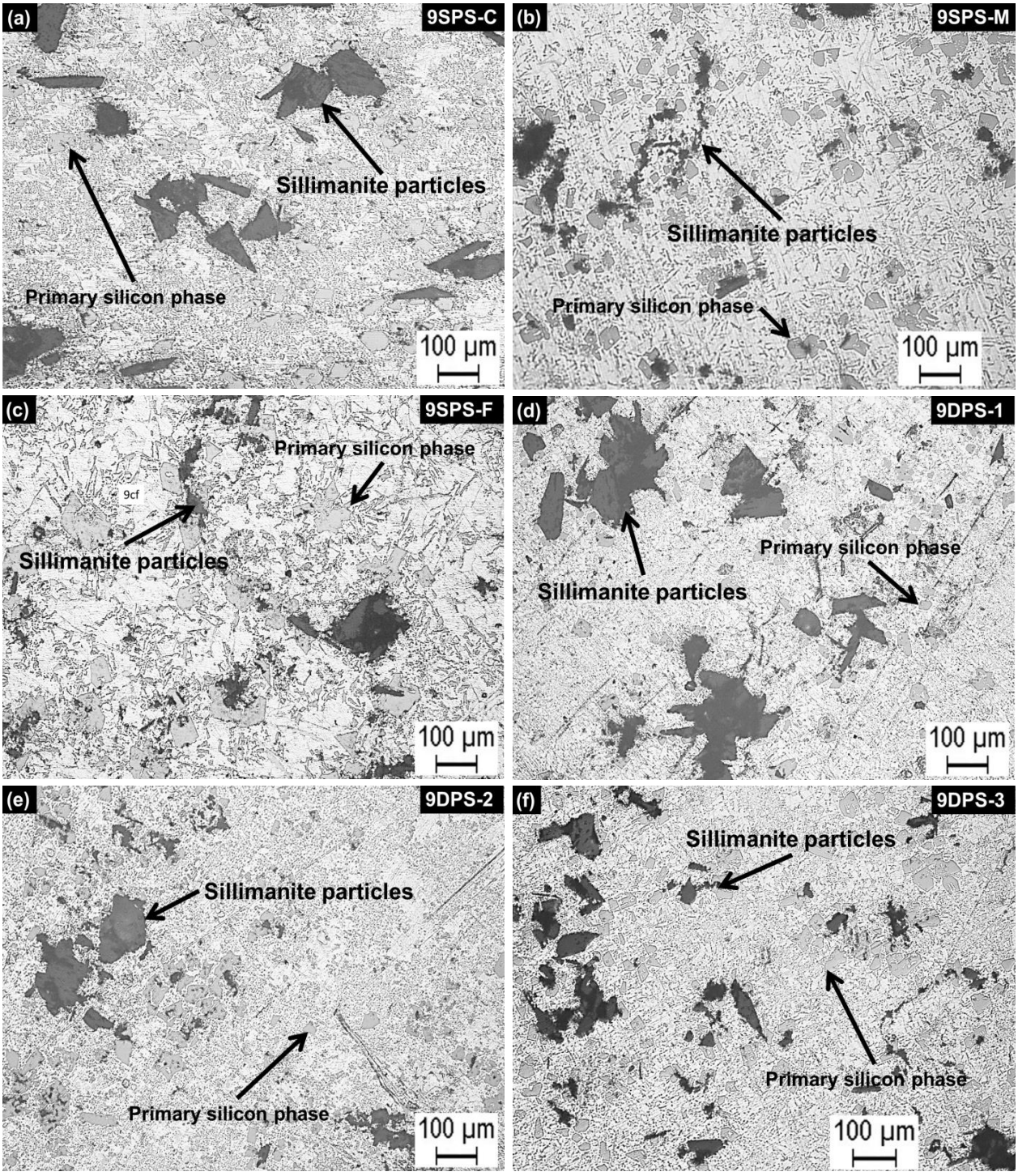

Figure 4.8 Optical micrographs of AMCs (a) 9SPS-C, (b) 9SPS-M, (c) 9SPS-F, (d) 9DPS-1, (e) 9DPS-2, and (f) 9DPS-3

It is reported that reinforced particles lead to modification of the dendritic structure which can be influenced by a variety of factors viz. dendrite fragmentation, dendritic growth restriction by the

particles, and thermal conductivity mismatch between the melt and the particles. Ceramic particles act as a barrier for dendritic growth. This phenomena is more pronounced when the cooling rate is high [160]. Higher cooling rate leads to formation of fine dendritic structure and gives rise to fine interparticle spacing. The interparticle spacing plays a crucial role in improving the mechanical and tribological properties of cast composites [65].

Figure 4.9a–f presents the optical micrographs of 12SPS-C, 12SPS-M, 12SPS-F, 12DPS-1, 12DPS-2, and 12DPS-3 composites reinforced with 12 wt.% of sillimanite sand particles in LM30 alloy matrix. The particles are uniformly distributed throughout the matrix. Clustering of particles increased with increase in reinforcement level. Further, the higher concentration of reinforced particles led to higher refinement in the microstructure. The primary silicon facets were smaller in size and were uniformly distributed throughout the matrix.

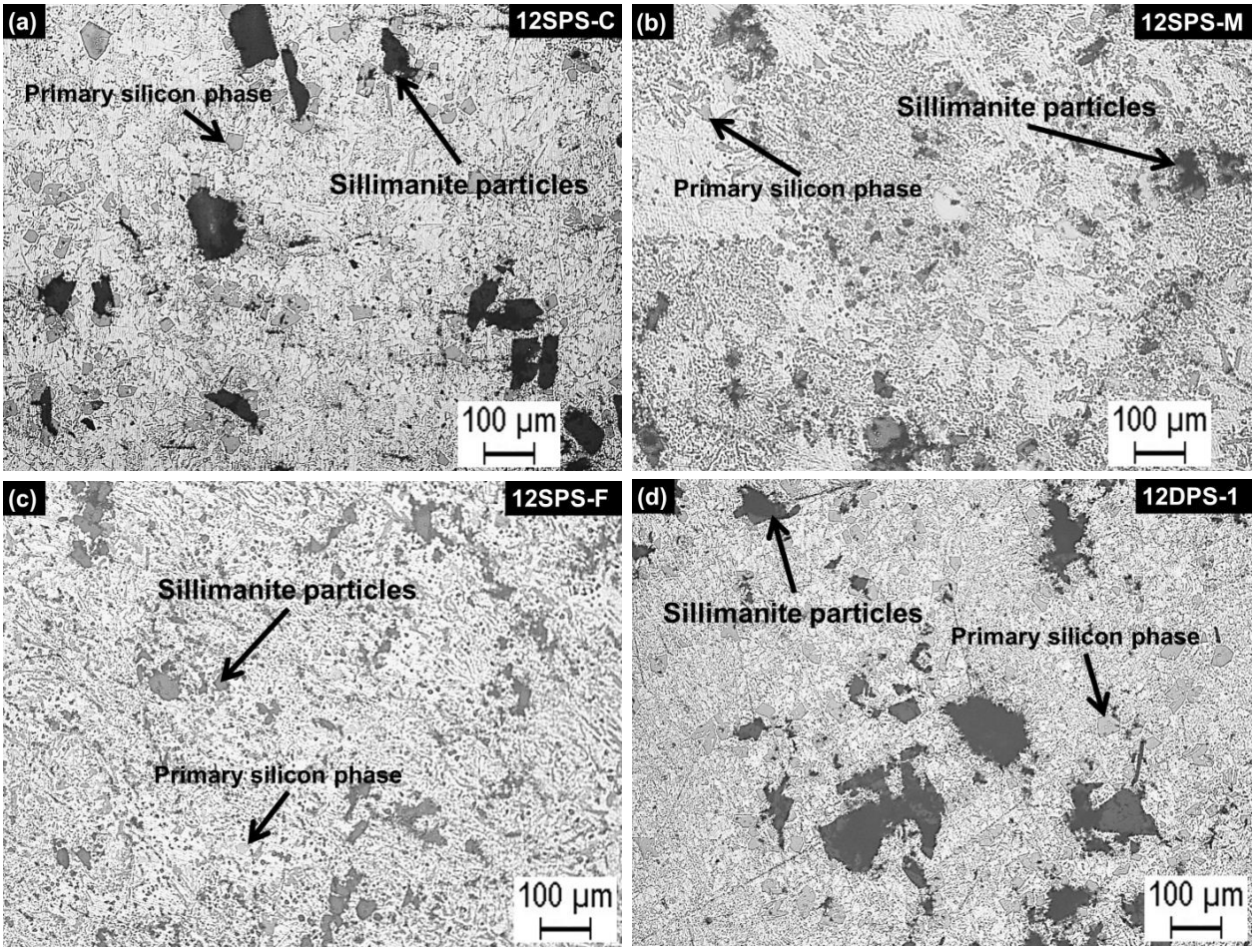

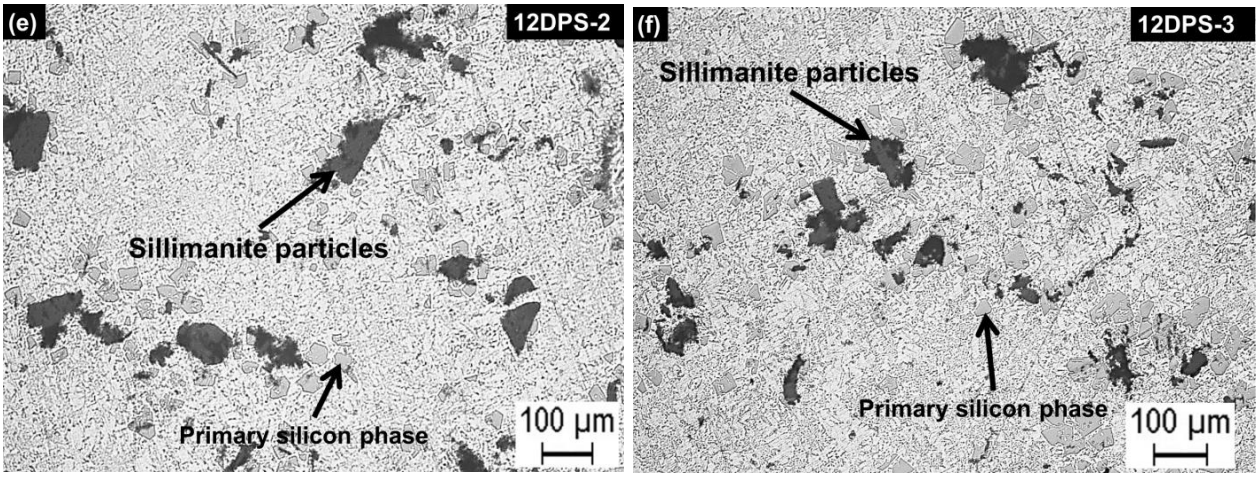

Figure 4.9 Optical micrographs of AMCs (a) 12SPS-C, (b) 12SPS-M, (c) 12SPS-F, (d) 12DPS-1, (e) 12DPS-2, and (f) 12DPS-3

Figure 4.10a–f presents the optical micrographs of 15SPS-C, 15SPS-M, 15SPS-F, 15DPS-1, 15DPS-2, and 15DPS-3 composites reinforced with 15 wt.% of sillimanite sand particles in LM30 alloy matrix. Figure 4.10g–f presents the high magnification micrographs of 15SPS-C and 15DPS-2 composites. For all the processed composites, particle distribution was nearly uniform throughout the matrix (Figure 4.10a–f). Such distribution of particles is essential to achieve better wear resistance of composites. The high shearing action of stirrer decreased the tendency of particles to settle down and provided a fairly uniform particle distribution inside the matrix [92].

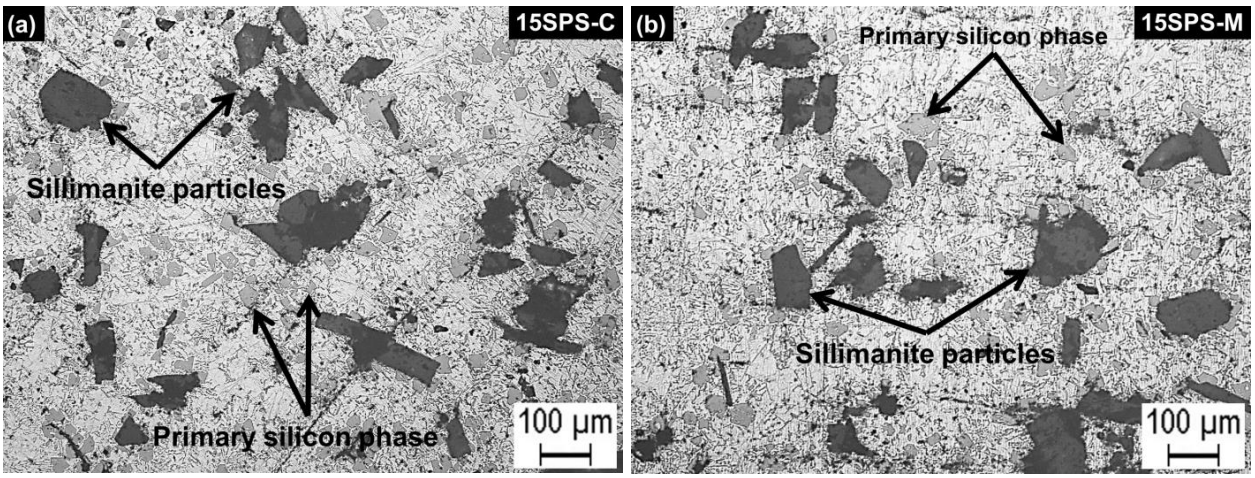

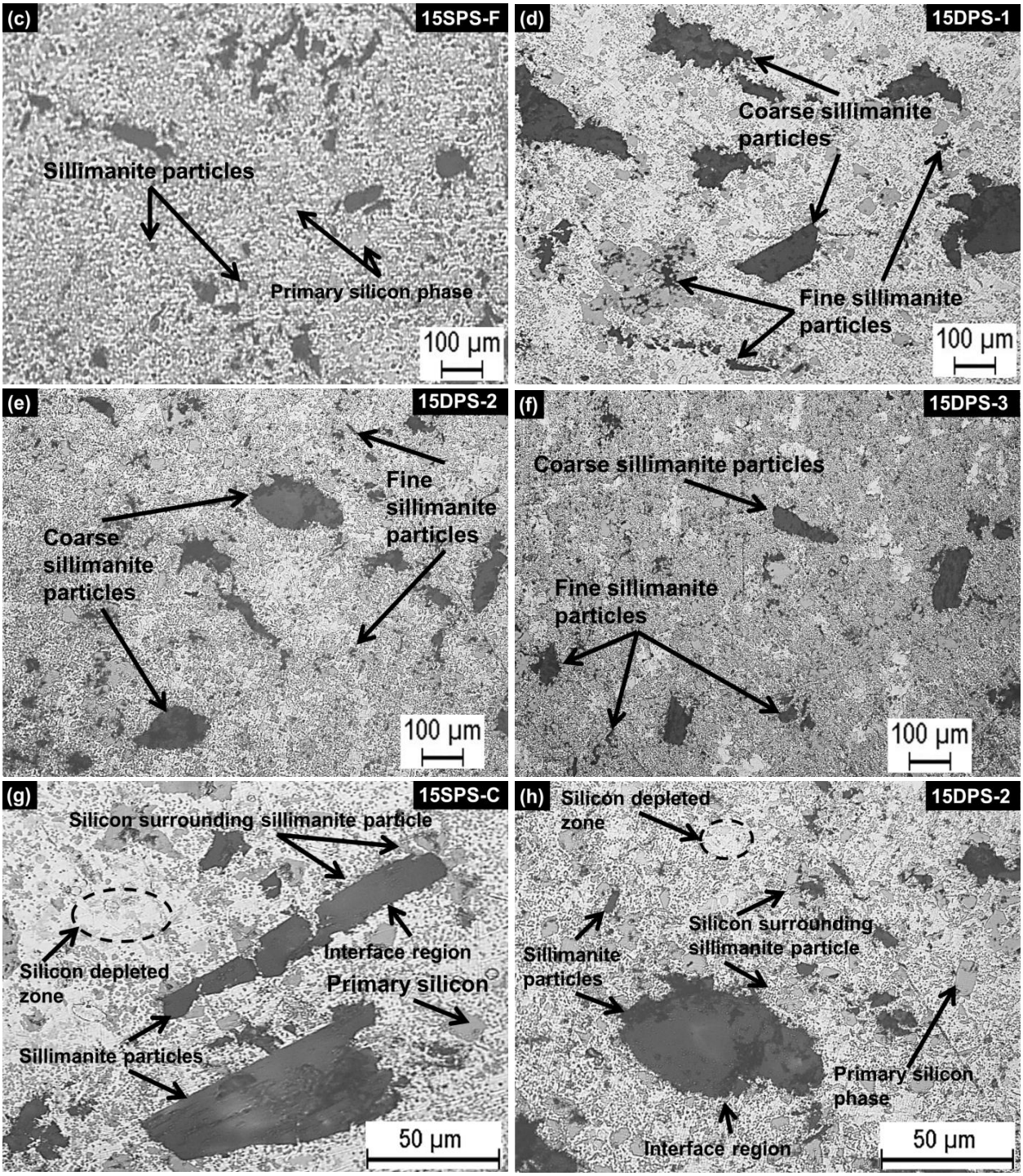

Figure 4.10 Optical micrographs of AMCs (a) 15SPS-C, (b) 15SPS-M, (c) 15SPS-F, (d) 15DPS-1, (e) 15DPS-2, (f) 15DPS-3, (g) 15SPS-C at high magnification, and (h) 15DPS-2 at high magnification

The microstructure of composites shown in Figure 4.10 reveals that the size of primary silicon phase was dramatically reduced in composites. Moreover, the morphology of eutectic silicon

also changed. The needle/acicular type of silicon morphology (of the base alloy) acquired a globular morphology in the vicinity of sillimanite particles in the AMCs (Figure 4.10f–g). Further, the primary silicon present in the vicinity of particles also got refined. The average size of primary silicon in the as-received Al-Si alloy was nearly 18.3 µm (Figure 4.3a) which got refined to 13.5 µm (Figure 4.7b) for 6SPS-M and 6.5 µm (Figure 4.10b) for 15SPS-M. This was because particles act as a heat sink and lead to rapid solidification of the melt. As stated earlier, higher reinforcement levels lead to formation of higher number of nuclei in the melt, and thus, result in refinement of primary silicon. Microstructure of various AMCs indicated that sillimanite particles have a significant influence on solidification behaviour of hypereutectic Al-Si matrix alloy. In contrast to the nucleation of primary silicon phase in hypereutectic Al-Si matrix, in AMCs, the primary Si phase nucleated in the vicinity of sillimanite particles (Figure 4.10a–f). Some agglomerates of primary Si phase in the vicinity of sillimanite particles was also observed. Further, some silicon depleted zones were observed in AMCs (Figure 4.10g–h). In the base alloy, silicon phase was uniformly present throughout the microstructure. However, in AMCs, silicon phase was concentrated near the reinforced sillimanite particles, thus creating silicon depleted zones. Considering the solidification kinetics, the melting temperature of silicon is much higher than aluminium. Temperature gradient exists between silicon phase and aluminium phase. Thus, for silicon phase, heterogeneous nucleation is followed. During the solidification of AMCs, the reinforcing particles are at a higher temperature than the surrounding melt. This increases the possibility of solidification of silicon in the vicinity of the particles [172]. Further, sillimanite particles have low thermal expansion and high thermal stability. Thus, when the solidification starts, sillimanite particles provide the necessary interface for nucleation for the solidification of silicon. Silicon in the neighbourhood of particles solidifies at faster rate than that away from the matrix. Silicon precipitates at a faster rate than aluminium, therefore, a higher concentration of silicon in the neighbourhood of the particles can be observed [172].

Figure 4.11a–b presents typical micrographs of 18SPS-F and 18DPS-3 AMCs. It was observed that the clustering tendency of particles increases with an increased amount of sillimanite particles (Figure 4.10 and Figure 4.11). However, the clustering tendency in 18 wt% reinforced composites was higher than 15 wt.% reinforced composites. Clustering of particles is an important phenomenon which affects the wear properties of composites. Clustering tendency of particles increases with decrease in the particle size and increase in the reinforcement level. The

smaller particles with the same amount of reinforcement in the matrix show a higher clustering tendency in comparison to coarser particles.

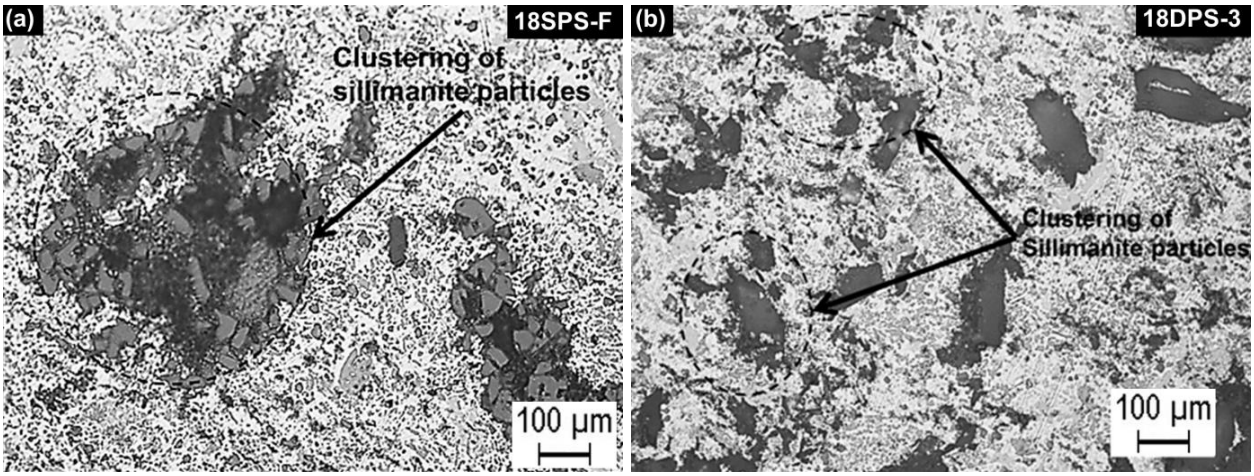

Figure 4.11 Optical micrograph of AMCs (a) 18SPS-F and (b) 18DPS-3

4.3.3 SEM MICROGRAPHS OF VARIOUS COMPOSITES

Figure 4.12a–f presents typical SEM micrographs of 15SPS-C, 15SPS-M, 15SPS-F, 15DPS-1, 15DPS-2, and 15DPS-3 composites. Uniform distribution of reinforced particles was observed. Further, addition of particles led to refinement of primary and eutectic silicon. The morphology of eutectic silicon changed from acicular (for base alloy) to globular (for AMCs). The refinement of primary and secondary silicon was very significant for 15SPS-F and 15DPS-3 composites. Maximum refinement in microstructure was observed for 15DPS-3 composites. Refinement of silicon increased with increase in proportion of fine particles in the matrix. As stated earlier, finer particles have higher surface area, and provide higher number of nucleation sites, thereby increasing the refinement of primary and secondary silicon. However, when only fine particles were added in the matrix, the refinement of primary and secondary silicon was lower than 15-DPS3 AMCs. This was attributed to clustering tendency of particles when only fine particles were present in the matrix. Thus, to achieve a higher concentration of reinforced particles in the matrix without any clustering, dual size particles (a mix of coarse and fine) were added to the matrix. Thus, 15-DPS-3 AMC provided maximum particle addition to the matrix without any clustering. This composite provided best refinement of silicon morphology.

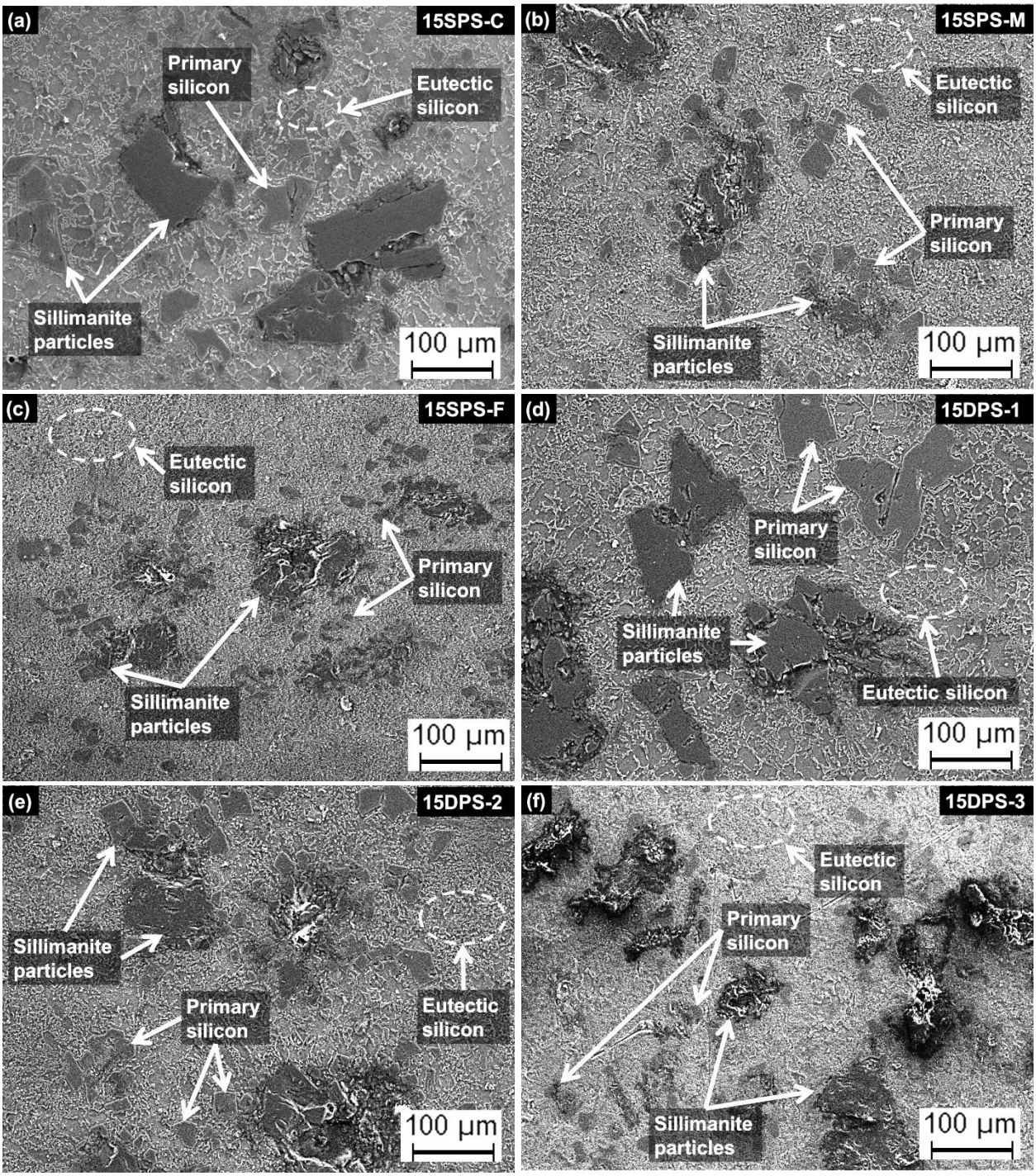

Figure 4.12 SEM micrographs of (a) 15SPS-C, (b) 15SPS-M, (c) 15SPS-F, (d) 15DPS-1, (e) 15DPS-2, and (f) 15DPS-3 composites

Figure 4.13 presents the results of line profile of 15SPS-C, 15SPS-M, 15SPS-F, 15DPS-1, 15DPS-2, and 15DPS-3 composites.. The distribution of silicon in the proximity of particles is observed (Figure 4.13). The higher concentration of silicon in the vicinity of the particles was

confirmed through X-ray line profile of the composites. Over the given line, other elements viz. aluminium and oxygen were also observed. The particles constituted of aluminium-silicon and oxygen. Since all the three elements were observed on the line, it indicated the presence of sillimanite particles (Figure 4.13). Further, the peaks of silicon in the vicinity of particle were high indicating a higher concentration of silicon at the particle-matrix interface. This was due to the thermal mismatch of particles and molten matrix. Sillimanite particles have low thermal expansion and high thermal stability. Thus, at the particle-matrix interface, thermal instability occurs. The sillimanite particles behave as a heat sink for the matrix. The matrix in the neighbourhood of the particles solidifies faster than that away from the matrix. Silicon solidifies faster than aluminium and therefore, a higher concentration of silicon in the neighbourhood of the particles was observed.

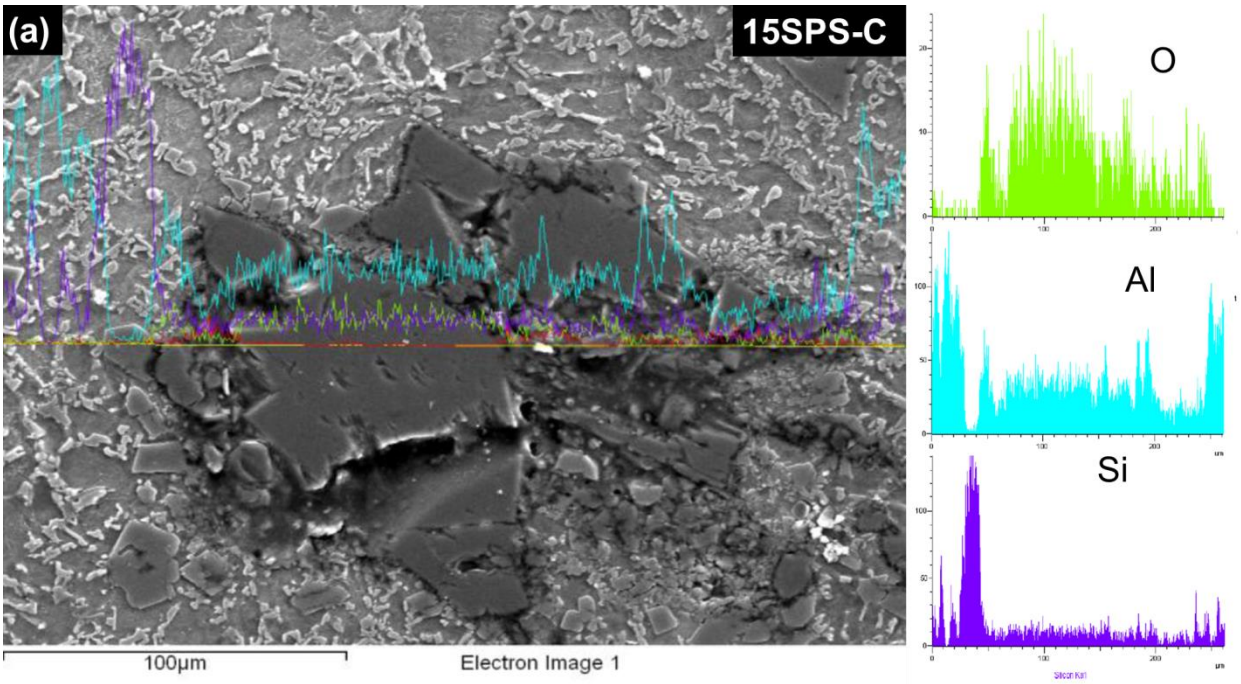

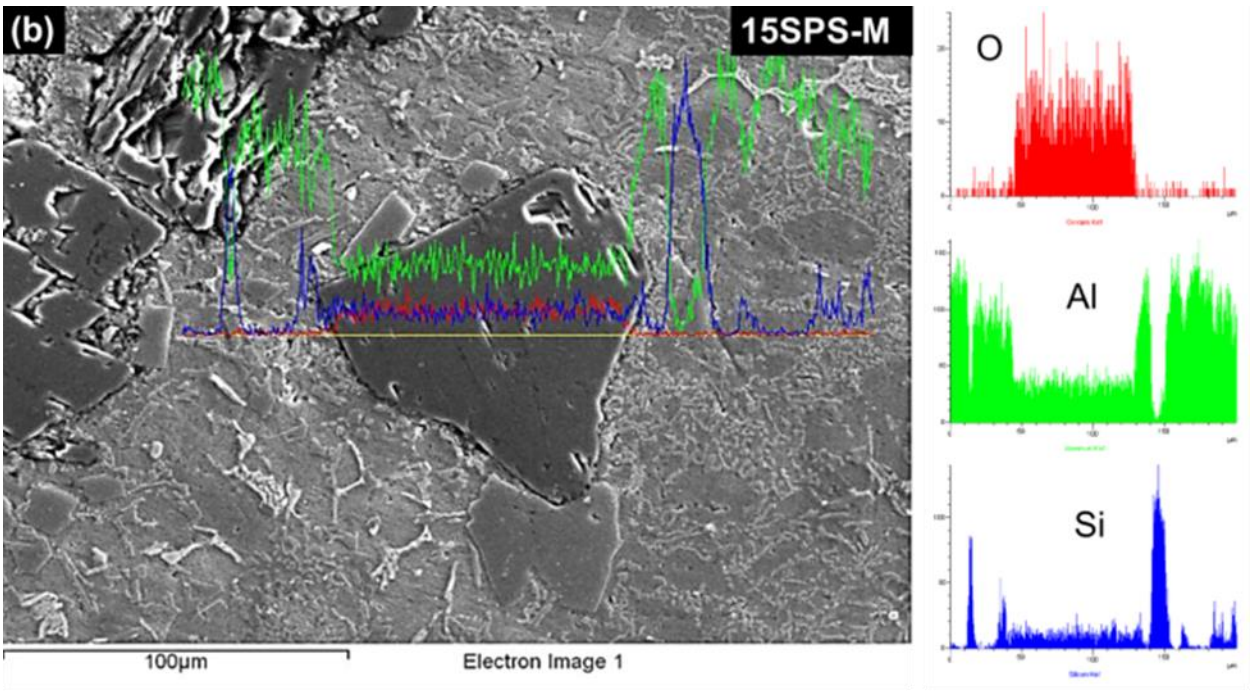
(b)
15SPS-M
100µm
Electron Image 1
O
Al
Si

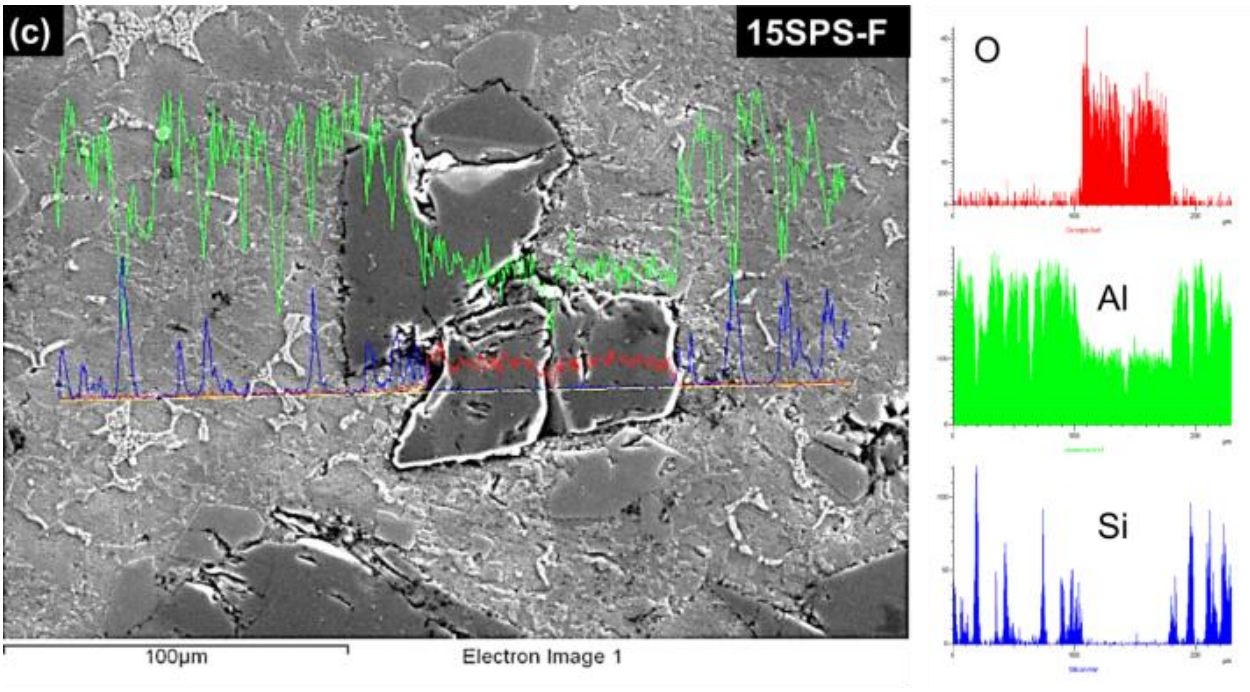
(c)
15SPS-F
100µm
Electron Image 1
O
Al
Si

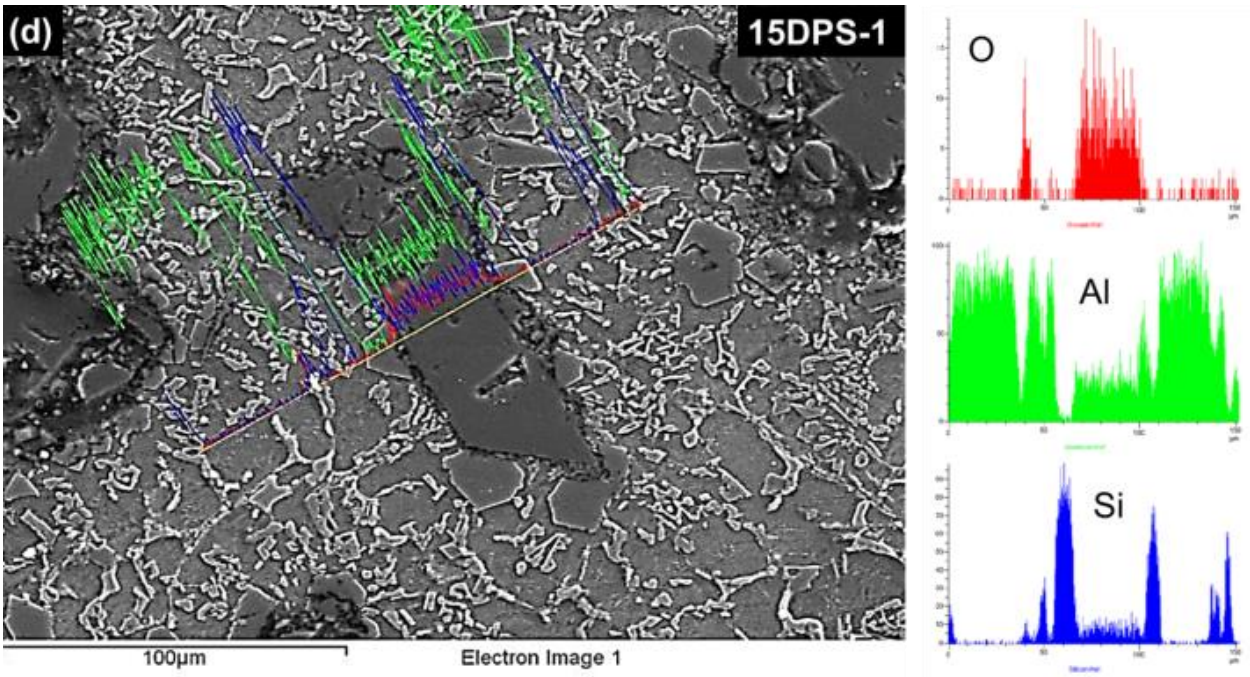
(d)
15DPS-1
100µm
Electron Image 1
O
Al
Si

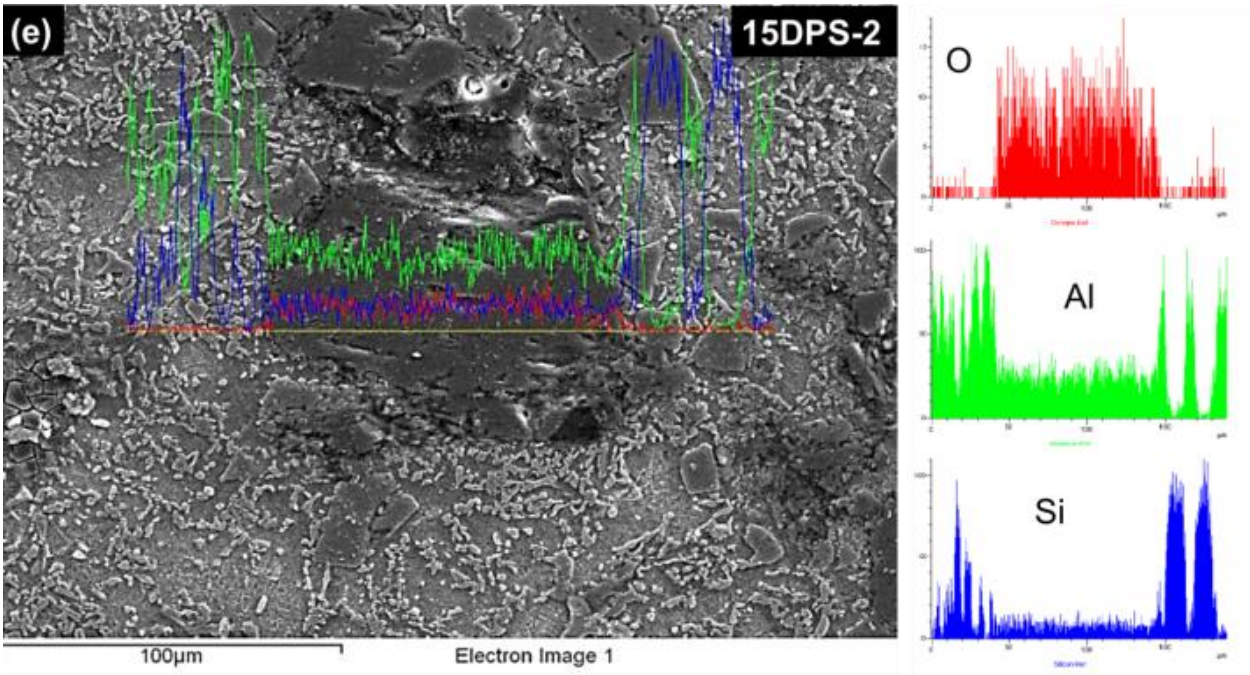
(e)
15DPS-2
100µm
Electron Image 1
O
Al
Si

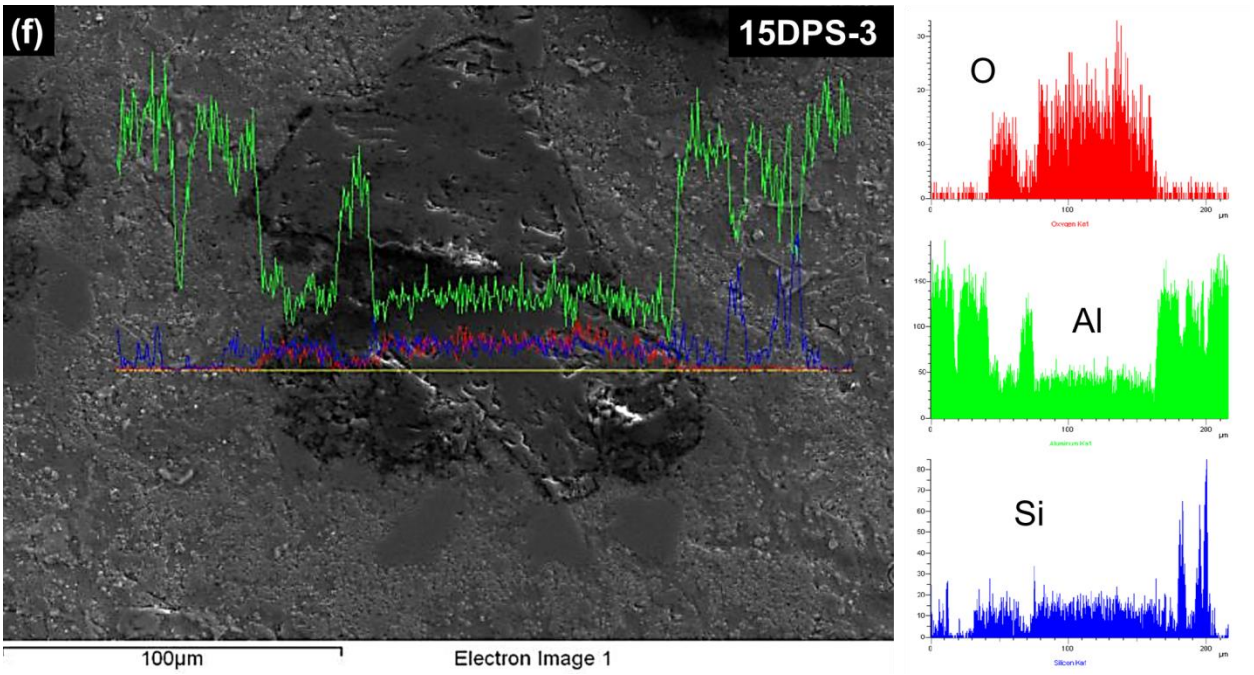

Figure 4.13 X-ray line profile of (a) 15SPS-C, (b) 15SPS-M, (c) 15SPS-F, (d) 15DPS-1, (e) 15DPS-2, and (f) 15DPS-3 composites

Figure 4.14 presents the X-ray dot mapping of 15SPS-C, 15SPS-M, 15SPS-F, 15DPS-1, 15DPS-2, and 15DPS-3 composites. A uniform particle distribution was evident from X-ray dot mapping (Figure 4.14). It was observed that particle addition refined the primary and eutectic silicon morphology. The refinement in primary silicon increased with increase in the portion of finer particles in the composites. The maximum refinement of primary and eutectic silicon was observed for 15DPS-3 composites. The sillimanite particles provided the necessary interface for the precipitation of silicon and the rise in the number of nucleation sites in the melt. The particles provide a chilling effect which disrupts the dendritic growth and hence leads to refinement/change of primary and eutectic silicon morphology from acicular to globular. Majorly, clustering of primary and secondary silicon was observed at the particle-matrix interface. A few primary silicon facets were observed at a distance from the particles. This is due to the process of convective forces. During solidification, a few facets are detached from the interface region [172]. Majority of the facets surround the sillimanite particles. The particles have low thermal conductivity and low coefficient of thermal expansion as compared to aluminium alloy. This creates a thermal gradient at the interface. The particles heat the neighbouring matrix, solidifying the aluminium matrix away from the reinforced particles. As

the melting temperature of silicon is higher than aluminium, the precipitation of silicon takes place in the vicinity of the reinforced particles leading to the enrichment of silicon in the vicinity of particles. Higher is the number of particles in the melt, higher are the nucleation sites for silicon, and higher is the refinement of matrix morphology.

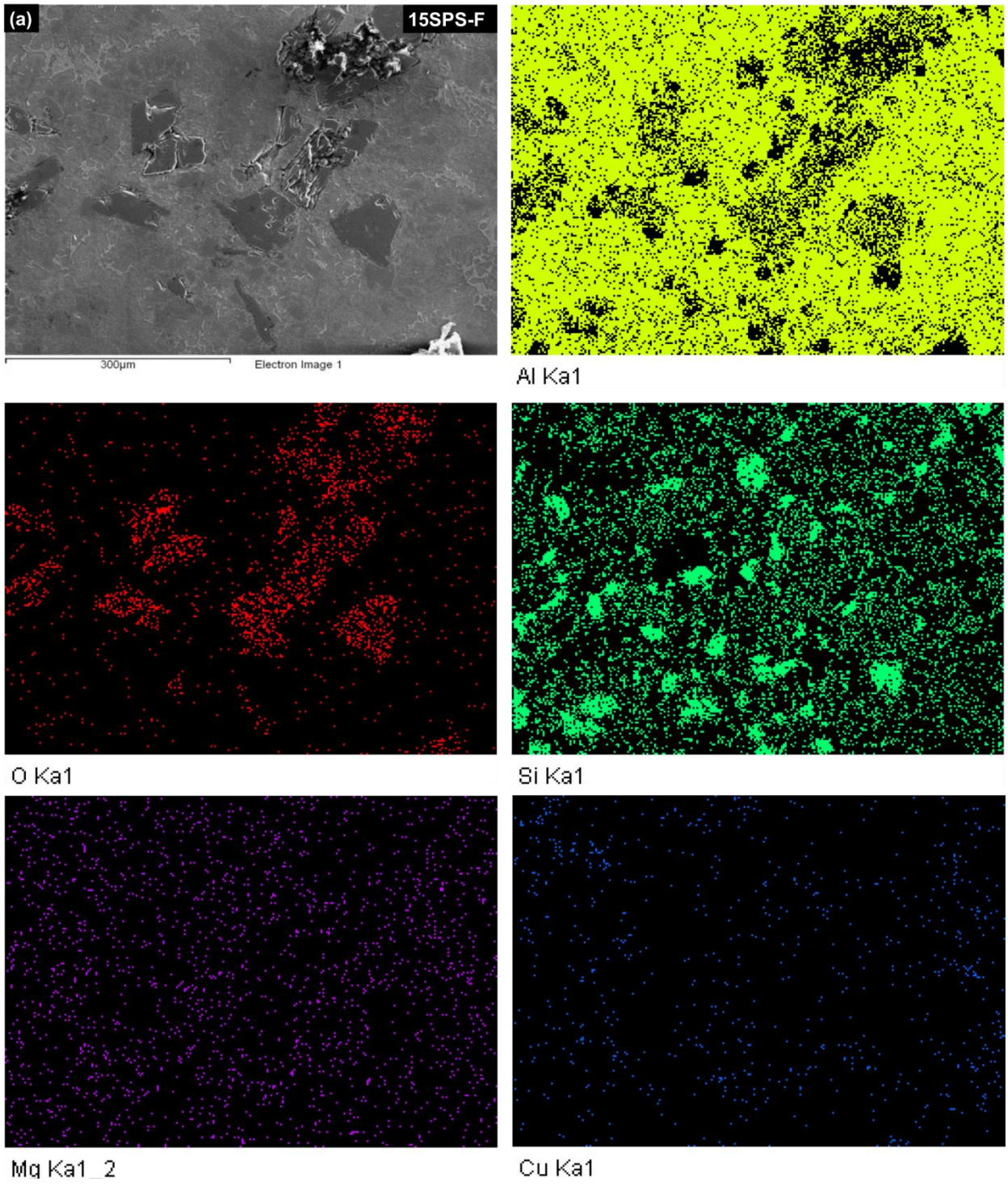
(a)
15SPS-F
300µm
Electron Image 1
Al Ka1
O Ka1
Si Ka1
Mg Ka1_2
Cu Ka1

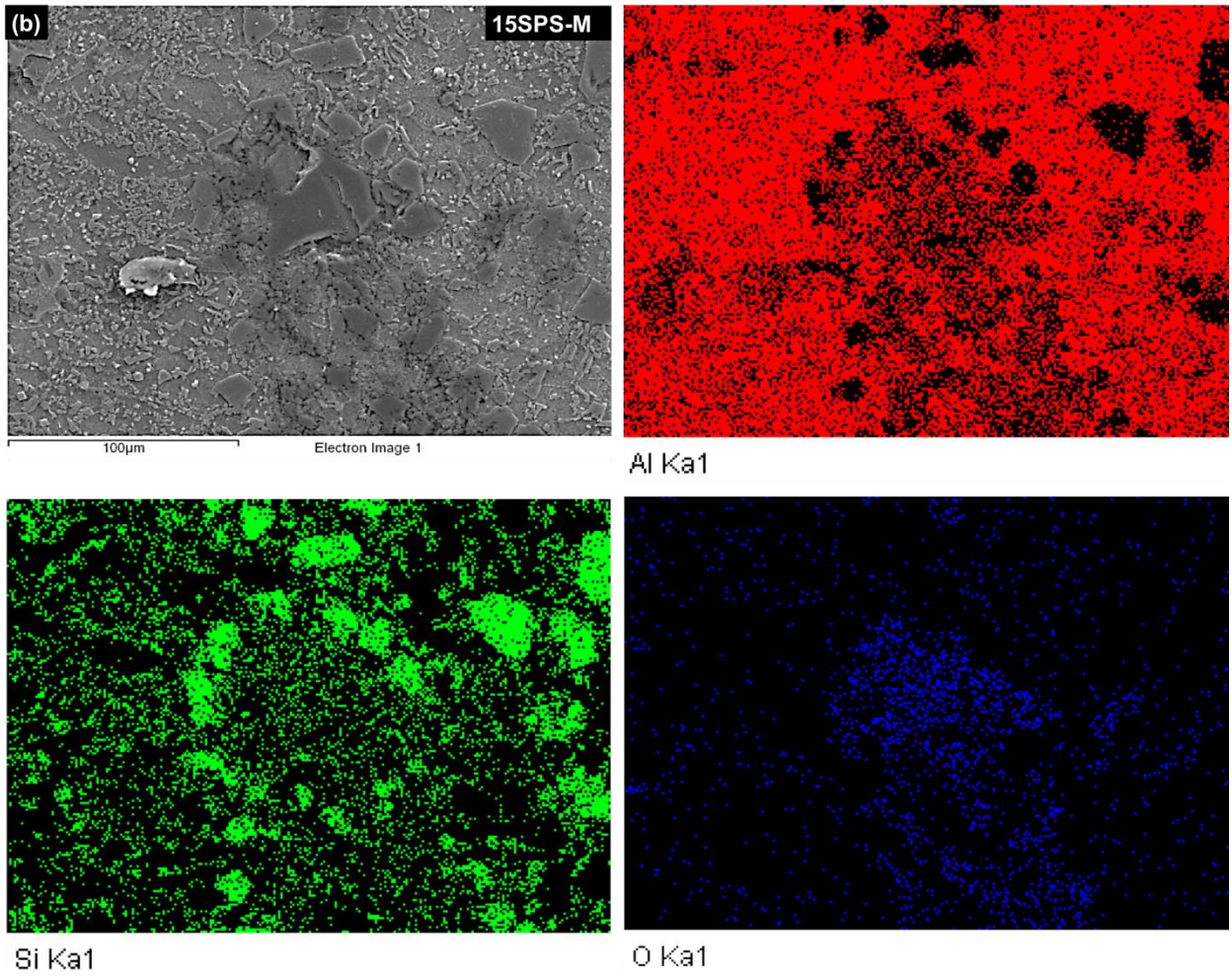
(b)
15SPS-M
100µm
Electron Image 1
Al Ka1
Si Ka1
O Ka1

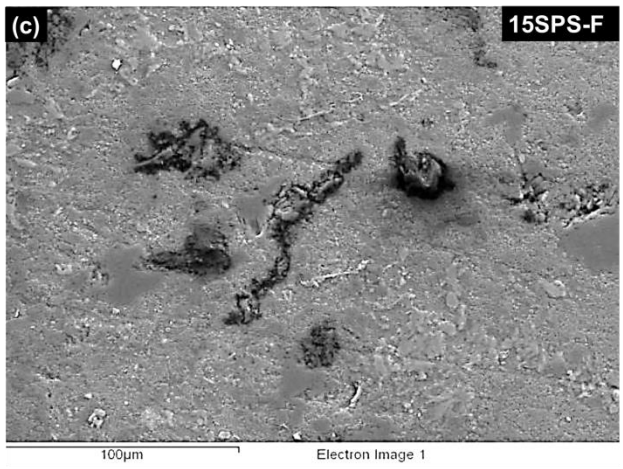

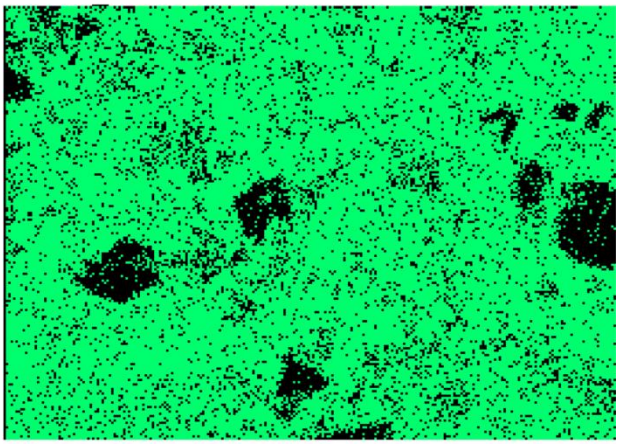

Al Ka1

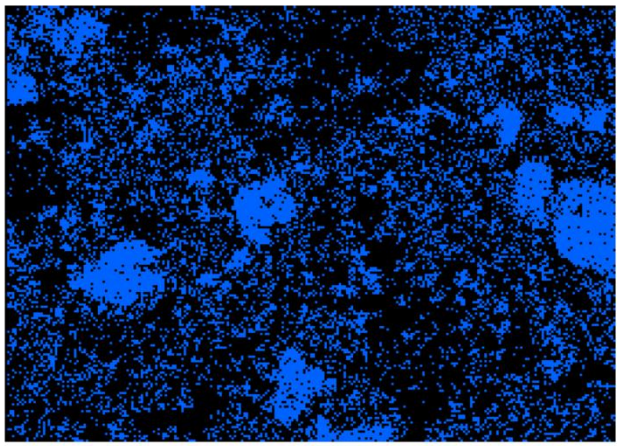

Si Ka1

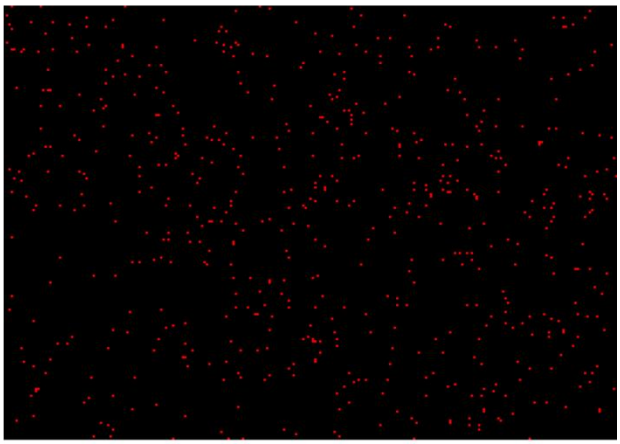

C Ka1 2

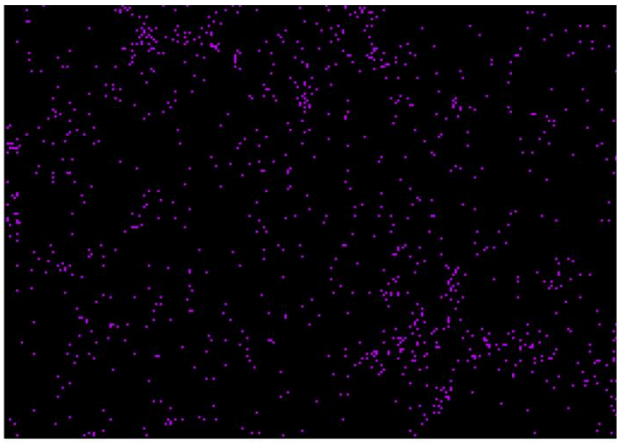

Cu Ka1

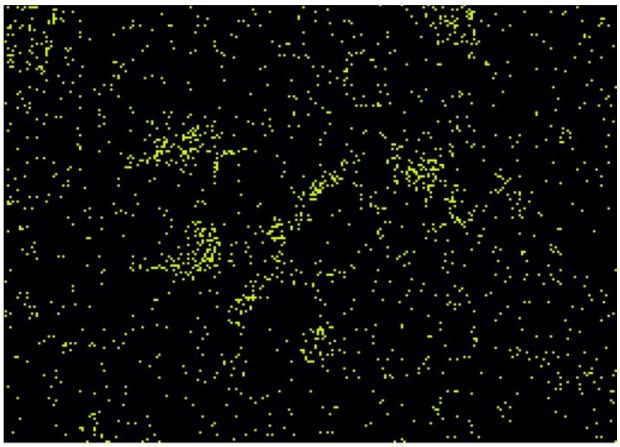

O Ka1

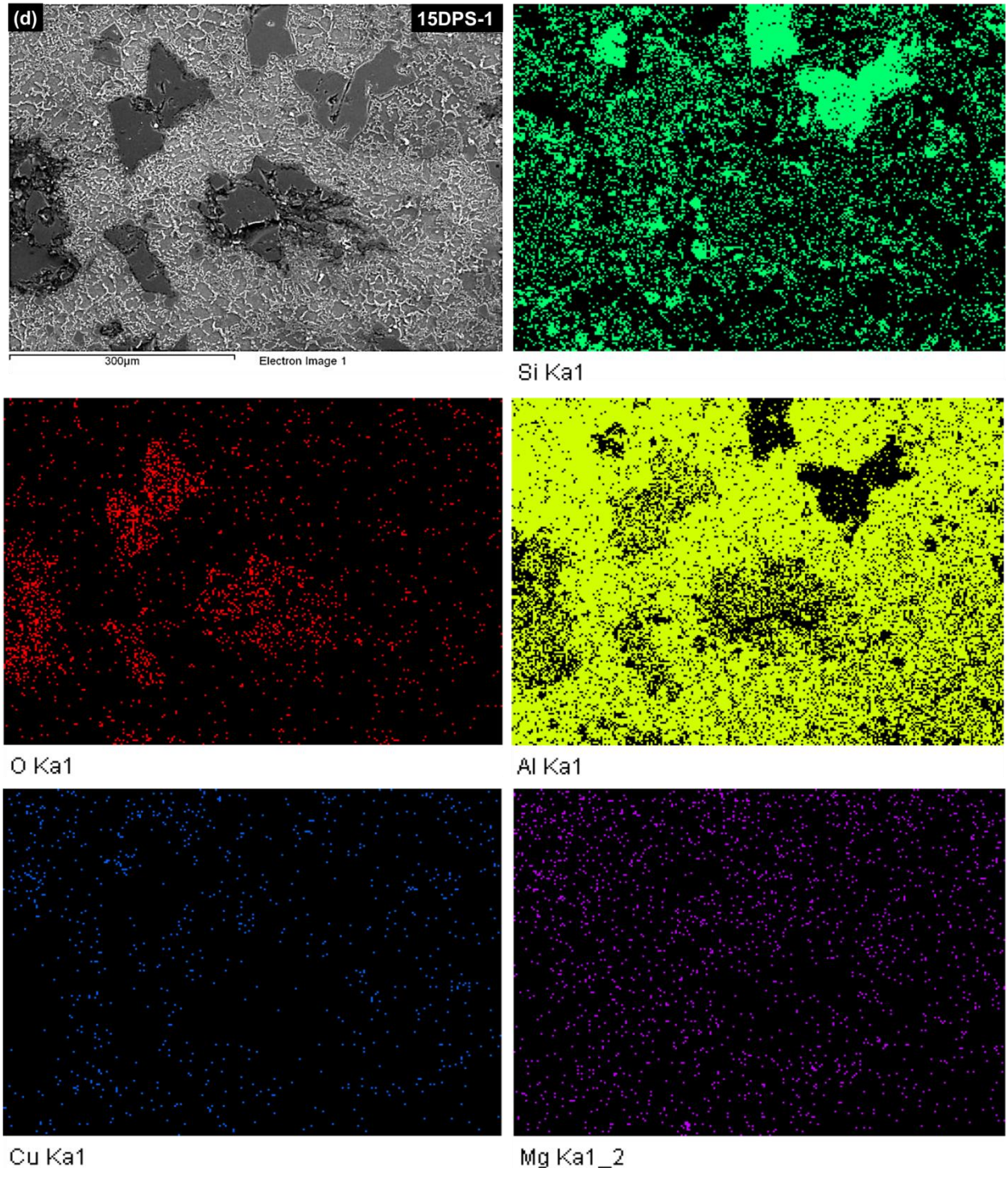
(d)
15DPS-1
300µm
Electron Image 1
Si Ka1
O Ka1
Al Ka1
Cu Ka1
Mg Ka1_2

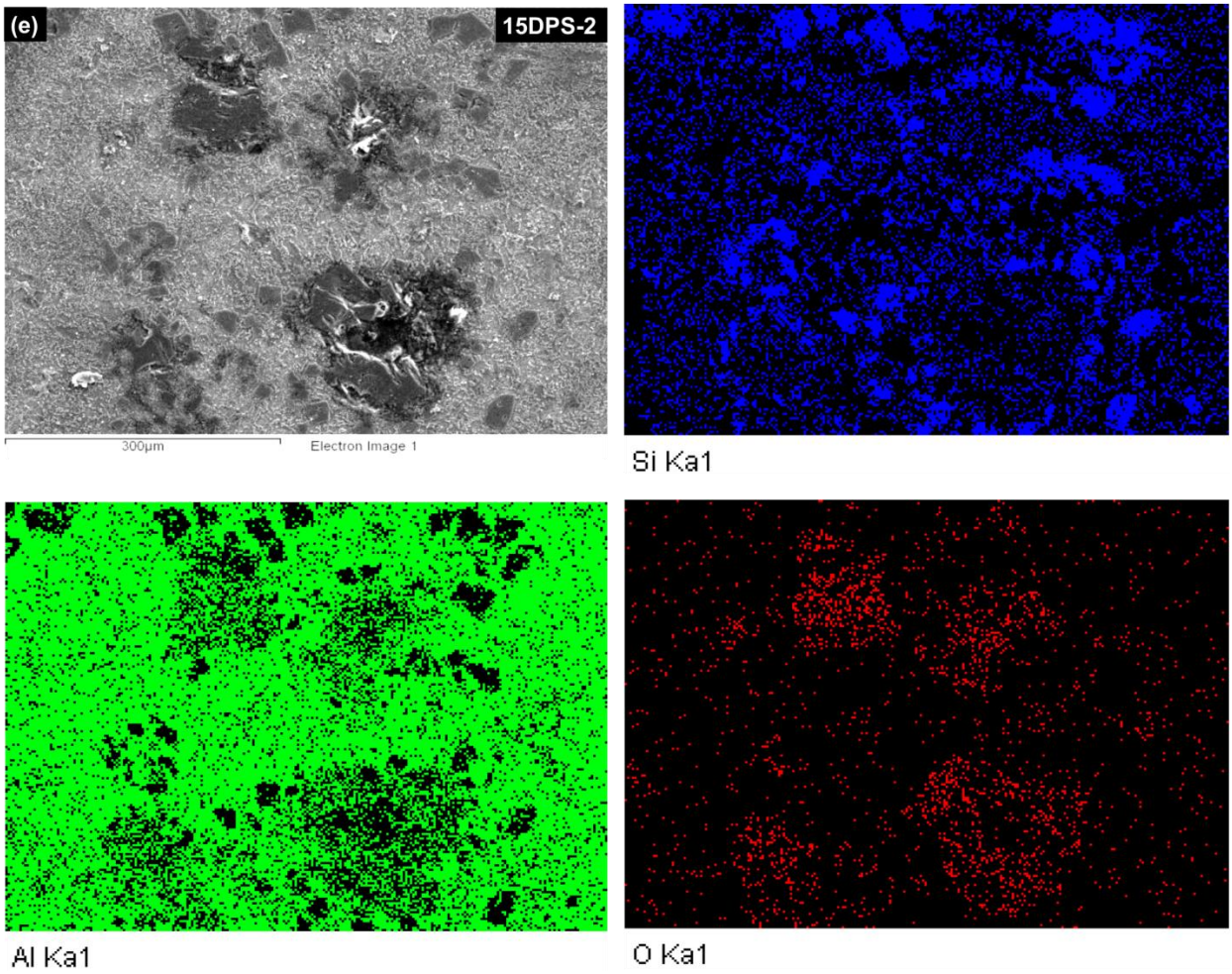
(e)
15DPS-2
300µm
Electron Image 1
Si Ka1
Al Ka1
O Ka1

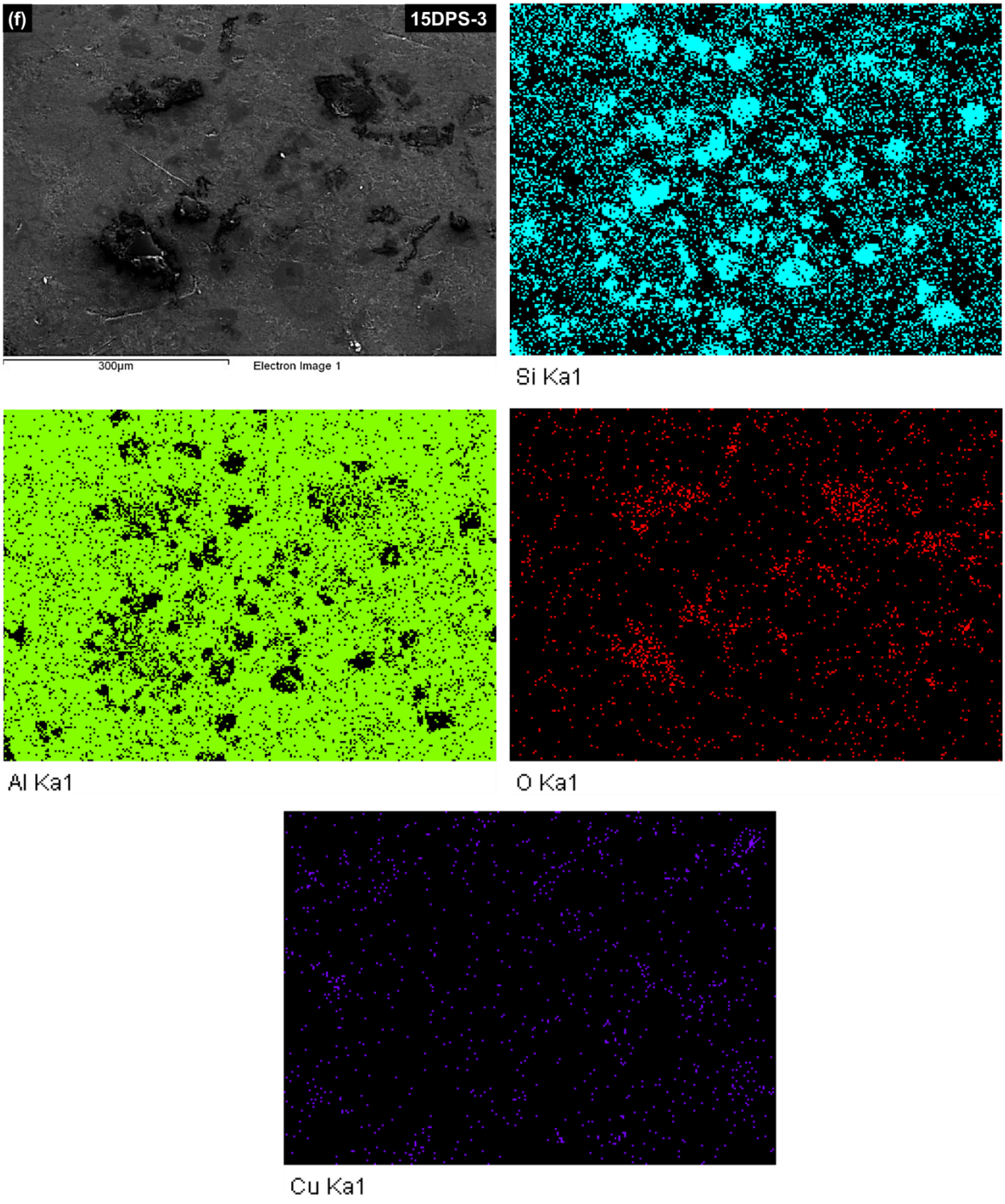

Figure 4.14 X-ray dot mapping of (a) 15SPS-C, (b) 15SPS-M, (c) 15SPS-F, (d) 15DPS-1, (e) 15DPS-2, and (f) 15DPS-3 composites

4.4 HARDNESS TESTING

4.4.1 NANOHARDNESS ANALYSIS

Nanoindentation tests were performed to characterize the various phases present in the base alloy and the processed AMCs. For the as-received LM30 base alloy, nanohardness testing was carried out on aluminium (eutectic aluminium) and silicon (proeutectic silicon) phases. Figure 4.15 presents the load-depth curves for the nanoindentation tests of the base alloy. Hardness values for the eutectic aluminium phase and primary silicon phase were calculated as 1.651±0.148 GPa and 10.787±0.085 GPa respectively.

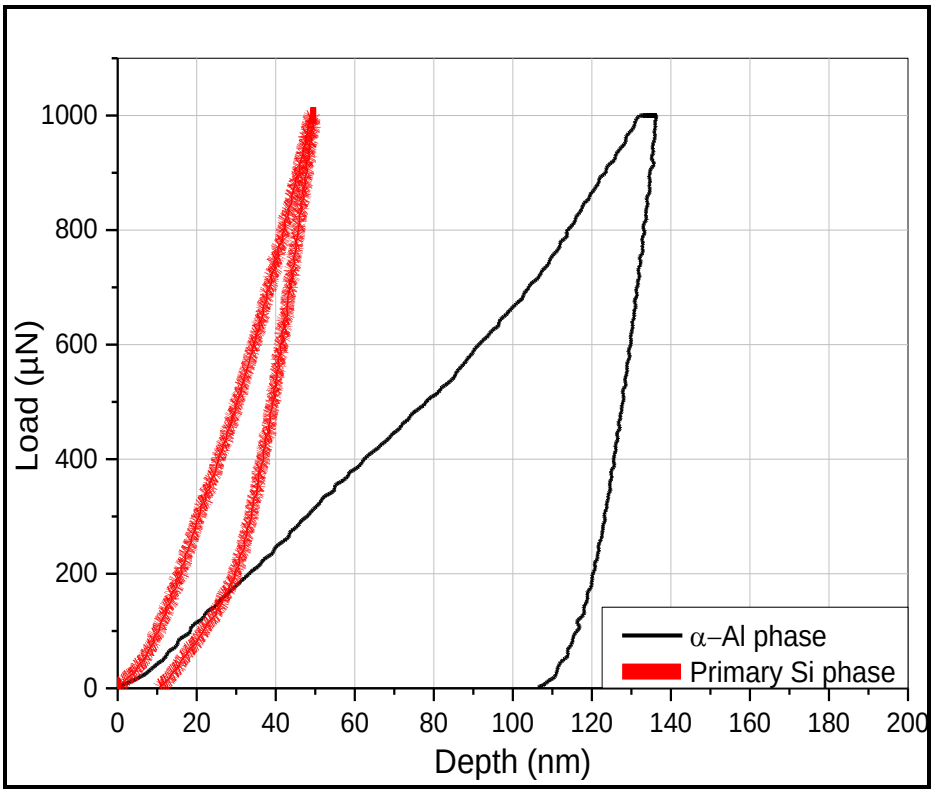

Figure 4.15 Load-depth (L-d) curves for the nanoindentation tests of as-received LM30 alloy

Nanohardness tests were also performed on various AMCs. For the composite system, three distinct phase regions were present. These included the aluminium matrix phase region, sillimanite particle region, and the interface region between Al matrix and sillimanite reinforcement. Nanoindentations were taken for all the three types of phase regions. Figure 4.16a–f presents the load-depth curves for various phases present in the 15 wt.% reinforced composites.

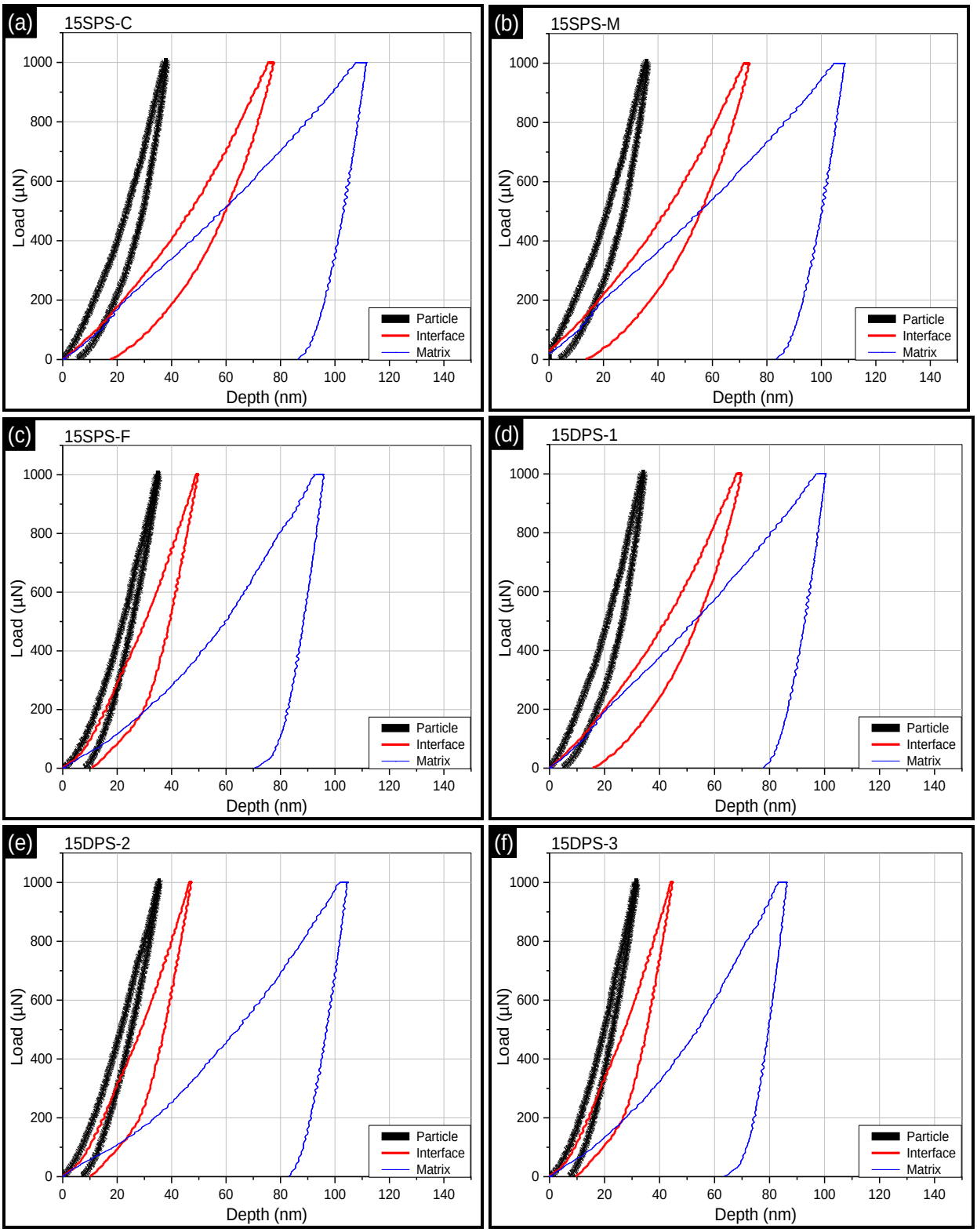

Figure 4.16 Load-depth (L-d) curves for nanoindentation tests of (a) 15SPS-C, (b) 15SPS-M, (c) 15SPS-F, (d) 15DPS-1, (e) 15DPS-2, and (f) 15DPS-3 composites

Table 4.1 presents the nanohardness values for different phase regions present in these composites. It was observed that all the composites contained a high hardness region with nearly similar hardness in the range of 18.78±0.78 to 21.42±2.31 GPa for different composites. This was the sillimanite particle phase region. Another region in all the composites was a low hardness phase region having low hardness in the range of 2.35±0.18 to 3.05±0.27 GPa for different composites indicating that this phase region was aluminium matrix region. Finally, all the composites contained a third distinct phase region where nanohardness value was in between the values obtained for matrix and particle regions, for a given composite formulation. This third phase in the composites was the interface region. For interface region (i.e. particle-matrix interface), high nanohardness value for all composites was obtained (Table 4.1) indicating good bonding between the matrix and reinforcement in various AMCs.

Table 4.1 Nanohardness values for different phases in AMCs containing 15 wt.% sillimanite

Composite Formulation	**Nanohardness (GPa) value at**		
	Aluminium matrix	***Interface***	***Sillimanite Reinforcement***
15SPS-C	2.35 ±0.18	9.76 ±1.12	18.78 ±0.78
15SPS-M	2.45±0.19	11.42±1.24	19.52±1.18
15SPS-F	3.05 ±0.27	13.20 ±1.47	20.79 ±1.31
15DPS-1	2.63±0.14	11.78±1.12	20.79±1.75
15DPS-2	2.64±0.17	13.82±154	21.42±2.31
15DPS-3	2.85±0.21	13.20±1.21	21.13±1.95

4.4.2 BRINELL HARDNESS TESTING

Brinell hardness testing was performed on various composites processed in the present research and also on cast iron specimen (considered as representative of the commercial material used for brake rotor applications). Table 4.2 presents the Brinell hardness values of various materials. The hardness of various AMCs increased with increase in sillimanite content. Brinell hardness of fabricated composites was found close to that of cast iron specimen used in brake rotor applications. Maximum hardness among composites was observed for 15DPS-3 sample (4.5% less than cast iron).

Table 4.2 Brinell hardness values for different materials

Material	Brinelll hardness (BHN)
Cast iron	203±8
15SPS-C	186±8
15SPS-M	187±7
15SPS-F	192±6
15DPS-1	184±9
15DPS-2	189±8
15DPS-3	194±7

4.5 WEAR TESTING

When two materials are in contact with each other, the relative motion between the surfaces leads to a progressive loss in material termed as wear. Wear analysis provides insights about the durability of the material under various contact conditions like contact pressure, operating temperature, environment etc. Hence, wear analysis of materials is very important for various engineering applications. The present section discusses the dry sliding wear rate behaviour of processed AMCs under different contact pressures at room temperature conditions. The section also compares the experimental wear results with theoretical wear analysis of the developed composites.

4.5.1 EXPERIMENTAL WEAR ANALYSIS

a) Effect of sliding distance on the wear rate

Figure 4.17 presents the wear rate behaviour (volume loss per sliding distance) of base alloy with respect to sliding distance (0–3000 m) under different contact pressure conditions (0.2–1 MPa). For any given contact pressure, the wear rate behaviour (of base alloy and various AMCs) with respect to sliding distance was observed to be divided into two distinct zones viz. an initial run-in-wear zone indicating a sharp change in wear rate with respect to sliding distance in the range of 0–2000 m followed by a steady-state-wear zone indicating constant wear rate over sliding distance in the range of 2000–3000 m. The run-in-wear zone indicated unstable nature of wear. This initial zone further comprised of two different sub-zones. The first sub-zone extended till a sliding distance of 500 m and showed an increase in wear rate with increase in sliding distance. The second sub-zone (500–2000 m) showed a decrease in wear rate with increase in sliding distance.

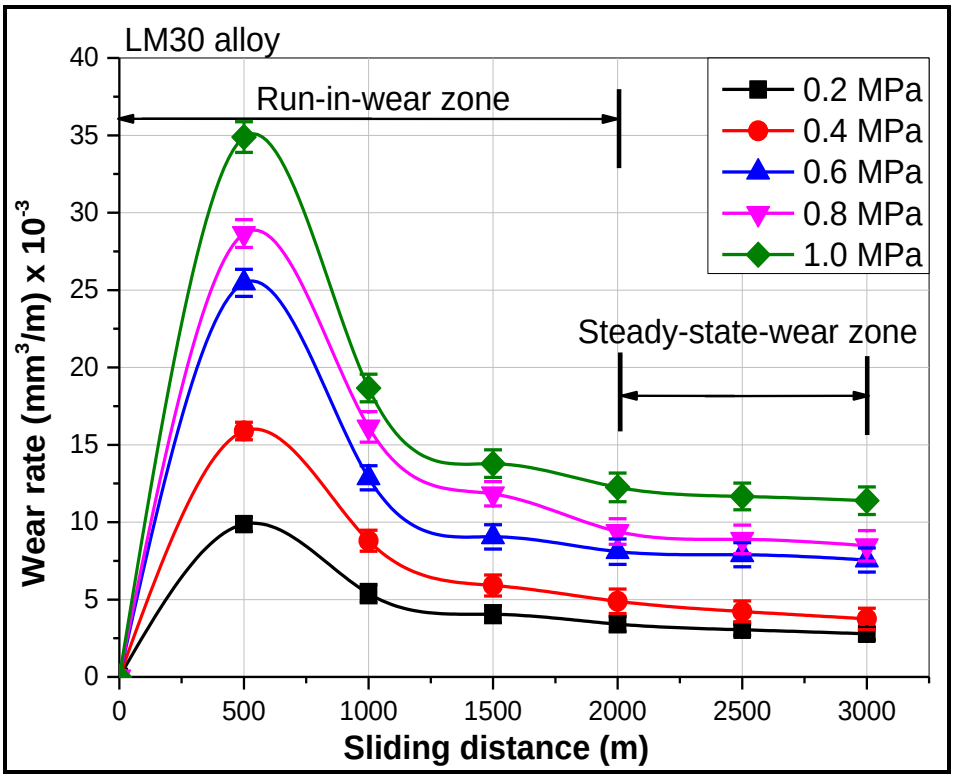

Figure 4.17 Wear rate behaviour of the as-received LM30 alloy

During the initial period of run, the two sliding counter surfaces (i.e. pin and disc) have asperity-to-asperity contact. These asperities are sharp and are in relative motion against each other. The greater degree of sharpness of asperities leads to high stress on asperity contact, thereby causing microcutting and microplowing action [173,174]. The asperities start acting as stress concentration points, get plastically deformed, and in the process, some very sharp asperities get fractured (thus, increasing the wear rate) under the combined action of normal stress, shear stress, and sliding speed. Also, during this initial part of the run-in-wear zone (0–500 m), the high frictional resistance between counter surfaces results in an increase in temperature at the contact of pin and disc [175]. This rise in temperature causes mechanical welding of the pin with disc resulting in plastic deformation of pin and hence higher wear rates [175–177]. Thus, an increase in wear rate was observed till a sliding distance of 500 m, mainly due to fragmentation of asperities and mechanical welding of pin with the disc. In the second sub-zone of run-in-wear period (500–2000 m), the debris formed due to wear of pin and disc materials starts aligning along the sliding direction in the wear tracks [175]. With increase in sliding distance, the valleys of the counter surfaces get occupied with wear debris resulting in compaction and continuous

grinding of wear debris which reduces the sharpness of debris. As a result, the abrasive action of counter surface asperities decreases, leading to a reduction in wear rate [134,162,175]. Also in this second sub-zone, with an increase in sliding distance, the interface temperature rises beyond a critical value, thus resulting in surface oxidation of the specimen (i.e. formation of oxide film on pin surface). The oxide layer on the pin surface acts as a protective layer and does not allow metal to metal contact, thereby reducing the effective wear rate [113,175]. Next, for the steady-state-wear zone (2000–3000 m), increase in sliding distance leads to further fragmentation and compaction of wear debris, counter surface materials, and the oxide layer. This compaction results in the formation of a mechanical mixed layer (MML) which protects the specimen surface from further wear [175]. However, an increase in sliding distance (2000–3000 m) also causes subsurface softening due to rise in temperature. The result is that the newly formed MML gets fractured and subsequently removed from the specimen surface. In the steady-state-wear zone, the formation and removal of MML occurs simultaneously with the rate of formation/growth of MML being equal to its rate of removal. Thus, the wear rate remains almost constant, with an increase in sliding distance in this zone [175].

The wear behaviour of 3 wt.%, 6 wt.%, 9 wt.%, 12 wt.%, and 15 wt.% sillimanite reinforced AMCs is shown in Figure 4.18 to 4.22

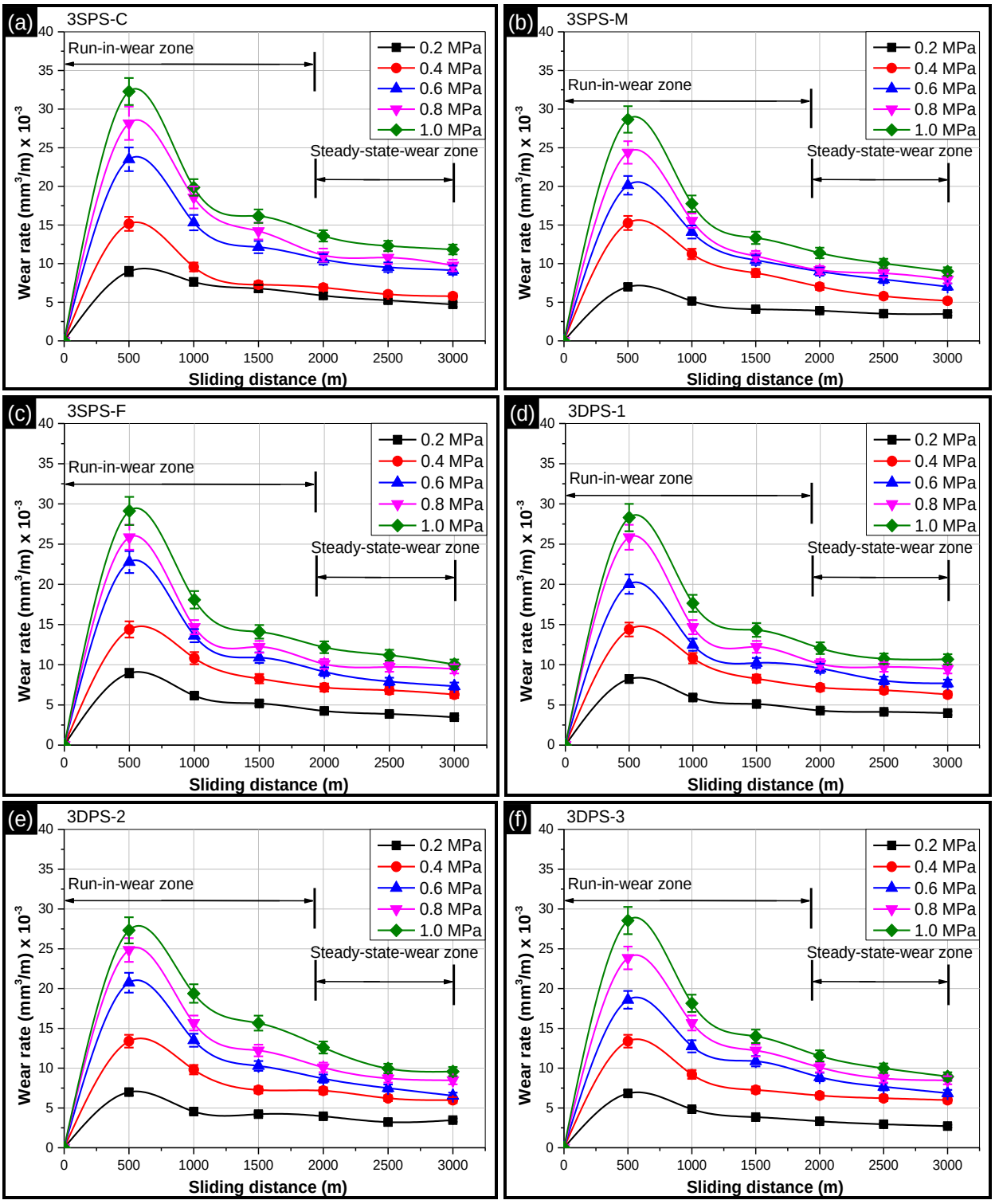

Figure 4.18 Wear behaviour of (a) 3SPS-C, (b) 3SPS-M, (c) 3SPS-F, (d) 3DPS-1, (e) 3DPS-2, and (f) 3DPS-3 composites

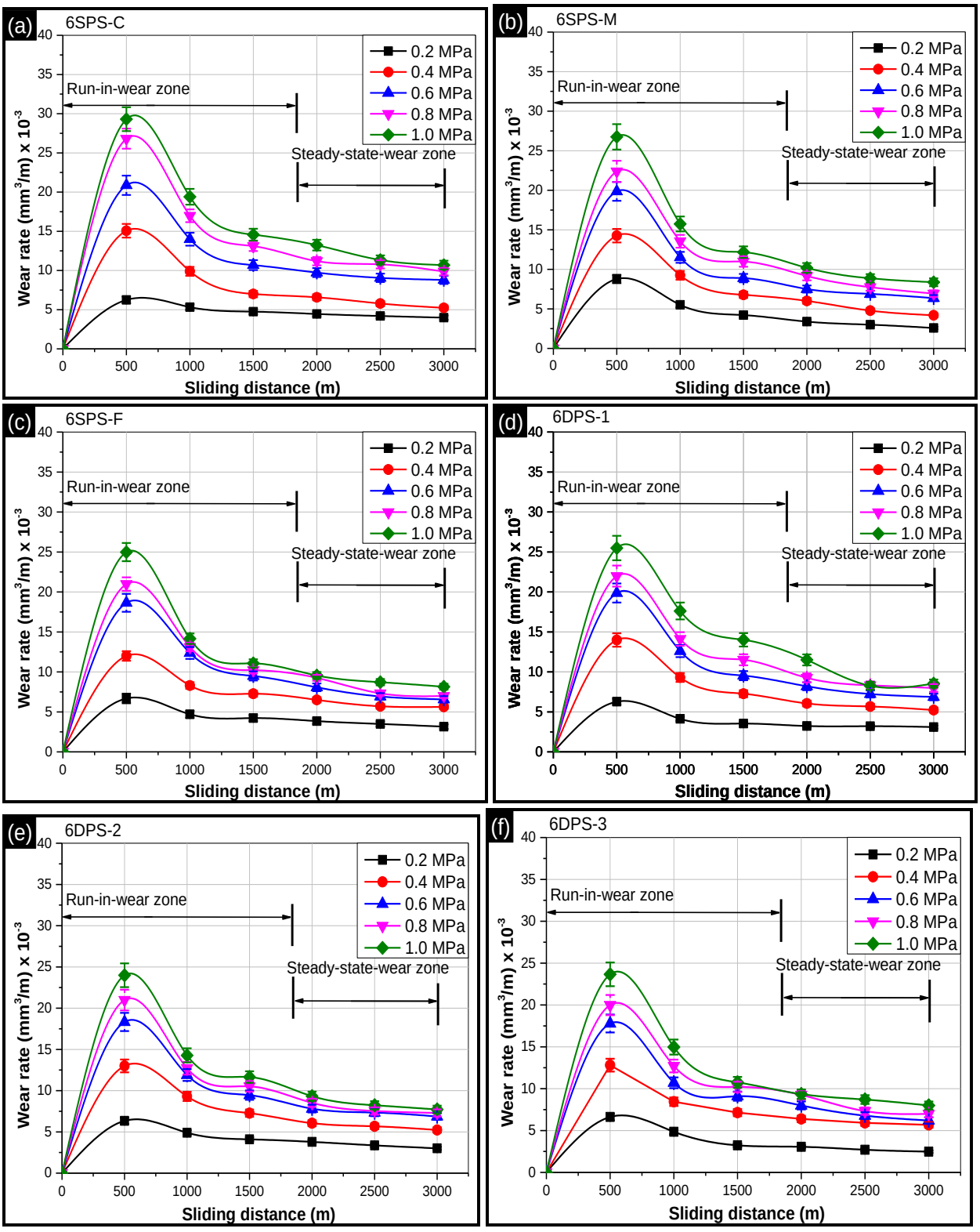

Figure 4.19 Wear behaviour of (a) 6SPS-C, (b) 6SPS-M, (c) 6SPS-F, (d) 6DPS-1, (e) 6DPS-2, and (f) 6DPS-3 composites

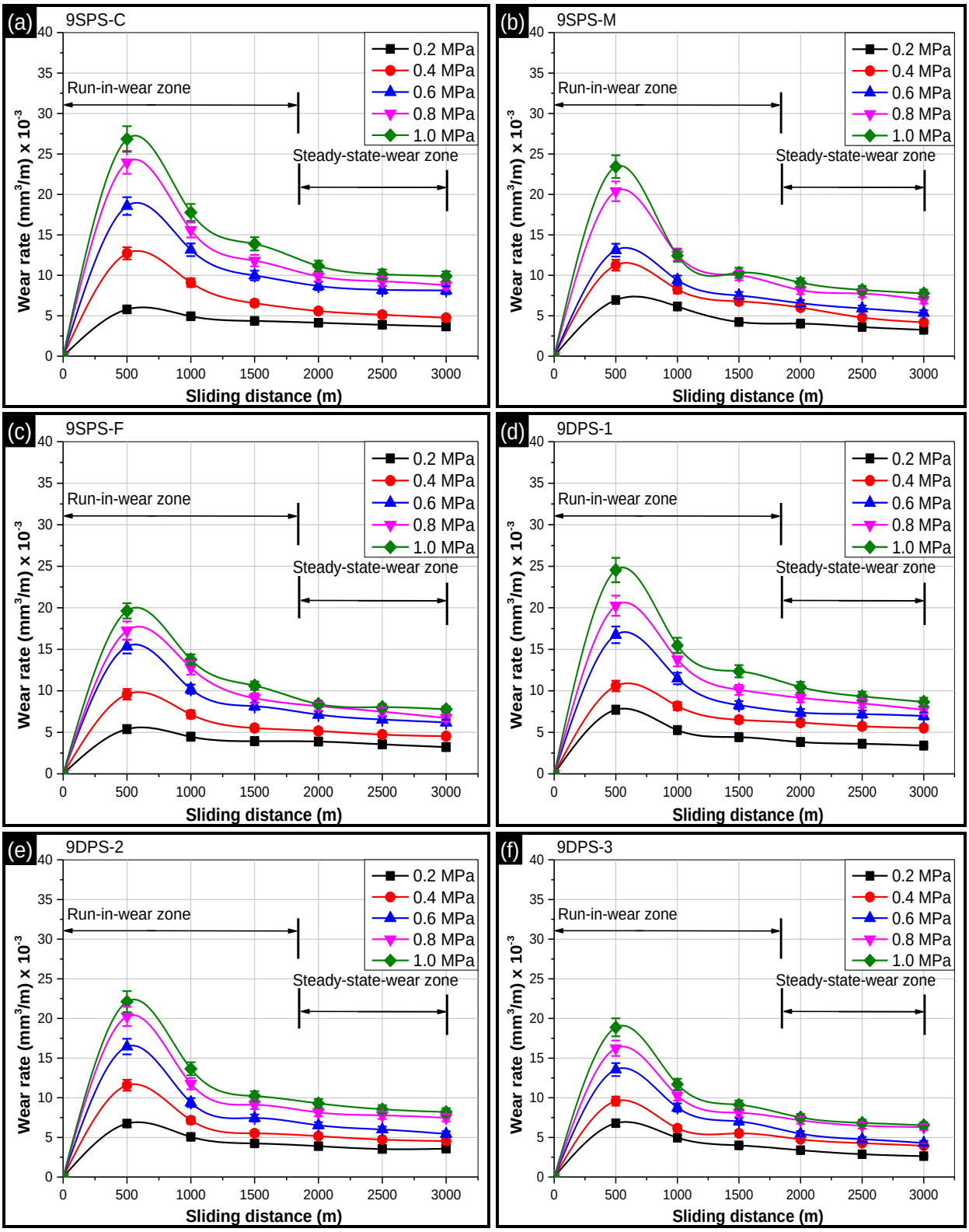

Figure 4.20 Wear behaviour of (a) 9SPS-C, (b) 9SPS-M, (c) 9SPS-F, (d) 9DPS-1, (e) 9DPS-2, and (f) 9DPS-3 composites

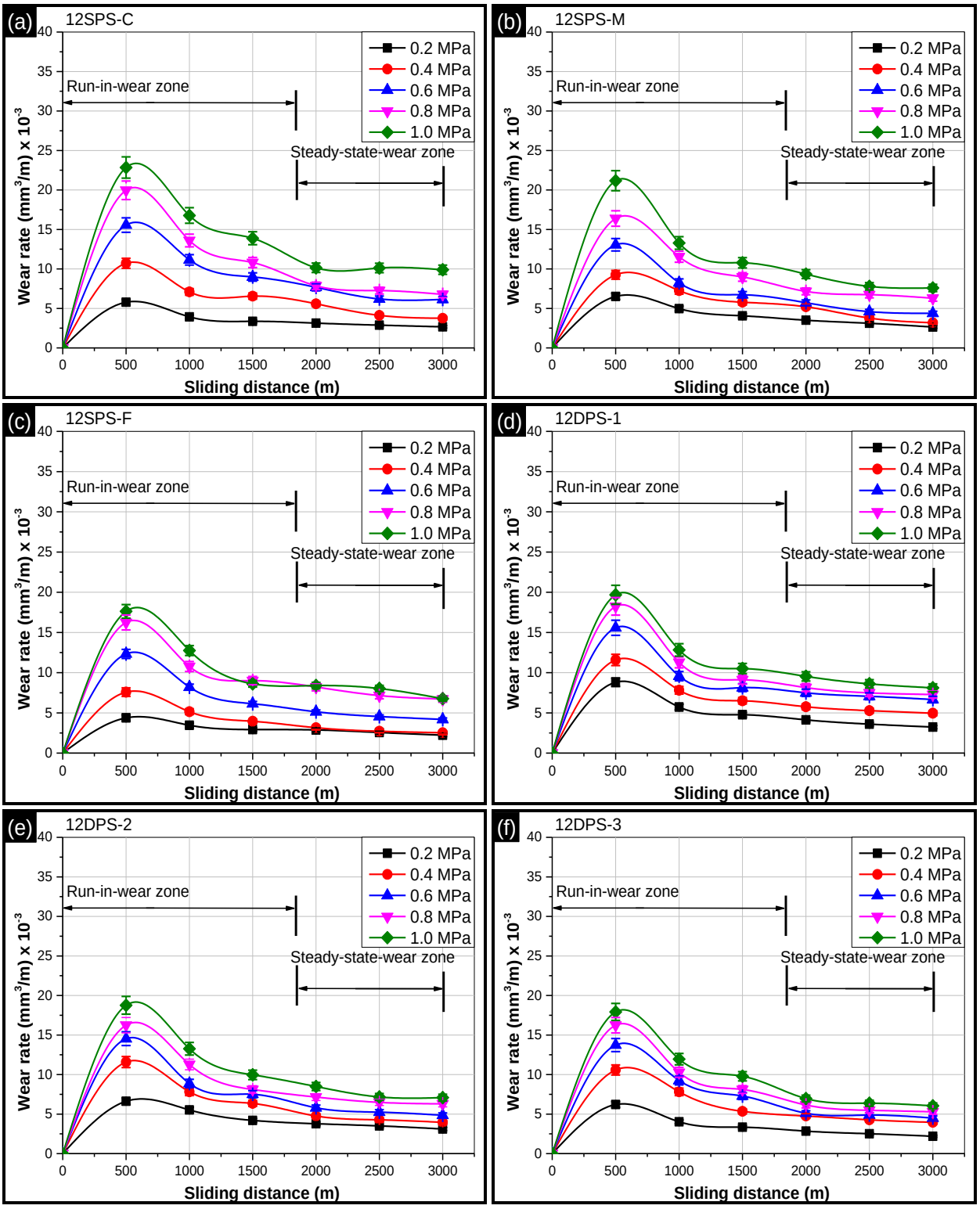

Figure 4.21 Wear behaviour of (a) 12SPS-C, (b) 12SPS-M, (c) 12SPS-F, (d) 12DPS-1, (e) 12DPS-2, and (f) 12DPS-3 composites

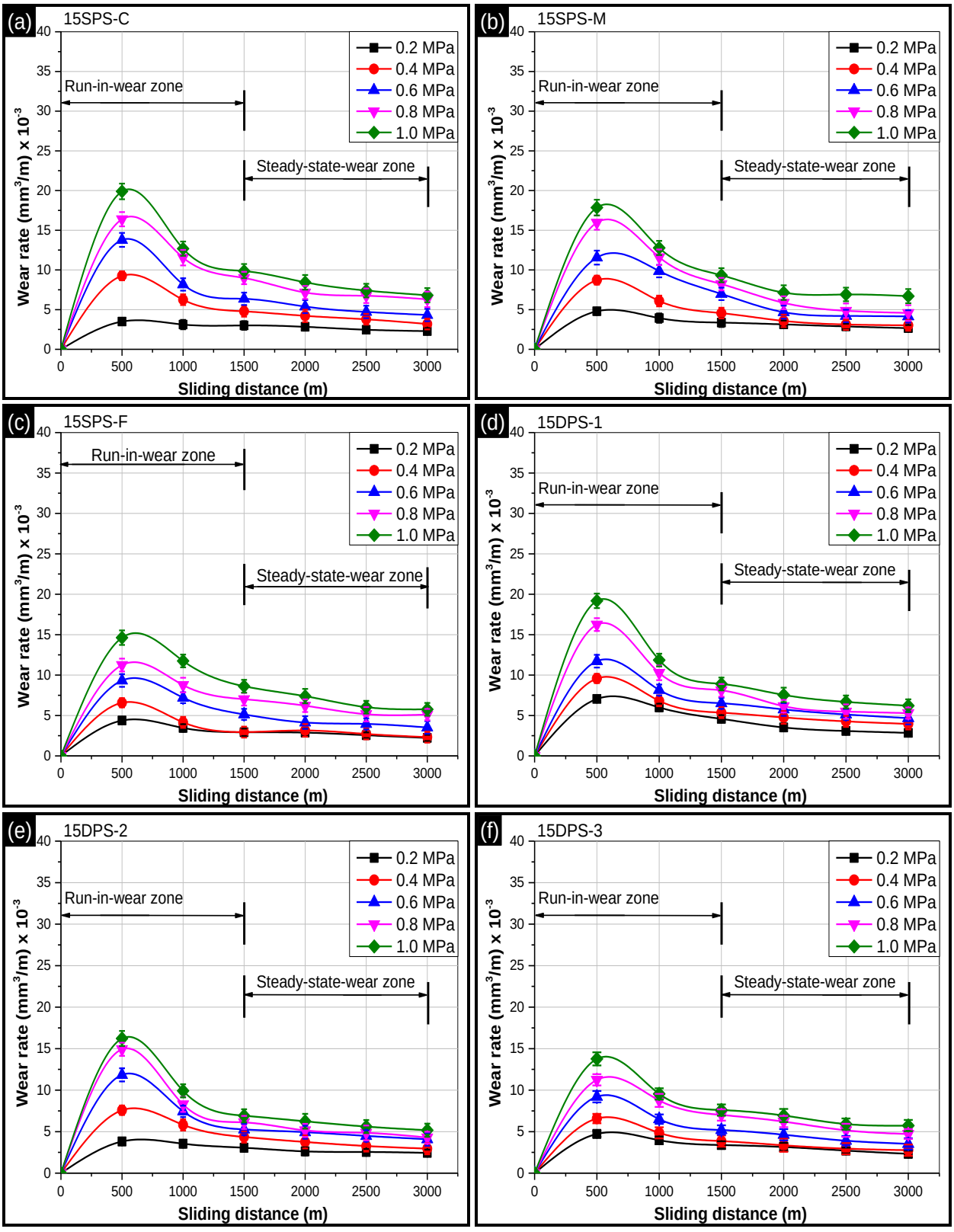

Figure 4.22 Wear behaviour of (a) 15SPS-C, (b) 15SPS-M, (c) 15SPS-F, (d) 15DPS-1, (e) 15DPS-2, and (f) 15DPS-3 composites

It was observed that presence of sillimanite particles in AMCs led to a reduction in wear rate (both run-in-wear and steady-state-wear) over the base alloy. Figure 4.18 to 4.22 show that wear rate (both run-in-wear and steady-state-wear) of AMCs reinforced with sillimanite decreased significantly with regards to that of the base alloy. The maximum wear rate of AMCs was significantly less when compared to the base alloy. Further, it was observed that the steady-state-wear zone for AMCs was achieved at a lesser sliding distance (for 15SPS-F composite, it was achieved at approximately 1500 m and for 15DPS-3 composite, it was achieved at 1200 m) as compared to that for base alloy (which achieved steady-state at 2000 m). Run-in wear of 15SPS-C composite was higher in comparison to other composite formulations. The run-in-wear was minimum for 15DPS-3 composites. This showed that a higher percentage of fine particles in DPS reinforced composites exhibited improved wear resistance.

Further, the wear analysis of cast iron pin (8 mm diameter) was carried out. Figure 4.23 presents the wear rate of cast iron specimen, 15SPS-F, and 15DPS-3 composites at a contact pressure of 1 MPa. It was observed that the wear rate of 15SPS-F and 15DPS-3 composites was found to be comparable with that of the cast iron specimen.

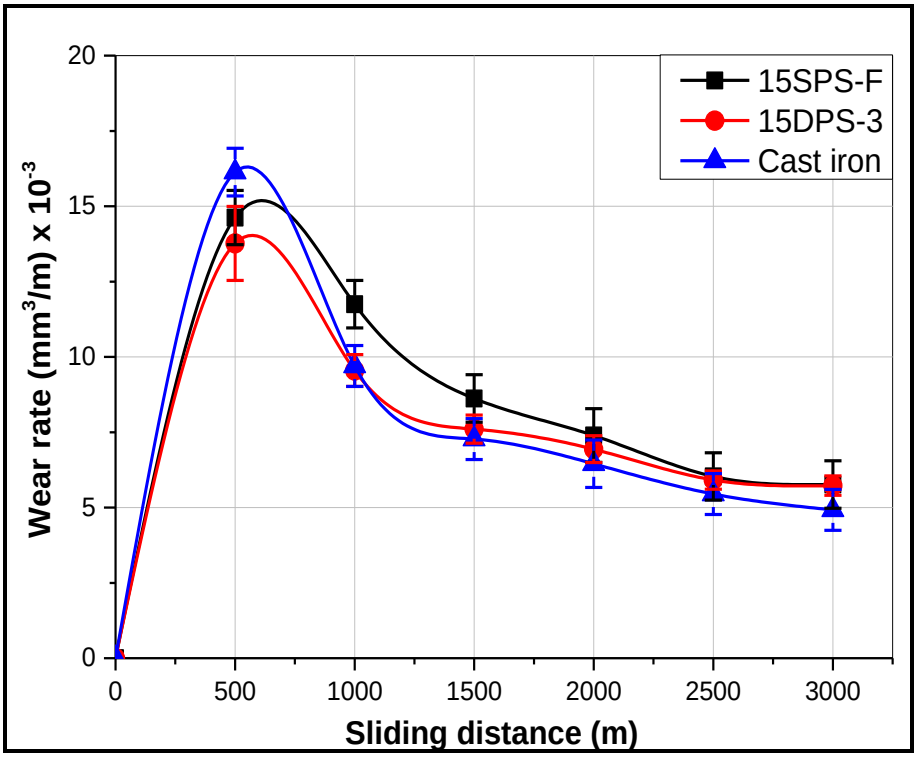

Figure 4.23 Comparison of wear rate of cast iron specimen with 15SPS-F and 15DPS-3 composites at a contact pressure of 1 MPa

The average steady-state wear values observed for 15SPS-F composite, 15DPS-3 composite, and cast iron were 6.944×10^{-3} mm^3/m, 6.537×10^{-3} mm^3/m and 6.050×10^{-3} mm^3/m respectively. The wear rate of the 15SPS-F composite and15DPS-3 composite was found to be just 13% and 8% higher than that of cast iron. On the contrary, the brake rotors fabricated using aluminium matrix composites are found to be 60 % lighter in comparison to the rotors made of cast iron [58]. Considering this factor and the comparable wear rate, the sillimanite reinforced LM30 aluminium matrix composites seemed to be a better option for industrial applications.

b) Effect of contact pressure, reinforcement level, and reinforcement particle size on the wear rate

Figure 4.24 presents the maximum wear rate of base alloy and various AMCs as a function of contact pressure. For the given sliding distance of 500 m, a linear relationship was observed between wear rate and contact pressure. Wear rate of the base alloy and various AMCs increased with increase in contact pressure from 0.2 to 1 MPa. This was because higher contact pressures increase the frictional resistance between counter surfaces causing an increase in interface temperature. The rise in temperature causes softening of material and hence increase in wear rate [175,178]. Also, at higher contact pressures, the hard oxide protective layer formed on pin surface during wear test becomes unstable and gets fractured, thus exposing the substrate materials (both, pin and disc). Consequently, small regions of substrate materials come into contact and get welded together and thereby, increase the wear rate. Also, at higher contact pressures, plastic deformation of substrate materials lead to subsurface crack initiation and increase in adhesive nature of pin with the disc, leading to increase in wear rate [179–182].

Further, it was observed that for a given reinforced particle size, wear rate decreased with increase in reinforcement level. The wear rate decreased significantly with increase in reinforcement level till 15 wt.%. This was attributed to the fact that the hard reinforced particles resist the grinding action of abrasives and protect the surface of composites against wear, thus reducing the wear rate. Also, addition of higher reinforcement content increases the hardness of composites and decreases the wear rate [49,183]. Further, it was observed that for a given reinforcement level, wear rate decreased with decrease in size of reinforced particles. For this reason, 15SPS-F showed better wear behaviour than 15SPS-M and 15SPS-C composites at all contact pressure. This was attributed to the fact that composites reinforced with finer particles

offer higher number of barriers per unit volume compared to those with relatively coarser particles [92,130]. Further, for a given reinforcement level in DPS composites (containing a mix of fine and coarse particles), wear rate decreased with increase in proportion of finer particles. For this reason, 15DPS-3 showed better wear resistance than 15DPS-2 and 15DPS-1 composites at any contact pressure. This was attributed to the fact that in DPS composites, the coarser particles bear a larger portion of the applied pressure, and thereby, the pressure on the finer particles and the matrix alloy decreases [184]. The coarse particles act as a buffer and protect the finer sized particles from the ploughing action of the abrasive. Thus, the finer particles continue to perform their wear resistance function for a longer time as compared to SPS (single particle size) composites. Further, for DPS composites, the critical pressure required for the particle fracture increases. Therefore, for DPS composites, by substituting a portion of fine-sized particles with coarser-sized particles, the critical pressure required for particle fracture increased. As a result, the highest reduction in maximum wear rate for AMCs was achieved for 15DPS-3 composites (59% reduction over base alloy). With single particle size composites, maximum reduction of 55% (over base alloy) was shown by 15SPS-F composite. Table 4.3 presents the highest reduction in maximum wear rate of various AMCs.

Table 4.3 Reduction in maximum wear rate of AMCs over the base alloy

S. No	Type of AMC	Reduction in maximum wear rate w.r.t. base alloy (%)
1.	15SPS- C	44
2.	15SPS-M	46
3.	15SPS- F	55
4.	15DPS-1	45
5.	15DPS-2	57
6.	15DPS-3	59

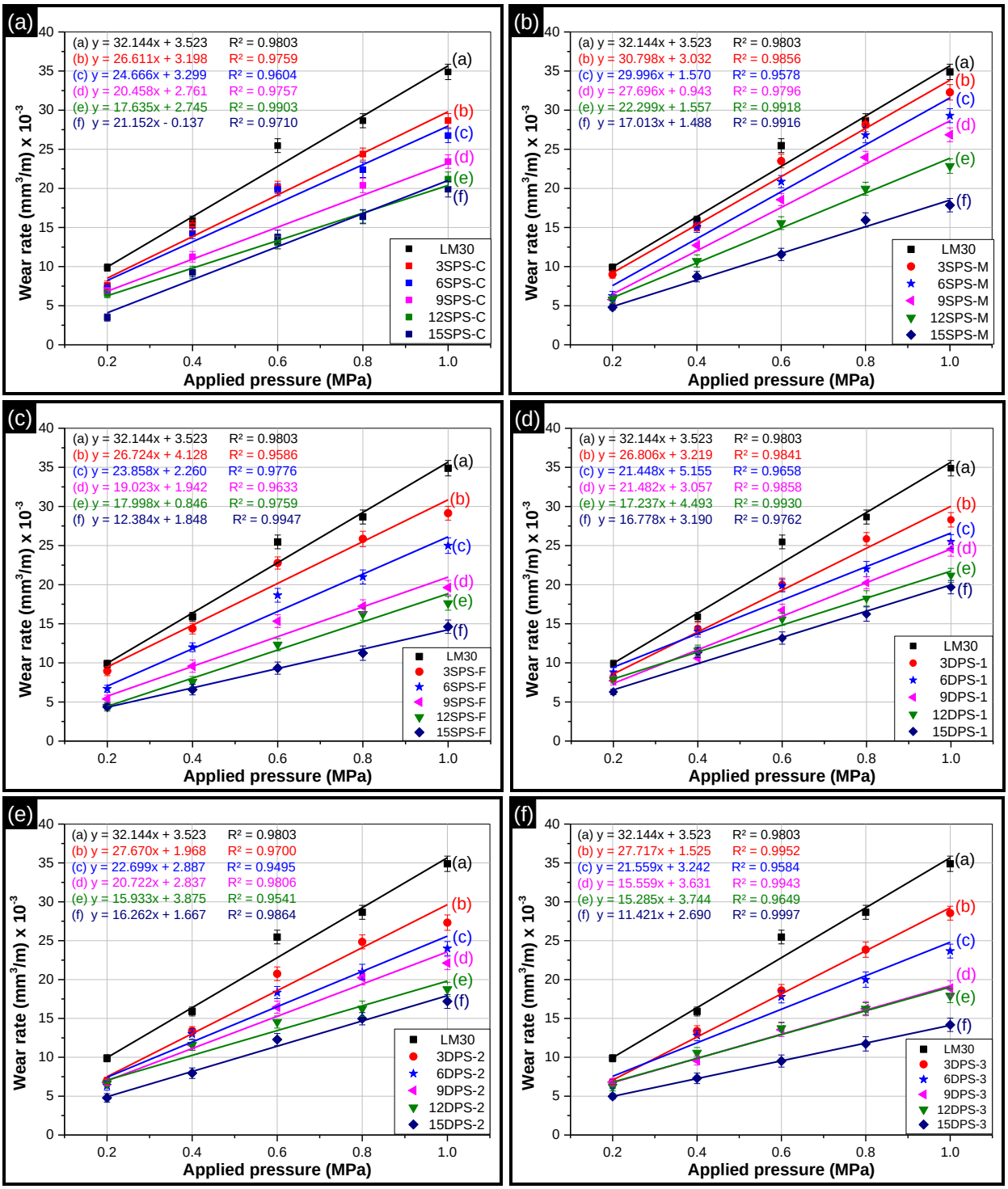

Figure 4.24 Maximum wear rate observed at a sliding distance of 500 m for base alloy and various AMCs (a) SPS-C, (b) SPS-M, (c) SPS-F, (d) DPS-1, (e) DPS-2, and (f) DPS-3 under different contact pressure conditions

4.5.2 MATHEMATICAL PREDICTION OF WEAR RATE

To validate the experimental results, mathematical modelling was performed. According to Archard's law, "the coefficient of wear is often considered to be inversely proportional to the hardness of the alloy and directly proportional to the contact pressure" (see Equation 4.1) [185].

$$Q = K\frac{PL}{H_V} \quad \text{..... (4.1)}$$

where,

Q: total volume of wear debris produced (mm^3)

K: dimensionless constant (has an approximate value of 4.0)

P: total normal load (N)

L: sliding distance (mm)

H_V: hardness of the softest contacting surfaces (N/mm^2)

However, contact pressure, sliding distance, and hardness are not the only parameters affecting the wear. Wear is also found to be inversely proportional to the size of reinforced particles and directly proportional to the spacing between particles and roughness of the counter plate surface. For a given sliding velocity and sliding distance, the wear loss for a hypereutectic Al-Si alloy is predicted according to Equation 4.2 [186].

$$W = K\frac{P}{H_V}\frac{R_{max}}{\frac{d_1}{\lambda_1}+\frac{d_2}{\lambda_2}} \quad \text{..... (4.2)}$$

where,

W: wear loss (μm)

P: pressure on sliding interface (N/mm^2)

R_{max}: counter plate surface roughness (μm)

H_V: Vickers hardness of softer contacting surface (N/mm^2)

K: constant, has an approximate value of 4.0

d_1: particle mean diameter (μm)

λ_1: particle mean spacing (μm)

d_2: primary silicon mean diameter (µm)

λ_2: primary silicon mean spacing (µm)

In the present work, Equation 4.2 was used to validate the experimental results. For the base alloy and various AMCs values of d_1, d_2, λ_1, and λ_2 were obtained through optical micrographs whereas, the values of hardness (Hv), contact pressure (P), and surface roughness (R_{max}) were obtained from the experimental results. The predicted wear loss results (W) are shown in Table 4.4.

The values of particle mean diameter (d_1), particle mean spacing (λ_1), primary silicon mean diameter (d_2), and primary silicon mean spacing (λ_2) were determined using image analysis software (ImageJ, National Institute of Health, USA). The counter plate surface roughness (R_{max}) was measured using a surface roughness tester (Surf test SJ-400, Mitutoyo, Japan). The average value for R_{max} was observed to be 25 µm. The sliding velocity was kept as constant at 1.6 m/s.

Using the predicted wear loss values (µm) as shown in Table 4.4, the wear rate (mm^3/m) values were calculated for different sliding distances (500–3000 m). Predictions of wear rate for base alloy and various AMCs is presented in Figure 4.25a–g. Close comparison was observed in the experimental and predicted wear rates as shown in Figure 4.25h–i. Maximum reduction in wear rate was predicted for 15DPS-3 composites showing 65% reduction in wear rate over the base alloy. The experimental results for 15DPS-3 composites were in close agreement showing 59% reduction in maximum wear rate.

Table 4.4 Predicted wear loss of base alloy and AMCs under various operating conditions

Alloys	Operating conditions							Wear loss
	P (N/mm^2)	R_{max} (µm)	H_V (N/mm^2)	d_1 (µm)	λ_1 (µm)	d_2 (µm)	λ_2 (µm)	W (µm)
Base alloy	0.2	25	610	-	-	60	150	0.082
	0.4							0.17
	0.6							0.25
	0.8							0.33
	1.0							0.41
15SPS-C	0.2	25	638	90	130	32	204.65	0.04
	0.4							0.07
	0.6							0.11
	0.8							0.15
	1.0							0.18
15SPS-M	0.2	25	675	40	100	17.75	90.25	0.05
	0.4							0.10
	0.6							0.15
	0.8							0.19
	1.0							0.24
15SPS-F	0.2	25	755	10	15	3	25.23	0.04
	0.4							0.07
	0.6							0.10
	0.8							0.14
	1.0							0.17
15DPS-1	0.2	25	625	80	120	10	208.33	0.05
	0.4							0.09
	0.6							0.14
	0.8							0.18
	1.0							0.23
15DPS-2	0.2	25	695	50	65	7	116.75	0.04
	0.4							0.07
	0.6							0.11
	0.8							0.14
	1.0							0.17
15DPS-3	0.2	25	789	29	32	3.5	37.33	0.03
	0.4							0.05
	0.6							0.08
	0.8							0.10
	1.0							0.13

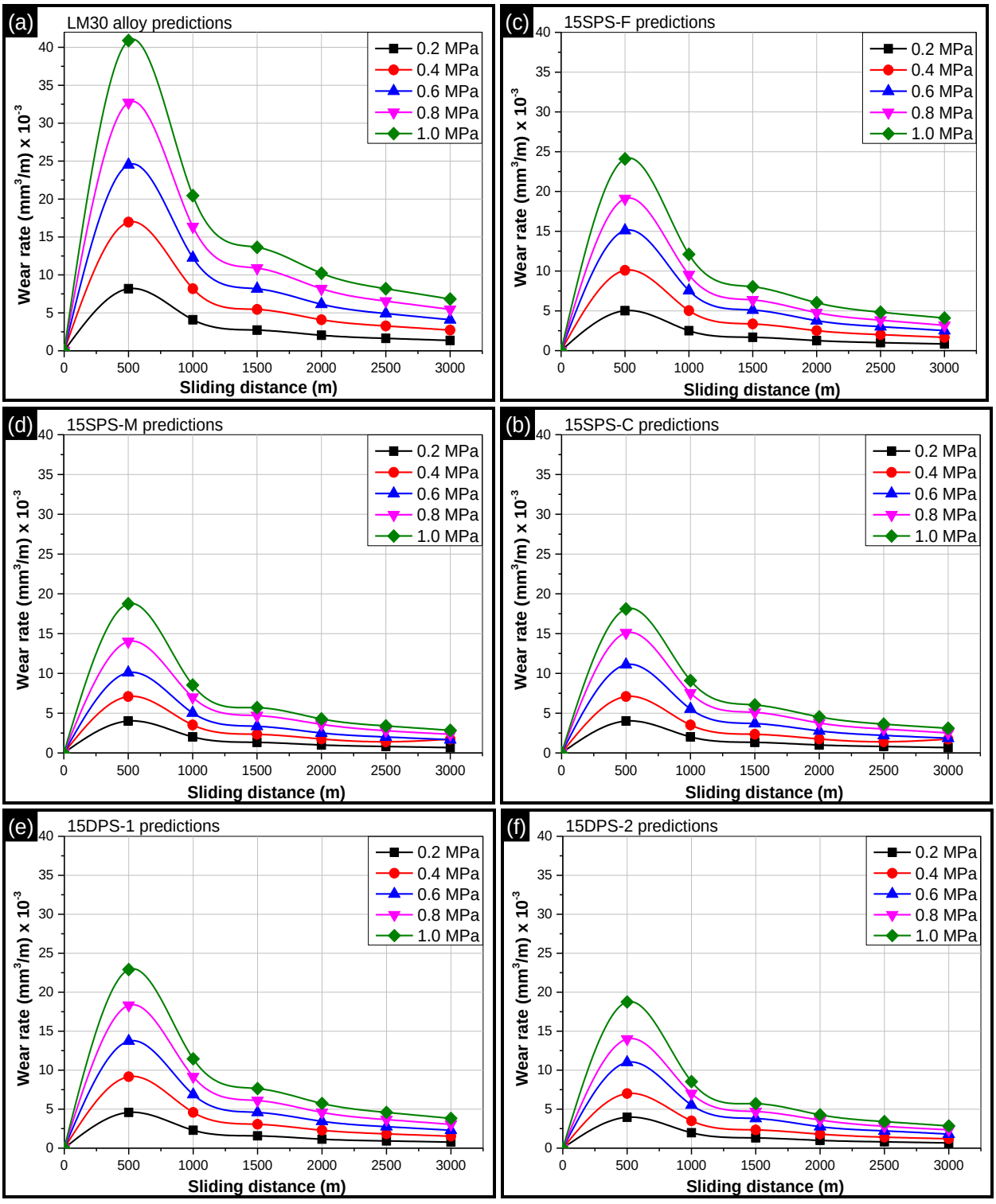
(a)
LM30 alloy predictions
(c)
15SPS-F predictions
(d)
15SPS-M predictions
(b)
15SPS-C predictions
(e)
15DPS-1 predictions
(f)
15DPS-2 predictions
0.2 MPa
0.4 MPa
0.6 MPa
0.8 MPa
1.0 MPa
Wear rate (mm³/m) x 10⁻³
Sliding distance (m)
0
5
10
15
20
25
30
35
40
0
500
1000
1500
2000
2500
3000

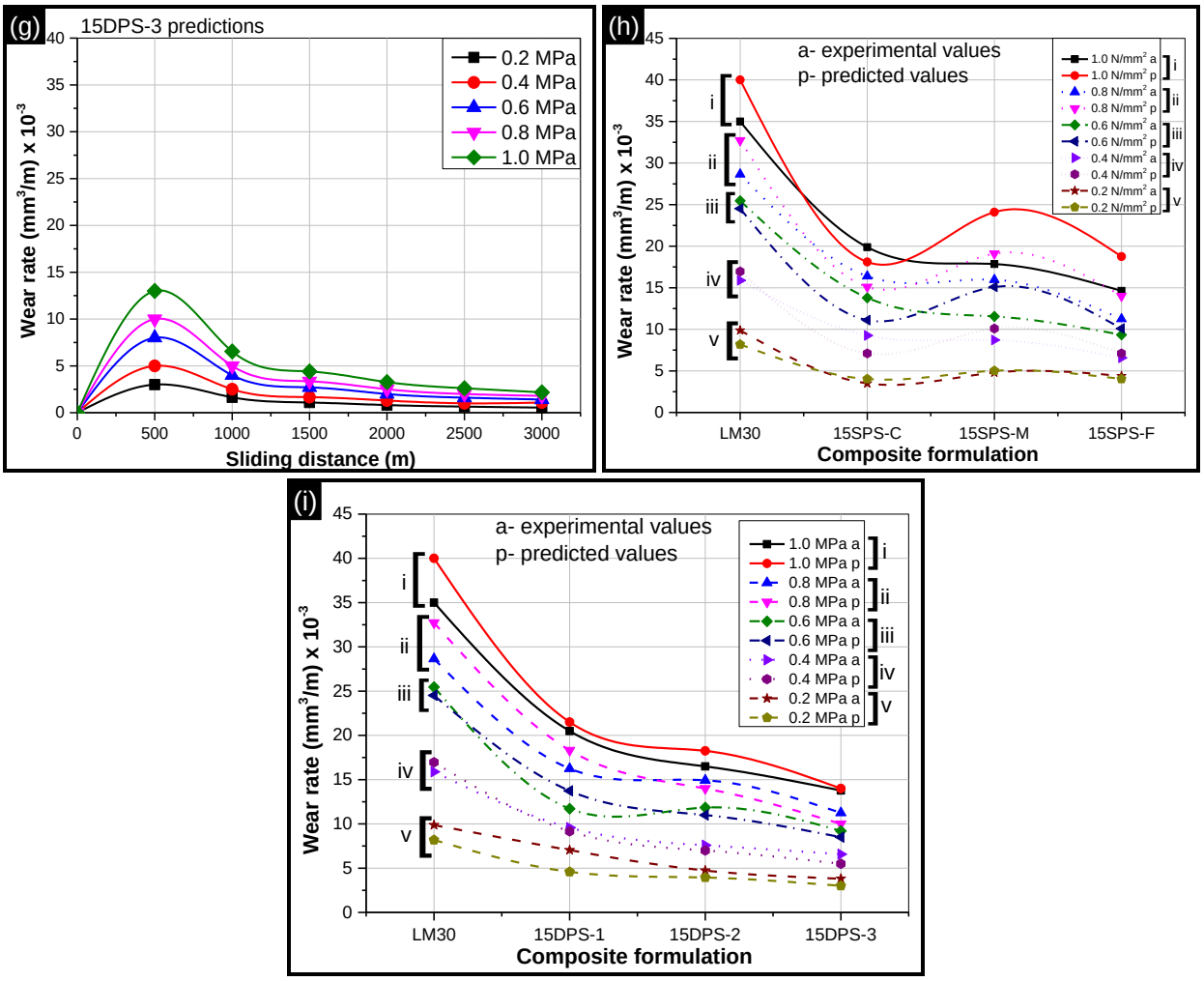

Figure 4.25 Predictions of wear rate against sliding distance at different contact pressure for (a) LM30 base alloy, (b) 15SPS-F, (c) 15SPS-M, (d) 15SPS-F, (e) 15DPS-1, (f) 15DPS-2, (g) 15DPS-3, (h) comparison of experimental and predicted maximum wear rate for single particle reinforced AMCs, and (i) comparison of experimental and predicted maximum wear rate for dual particle reinforced AMCs

4.6 FRICTION TESTING

Figure 4.26 and Figure 4.27 present the coefficient of friction (COF) values for base alloy and various AMCs. For any contact pressure, the base alloy (LM30) showed maximum COF value and the dual particle reinforced composite (15DPS-3) showed minimum value. For the base alloy, the interaction of alloy surface with steel disc at asperities level is relatively more as compared to that in composites (because of the absence of the hard mineral reinforcement in the base alloy). As a result, steel disc asperities dig more into the base alloy surface as compared to

composites. More is the digging, more is the frictional force required to keep the counter surfaces in motion, and hence higher is the COF value.

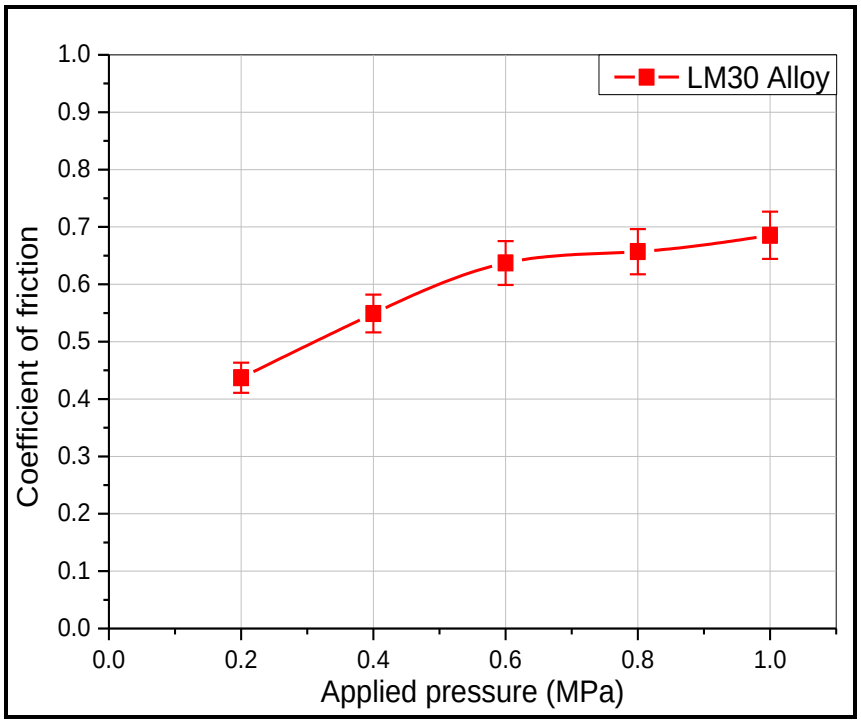

Figure 4.26 Coefficient of friction of LM30 base alloy at different contact pressures

Figure 4.27 presents the COF values for different composite formulations. In case of composites, presence of mineral particles results in two main effects: (a) mineral reinforcement improves hardness of the alloy matrix, and (b) the hard reinforced particles also interact with the steel disc, in addition to interaction of alloy matrix with steel disc. This means that in composites, there is a decrease in the matrix to steel disc surface contact ratio, as compared to base alloy. Due to a decrease in this ratio, few junction points are created from where the shearing starts during sliding. These effects help in increasing the load bearing capacity of the composite surface more effectively and reduce the digging depth on the composite surface due to steel disc asperities. As digging is less, frictional force and hence COF value is less in composites [175,187].

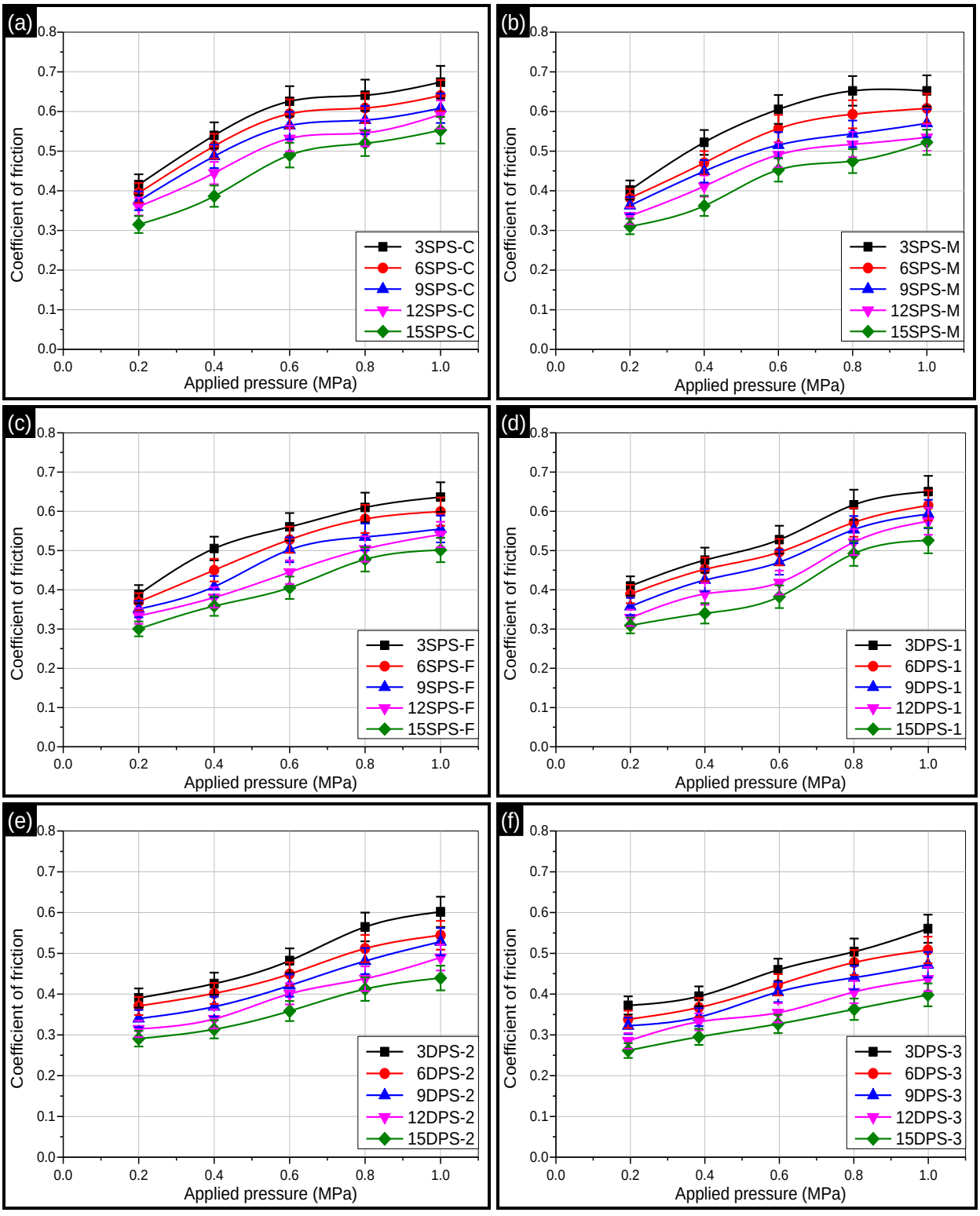

Figure 4.27 Coefficient of friction values for various AMCs (a) SPS-C, (b) SPS-M, (c) SPS-F, (d) DPS-1, (e) DPS-2, and (f) DPS-3 composites under different contact pressures

It was observed that COF values of composites decreased with increase in sillimanite weight percentage. Further, a decrement in COF was also observed with decrease in particle size. Also, for dual particle reinforced AMCs, decrease in COF values was observed with increase in proportion of fine particles in the dual particle size mixture. Maximum reduction in COF was obtained in 15DPS-3 composite (42% less compared to base alloy). Table 4.5 presents the reduction in COF values obtained for various AMCs containing 15 wt.% reinforcement.

Table 4.5 Reduction in COF values of AMCs over the base alloy

S. No.	Type of AMC	Percentage reduction in COF values (%)
1.	15SPS-C	20
2.	15SPS-M	24
3.	15SPS-F	28
4.	15DPS-1	24
5.	15DPS-2	36
6.	15DPS-3	42

4.7 WEAR TRACK AND WEAR DEBRIS ANALYSIS

4.7.1 LM30 BASE ALLOY

Figure 4.28a–d presents the wear track and wear debris for LM30 base alloy under the extreme contact pressure conditions of 0.2 MPa and 1 MPa respectively. Abrasive grooves with some delaminated areas can be observed for the wear track at 0.2 MPa (Figure 4.28a). For the contact pressure of 1MPa, wider grooves with larger delaminated areas were observed. During the initial period of run, the asperities of countersurfaces are in relative motion against each other. This leads to generation of high stresses on asperity contact, thereby causing microcutting and microplowing action [173,174]. Under the combined action of sliding distance and contact pressure, the microplowing action is converted to abrasive grooves. The sharp asperities act as stress concentration points and get plastically deformed in the process. The stress concentration causes the asperities to fracture, and thus, an increase in wear rate is observed [159]. Under even higher contact pressures (here, 1 MPa), the larger frictional resistance between countersurfaces results in higher increase in temperature which causes mechanical welding of pin with the disc resulting in greater plastic deformation and tearing of material causing wider grooves and larger delamination areas. Large delaminated area indicates higher wear rate under the given testing condition [188]. The formation of crater pattern on the pin surface is the evidence of wear by delamination [189].

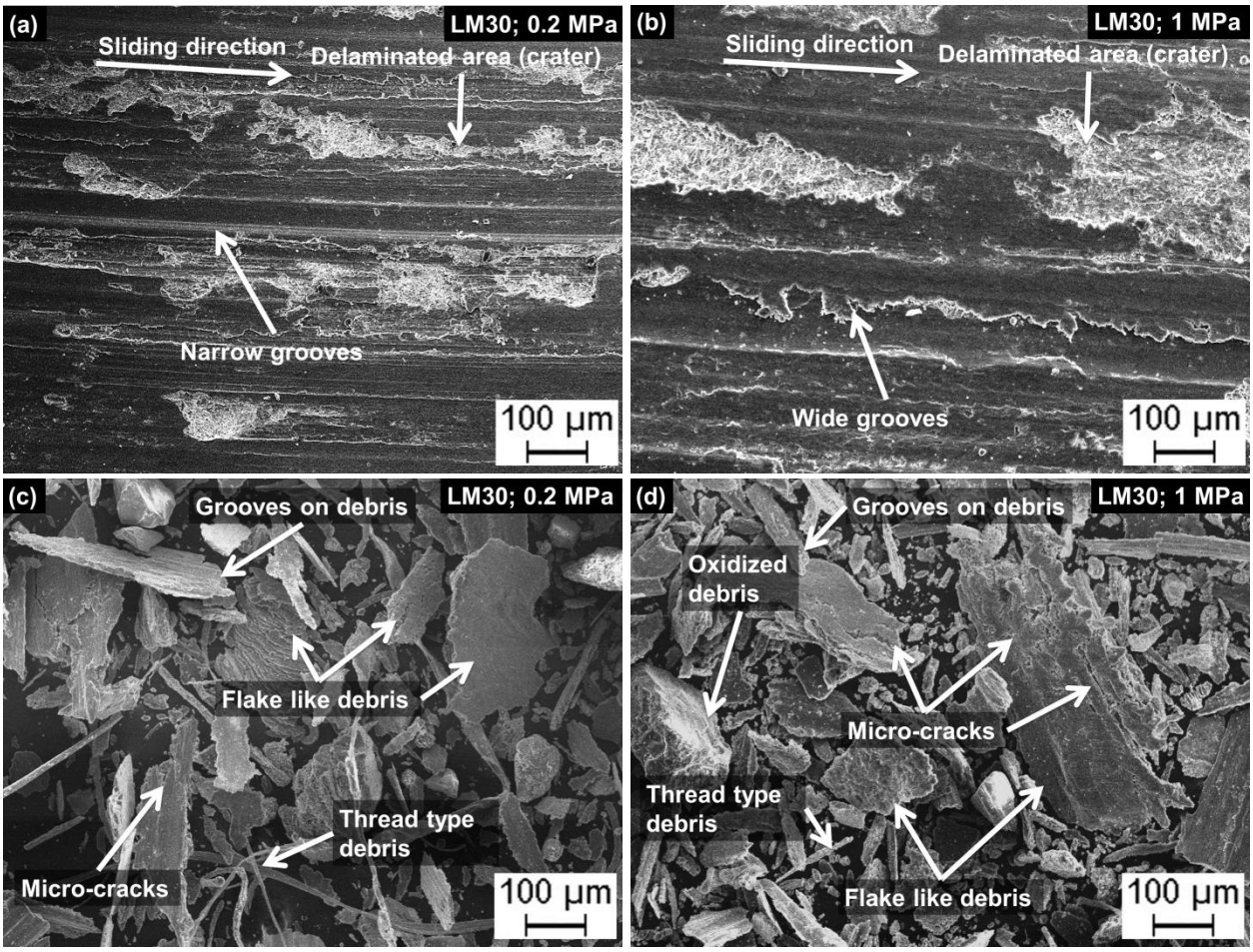

Figure 4.28 Wear track and wear debris analysis of base alloy (a) wear track at 0.2 MPa, (b) wear track at 1MPa, (c) wear debris at 0.2 MPa, and (d) wear debris at 1 MPa

Flake like debris were majorly observed for base alloy tested at 0.2 MPa and 1 MPa respectively (Figure 4.28c–d). The grooves on flake like debris are a representative of the abrasive wear mechanism at the initial stages of the run. Further, for longer sliding distances, the adhesive/delamination wear mechanism was dominant. Apart from this feature, several micro-cracks were also observed in the wear debris indicating removal of material by delamination (Figure 4.28c–d). This indicated that the initial abrasive wear mechanism (mainly because of micro-ploughing action) was followed by adhesive wear mechanism (due to formation of micro cracks) [92]. Oxides were also observed on the debris. The constant sliding increases the contact temperature between countersurfaces and causes oxidation of the debris. The presence of oxide

layer between the surface of sample and countersurface improves the wear resistance of the materials, as they avoid direct metal-to-metal contact between the surfaces [190].

4.7.2 COMPOSITE FORMULATIONS

Figure 4.29 to 4.33 present the SEM micrographs of wear track of 3 wt.%, 6 wt.%, 9 wt.%, 12 wt.%, and 15 wt.% sillimanite reinforced AMCs obtained for conditions of 0.2 MPa and 1 MPa respectively. For the contact pressure of 0.2 MPa, narrow grooves running along the sliding direction having some delaminated area were observed on the worn-out pin surface as shown in Figure 4.29(a, c, e, g, i, k), Figure 4.30(a, c, e, g, i, k), Figure 4.31(a, c, e, g, i, k), Figure 4.32(a, c, e, g, i, k), and Figure 4.33(a, c, e, g, i, k). However, for the higher contact pressure (1 MPa), wider grooves with larger delamination area on the worn-out pin surface were observed as shown in Figure 4.29(b, d, f, h, j, l), Figure 4.30(b, d, f, h, j, l), Figure 4.31(b, d, f, h, j, l), Figure 4.32(b, d, f, h, j, l), and Figure 4.33(b, d, f, h, j, l)). As reported earlier, abrasive grooves were the result of initial microploughing action created by the asperities. At low contact pressure (0.2 MPa), the ploughing action was low, and thus, smaller abrasive grooves were observed. However, at higher contact pressure (1 MPa), the asperities deformed and their sharpness decreased, causing formation of wider abrasive grooves. The continuous sliding led to generation of frictional heat and caused localized melting and welding of countersurfaces. Due to the action of sliding, these welds were broken and tearing of material took place. This tearing led to generation and propagation of microcracks on the pin surface as shown in Figure 4.31f, Figure 4.32l, and Figure 4.33(f, h). Hence, removal of material took place in the form of delamination. Higher contact pressure increased frictional heating, and thus, the delamination phenomenon increased. Also, the constant sliding action caused the compaction and grinding of debris. A few debris were observed to be embedded in the pin surface as can be observed in Figure 4.30(e, h, j, k, l), Figure 4.31(c, j, k), Figure 4.32(d, i), and Figure 4.33(d, i). As the sliding distance increased, the debris (containing countersurface materials and sillimanite particles) got fractured. Sillimanite particles carry a major portion of the contact pressure, get fractured and removed from the matrix resulting in formation of fractured particles as shown in Figure 4.30(g, h). Further, a few debris were observed to be entrapped in the delaminated areas of the worn-out pin surface as shown in Figure 4.33b.

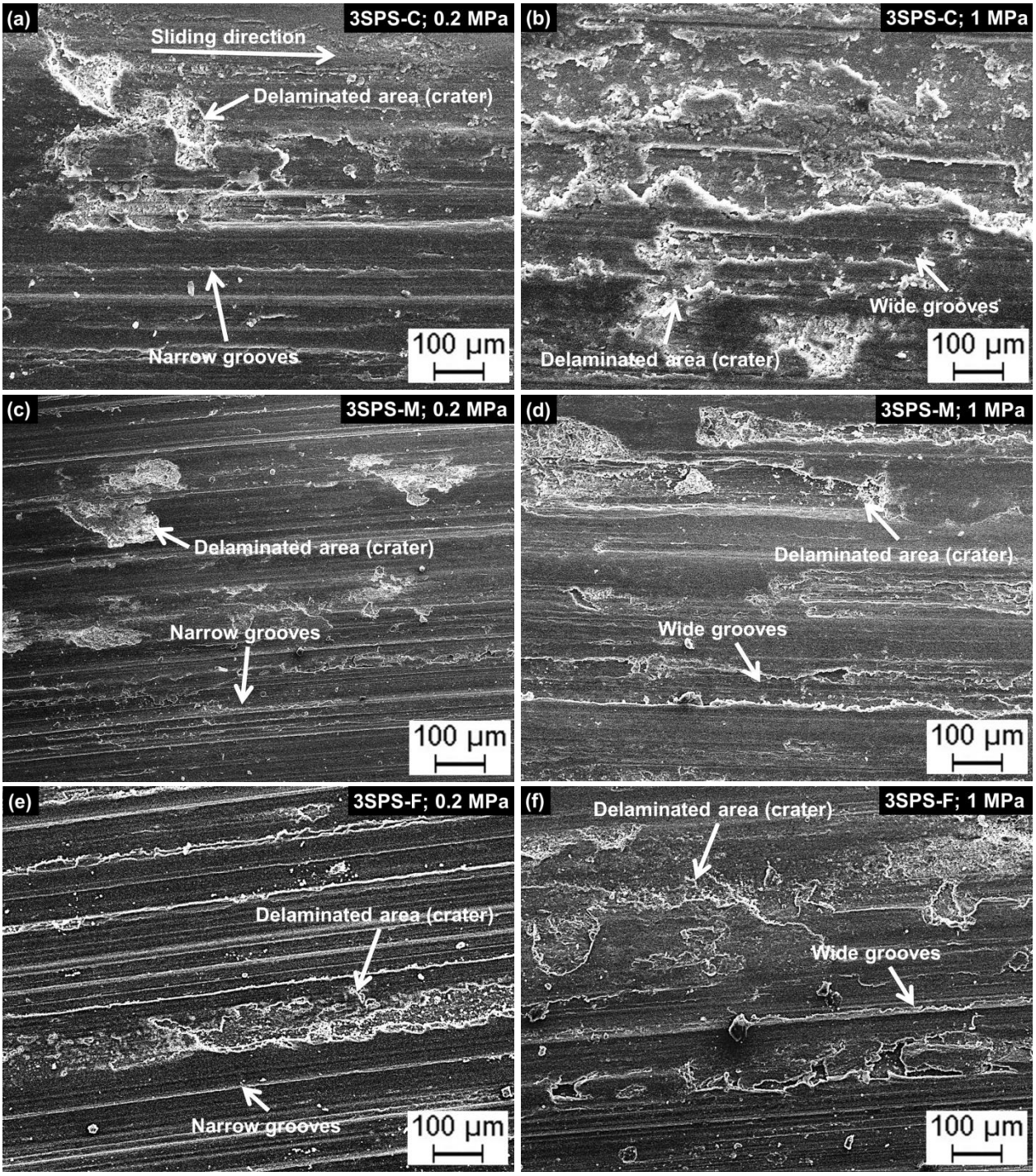
(a)
3SPS-C; 0.2 MPa
Sliding direction
Delaminated area (crater)
Narrow grooves
100 μm
(b)
3SPS-C; 1 MPa
Wide grooves
Delaminated area (crater)
100 μm
(c)
3SPS-M; 0.2 MPa
Delaminated area (crater)
Narrow grooves
100 μm
(d)
3SPS-M; 1 MPa
Delaminated area (crater)
Wide grooves
100 μm
(e)
3SPS-F; 0.2 MPa
Delaminated area (crater)
Narrow grooves
100 μm
(f)
3SPS-F; 1 MPa
Delaminated area (crater)
Wide grooves
100 μm

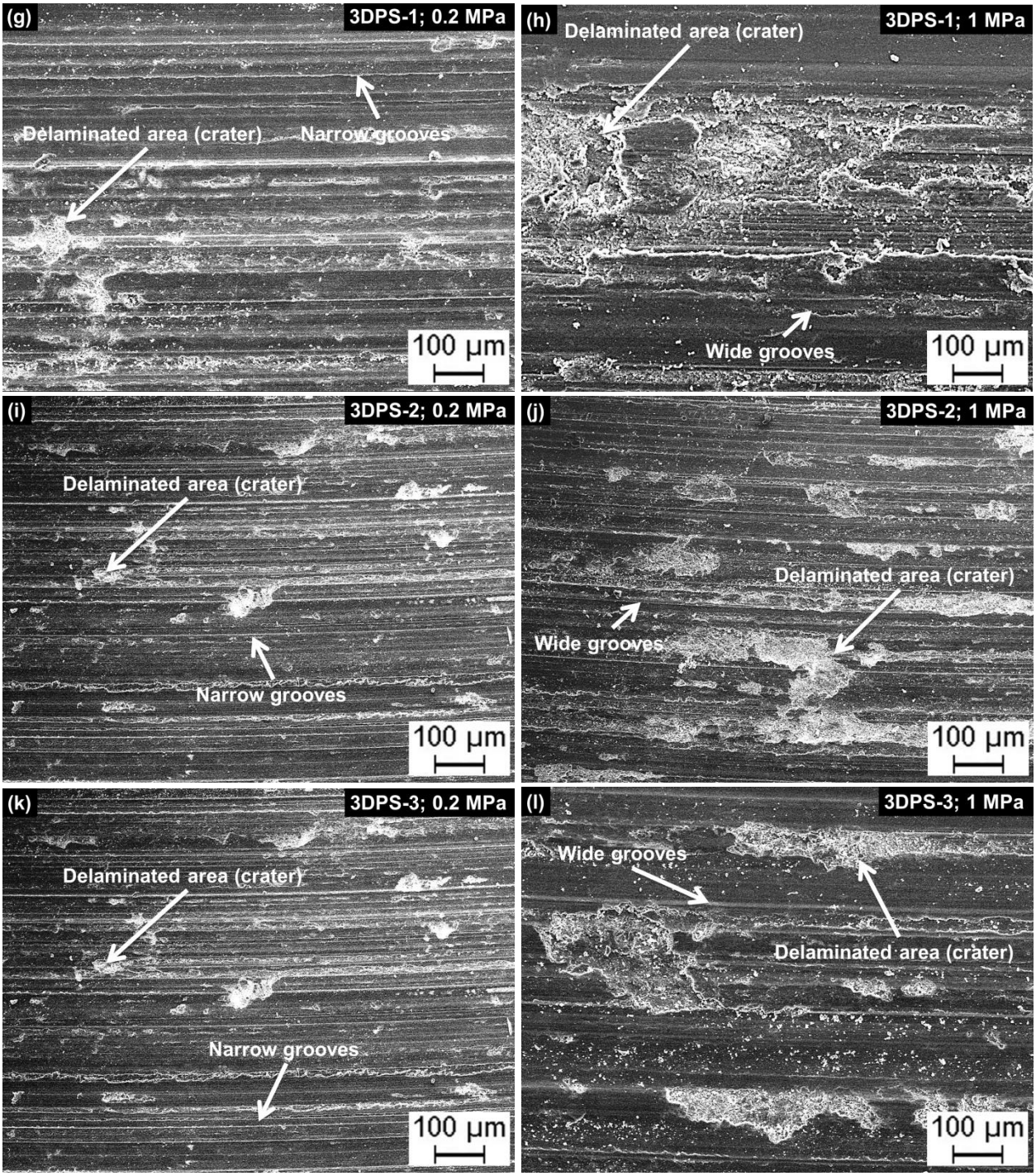

Figure 4.29 SEM micrographs of wear tracks of (a) 3SPS-C composite at 0.2 MPa, (b) 3SPS-C composite at 1 MPa, (c) 3SPS-M composite at 0.2 MPa, (d) 3SPS-M composite at 1 MPa, (e) 3SPS-F composite at 0.2 MPa, (f) 3SPS-F composite at 1 MPa, (g) 3DPS-1 composite at 0.2 MPa, (h) 3DPS-1 composite at 1 MPa, (i) 3DPS-2 composite at 0.2 MPa, (j) 3DPS-2 composite at 1 MPa, (k) 3DPS-3 composite at 0.2 MPa, and (l) 3DPS-3 composite at 1 MPa

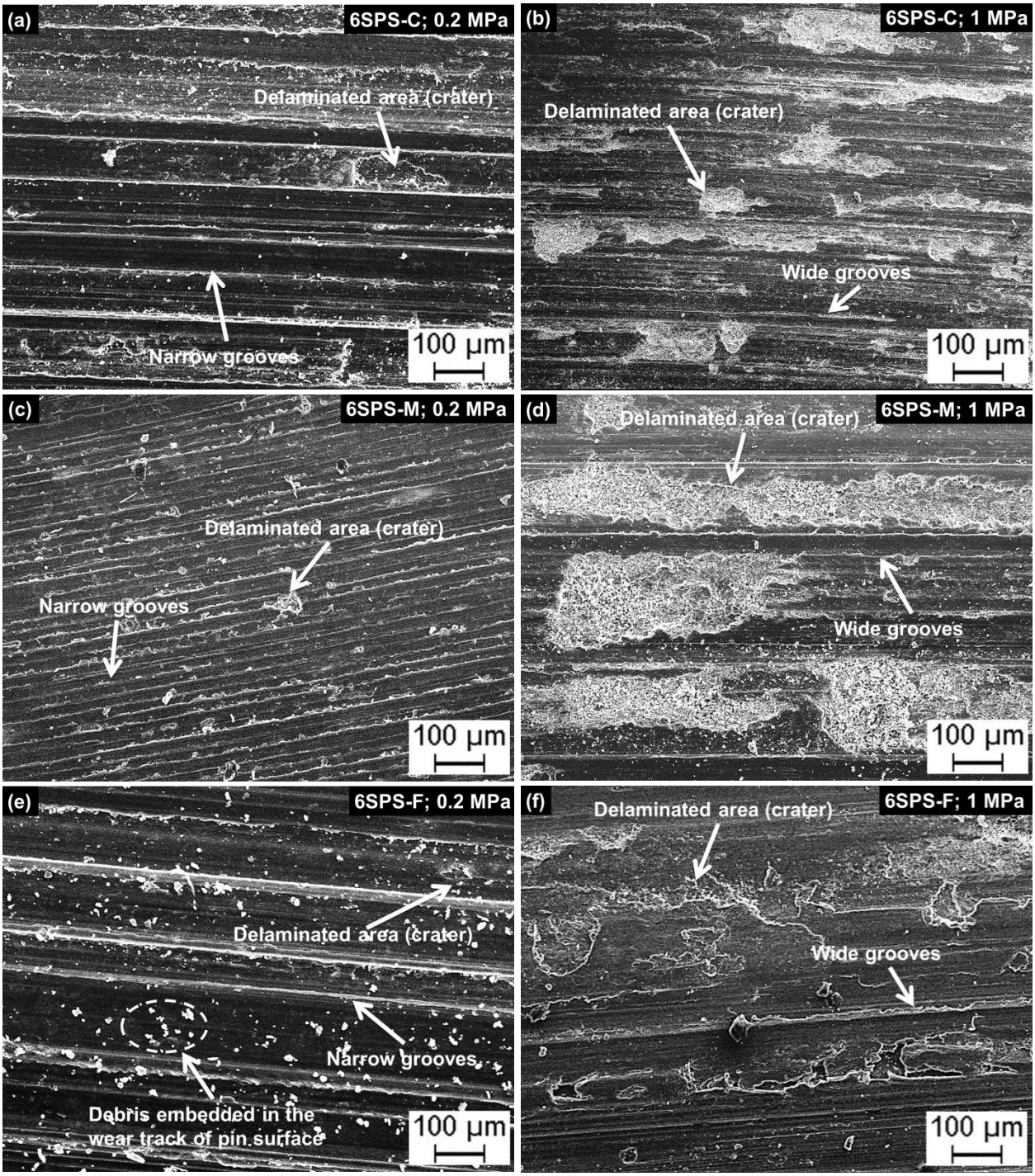
(a)
6SPS-C; 0.2 MPa
Delaminated area (crater)
Narrow grooves
100 µm
(b)
6SPS-C; 1 MPa
Delaminated area (crater)
Wide grooves
100 µm
(c)
6SPS-M; 0.2 MPa
Delaminated area (crater)
Narrow grooves
100 µm
(d)
Delaminated area (crater)
6SPS-M; 1 MPa
Wide grooves
100 µm
(e)
6SPS-F; 0.2 MPa
Delaminated area (crater)
Narrow grooves
Debris embedded in the wear track of pin surface
100 µm
(f)
Delaminated area (crater)
6SPS-F; 1 MPa
Wide grooves
100 µm

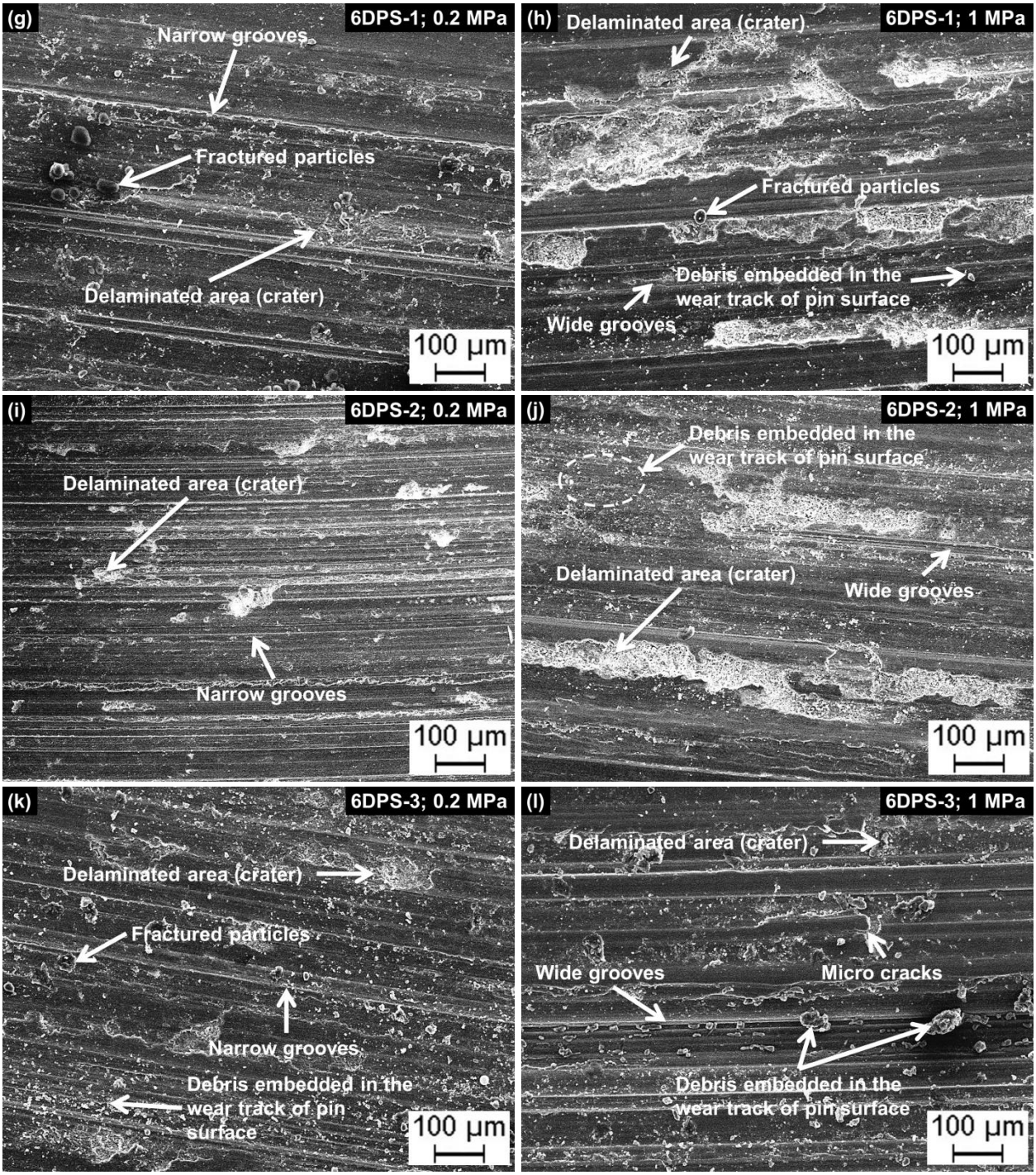

Figure 4.30 SEM micrographs of wear tracks of (a) 6SPS-C composite at 0.2 MPa, (b) 6SPS-C composite at 1 MPa, (c) 6SPS-M composite at 0.2 MPa, (d) 6SPS-M composite at 1 MPa, (e) 6SPS-F composite at 0.2 MPa, (f) 6SPS-F composite at 1 MPa, (g) 6DPS-1 composite at 0.2 MPa, (h) 6DPS-1 composite at 1 MPa, (i) 6DPS-2 composite at 0.2 MPa, (j) 6DPS-2 composite at 1 MPa, (k) 6DPS-3 composite at 0.2 MPa, and (l) 6DPS-3 composite at 1 MPa

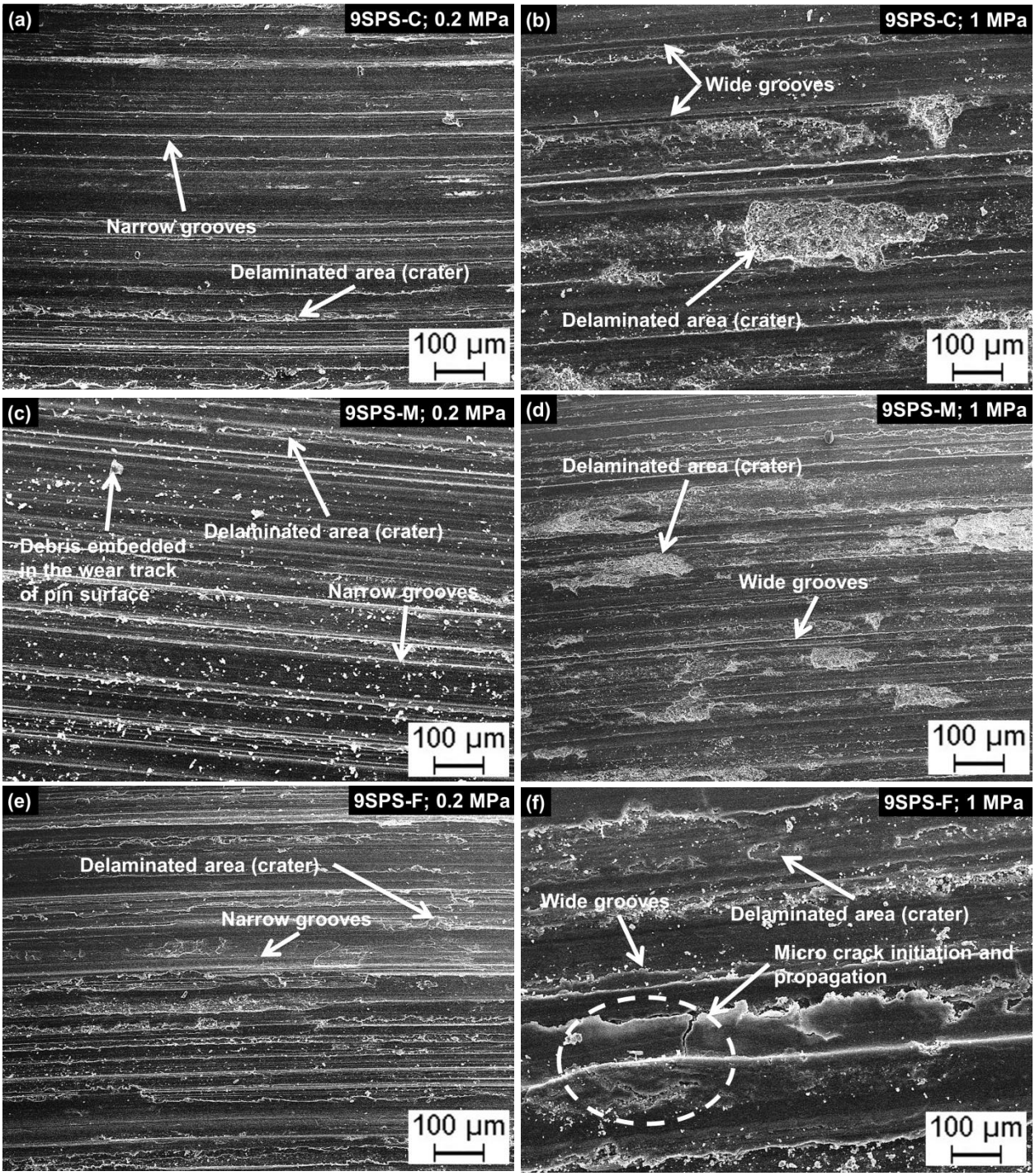
(a)
9SPS-C; 0.2 MPa
Narrow grooves
Delaminated area (crater)
100 µm
(b)
9SPS-C; 1 MPa
Wide grooves
Delaminated area (crater)
100 µm
(c)
9SPS-M; 0.2 MPa
Debris embedded in the wear track of pin surface
Delaminated area (crater)
Narrow grooves
100 µm
(d)
9SPS-M; 1 MPa
Delaminated area (crater)
Wide grooves
100 µm
(e)
9SPS-F; 0.2 MPa
Delaminated area (crater)
Narrow grooves
100 µm
(f)
9SPS-F; 1 MPa
Wide grooves
Delaminated area (crater)
Micro crack initiation and propagation
100 µm

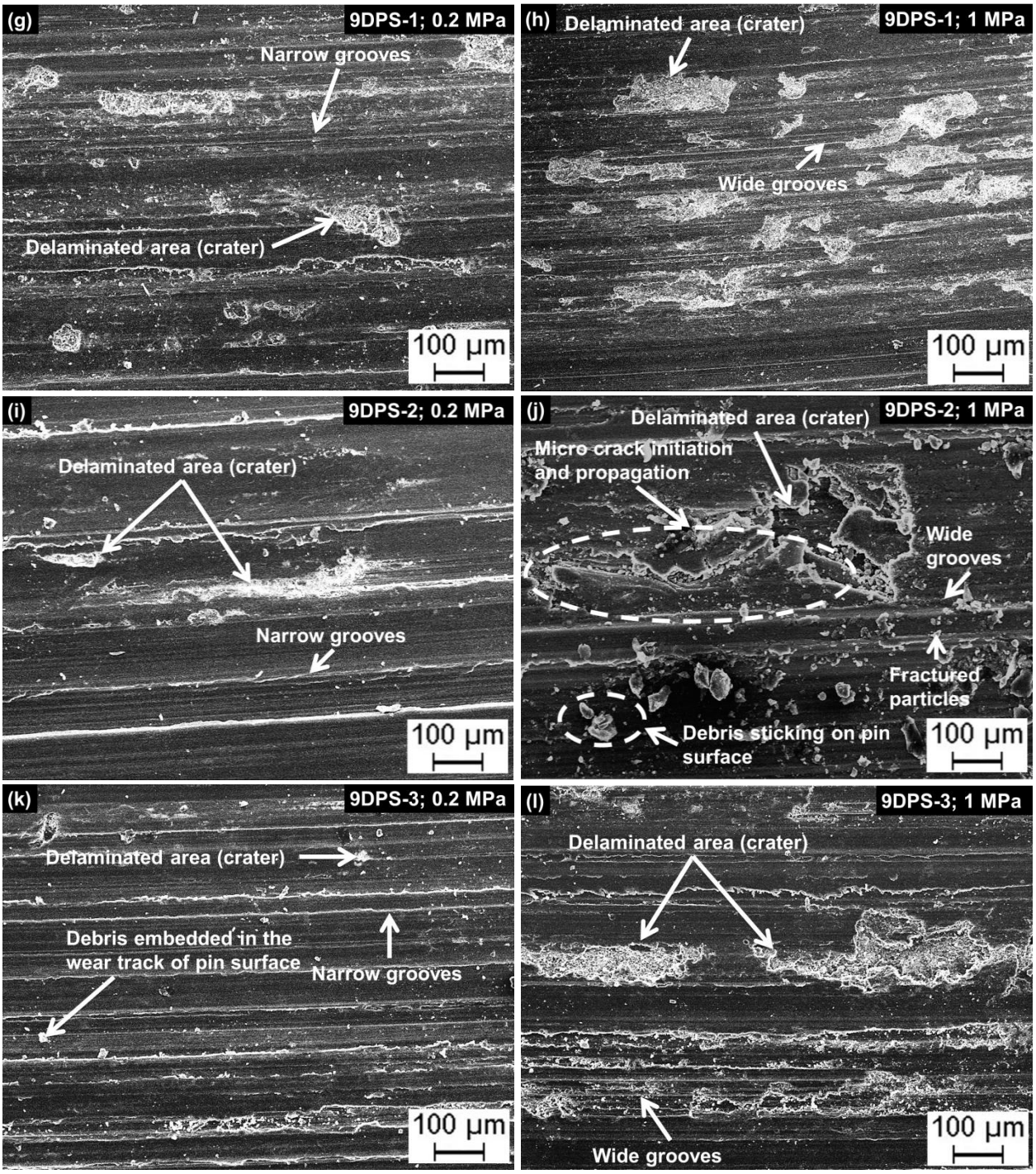

Figure 4.31 SEM micrographs of wear tracks of (a) 9SPS-C composite at 0.2 MPa, (b) 9SPS-C composite at 1 MPa, (c) 9SPS-M composite at 0.2 MPa, (d) 9SPS-M composite at 1 MPa, (e) 9SPS-F composite at 0.2 MPa, (f) 9SPS-F composite at 1 MPa, (g) 9DPS-1 composite at 0.2 MPa, (h) 9DPS-1 composite at 1 MPa, (i) 9DPS-2 composite at 0.2 MPa, (j) 9DPS-2 composite at 1 MPa, (k) 9DPS-3 composite at 0.2 MPa, and (l) 9DPS-3 composite at 1 MPa

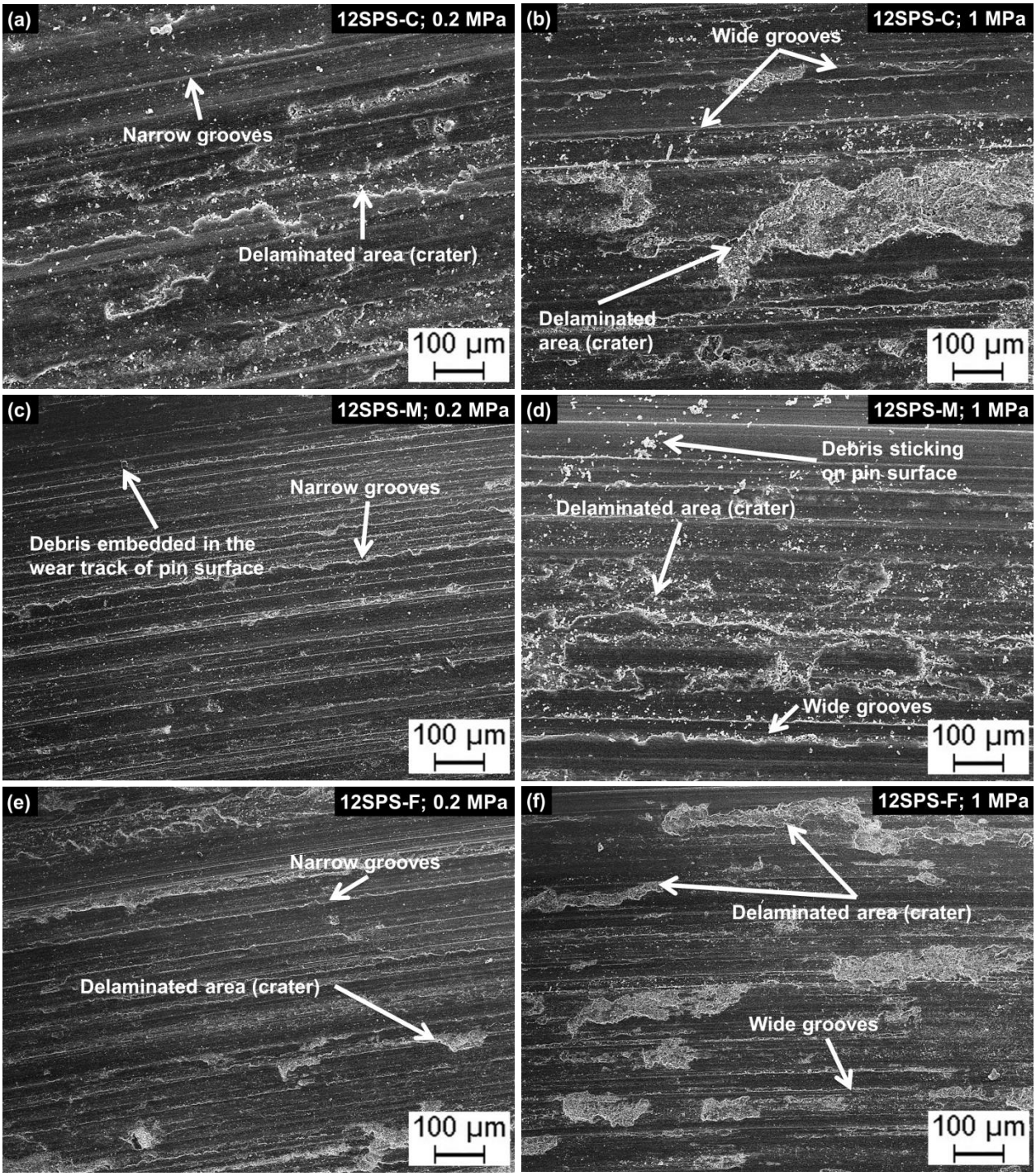
(a)
12SPS-C; 0.2 MPa
Narrow grooves
Delaminated area (crater)
100 µm
(b)
12SPS-C; 1 MPa
Wide grooves
Delaminated area (crater)
100 µm
(c)
12SPS-M; 0.2 MPa
Narrow grooves
Debris embedded in the wear track of pin surface
100 µm
(d)
12SPS-M; 1 MPa
Debris sticking on pin surface
Delaminated area (crater)
Wide grooves
100 µm
(e)
12SPS-F; 0.2 MPa
Narrow grooves
Delaminated area (crater)
100 µm
(f)
12SPS-F; 1 MPa
Delaminated area (crater)
Wide grooves
100 µm

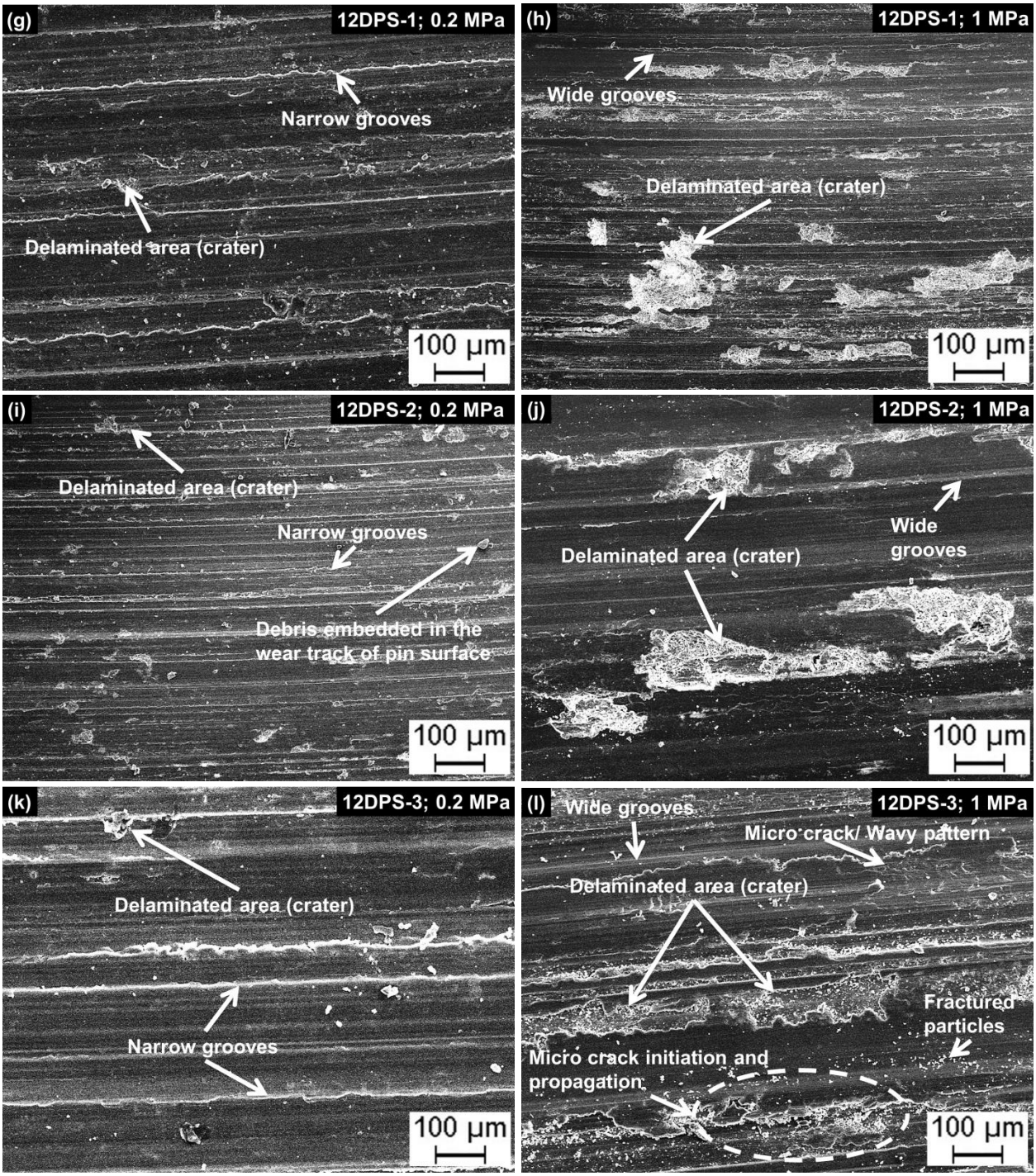

Figure 4.32 SEM micrographs of wear tracks of (a) 12SPS-C composite at 0.2 MPa, (b) 12SPS-C composite at 1 MPa, (c) 12SPS-M composite at 0.2 MPa, (d) 12SPS-M composite at 1 MPa, (e) 12SPS-F composite at 0.2 MPa, (f) 12SPS-F composite at 1 MPa, (g) 12DPS-1 composite at 0.2 MPa, (h) 12DPS-1 composite at 1 MPa, (i) 12DPS-2 composite at 0.2 MPa, (j) 12DPS-2 composite at 1 MPa, (k) 12DPS-3 composite at 0.2 MPa, and (l) 12DPS-3 composite at 1 MPa

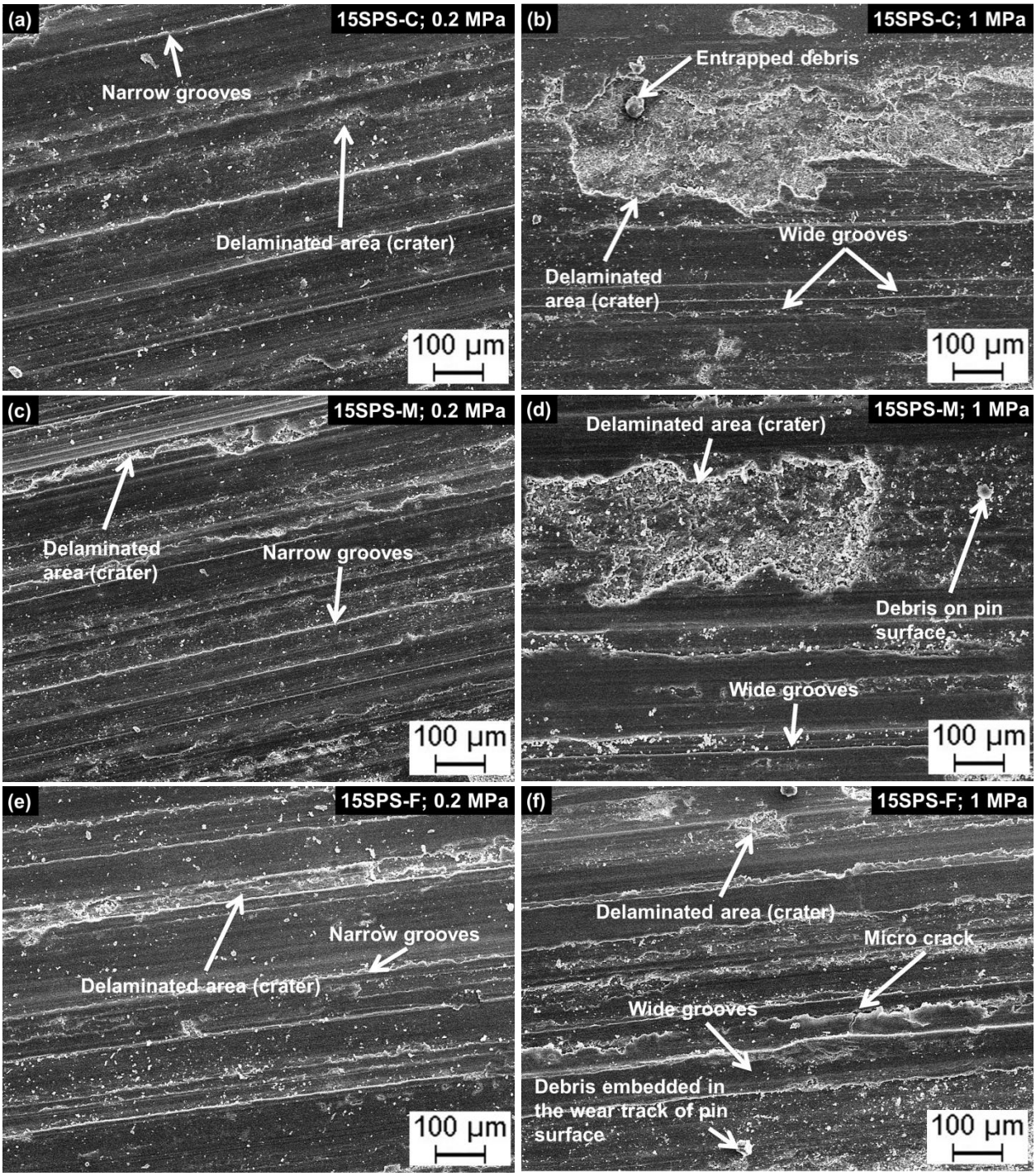
(a)
15SPS-C; 0.2 MPa
Narrow grooves
Delaminated area (crater)
100 µm
(b)
15SPS-C; 1 MPa
Entrapped debris
Delaminated area (crater)
Wide grooves
100 µm
(c)
15SPS-M; 0.2 MPa
Delaminated area (crater)
Narrow grooves
100 µm
(d)
15SPS-M; 1 MPa
Delaminated area (crater)
Debris on pin surface
Wide grooves
100 µm
(e)
15SPS-F; 0.2 MPa
Narrow grooves
Delaminated area (crater)
100 µm
(f)
15SPS-F; 1 MPa
Delaminated area (crater)
Micro crack
Wide grooves
Debris embedded in the wear track of pin surface
100 µm

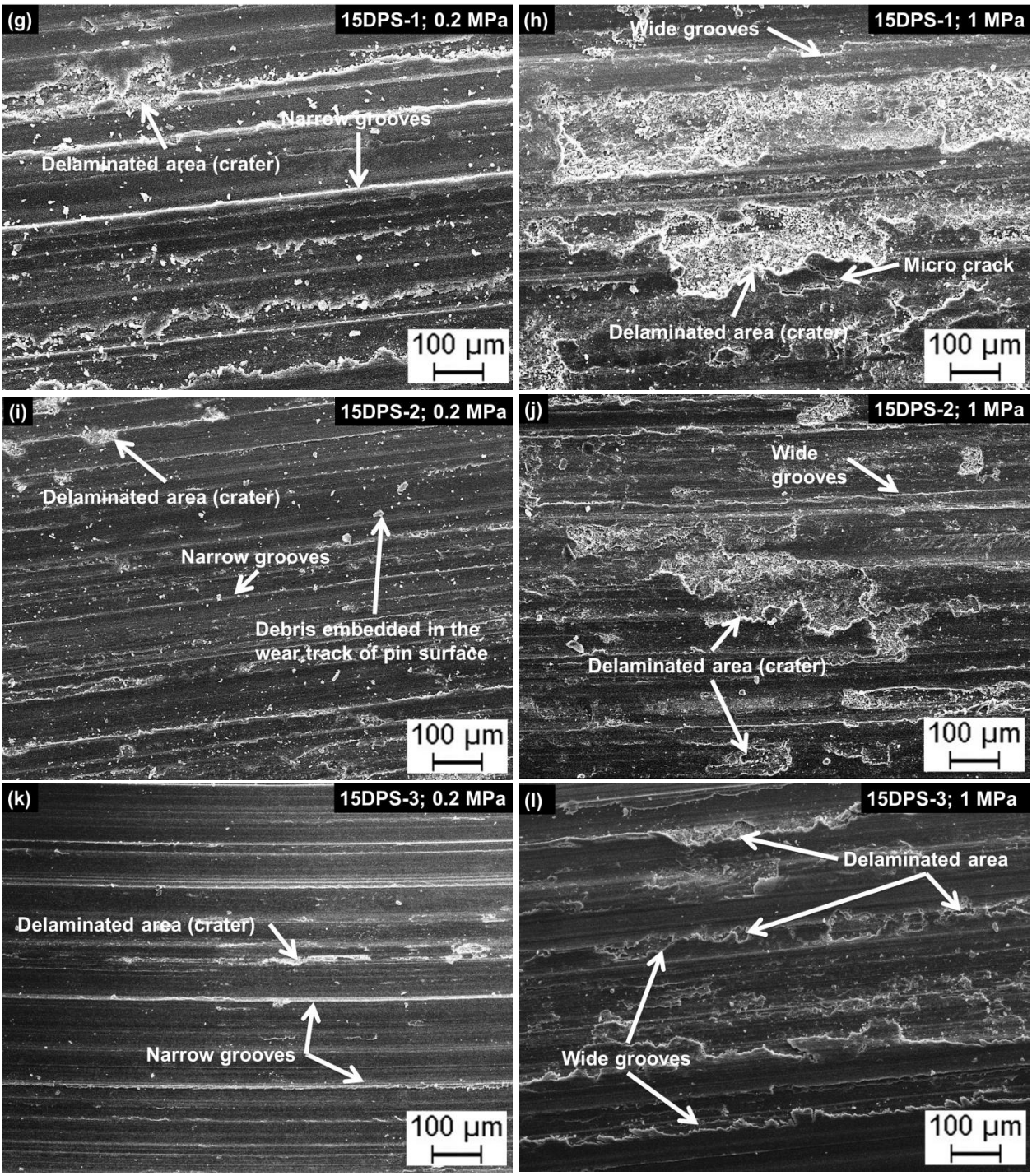

Figure 4.33 SEM micrographs of wear tracks of (a) 15SPS-C composite at 0.2 MPa, (b) 15SPS-C composite at 1 MPa, (c) 15SPS-M composite at 0.2 MPa, (d) 15SPS-M composite at 1 MPa, (e) 15SPS-F composite at 0.2 MPa, (f) 15SPS-F composite at 1 MPa, (g) 15DPS-1 composite at 0.2 MPa, (h) 15DPS-1 composite at 1 MPa, (i) 15DPS-2 composite at 0.2 MPa, (j) 15DPS-2 composite at 1 MPa, (k) 15DPS-3 composite at 0.2 MPa, and (l) 15DPS-3 composite at 1 MPa

Figure 4.34 to 4.38 present the SEM micrographs of wear debris of 3 wt.%, 6 wt.%, 9 wt.%, 12 wt.%, and 15 wt.% sillimanite reinforced AMCs at 0.2 MPa and 1 MPa respectively. It was observed that majorly the debris were flake like with grooves present on some of the debris (Figure 4.34 to 4.38). The grooves visible on debris were due to microploughing action and indicated the abrasive nature of wear in the initial stages [92]. Further, micro-cut debris were observed which form as a result of microploughing action of asperities on the countersurfaces. Micro-cut debris were observed in Figure 4.34b, Figure 4.35(c, j), Figure 4.36a, and Figure 4.37g. Several micro cracks were also observed on wear debris. Micro cracks indicated the removal of material by delamination (Figure 4.34 to 4.38). This indicated that the initial abrasive wear mechanism (mainly because of microploughing action) was followed by adhesive wear mechanism (due to formation of micro-cracks leading to delamination). Twisted and layered debris (corrugated structured debris) were also visible as shown in Figure 4.34e, Figure 4.35(c, g, h, j), Figure 4.36(a, c, f, g, h, j), Figure 4.37(a, c, d, e, f, j, k), and Figure 4.38(a, d, h, I, l). This indicated repetitive nature of stress due to continuous rubbing action occurring under constant load sliding conditions [159]. Further, the constant sliding during wear test of AMCs increased the contact temperature of countersurfaces and led to formation of oxides on the debris (oxide debris) as shown in Figure 4.34(d, h, j, k), Figure 4.35(d, h, k), Figure 4.36b, and Figure 4.37(a, g, h, j). Moreover, the constant sliding under various contact pressure conditions lead to localized melting resulting in the appearance of molten debris [160]. These are shown in Figure 4.34(a, d, f, g, h, i, j), Figure 4.36(b, e), Figure 4.37(i, j), and Figure 4.38(b, c, h, i). Thread type debris were also observed indicating pull out of ductile material from the pin surface (Figure 4.34 to 4.38). Also, the fracturing of debris was observed. The fracturing of debris occurred due to entrapment of debris between the specimen and counter surface [160]. Fractured debris were observed as marked in Figure 4.38(f, l).

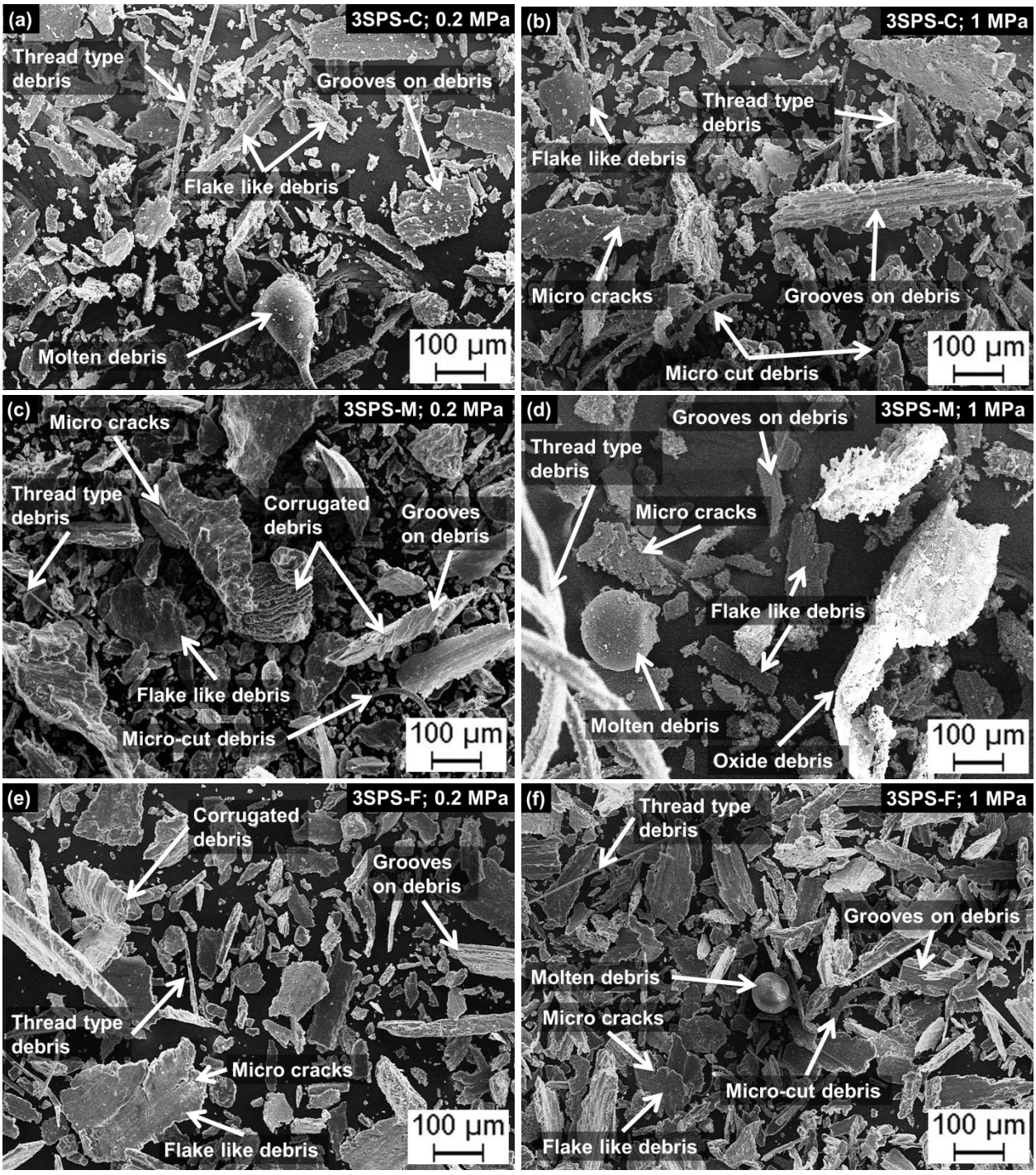
(a)
3SPS-C; 0.2 MPa
Thread type debris
Grooves on debris
Flake like debris
Molten debris
100 µm
(b)
3SPS-C; 1 MPa
Thread type debris
Flake like debris
Micro cracks
Grooves on debris
Micro cut debris
100 µm
(c)
3SPS-M; 0.2 MPa
Micro cracks
Thread type debris
Corrugated debris
Grooves on debris
Flake like debris
Micro-cut debris
100 µm
(d)
3SPS-M; 1 MPa
Grooves on debris
Thread type debris
Micro cracks
Flake like debris
Molten debris
Oxide debris
100 µm
(e)
3SPS-F; 0.2 MPa
Corrugated debris
Grooves on debris
Thread type debris
Micro cracks
Flake like debris
100 µm
(f)
3SPS-F; 1 MPa
Thread type debris
Grooves on debris
Molten debris
Micro cracks
Micro-cut debris
Flake like debris
100 µm

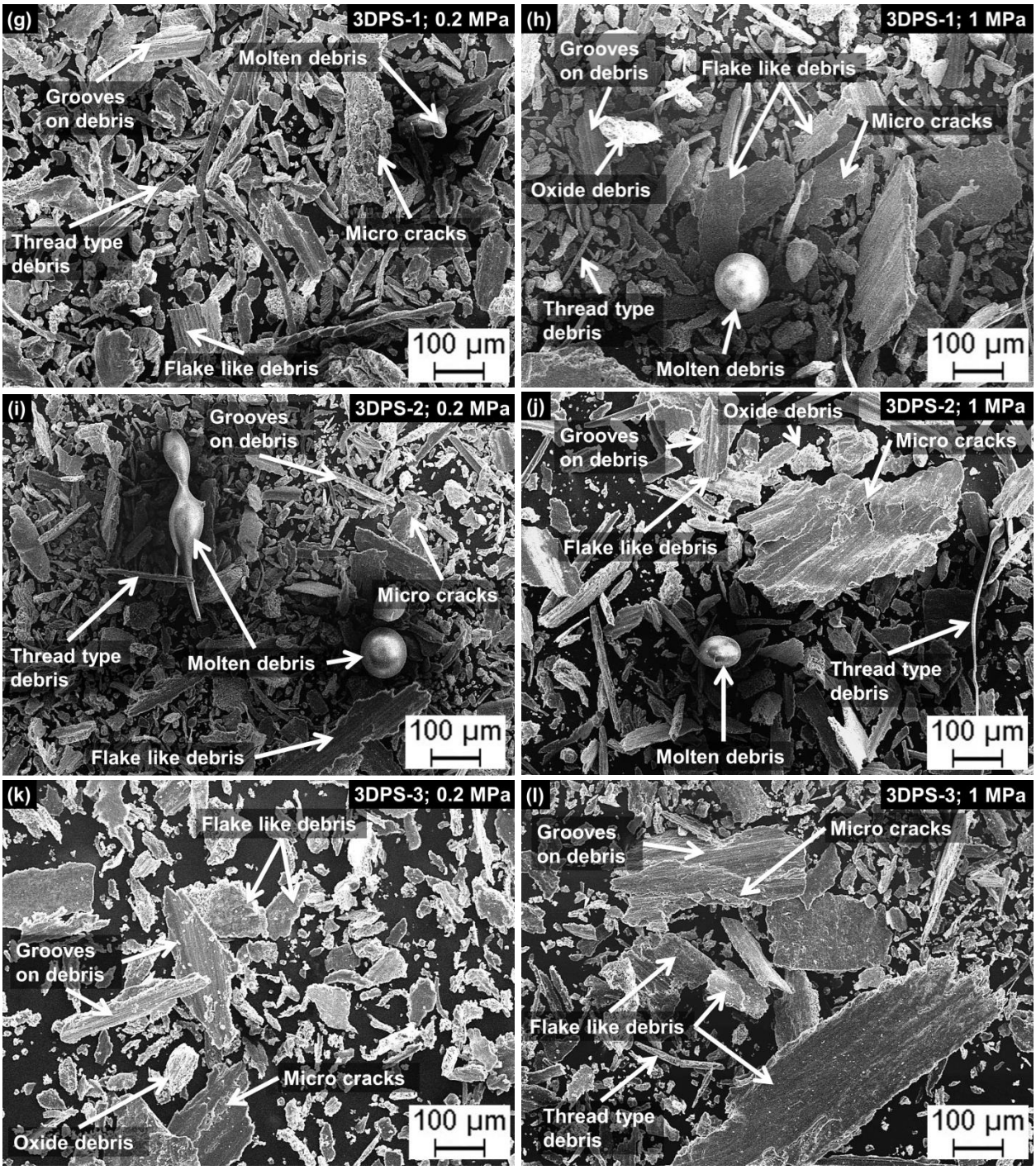

Figure 4.34 SEM micrographs of wear debris of (a) 3SPS-C at 0.2 MPa, (b) 3SPS-C composite at 1 MPa, (c) 3SPS-M composite at 0.2 MPa, (d) 3SPS-M composite at 1 MPa, (e) 3SPS-F composite at 0.2 MPa, (f) 3SPS-F composite at 1 MPa, (g) 3DPS-1 composite at 0.2 MPa, (h) 3DPS-1 composite at 1 MPa, (i) 3DPS-2 composite at 0.2 MPa, (j) 3DPS-2 composite at 1 MPa, (k) 3DPS-3 composite at 0.2 MPa, and (l) 3DPS-3 composite at 1 MPa

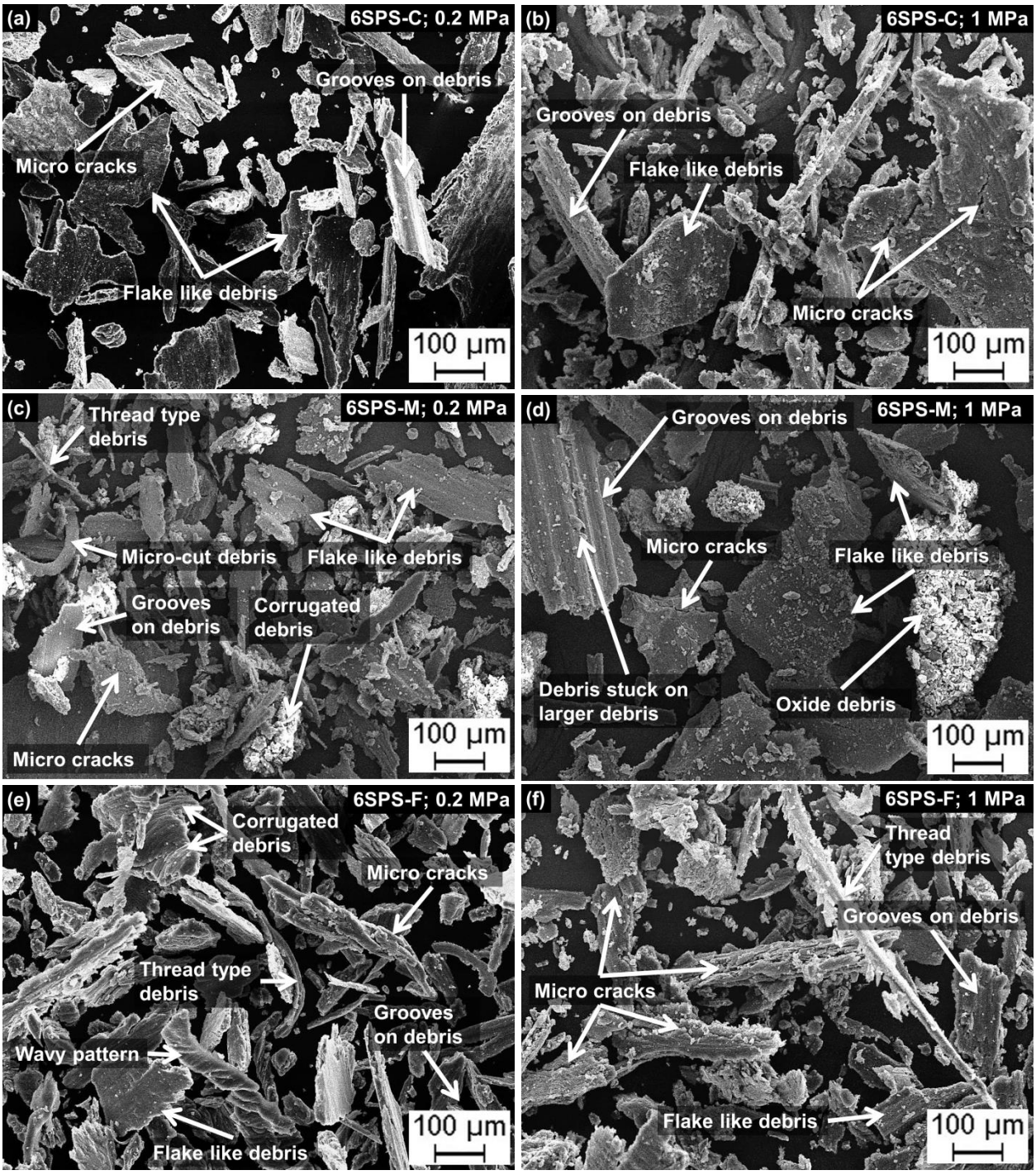
(a)
6SPS-C; 0.2 MPa
Grooves on debris
Micro cracks
Flake like debris
100 µm
(b)
6SPS-C; 1 MPa
Grooves on debris
Flake like debris
Micro cracks
100 µm
(c)
6SPS-M; 0.2 MPa
Thread type debris
Micro-cut debris
Flake like debris
Grooves on debris
Corrugated debris
Micro cracks
100 µm
(d)
6SPS-M; 1 MPa
Grooves on debris
Micro cracks
Flake like debris
Debris stuck on larger debris
Oxide debris
100 µm
(e)
6SPS-F; 0.2 MPa
Corrugated debris
Micro cracks
Thread type debris
Grooves on debris
Wavy pattern
Flake like debris
100 µm
(f)
6SPS-F; 1 MPa
Thread type debris
Grooves on debris
Micro cracks
Flake like debris
100 µm

Figure 4.35 SEM micrographs of wear debris of (a) 6SPS-C composite at 0.2 MPa, (b) 6SPS-C composite at 1 MPa, (c) 6SPS-M composite at 0.2 MPa, (d) 6SPS-M composite at 1 MPa, (e) 6SPS-F composite at 0.2 MPa, (f) 6SPS-F composite at 1 MPa, (g) 6DPS-1 composite at 0.2 MPa, (h) 6DPS-1 composite at 1 MPa, (i) 6DPS-2 composite at 0.2 MPa, (j) 6DPS-2 composite at 1 MPa, (k) 6DPS-3 composite at 0.2 MPa, and (l) 6DPS-3 composite at 1 MPa

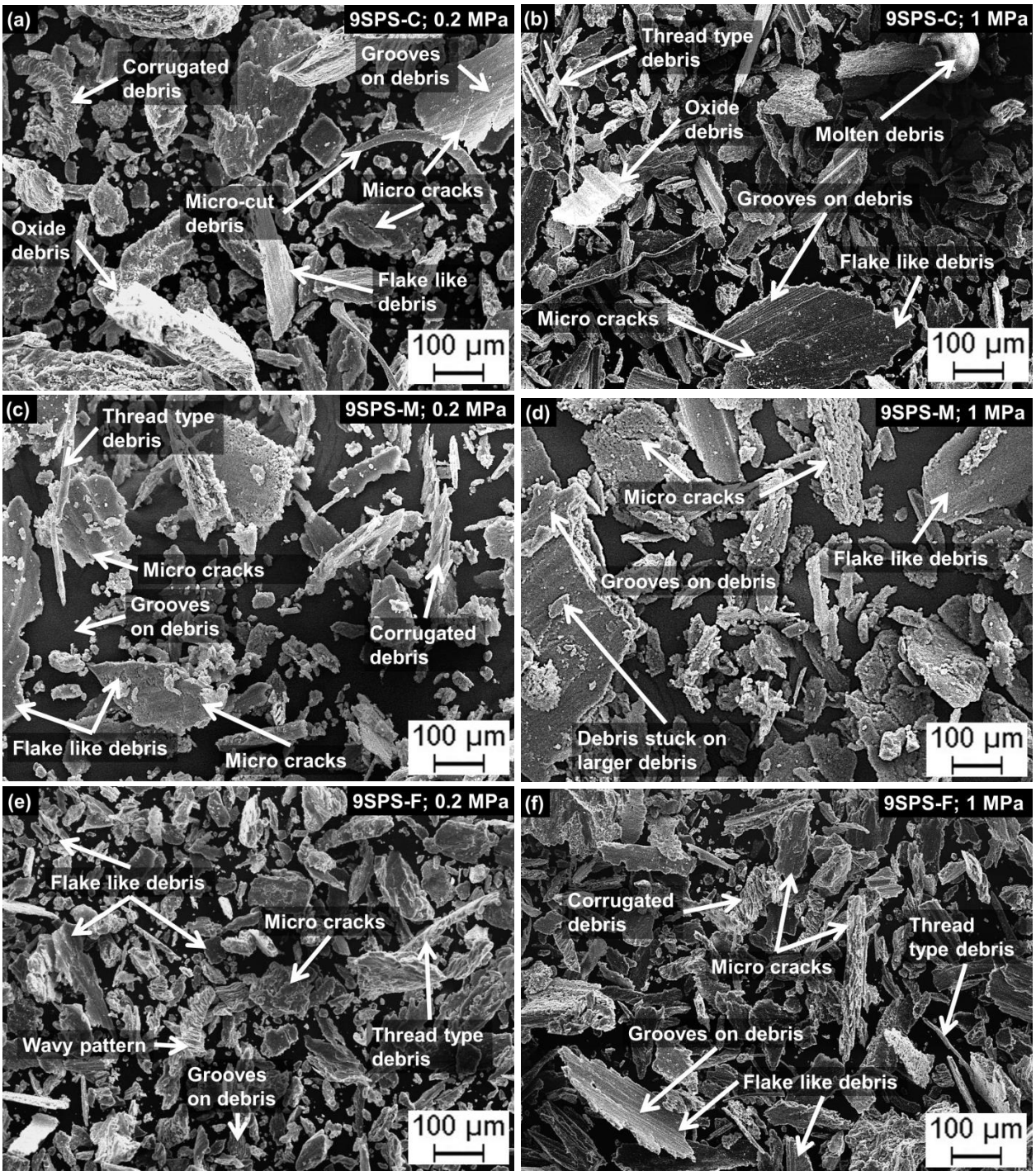
(a)
9SPS-C; 0.2 MPa
Corrugated debris
Grooves on debris
Micro-cut debris
Micro cracks
Oxide debris
Flake like debris
100 µm
(b)
9SPS-C; 1 MPa
Thread type debris
Oxide debris
Molten debris
Grooves on debris
Flake like debris
Micro cracks
100 µm
(c)
9SPS-M; 0.2 MPa
Thread type debris
Micro cracks
Grooves on debris
Corrugated debris
Flake like debris
Micro cracks
100 µm
(d)
9SPS-M; 1 MPa
Micro cracks
Flake like debris
Grooves on debris
Debris stuck on larger debris
100 µm
(e)
9SPS-F; 0.2 MPa
Flake like debris
Micro cracks
Wavy pattern
Thread type debris
Grooves on debris
100 µm
(f)
9SPS-F; 1 MPa
Corrugated debris
Micro cracks
Thread type debris
Grooves on debris
Flake like debris
100 µm

Figure 4.36 SEM micrographs of wear debris of (a) 9SPS-C composite at 0.2 MPa, (b) 9SPS-C composite at 1 MPa, (c) 9SPS-M composite at 0.2 MPa, (d) 9SPS-M composite at 1 MPa, (e) 9SPS-F composite at 0.2 MPa, (f) 9SPS-F composite at 1 MPa, (g) 9DPS-1 composite at 0.2 MPa, (h) 9DPS-1 composite at 1 MPa, (i) 9DPS-2 composite at 0.2 MPa, (j) 9DPS-2 composite at 1 MPa, (k) 9DPS-3 composite at 0.2 MPa, and (l) 9DPS-3 composite at 1 MPa

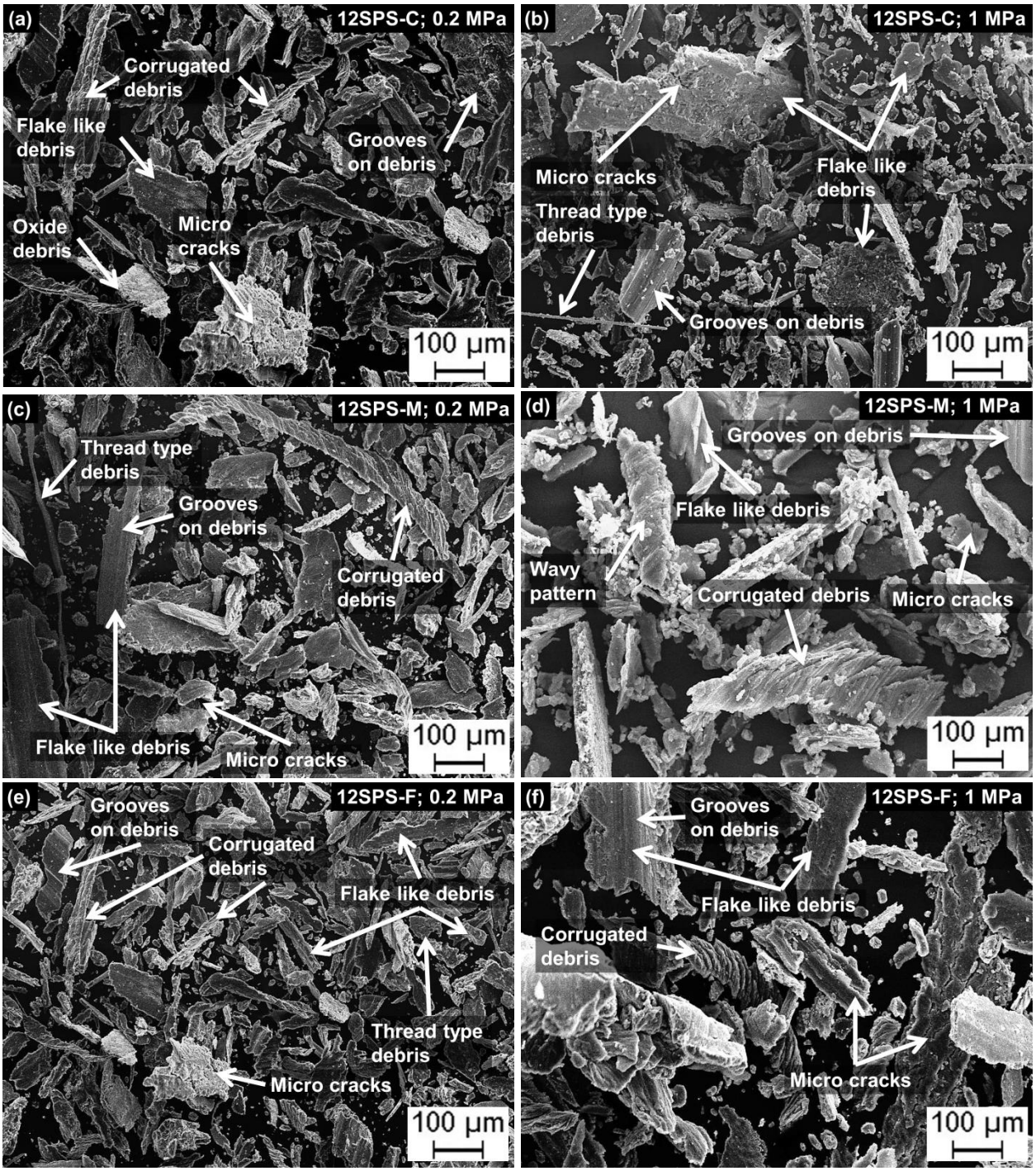
(a)
12SPS-C; 0.2 MPa
Corrugated debris
Flake like debris
Grooves on debris
Oxide debris
Micro cracks
100 µm
(b)
12SPS-C; 1 MPa
Micro cracks
Flake like debris
Thread type debris
Grooves on debris
100 µm
(c)
12SPS-M; 0.2 MPa
Thread type debris
Grooves on debris
Corrugated debris
Flake like debris
Micro cracks
100 µm
(d)
12SPS-M; 1 MPa
Grooves on debris
Flake like debris
Wavy pattern
Corrugated debris
Micro cracks
100 µm
(e)
12SPS-F; 0.2 MPa
Grooves on debris
Corrugated debris
Flake like debris
Thread type debris
Micro cracks
100 µm
(f)
12SPS-F; 1 MPa
Grooves on debris
Flake like debris
Corrugated debris
Micro cracks
100 µm

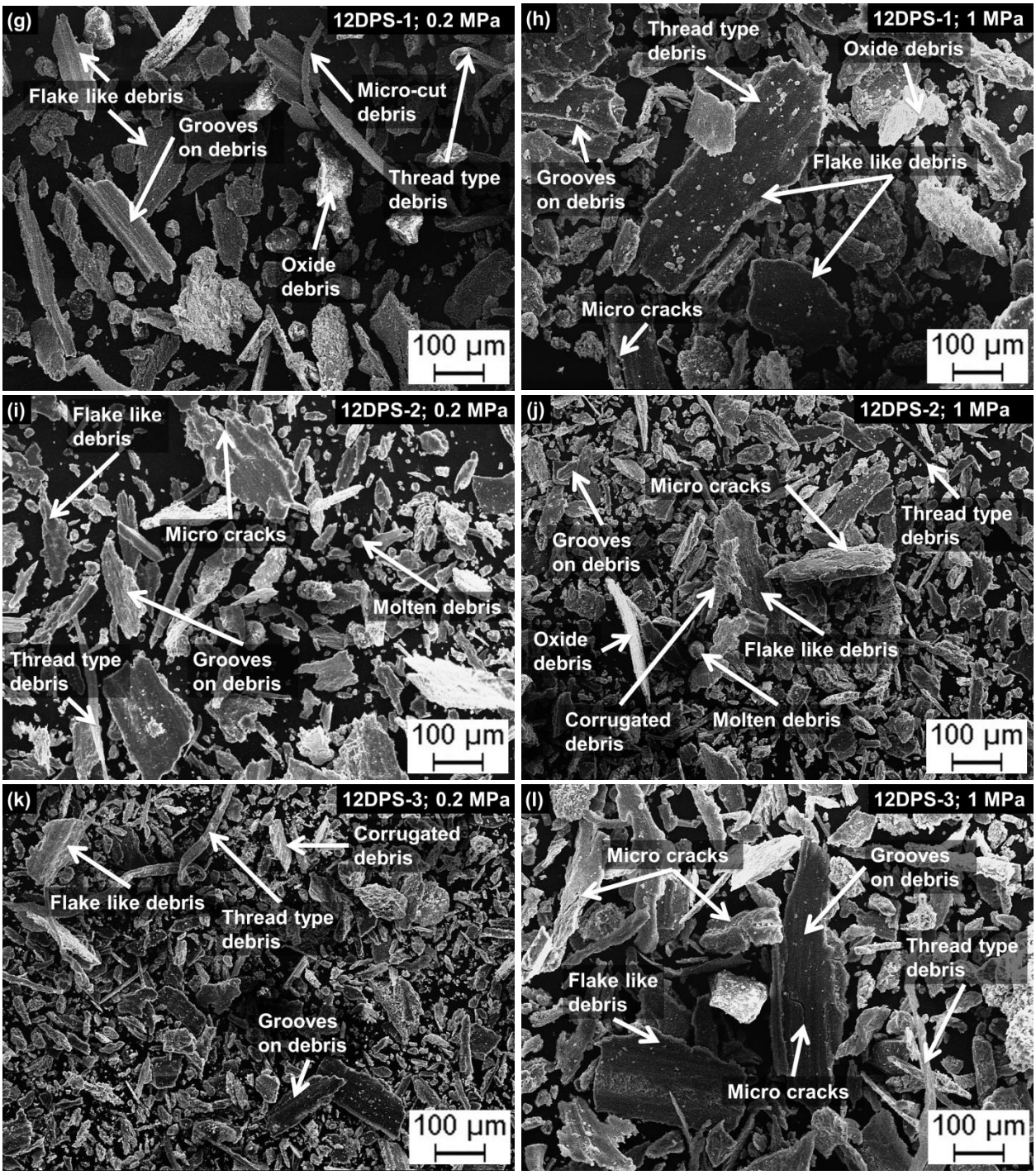

Figure 4.37 SEM micrographs of wear debris of (a) 12SPS-C composite at 0.2 MPa, (b) 12SPS-C composite at 1 MPa, (c) 12SPS-M composite at 0.2 MPa, (d) 12SPS-M composite at 1 MPa, (e) 12SPS-F composite at 0.2 MPa, (f) 12SPS-F composite at 1 MPa, (g) 12DPS-1 composite at 0.2 MPa, (h) 12DPS-1 composite at 1 MPa, (i) 12DPS-2 composite at 0.2 MPa, (j) 12DPS-2 composite at 1 MPa, (k) 12DPS-3 composite at 0.2 MPa, and (l) 12DPS-3 composite at 1 MPa

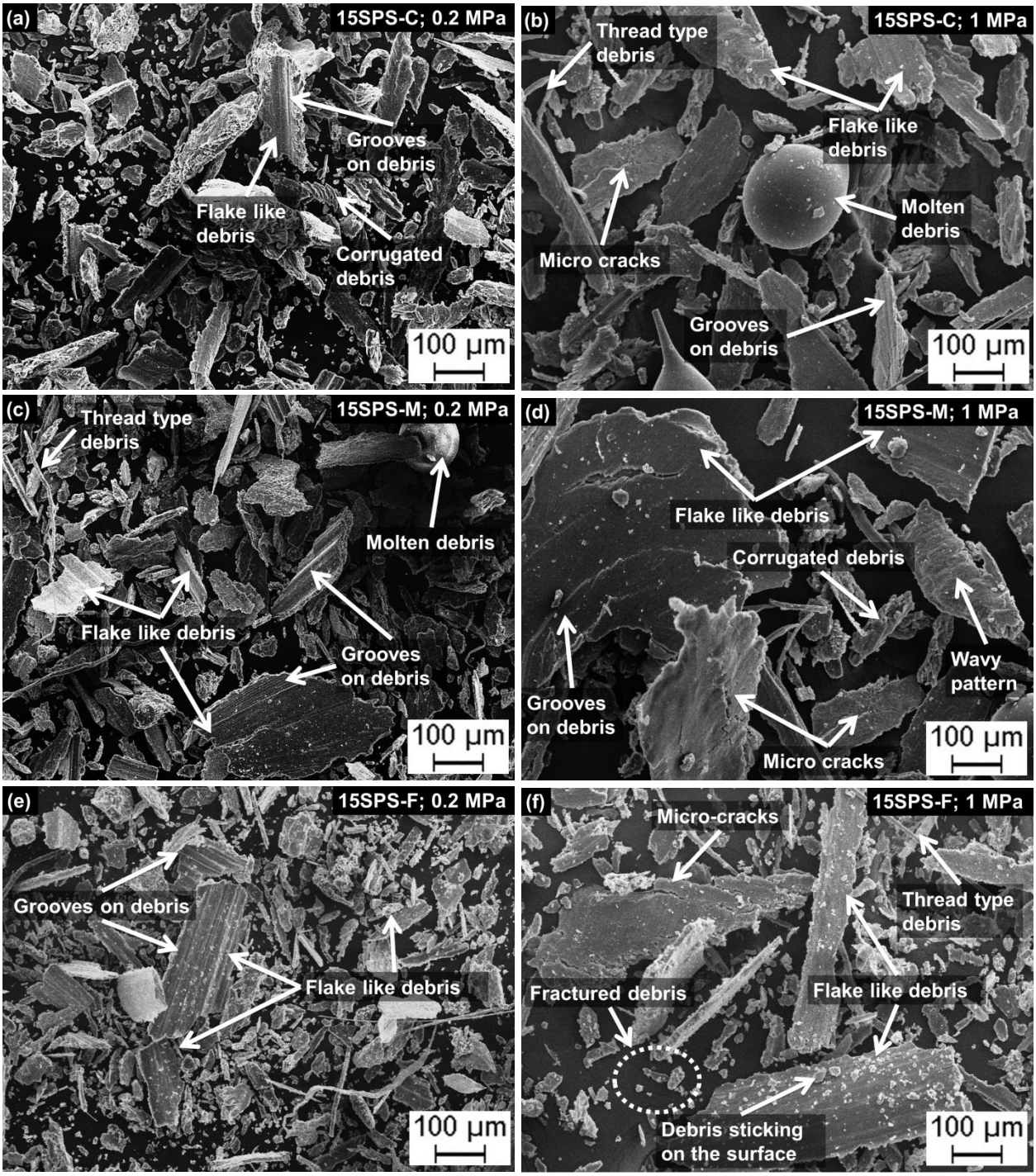
(a)
15SPS-C; 0.2 MPa
Grooves on debris
Flake like debris
Corrugated debris
100 µm
(b)
15SPS-C; 1 MPa
Thread type debris
Flake like debris
Molten debris
Micro cracks
Grooves on debris
100 µm
(c)
15SPS-M; 0.2 MPa
Thread type debris
Molten debris
Flake like debris
Grooves on debris
100 µm
(d)
15SPS-M; 1 MPa
Flake like debris
Corrugated debris
Wavy pattern
Grooves on debris
Micro cracks
100 µm
(e)
15SPS-F; 0.2 MPa
Grooves on debris
Flake like debris
100 µm
(f)
15SPS-F; 1 MPa
Micro-cracks
Thread type debris
Fractured debris
Flake like debris
Debris sticking on the surface
100 µm

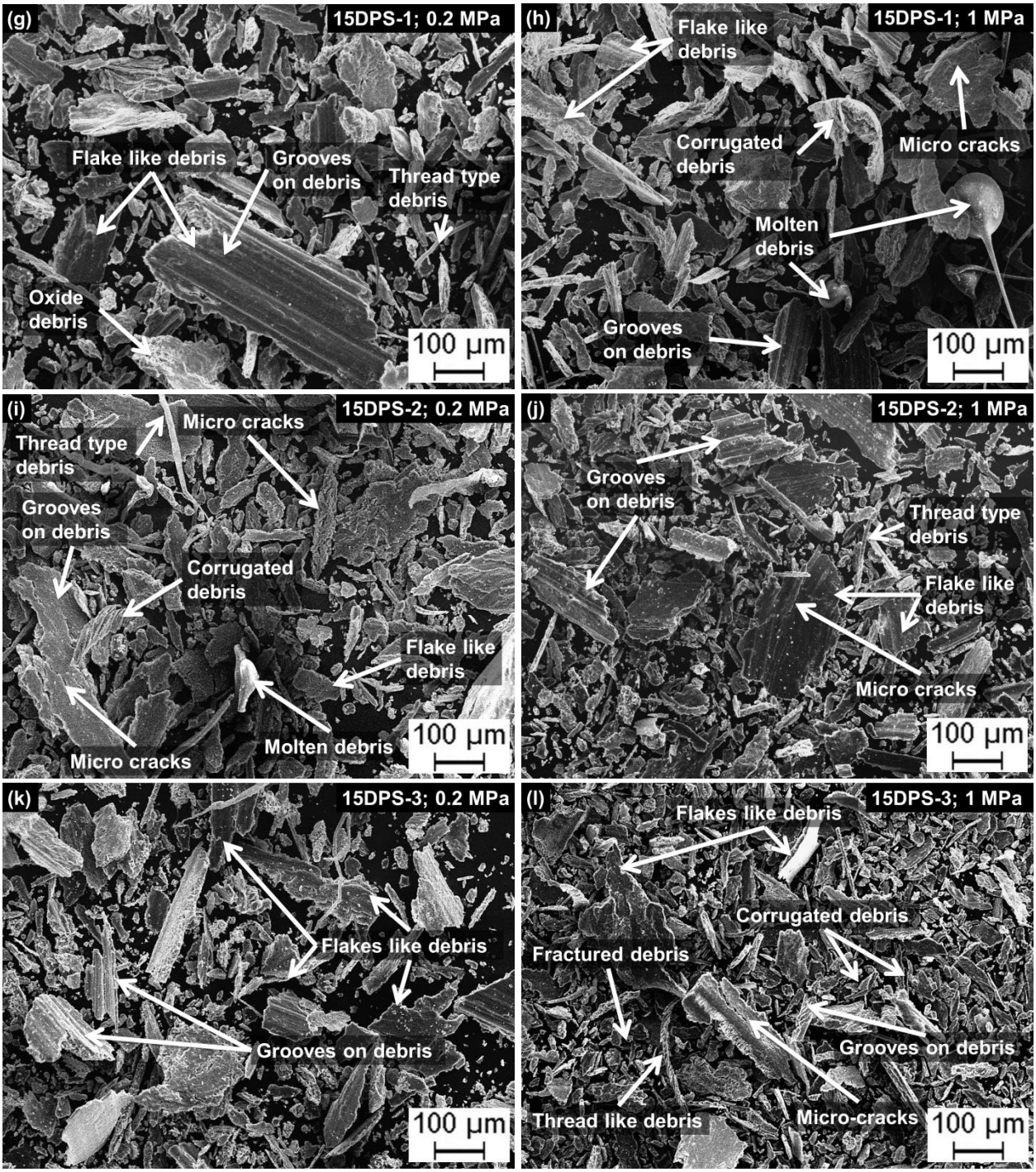

Figure 4.38 SEM micrographs of wear debris of (a) 15SPS-C composite at 0.2 MPa, (b) 15SPS-C composite at 1 MPa, (c) 15SPS-M composite at 0.2 MPa, (d) 15SPS-M composite at 1 MPa, (e) 15SPS-F composite at 0.2 MPa, (f) 15SPS-F composite at 1 MPa, (g) 15DPS-1 composite at 0.2 MPa, (h) 15DPS-1 composite at 1 MPa, (i) 15DPS-2 composite at 0.2 MPa, (j) 15DPS-2 composite at 1 MPa, (k) 15DPS-3 composite at 0.2 MPa, and (l) 15DPS-3 composite at 1 MPa

SEM analysis of wear tracks and wear debris indicated that at lower contact pressure (0.2 MPa), abrasive wear was dominant. This was evident from the SEM images of the wear tracks where narrow abrasive grooves were visible. The increase in particle addition led to decrement in wear rate as was evident from the wear track analysis. For the contact pressure of 0.2 MPa, as the concentration of particles increased, the delamination areas on the wear tacks decreased. This indicated that for the contact pressure of 0.2 MPa, the addition of sillimanite particles transformed the wear mechanism from abrasive/adhesive (for base alloy) to dominantly abrasive type (for composites). Further, for the contact pressure of 1 MPa, a decrement in delaminated areas was observed. The wear mechanism of sillimanite reinforced composites transformed from dominantly adhesive wear regime (for base alloy) to a combination of abrasive and adhesive wear regime (for the composites). Next, for wear debris, the size of debris decreased with increase in sillimanite particle addition. Flake type of debris is a result of adhesive wear mechanism. The reduction in the size of flakes indicates the decrease in the adhesive wear mechanism for the composites.

Figure 4.39a–d presents the EDS analysis of wear track of 15SPS-F and 15DPS-3 AMCs at low contact pressure (0.2 MPa) and high contact pressure (1 MPa) respectively. At contact pressure of 0.2 MPa, the wear track surface of both the AMCs mainly consisted of aluminium, silicon, and oxygen. This showed that at low contact pressures, the oxides formed were mainly of the matrix material. However, at high contact pressure (1 MPa), iron was also observed in addition to aluminium, silicon, and oxygen. The source of iron was the EN32 steel disc. The presence of iron indicated that at high contact pressures, wear of countersurface also occurred along with the pin surface. Figure 4.40a–d presents the EDS analysis of wear debris of 15SPS-F and 15DPS-3 composites at low contact pressure (0.2 MPa) and high contact pressure (1 MPa) conditions respectively.

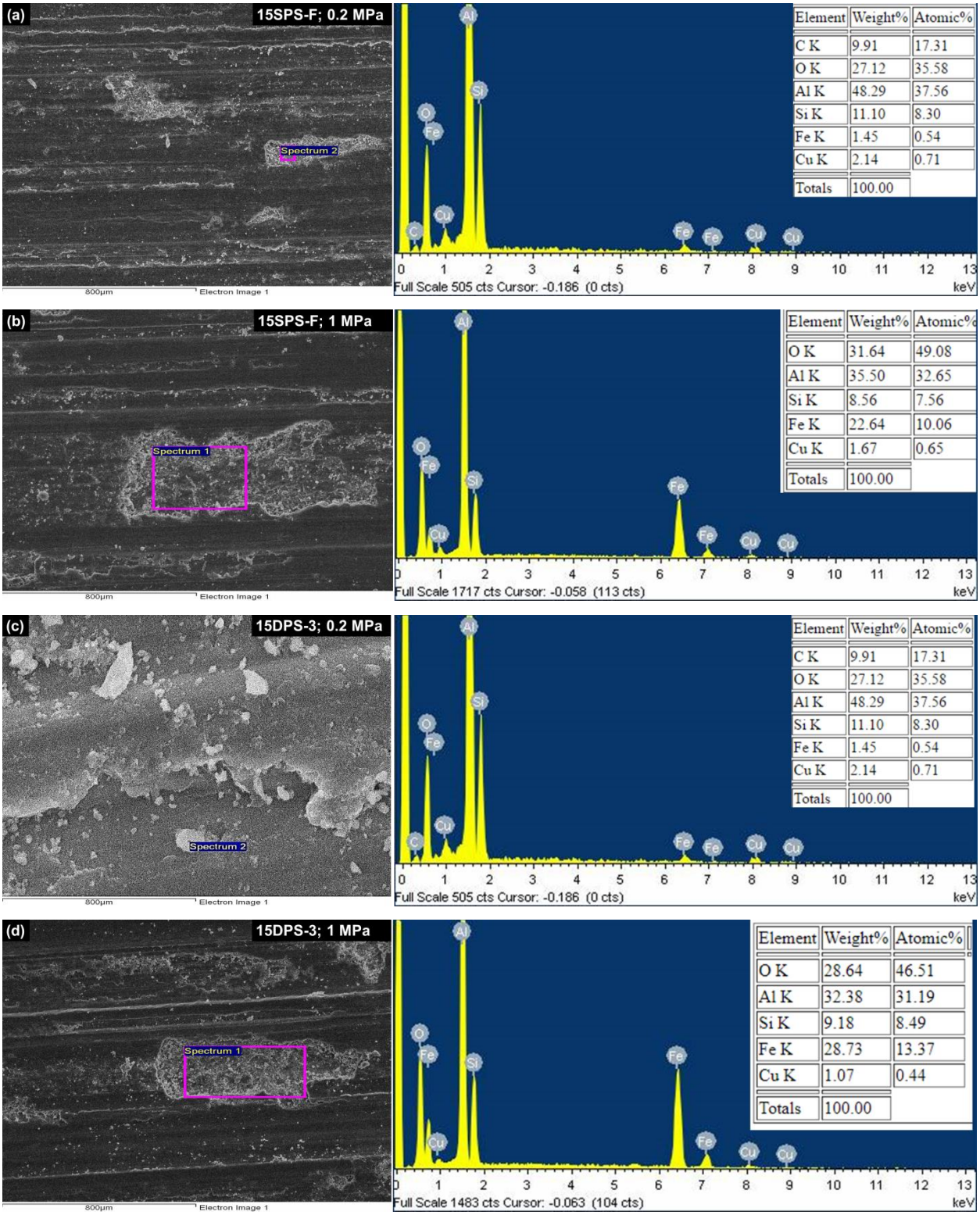

Figure 4.39 EDS analysis of wear track of (a) 15SPS-F composite at 0.2 MPa, (b) 15SPS-F composite at 1 MPa, (c) 15DPS-3 composite at 0.2 MPa, and (d) 15DPS-3 composite at 1 MPa

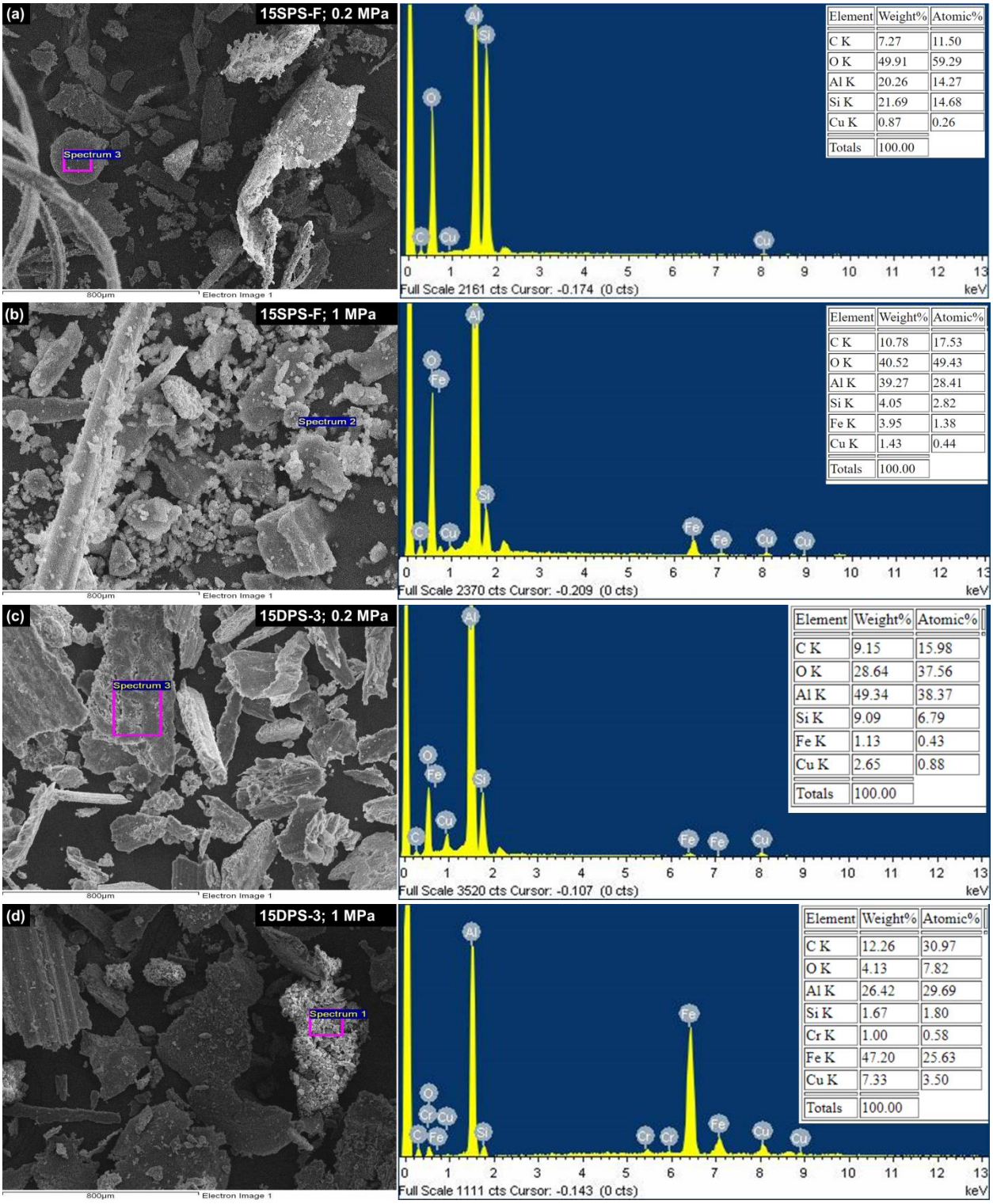

Figure 4.40 EDS analysis of wear debris of (a) 15SPS-F composite at 0.2 MPa, (b) 15SPS-F composite at 1 MPa, (c) 15DPS-3 composite at 0.2 MPa, and (d) 15DPS-3 composite at 1 MPa

For the low contact pressure of 0.2 MPa, EDS confirmed the presence of oxides which were mainly of aluminium (due to wear of only pin surface). However, at high contact pressure conditions, the oxides of iron were also formed (due to wear of steel disc surface also) in addition to oxides of aluminium. This indicated that under high contact pressure conditions, a mechanical mixed layer (comprising of oxide of aluminium from pin surface and oxides of iron from steel disc surface) got formed. This compaction resulted in the formation of a mechanical mixed layer (MML), also known as transfer film [191]. MML protects the specimen surface from further wear [175]. Under the action of contact pressure, the deformation of transfer film results in strain hardening of wear debris, thereby increasing the hardness of transfer film. The hardness of the MML is much higher than the countersurfaces. This work-hardened layer reduces the wear rate of the AMCs [191]. The formation and removal of transfer film remains constant and it also prevents metal to metal contact. Thus, the wear rate remains constant in the steady-state-wear zone [175,192]. For these reasons, at low contact pressures, the wear in the processed AMC can be referred to as mild wear (mainly abrasive nature of wear). However, for high contact pressure conditions, the wear can be referred to as sever wear due to formation of the oxide-rich layer comprising of iron oxide and aluminium oxide (mainly adhesive nature of wear).

The next chapter presents the results and discussion pertaining to characterization, wear testing, and friction testing of various AMCs under elevated temperature conditions.

CHAPTER 5
RESULTS AND DISCUSSION
(Characterization and testing of AMCs at elevated temperatures)

OVERVIEW

This chapter presents the results of wear tests conducted at elevated temperatures. Composites containing different fractions of sillimanite minerals were tested for wear behaviour. The results have been explained on the basis of thermal stability of mineral and also the variation in coefficient of thermal expansion (CTE). The wear tracks and wear debris so obtained have been analyzed under SEM and also by X-ray diffraction technique to predict the wear mechanisms at elevated temperatures. The existence of MML has been confirmed by EDS analysis of the worn surfaces and debris.

5.1 DTG-TGA AND DSC ANALYSIS OF SILLIMANITE PARTICLES

DTG-TGA and DSC analysis of sillimanite particles was done to observe its thermal stability. Figure 5.1 presents the results of DTG-TGA and DSC analysis of sillimanite particles used in the present study. DTG-TGA results revealed that there was an insignificant weight change (1.5% only) of the sample when heated till a temperature of 300 ℃. The DSC curve showed two peaks in the temperature range of 50–250 ℃. These peaks were associated with the removal of moisture and volatile matter. Beyond 250 ℃, the sillimanite particles showed thermal stability till 900 ℃.

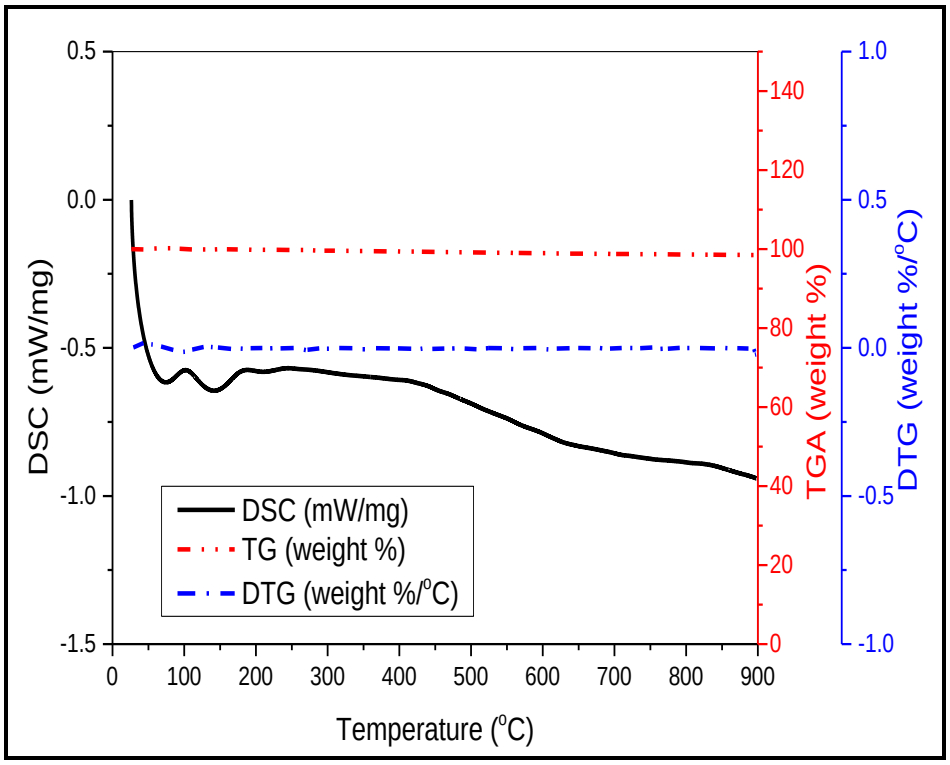

Figure 5.1 Results of DTG-TGA and DSC analysis of sillimanite particles

5.2 CTE ANALYSIS

Figure 5.2a–l presents the thermal strain versus temperature and CTE versus temperature graphs for various AMCs. CTE analysis in the present work was conducted till a high temperature of 400 ℃ (higher than the temperature of 300 ℃ selected for wear testing). Experimentally, CTE values were calculated as per Equation 5.1.

$$\alpha_c = \frac{\Delta L}{L} \times \frac{1}{\Delta T} \quad \text{……. (5.1)}$$

Where,

α_c: CTE ($℃^{-1}$)

$\frac{\Delta L}{L}$: Thermal strain

ΔT: Change in temperature (℃)

It was observed from Figure 5.2a–l that for any AMC composition at any given temperature, the thermal strain and CTE values were lower as compared to those of the base alloy. Thus, addition of sillimanite particles to the base alloy decreased the CTE of the resulting AMCs. However, with increase in temperature, there was an increase in the thermal strain and CTE values of base alloy and various AMCs. Also, CTE values of AMCs further decreased with increase in the reinforcement level (Figure 5.2b, d, f, h, j, l). For a given AMC composition, a slight decrease in thermal strain and CTE was observed with a decrease in sillimanite particle size [190]. Further, for DPS composites, CTE value decreased with increase in the proportion of finer particles. Thus, the results showed that addition of sillimanite particles is useful to tailor the CTE value of base alloy. In the present work, 15SPS-F (for SPS composites) and 15DPS-3 (for DPS composites) AMCs showed the maximum reduction in CTE values (25% and 28% respectively over the base alloy).

CTE of composites depends on (i) the relative difference in CTE values of individual constituents of matrix and reinforcement, and (ii) the relative strength of interfacial bonding between matrix and reinforcement. CTE value reported for sillimanite is 2.1×10^{-6} $℃^{-1}$ [193]. CTE value obtained for the base alloy in the present work was 24×10^{-6} $℃^{-1}$. During heating, due to the high CTE value of base alloy, the rate of expansion of the matrix was higher than the sillimanite particles. Presence of reinforcement in the matrix restricts the expansion of matrix by exerting an opposing force due to its relatively lower CTE value. With regards to interfacial bonding factor, higher is the interfacial bonding strength between the matrix and reinforcement, greater is the resistance to expansion on heating, and thus lower is the CTE of composite [194,195]. The lower CTE value for composites signified a strong interfacial bonding between matrix and reinforcement in these AMCs.

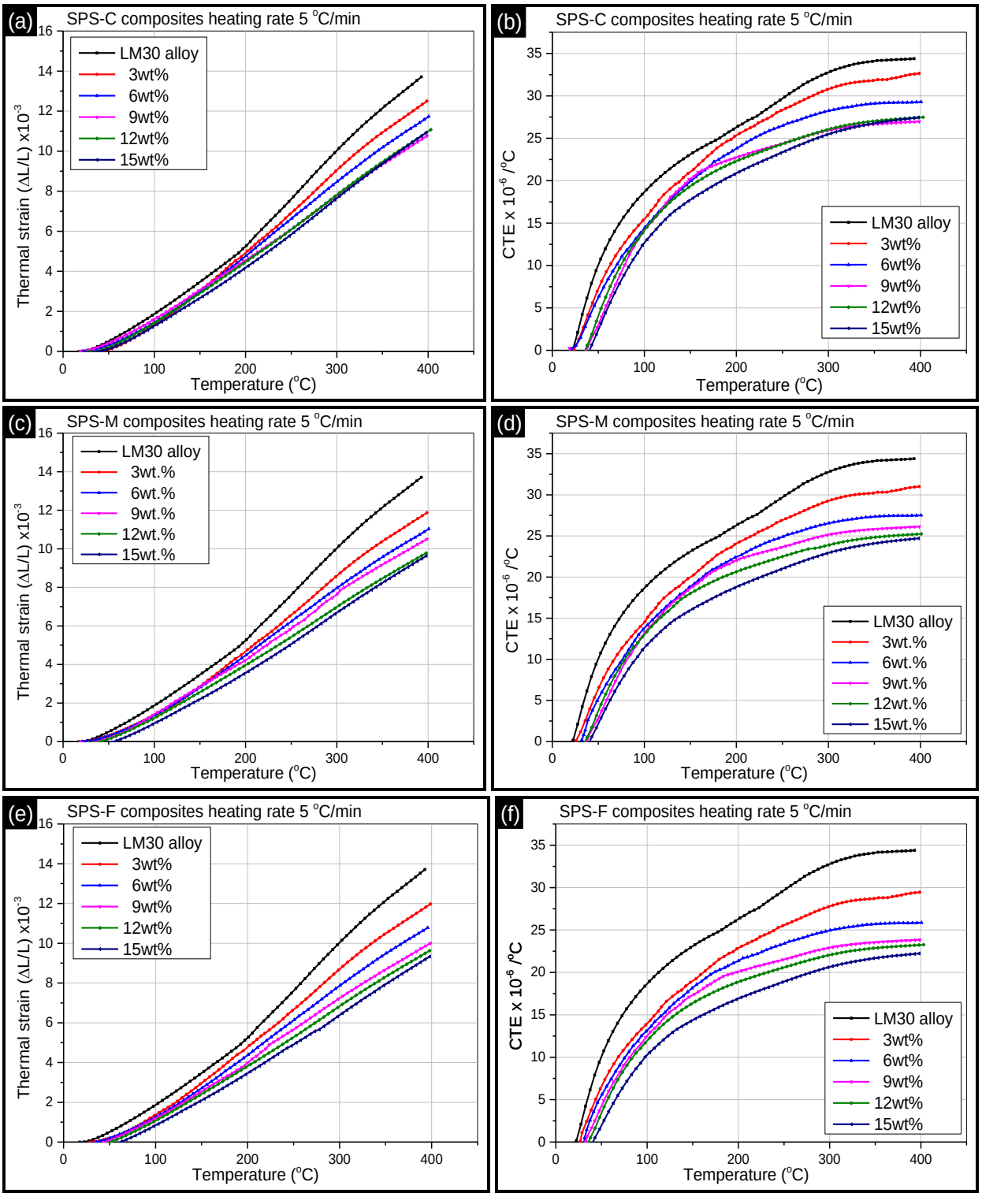
(a)
SPS-C composites heating rate 5 °C/min
Thermal strain (ΔL/L) x10-3
Temperature (°C)
LM30 alloy
3wt%
6wt%
9wt%
12wt%
15wt%
(b)
SPS-C composites heating rate 5 °C/min
CTE x 10-6 /°C
Temperature (°C)
LM30 alloy
3wt%
6wt%
9wt%
12wt%
15wt%
(c)
SPS-M composites heating rate 5 °C/min
Thermal strain (ΔL/L) x10-3
Temperature (°C)
LM30 alloy
3wt.%
6wt.%
9wt.%
12wt.%
15wt.%
(d)
SPS-M composites heating rate 5 °C/min
CTE x 10-6 /°C
Temperature (°C)
LM30 alloy
3wt.%
6wt.%
9wt.%
12wt.%
15wt.%
(e)
SPS-F composites heating rate 5 °C/min
Thermal strain (ΔL/L) x10-3
Temperature (°C)
LM30 alloy
3wt%
6wt%
9wt%
12wt%
15wt%
(f)
SPS-F composites heating rate 5 °C/min
CTE x 10-6 /°C
Temperature (°C)
LM30 alloy
3wt%
6wt%
9wt%
12wt%
15wt%

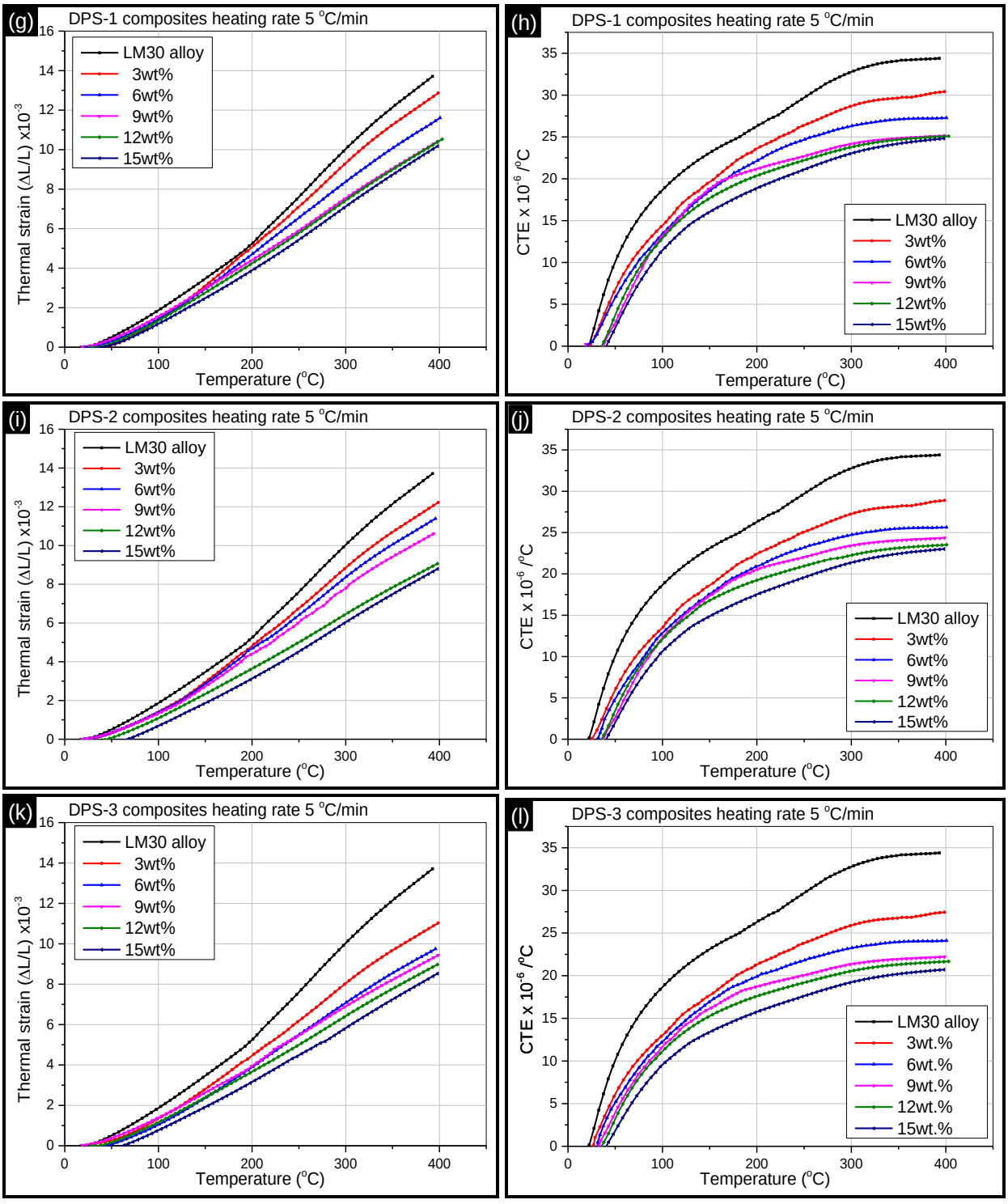

Figure 5.2 (a) Thermal strain of SPS-C composites, (b) CTE of SPS-C composites, (c) thermal strain of SPS-M composites, (d) CTE of SPS-M composites, (e) thermal strain of SPS-F composites, (f) CTE of SPS-F composites, (g) thermal strain of DPS-1 composites, (h) CTE of DPS-1 composites, (i) thermal strain of DPS-2 composites, (j) CTE of DPS-2 composites, (k) thermal strain of DPS-3 composites, and (l) CTE of DPS-3 composites

The experimental CTE values were also compared with the CTE values obtained using different mathematical models. Table 5.1 presents the various mathematical models used for predicting CTE values [190,196]. Table 5.2 presents the details of various properties of the base alloy and sillimanite particles.

Table 5.1 Predictions of CTE for a two-phase material [190,196]

Model	***Prediction Equation***	
ROM*	$\alpha_c = \alpha_m V_m + \alpha_p V_p$	……(5.2)
Turner	$\alpha_c = \frac{\alpha_m K_m V_m + \alpha_p K_p V_p}{K_m V_m + K_p V_p}$	……(5.3)
Kerner	$\alpha_c = \alpha_m V_m + \alpha_p V_p + V_m V_p (\alpha_p - \alpha_m) \frac{K_p - K_m}{V_m K_m + V_p K_p + 3 K_m K_p / 4G_m}$	……(5.4)

Where
$\boldsymbol{\alpha_c}$**:** CTE of the composite
$\boldsymbol{\alpha_m}$**:** CTE of the matrix phase
$\boldsymbol{\alpha_p}$**:** CTE of the particles
$\boldsymbol{V_m}$**:** volume fraction of matrix in the composite
$\boldsymbol{V_p}$**:** volume fraction of particle in the composite
$\boldsymbol{K_m}$**:** bulk modulus of the matrix
$\boldsymbol{K_p}$**:** bulk modulus of particles
$\boldsymbol{G_m}$**:** shear modulus of the matrix
* ROM: rule of mixtures

Table 5.2 Physical, mechanical, and thermal properties of aluminium alloy and sillimanite particles [193,197,198]

	Density (g/cm^3)	**Shear modulus (GPa)**	**Elastic modulus (GPa)**	**Bulk modulus (GPa)**	**CTE ($\times 10^{-6}$/℃)**
LM30 aluminium alloy	2.73	34	88.5	106	24
Sillimanite	3.25	87.8	224.9	170.9	2.1

Figure 5.3 presents the mean CTE values (both, predicted as well as experimental values) for base alloy and various AMCs with different reinforcement content. Close agreement in the predicted and experimental values was observed. The closest comparison was obtained with the Turner model.

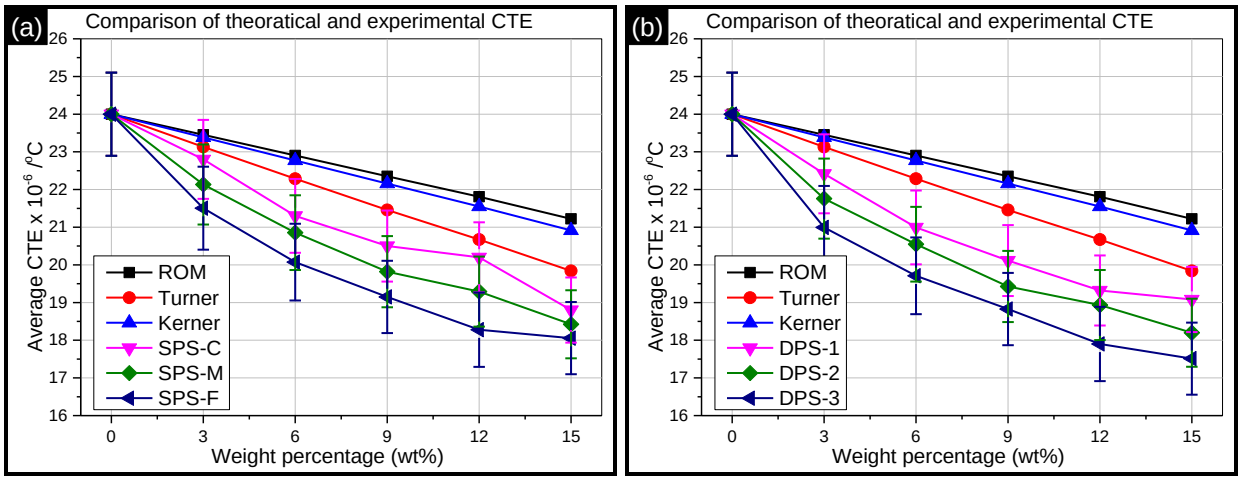

Figure 5.3 Average CTE value versus reinforcement content in AMCs for (a) SPS composites, and (b) DPS composites

5.3 WEAR TESTING

5.3.1 RESULTS OF WEAR TESTING OF BASE ALLOY

The operating temperature of wear test is a crucial factor which defines the wear behavior of materials. At a critical temperature range of $0.4T_m$–$0.6T_m$ (T_m being the melting point of the material in K), strong adhesion of surfaces (pin and countersurface) takes place [190]. Wear testing in the critical temperature range leads to thermal and mechanical activation of the deformation process causing thermal softening of the pin. In the present work, for the wear testing at elevated temperatures, the mean steady-state wear rate of pin surface was obtained for various operating temperatures. For calculating the mean steady-state wear rate of base alloy/AMCs at a given elevated temperature, the wear rates obtained for each formulation over a continuous sliding range of 1500–3000 m were considered.

Figure 5.4 shows the mean steady-state wear rate of base alloy obtained at various elevated temperatures (50–300 ℃; at interval of 50 ℃). Firstly, for 0.2 MPa contact pressure, a slight decrease in steady-state wear rate of base alloy was observed till 200 ℃. This decrease in wear rate was attributed to the development of an oxide film which develops during wear testing at higher temperatures of 150–200 ℃. Oxide layer inhibits direct metal-to-metal contact of the countersurfaces [51]. For operating temperature beyond 200 ℃, an increase in steady-state wear rate was observed. At high temperatures, thermal softening of the material decreased the mechanical stability of oxide film and hence increased the wear rate [190]. Thus, for the base alloy, at low contact pressure of 0.2 MPa, mild-to-severe wear transition took place at an

operating temperature of 200 ℃. Severe wear signifies excessive plastic deformation along the sliding direction causing extensive surface damage at the contact zone [92].

For contact pressure of 0.6 MPa and 1 MPa, the trend observed for mean steady-state wear rate was different from that of 0.2 MPa. Unlike the case of 0.2 MPa, for contact pressure of 0.6 MPa and 1 MPa, a continuous increase in wear rate was noted for the entire range of operating temperatures (50–300 ℃). The increase in wear rate with operating temperature was gradual till 150 ℃. This means that for change in operating temperature in the range of 50–150 ℃, the combined effect of high contact pressure and operating temperature caused thermal softening of material and tearing of oxide film which resulted in gradual increase in wear rate. However, beyond this operating temperature (i.e. 150–300℃), a sharp increase in wear rate was observed. This sharp increase in wear rate (severe wear) was attributed to the complete removal of oxide film which leads to exposure of new metallic areas to the wear environment [92,190]. At the operating temperature of 300 ℃, complete wear of the base alloy was detected at a sliding distance of about 1850 m. Complete wear refers to the complete working range of the LVDT used in the present research that measured the height loss (i.e. 2 mm).

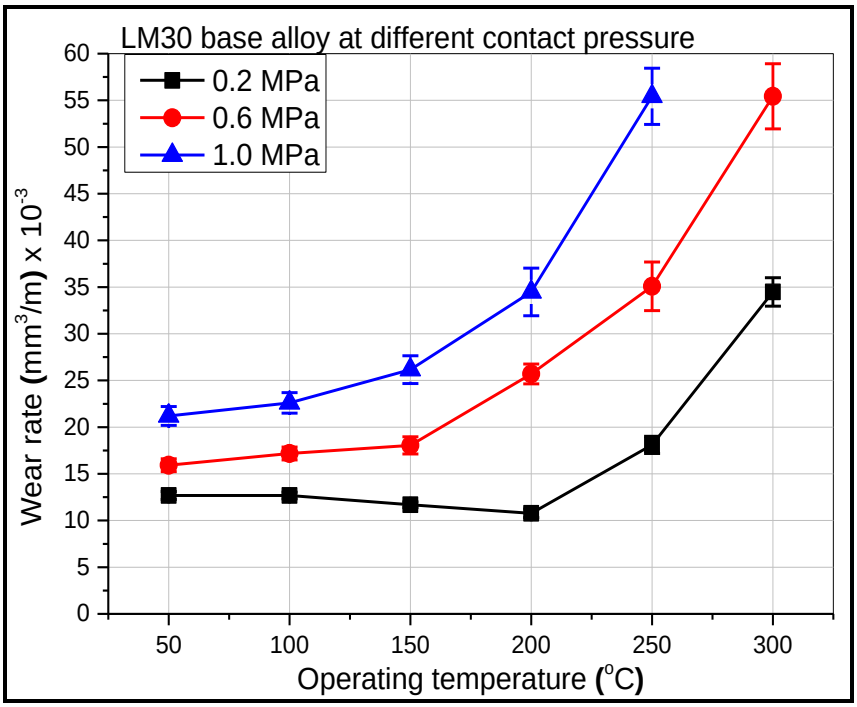

Figure 5.4 Change in steady-state wear rate of base alloy as a function of operating temperature for various contact pressures

5.3.2 RESULTS OF WEAR TESTING OF AMCs

Figure 5.5 to 5.7 present the wear behavior of various AMCs at different elevated temperatures in the range of 50–300 ℃ at contact pressure of 0.2 MPa, 0.6 MPa, and 1 MPa respectively. As observed from Figure 5.5, wear rate trend shown by various AMCs at 0.2 MP was similar to that of the base alloy (Figure 5.4). Further, for a given operating temperature, the steady-state wear rate was lower for AMCs with higher reinforcement content. It was reported in an earlier section that increase in sillimanite content in AMCs decreased the CTE of the composite system. Thus, increase in sillimanite reinforcement level in AMCs increased their thermal stability and decreased the wear rate.

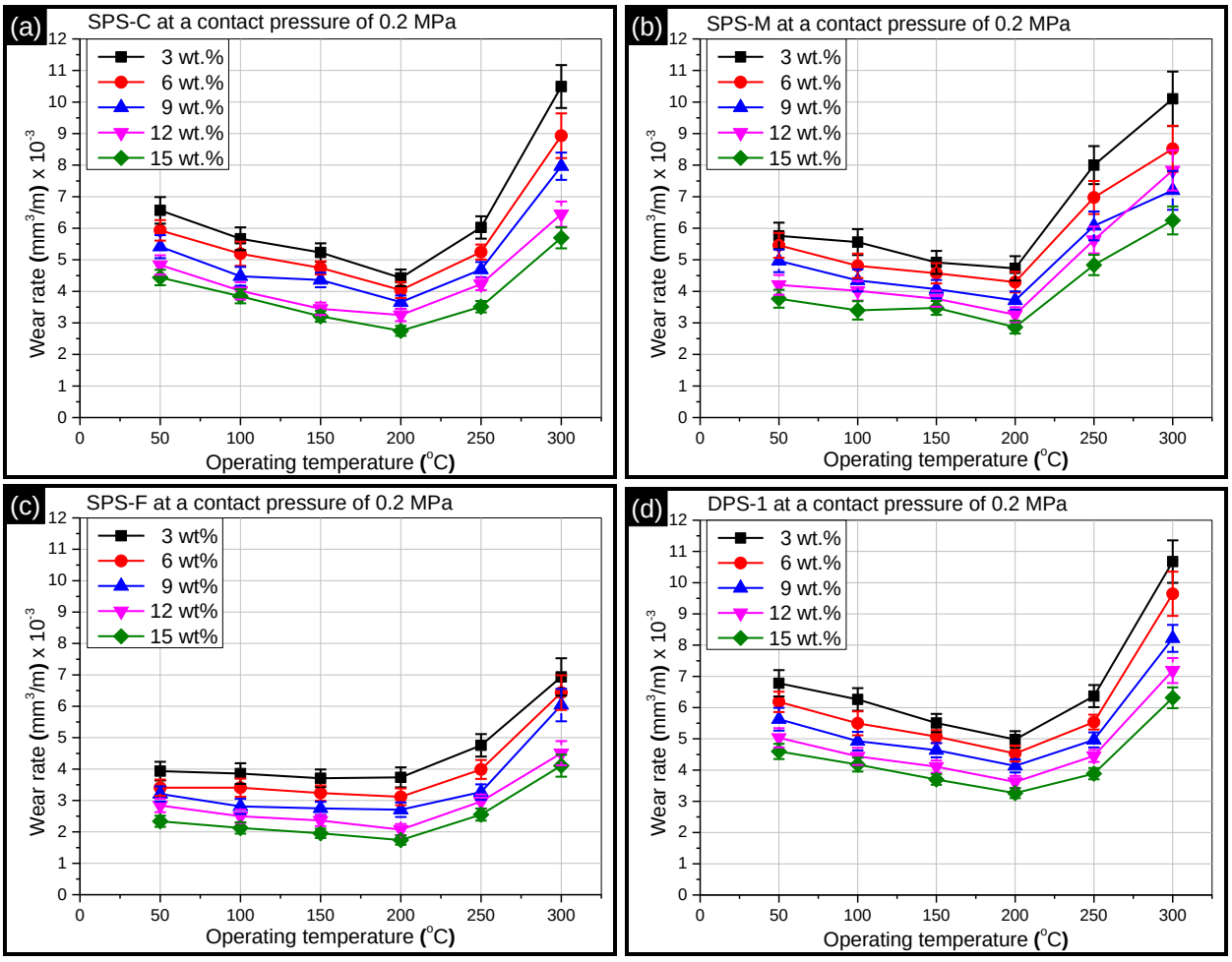

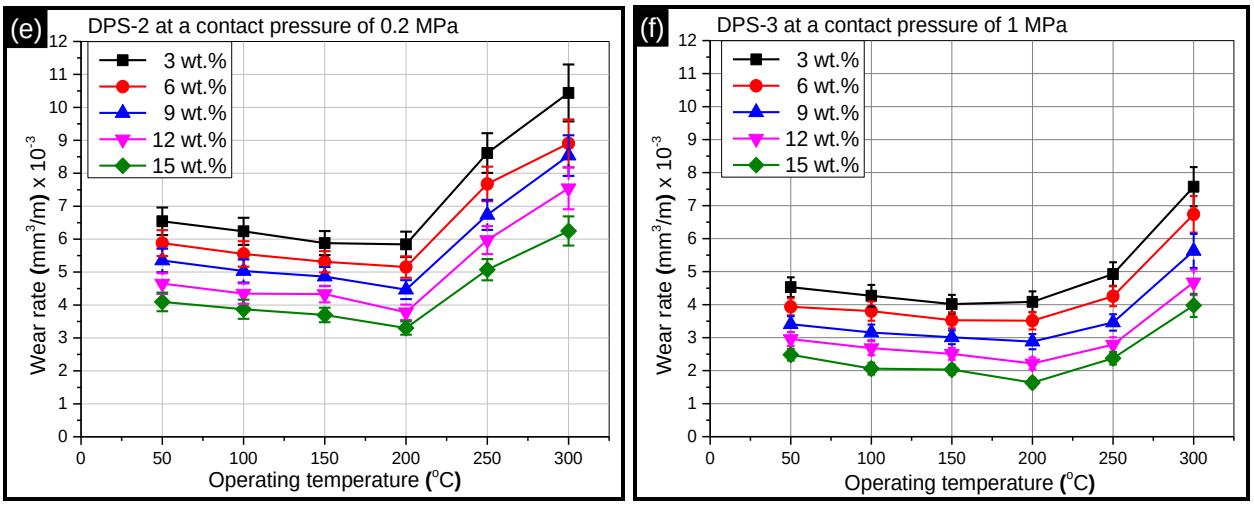

Figure 5.5 Wear rate vs. operating temperature at contact pressure of 0.2 MPa for (a) SPS-C, (b) SPS-M, (c) SPS-F, (d) DPS-1, (e) DPS-2, and (f) DPS-3 composites

As observed from Figure 5.6, wear rate trend of AMCs at 0.6 MPa was slightly different than that of the base alloy (Figure 5.4). For AMCs at 0.6 MPa, wear rate initially decreased with increase in operating temperature till 200 ℃ and thereafter increased. Also, it was noted that mild-to-severe wear transition temperature for AMCs at 0.6 MPa was higher (200 ℃) than that for base alloy (150 ℃).

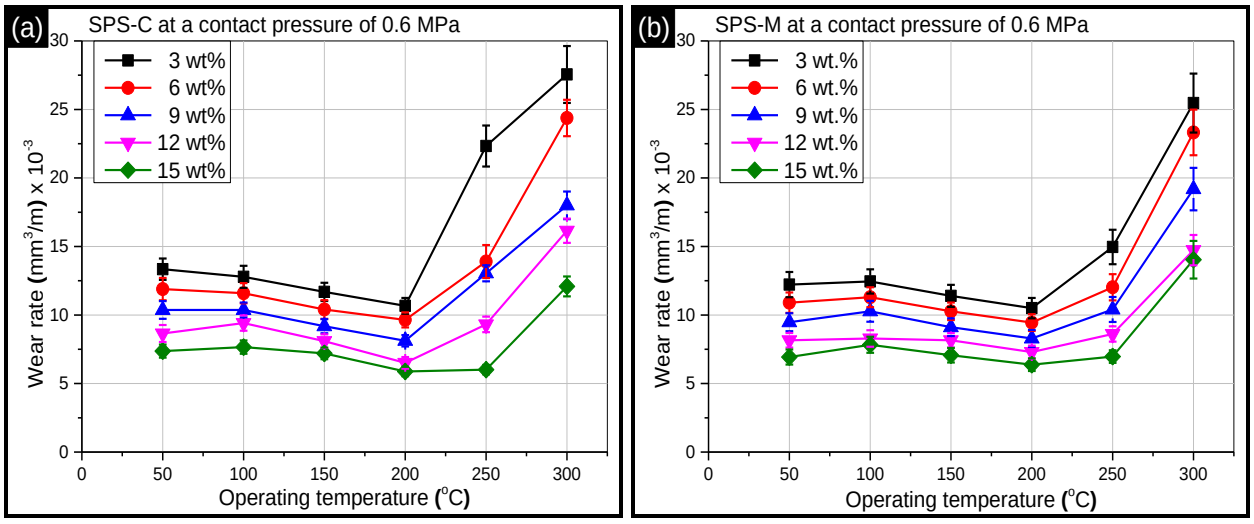

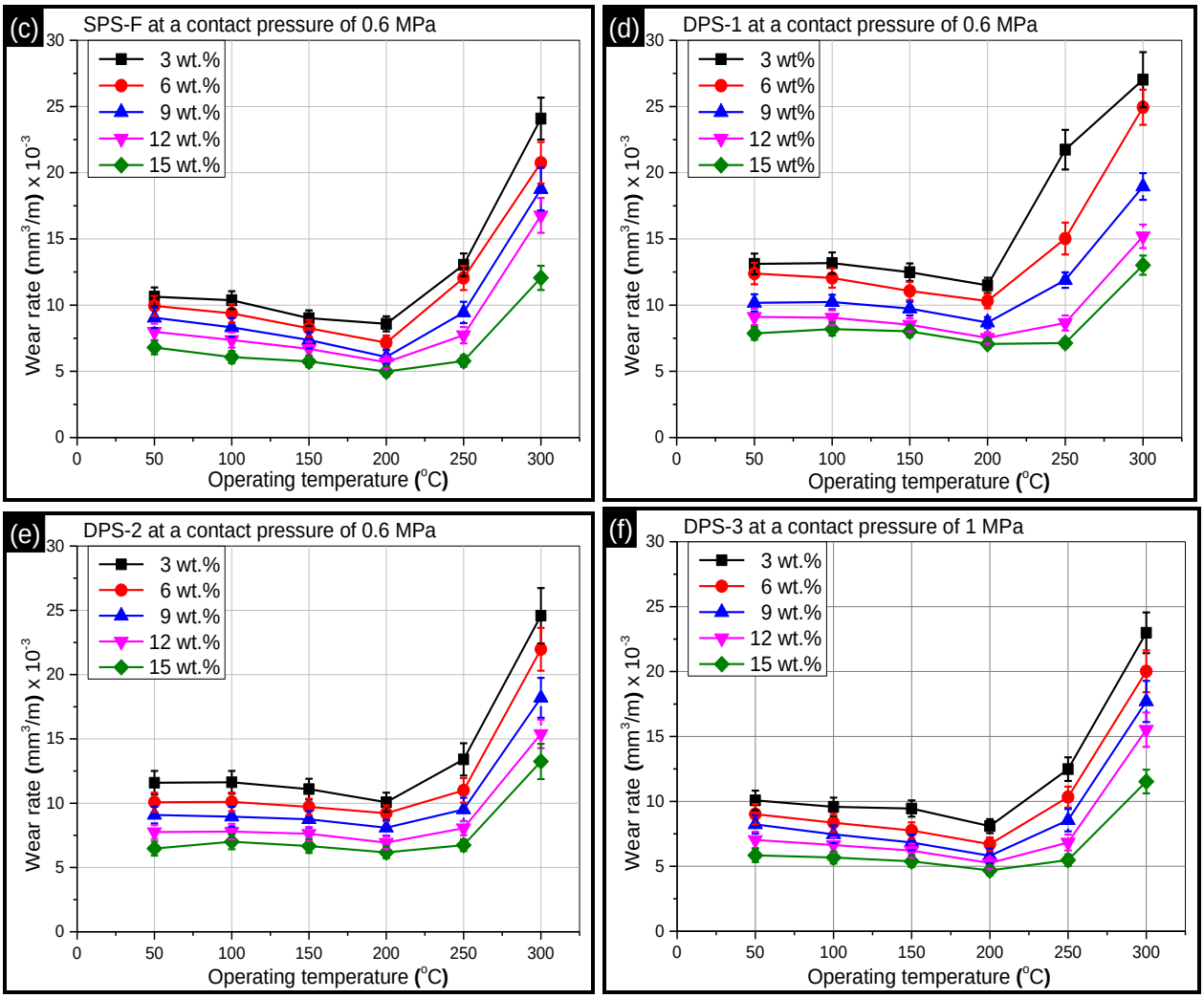

Figure 5.6 Wear rate vs. operating temperature at contact pressure of 0.6 MPa for (a) SPS-C, (b) SPS-M, (c) SPS-F, (d) DPS-1, (e) DPS-2, and (f) DPS-3 composites

From Figure 5.7, it can be observed that wear rate trend shown by various AMCs at 1 MPa was similar to that of the base alloy (Figure 5.4). However, the following was noted, (i) compared to the base alloy where mild-to-severe transition occurred at 150 ℃, for the AMCs it occurred at slightly higher temperature (200 ℃), and (ii) compared to the base alloy where at 300 ℃, complete wear was observed at 1850 m, the AMCs could withstand this high temperature of 300 ℃.

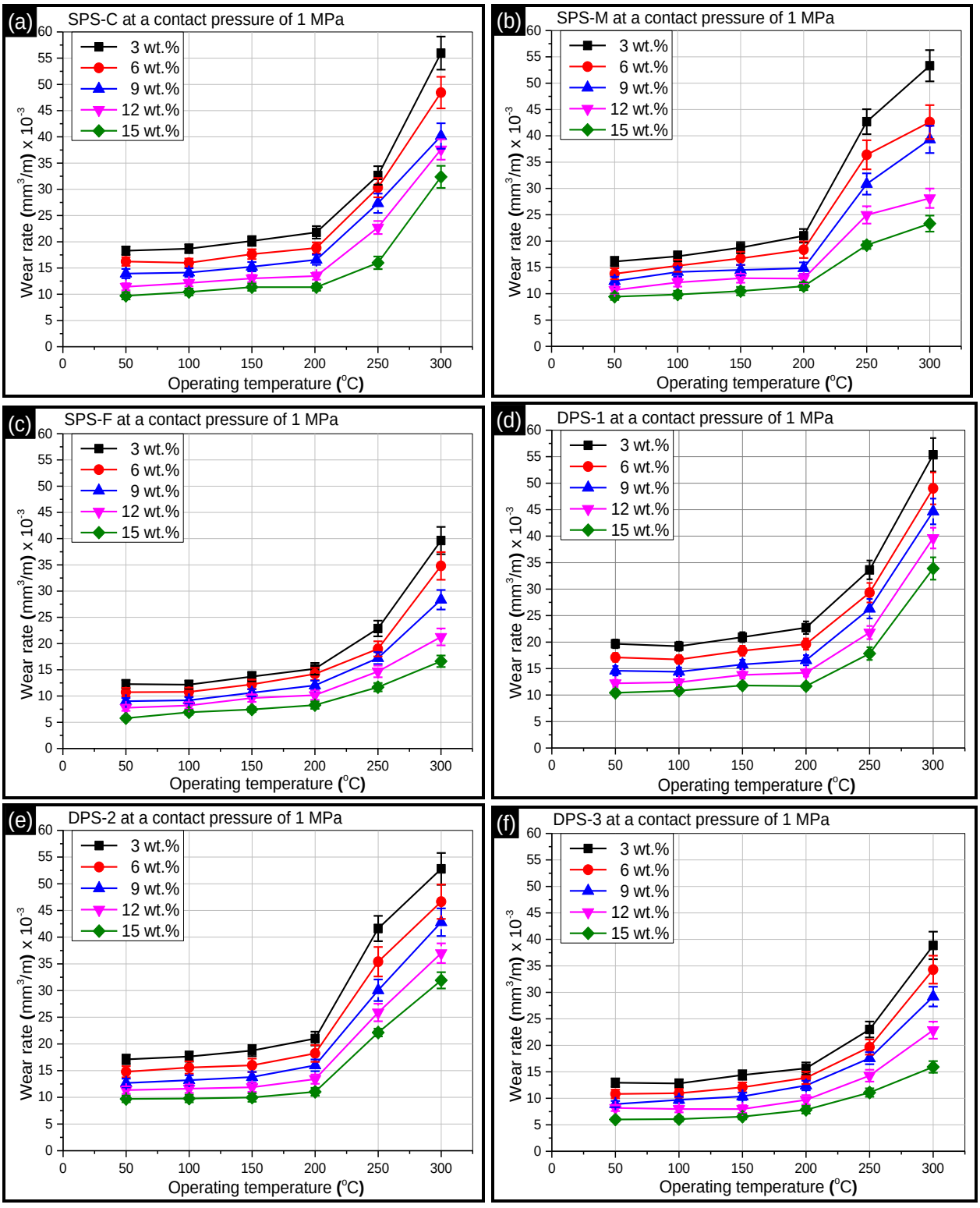

Figure 5.7 Wear rate vs. operating temperature at contact pressure of 1 MPa for (a) SPS-C, (b) SPS-M, (c) SPS-F, (d) DPS-1, (e) DPS-2, and (f) DPS-3 composites

For all contact pressure and operating temperature combinations, the AMCs showed significantly lower wear rate than the base alloy. For SPS composites, a decrease in wear rate was observed with increase in sillimanite content. Also, for DPS composites, wear rate decreased with increase in proportion of finer particles in the mixture. The best wear results were observed for 15DPS-3 composites. The high wear resistance shown by 15DPS-3 composites was due to the higher proportion of finer particles in the composites along with some coarse particles. The coarser particles shielded the smaller particles and the matrix from wear and decreased the wear rate of AMCs. Majority of the load was borne by the coarser particles, and therefore, the load on finer particles reduced. Finally, when the coarser particles got crushed under the contact pressure, the load was transferred to the finer particles, keeping the matrix material protected from wear. Table 5.3 presents the percentage decrease in wear rate (over LM30 alloy) for 15SPS-C, 15SPS-M, 15SPS-F, 15DPS-1, 15DPS-2, and 15DPS-3 AMCs at contact pressure and operating temperature condition of 1 MPa and 200 ℃ respectively. It can be noted that 15SPS-F and 15DPS-3 composites showed the highest reduction in wear rate of AMCs over the base alloy (78% and 80% reduction respectively).

Table 5.3 Reduction in wear rate (over base alloy) at a given operating temperature (200 ℃) and contact pressure (1 MPa)

Composite	*Percentage decrease in mean wear rate (over base alloy)*
15SPS-C	64%
15SPS-M	67%
15SPS-F	78%
15DPS-1	68%
15DPS-2	70%
15DPS-3	80%

The wear rate of 15SPS-F and 15DPS-3 composites was compared to the commercially used grey cast iron material utilized for fabrication of automobile brake rotors. Figure 5.8a presents the mean steady-state wear rate at various operating temperatures for 15SPS-F, 15DPS-3 composites, and the cast iron specimen. It was observed that till a high operating temperature of 200 ℃, the wear rates of 15SPS-F/15DPS-3 AMCs processed in the present work were comparable to the commercial material. However, beyond 200 ℃, the performance of cast iron specimen was superior to that of AMCs. To elaborate this further, Figure 5.8b presents the derivative of wear rate as a function of operating temperature. Figure 5.8b shows that for any

given working condition (i.e. for any derivative of wear rate w.r.t. operating temperature), the cast iron specimen can operate till a higher temperature. For example, at a derivative value of 0.05 $mm^3m^{-1}{}^{\circ}C^{-1}$, the AMCs (15SPS-F and 15DPS-3) can operate till a temperature of 200 ℃ only, whereas the cast iron specimen can operate till a higher temperature of 300 ℃. From these observations, it can be noted that working range of AMCs processed in the present work is till 200 ℃, whereas for the commercial material it is till 300 ℃. Though in terms of wear performance, cast iron is superior to AMCs, however, the brake drums fabricated using AMCs are about 60% lighter in weight in comparison to the cast iron brake drums [58]. Considering these aspects (comparable wear rate till temperatures of 200 ℃ and significant weight reduction), the sillimanite reinforced AMCs appear to be a better material for processing brake drums for light vehicles.

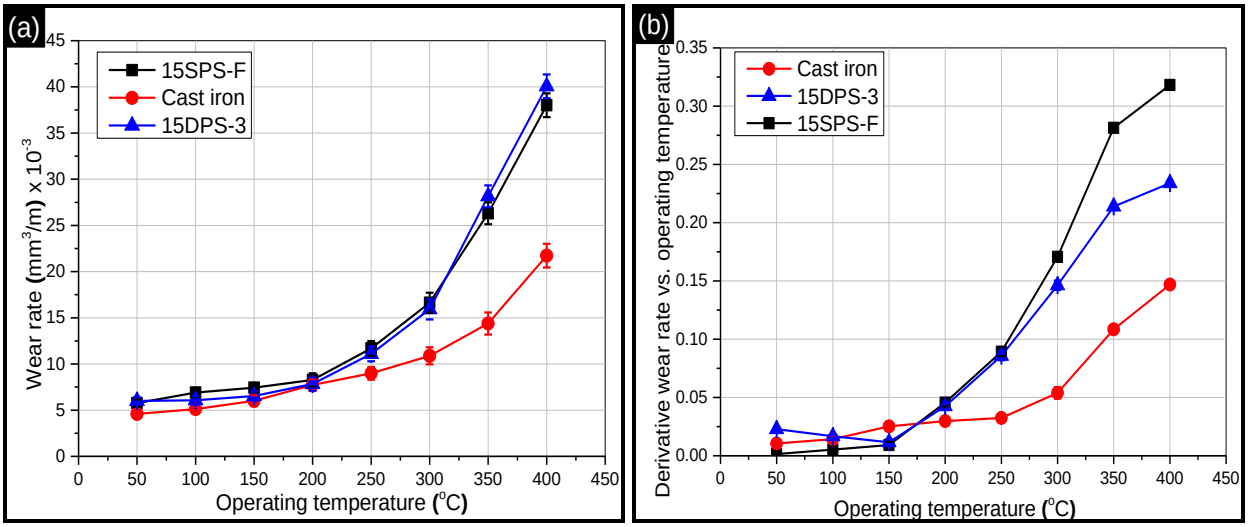

Figure 5.8 (a) Wear rate comparison of GCI, 15DPS-3, and 15SPS-F AMCs at 1MPa, and (b) Derivative of wear rate with respect to operating temperature of GCI, 15DPS-3, and 15SPS-F AMCs

5.3.3 WEAR MECHANISMS FOR MATERIAL LOSS

From the results of wear test of the present research work and the available literature, the tentative wear mechanism causing material loss due to wear at elevated temperatures is depicted in Figure 5.9a–d. Figure 5.9a shows that initially the countersurfaces have asperity-to-asperity contact. As the wear proceeds at a given operating temperature, the relative motion between the asperities of countersurfaces lead to generation of mocroploughing action, thus forming abrasive

grooves on the pin surface (Figure 5.9a). In this period thes hard reinforcements bear the abrasion until they are leveled with the matrix .Therefore, the surface damage is only restrained to the abrasion of the contact surface and results in inferior wear rate [199,200]. As the sliding continues, the asperities deform leading to generation of wear debris and wider grooves (Figure 5.9b). Further increase in the sliding distance increases the area of contact between the countersurfaces and also causes higher deformation of the pin surface. Moreover, at this high contact pressure and operating temperature condition, micro-crack initiation is observed on the pin surface (Figure 5.9c). With progression in sliding distance these micro-cracks propagate into the matrix material and finally meet each other. These results in huge volume loss of material causing large surface damage and hence high wear rates [61]. This material loss appears as large delaminated areas indicating adhesive/delamination wear (Figure 5.9d).

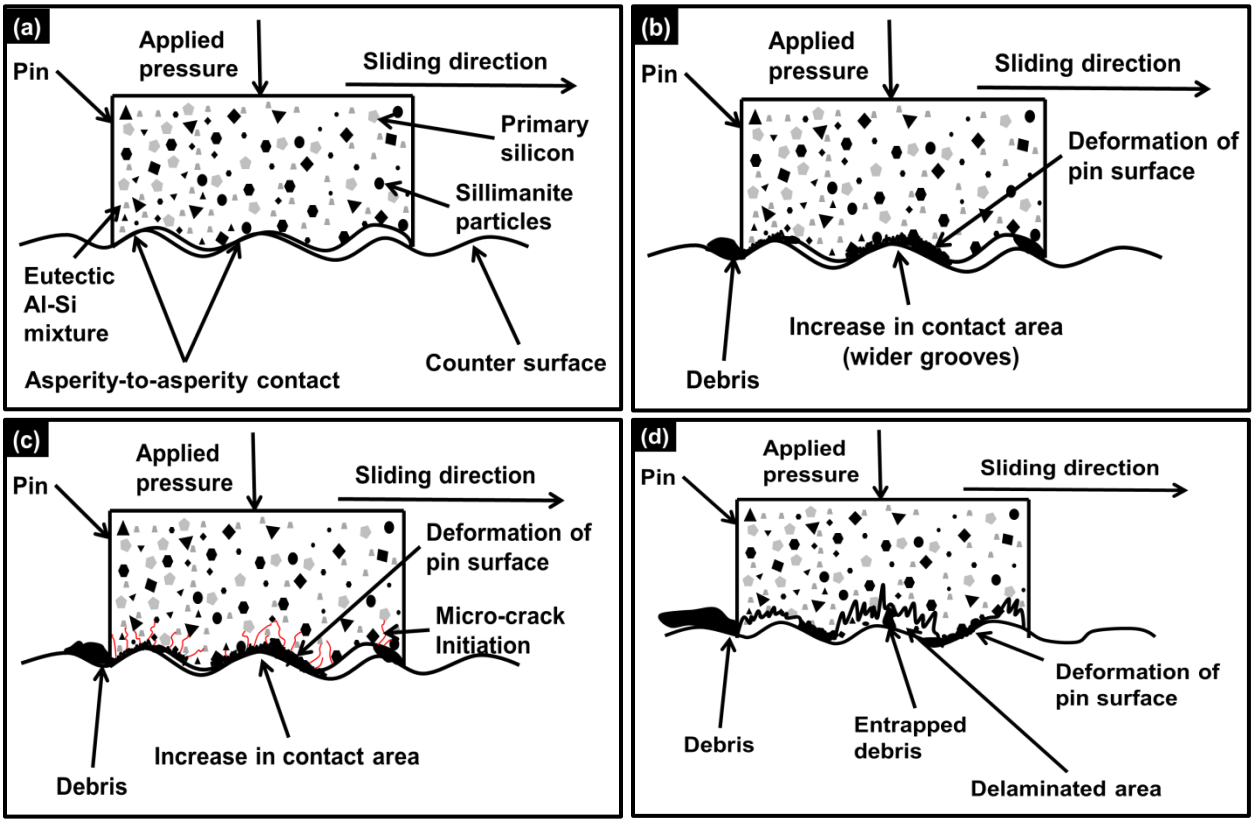

Figure 5.9 (a–d) Schematic of the tentative wear mechanisms causing material loss in AMCs

5.4 XRD OF WEAR TRACKS AND WEAR DEBRIS

Figure 5.10a–d presents the XRD analysis of wear tracks of base alloy and 15DPS-3 composite at a contact pressure of 0.2 MPa and 1 MPa respectively at operating temperature of 200 ℃.

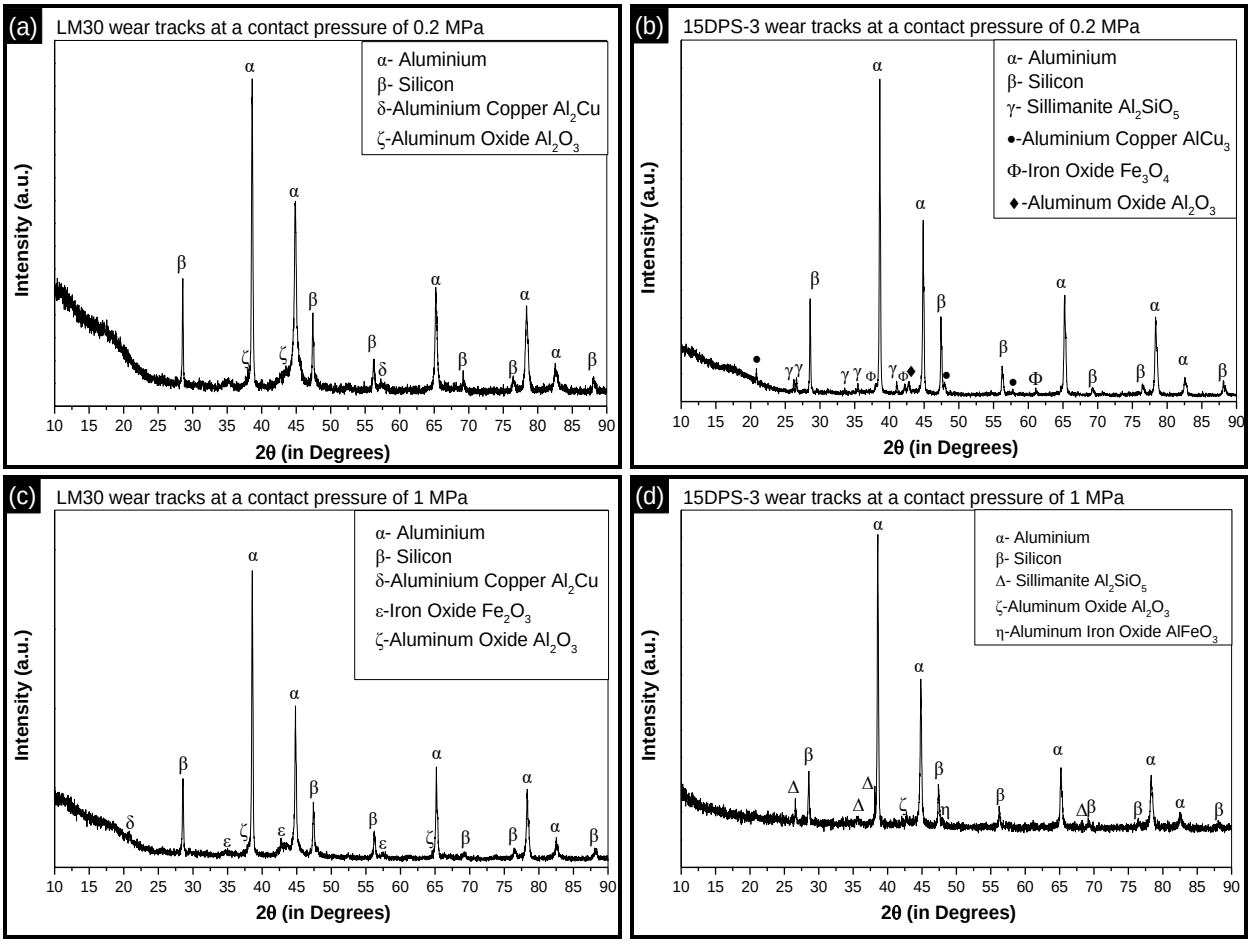

Figure 5.10 XRD analysis of wear track for (a) base alloy at contact pressure of 0.2 MPa, (b) 15DPS-3 AMC at contact pressure of 0.2 MPa, (c) base alloy at contact pressure of 1 MPa, and (d) 15DPS-3 AMC at contact pressure of 1 MPa (all at the operating temperature of 200 ℃)

The XRD of wear tracks of base alloy clearly shows the presence of Al_2O_3, and SiO_2 phases (Figure 5.10a–d). The presence of these phases is a resultant of the reaction of matrix with the atmospheric oxygen. For 0.2 MPa contact pressure, XRD of wear tracks shows presence of oxides of the matrix i.e. aluminium and silicon (Figure 5.14a–b). Apart from these phases, oxides of iron are also observed for wear at 1 MPa contact pressure. The source of iron is the EN32 steel disc. At high contact pressures, the high frictional heat at the interfacial regions causes the

localized welding of the pin and disc. Due to the sliding motion of pin on the disc, the weld is broken and particles of iron oxide get embedded in the pin surface.

Figure 5.11a–d presents the XRD results of wear debris of base alloy/15DPS-3 composite under various conditions. Several oxides (viz. Al_2O_3, SiO_2, Fe_2O_3, $AlFeO_3$, Fe_3O_4 etc.) were observed. The extent of oxides observed in the wear debris was significantly more as compared to wear tracks. This confirmed the tearing and removal of oxide film from the pin surface.

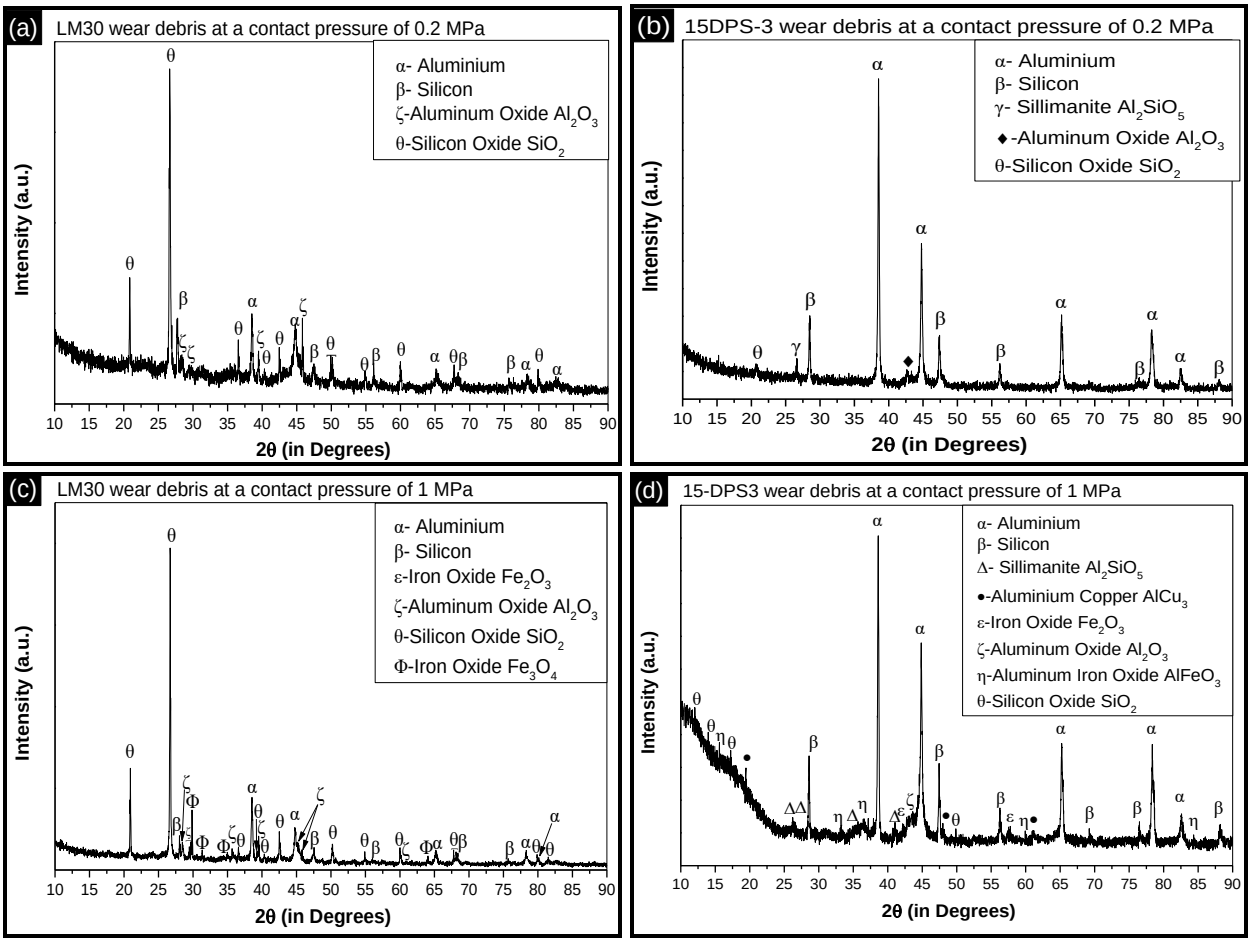

Figure 5.11 XRD analysis of wear debris for (a) base alloy at contact pressure of 0.2 MPa, (b) 15DPS-3 AMC at contact pressure of 0.2 MPa, (c) base alloy at contact pressure of 1 MPa, and (d) 15DPS-3 AMC at contact pressure of 1 MPa (all at the operating temperature of 200 ℃)

For 15DPS-3 composites, the wear debris clearly indicated a blend of different oxides (aluminium oxide, silicon oxide, and iron oxide), sillimanite particles, and various other phases like aluminium, silicon and aluminium copper etc. (Figure 5.11a–d). This blend of various

oxides at the contact of pin and disc is generally termed as a tribochemical layer (TL) or mechanically mixed layer (MML) or glaze layer (GL). The GL formation increases with increase in sillimanite weight percentage and decreases the wear rate of AMCs.

The maximum intensity peaks observed for the base alloy were of silicon oxide, whereas for the composites, the maximum intensity peaks observed were of aluminium (Figure 5.11c–d). This indicated that at high operating temperature of 200 ℃, the oxide film was stable on the wear tracks of AMCs whereas for the base alloy, the oxide film got removed and higher concentration of oxides were observed in the wear debris. Thus, the addition of sillimanite particles led to the formation of a stable oxide film and improved the wear resistance of AMCs.

5.5 FRICTION TESTING

5.5.1 RESULTS OF FRICTION TESTING OF BASE ALLOY

Coefficient of friction (COF) value for steady-state wear at different operating temperatures was obtained separately. The mean steady-state COF value (for base alloy/AMCs) at any given operating temperature was obtained by averaging various COF values obtained for different sliding distances in steady-state wear range (in the range of 1500–3000 m) at that operating temperature.

Figure 5.12 presents the mean steady-state COF values for base alloy obtained at various elevated temperatures (50–300 ℃; at interval of 50 ℃). At any given contact pressure, the mean steady-state COF value (as a function of operating temperature) of AMCs initially decreased and then increased. For contact pressure of 0.2 MPa and 0.6 MPa, the mean COF value decreased initially till operating temperature of 150 ℃, and beyond this temperature, mean COF value continuously increased. The oxide layer was stable till a temperature of 150 ℃ and prevented direct metal-to-metal contact, thus, a decrease in COF was observed [51]. Beyond this temperature, the tearing of oxide layer occurred and hence COF increased. Further, for contact pressure of 1 MPa, the COF value decreased till 100 ℃, and thereafter showed a continuous sharp increase. COF was not observed for the temperature of 300 ℃ as the material was completely worn out at a sliding distance of 1850 m.

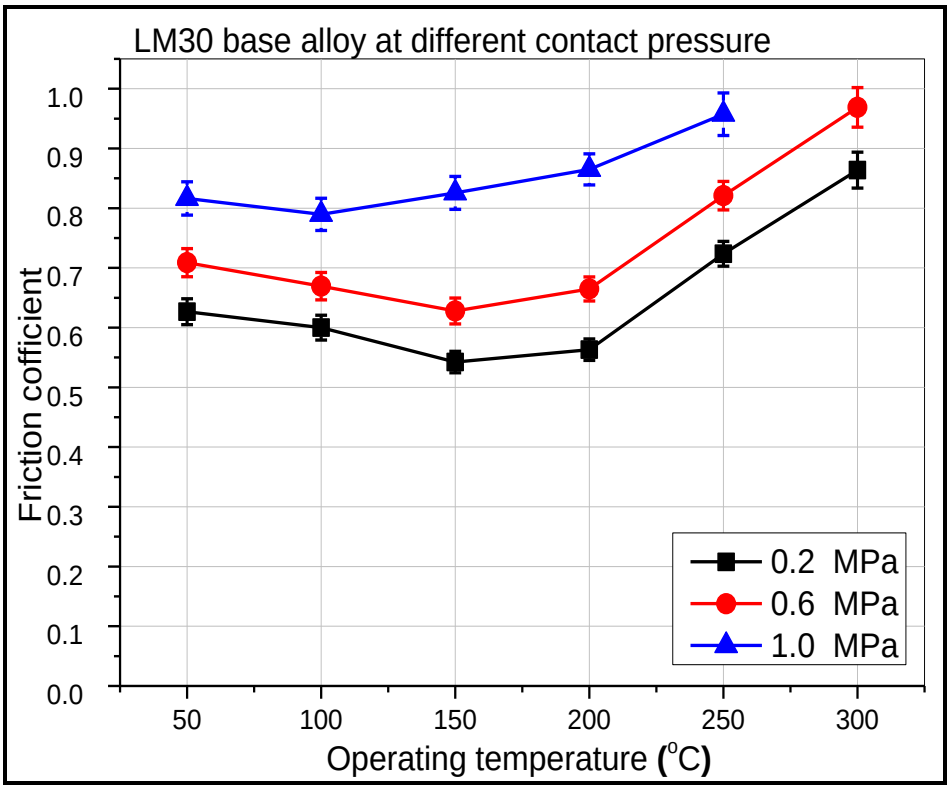

Figure 5.12 Coefficient of friction values of base alloy as a function of operating temperature at various contact pressures

5.5.2 RESULTS OF FRICTION TESTING OF AMCs

Figure 5.13 to 5.15 present the mean COF values of various AMCs obtained at operating temperatures in the range of 50–300 ℃ for various contact pressures of 0.2 MPa, 0.6 MPa, and 1 MPa. For the contact pressure of 0.2 MPa and 0.6 MPa, the trend in COF values of AMCs as a function of operating temperature was similar to that shown by base alloy. However, for AMCs, the COF values decreased till a relatively higher temperature of 200 ℃ beyond which an increase in COF values was observed. Further, for the contact pressure of 1 MPa, the trend in COF values of AMCs as a function of operating temperature was different from that obtained for the base alloy. At this condition of high contact pressure (1 MPa), the mean COF value of AMCs remained almost constant with increase in operating temperature till 200 ℃ and thereafter increased. For any contact pressure and operating temperature condition, the AMCs processed in the present work showed significantly lower COF values compared to the base alloy.

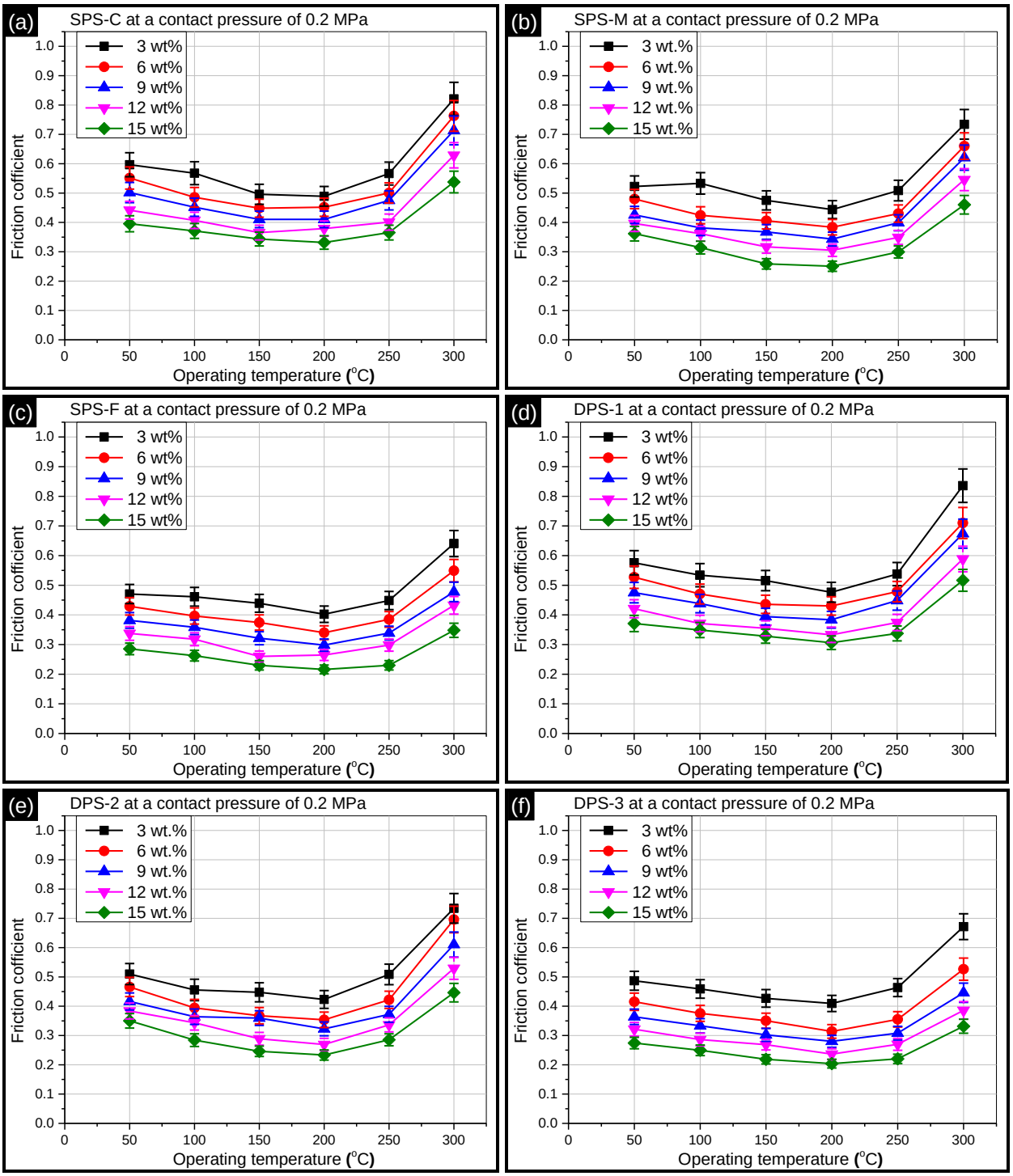

Figure 5.13 Coefficient of friction values of AMCs as a function of operating temperature at 0.2 MPa for (a) SPS-C, (b) SPS-M, (c) SPS-F, (d) DPS-1, (e) DPS-2, and (f) DPS-3 composites

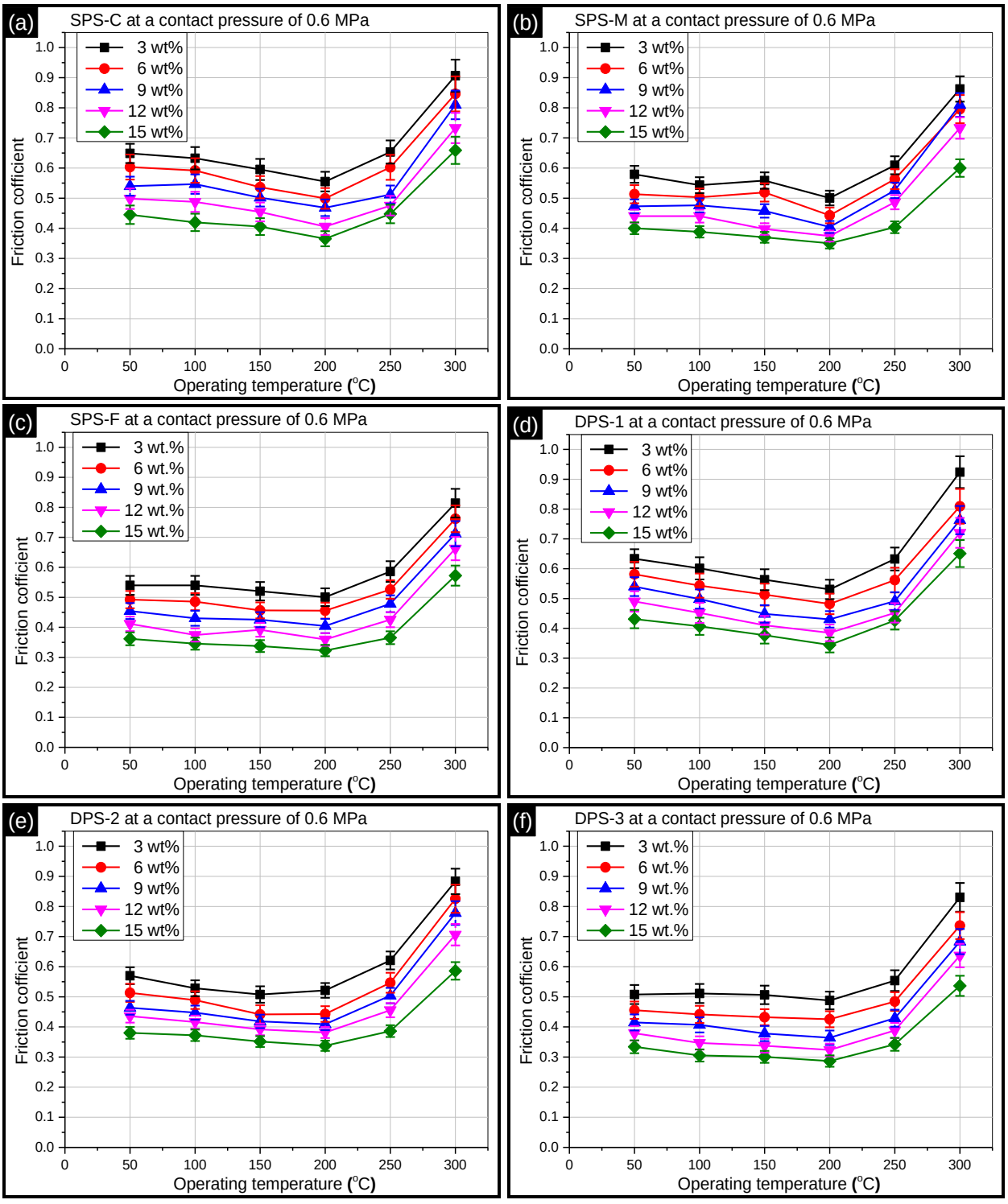

Figure 5.14 Coefficient of friction values of AMCs as a function of operating temperature at 0.6 MPa for (a) SPS-C, (b) SPS-M, (c) SPS-F, (d) DPS-1, (e) DPS-2, and (f) DPS-3 composites

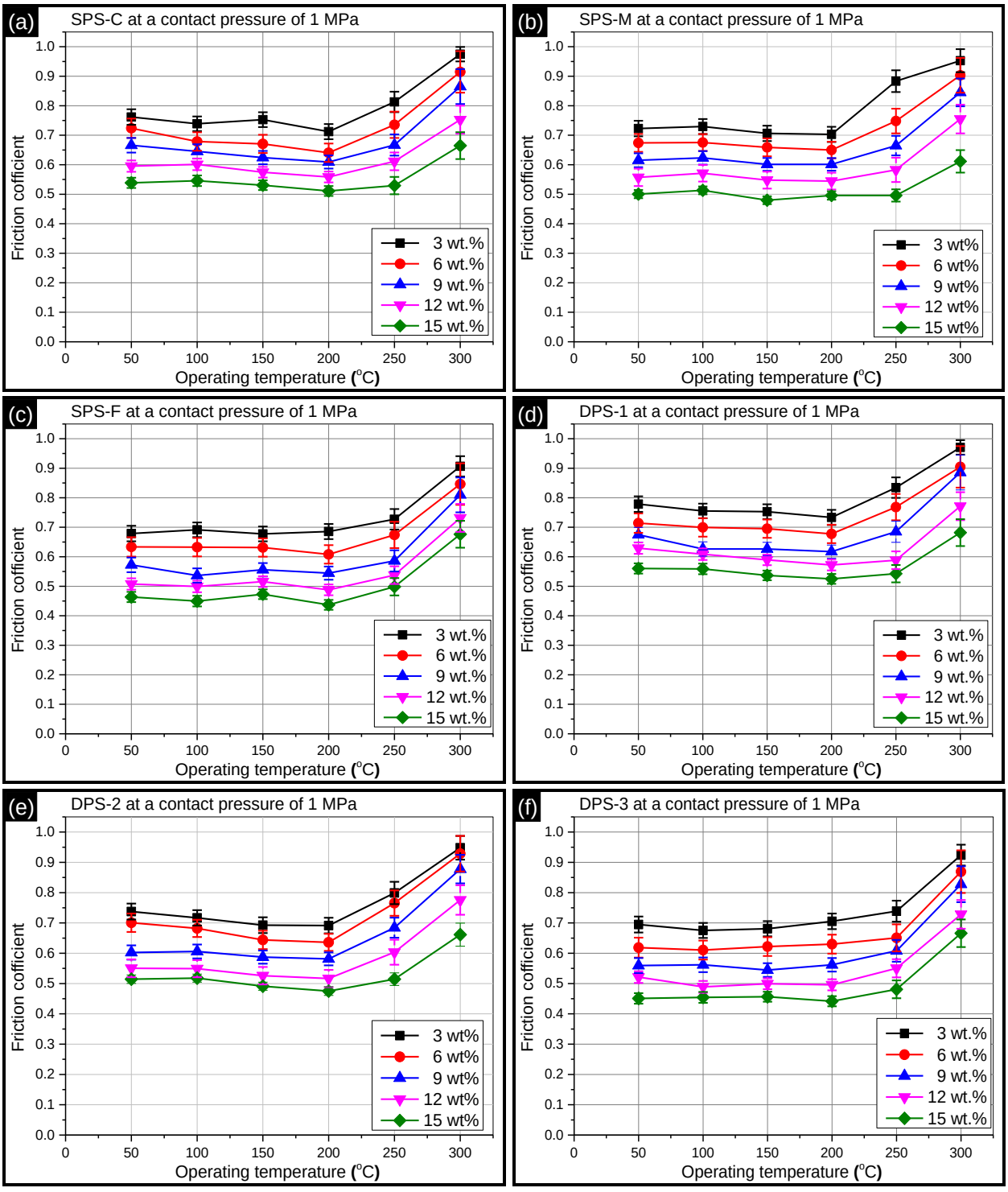

Figure 5.15 Coefficient of friction values of AMCs as a function of operating temperature at 1 MPa for (a) SPS-C, (b) SPS-M, (c) SPS-F, (d) DPS-1, (e) DPS-2, and (f) DPS-3 composites

Sillimanite particle reinforcement in the base alloy acts as a load bearing element. Under any given contact pressure and operating temperature condition, the reinforced particles carry a significant portion of the contact pressure, and thus, resist the wear of the matrix material [51]. Also sillimanite particles have high thermal stability, high hardness, and low CTE values. Due to these characteristics, sillimanite reinforcement makes the AMCs an anti-frictional material displaying low COF values.

Table 5.4 illustrates the reduction in mean steady-state COF value of various AMCs over the base alloy evaluated for contact pressure and operating temperature condition of 1 MPa-200 ℃.

Table 5.4 Percentage reduction obtained in the mean COF value of AMCs over base alloy

Composite	*Percentage decrease in mean COF (over base alloy)*
15SPS-C	40 %
15SPS-M	43 %
15SPS-F	52 %
15DPS-1	43 %
15DPS-2	44 %
15DPS-3	54 %

It can be observed from Table 5.4 that 15SPS-F and 15DPS-3 AMCs showed maximum reduction in mean COF value (52% and 54% reduction respectively, over the base alloy). Finally mean steady-state COF value (at 1 MPa and 200 ℃ condition) for the cast iron specimen was observed to be 0.39. The COF values of 15SPS-F and 15DPS-3 AMCs were close to that of the commercial material (0.42 and 0.41 respectively).

5.6 WEAR TRACK AND WEAR DEBRIS ANALYSIS

5.6.1 LM30 BASE ALLOY

Figure 5.16a–d presents the SEM micrographs of wear track and wear debris for LM30 base alloy under the extreme contact pressure conditions of 0.2 and 1 MPa at an operating temperature of 200 ℃. Operating temperature value of 200 ℃ was selected for investigation as this temperature appeared to be the transition temperature reflecting mild-to-severe wear transition. The wear testing results of base alloy at operating temperature of 200 ℃ revealed that wear rate increased with increase in contact pressure (Figure 5.4). The same can be observed from the SEM micrographs of wear track of pin surface of base alloy showing an increase in delamination area (Figure 5.16a–d) with increase in contact pressure. At the low contact pressure of 0.2 MPa,

fine abrasive grooves with some delamination area were observed (Figure 5.16a). The fine abrasive grooves developed as a result of entrapment of hard particles in-between the countersurfaces (pin and steel disc) [190]. At the high contact pressure of 1 MPa, wider grooves with larger delaminated area were observed (Figure 5.16b). Higher contact pressure caused deformation of the material in the direction of sliding leading to generation of cavities, and thus, caused tearing/delamination of the pin surface [92].

Figure 5.16 c–d presents the SEM micrographs of wear debris of base alloy at contact pressure of 0.2 MPa and 1 MPa respectively for operating temperature of 200 ℃. Flake like debris were mainly observed indicating abrasive wear mechanism at the initial stages of wear test. However, features like grooves on debris, thread type debris, oxidized debris, corrugated debris, molten debris were also observed. The presence of micro-cracks indicated removal of material by delamination also. Thus, even at high operating temperature conditions, the initial wear mechanism was abrasive wear followed by delamination/adhesive wear. Further, Figure 5.16e presents the generation of micro cracks on the wear debris. Micro cracks indicate the plastic deformation and fracture of pin surface.

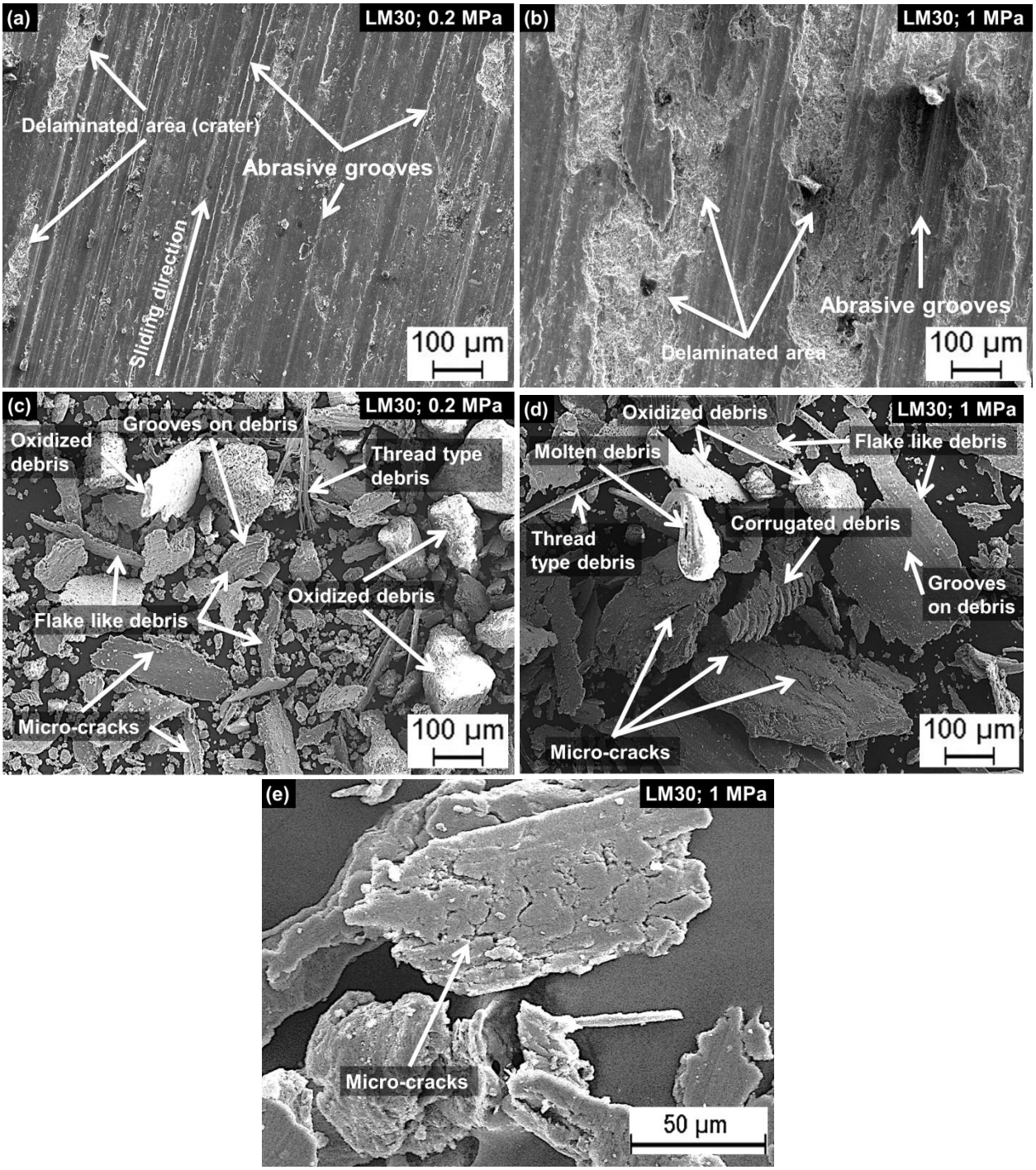

Figure 5.16 Wear tracks and debris analysis of LM30 base alloy at a temperature of 200 ℃ (a) wear tracks at 0.2 MPa, (b) wear tracks at 1MPa, (c) wear debris at 0.2 MPa, (d) wear debris at 1 MPa, and (g) high magnification debris analysis of LM30 base alloy at 1 MPa

5.6.2 COMPOSITE FORMULATIONS

Figure 5.17 to 5.21 present the SEM micrographs of wear tracks of 3 wt.%, 6 wt.%, 9 wt.%, 12 wt.%, and 15 wt.% sillimanite reinforced AMCs under the extreme contact pressure conditions of 0.2 MPa and 1 MPa at an operating temperature of 200 ℃. For any contact pressure and operating temperature condition, SEM micrographs clearly showed less surface damage in AMCs compared to the base alloy. Further, for a given AMC composition, micrographs revealed relatively more surface damage at higher contact pressure condition. The rise in surface damage is a representative of increment in wear rate and COF values of a material, and thus, SEM microscopy results of wear track were in agreement with the results of COF analysis/wear testing. For the contact pressure of 0.2 MPa, narrow grooves running along the sliding direction having some delaminated area were observed on the worn-out pin surface as shown in Figure 5.17(a, c, e, g, i, k), Figure 5.18(a, c, e, g, i, k), Figure 5.19(a, c, e, g, i, k), Figure 5.20(a, c, e, g, i, k), and Figure 5.21(a, c, e, g, i, k). However, for higher contact pressure (1 MPa), wider grooves with larger delamination area on the worn-out pin surface were observed as shown in Figure 5.17(b, d, f, h, j, l), 5.18(b, d, f, h, j, l), 5.19(b, d, f, h, j, l), 5.20(b, d, f, h, j, l), and 5.21(b, d, f, h, j, l). SEM micrographs of the wear track of AMCs also displayed some characteristic features like presence of micro cracks as shown in Figure 5.17j, Figure 5.19d, Figure 5.20h, Figure 5.21(c, k) and also presence of some wear debris embedded in pin surface as shown in 5.17(a, b, g, i), 5.18(a, j), 5.19(b, c, k), Figure 5.20 (b, c), and Figure 5.21(a, c, l).

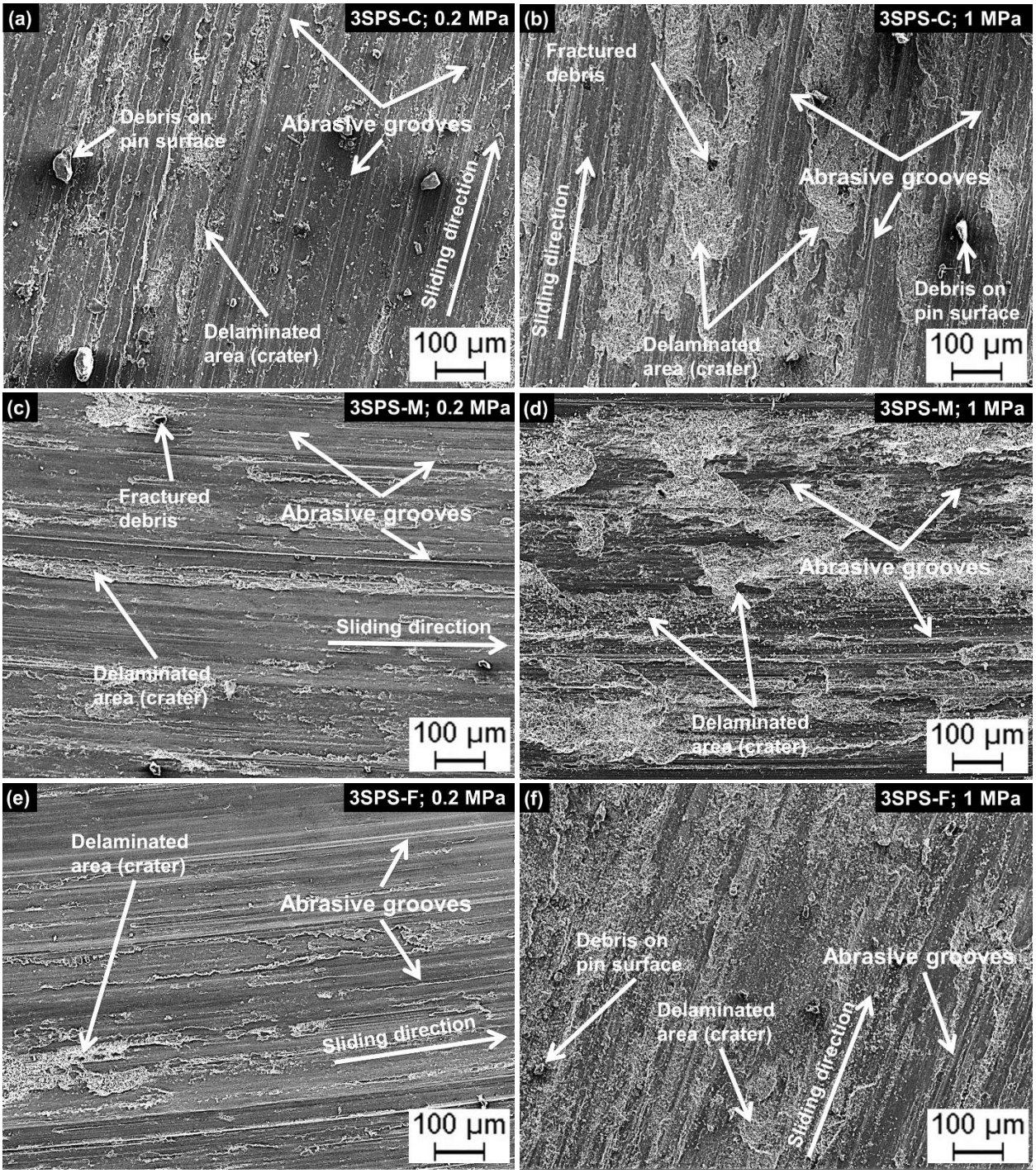
(a)
3SPS-C; 0.2 MPa
Debris on pin surface
Abrasive grooves
Sliding direction
Delaminated area (crater)
100 µm
(b)
3SPS-C; 1 MPa
Fractured debris
Abrasive grooves
Sliding direction
Debris on pin surface
Delaminated area (crater)
100 µm
(c)
3SPS-M; 0.2 MPa
Fractured debris
Abrasive grooves
Sliding direction
Delaminated area (crater)
100 µm
(d)
3SPS-M; 1 MPa
Abrasive grooves
Delaminated area (crater)
100 µm
(e)
3SPS-F; 0.2 MPa
Delaminated area (crater)
Abrasive grooves
Sliding direction
100 µm
(f)
3SPS-F; 1 MPa
Debris on pin surface
Abrasive grooves
Delaminated area (crater)
Sliding direction
100 µm

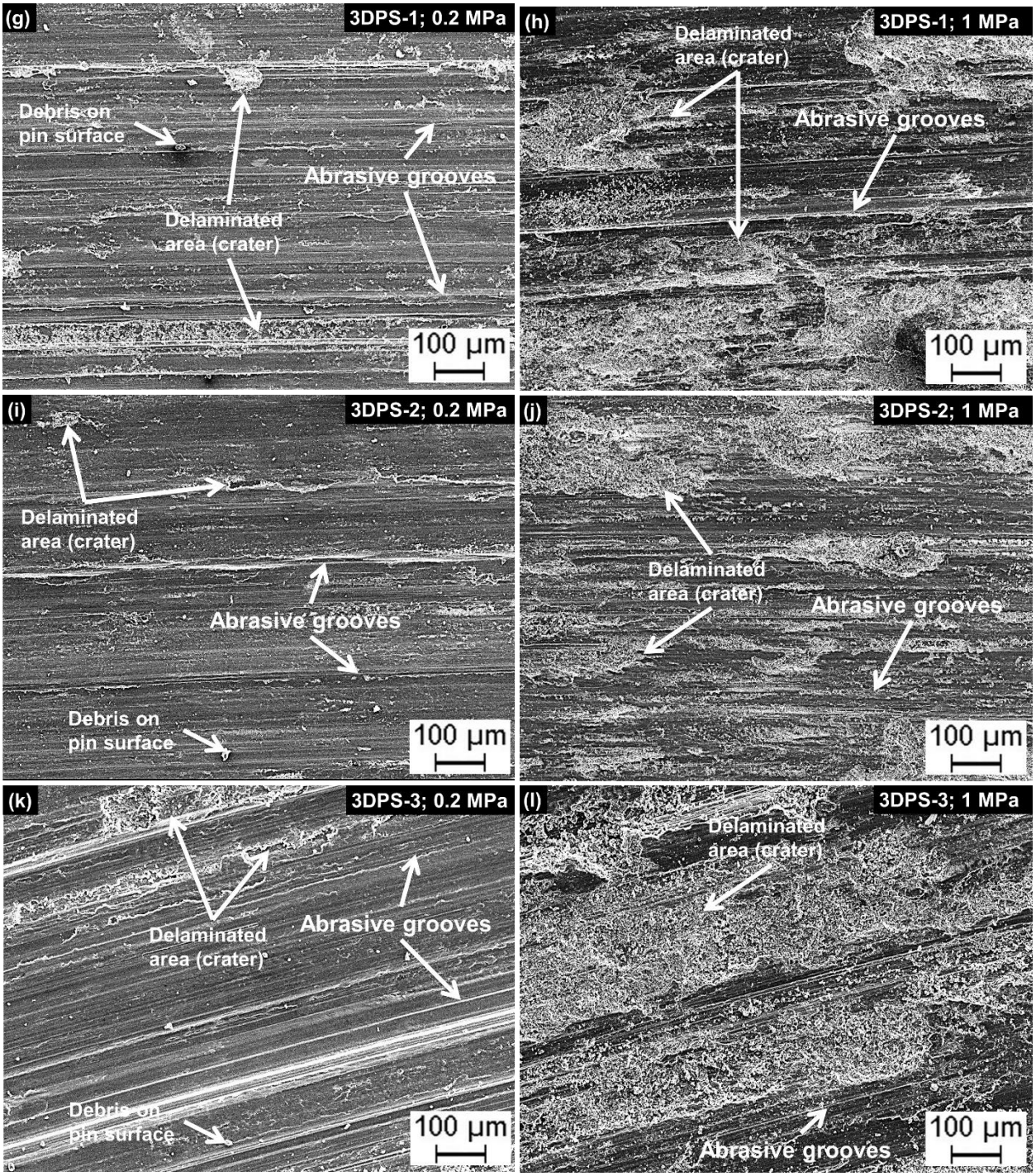

Figure 5.17 SEM micrographs of wear tracks of (a) 3SPS-C composite at 0.2 MPa, (b) 3SPS-C composite at 1 MPa, (c) 3SPS-M composite at 0.2 MPa, (d) 3SPS-M composite at 1 MPa, (e) 3SPS-F composite at 0.2 MPa, (f) 3SPS-F composite at 1 MPa, (g) 3DPS-1 composite at 0.2 MPa, (h) 3DPS-1 composite at 1 MPa, (i) 3DPS-2 composite at 0.2 MPa, (j) 3DPS-2 composite at 1 MPa, (k) 3DPS-3 composite at 0.2 MPa, and (l) 3DPS-3 composite at 1 MPa (all at the operating temperature of 200 ℃)

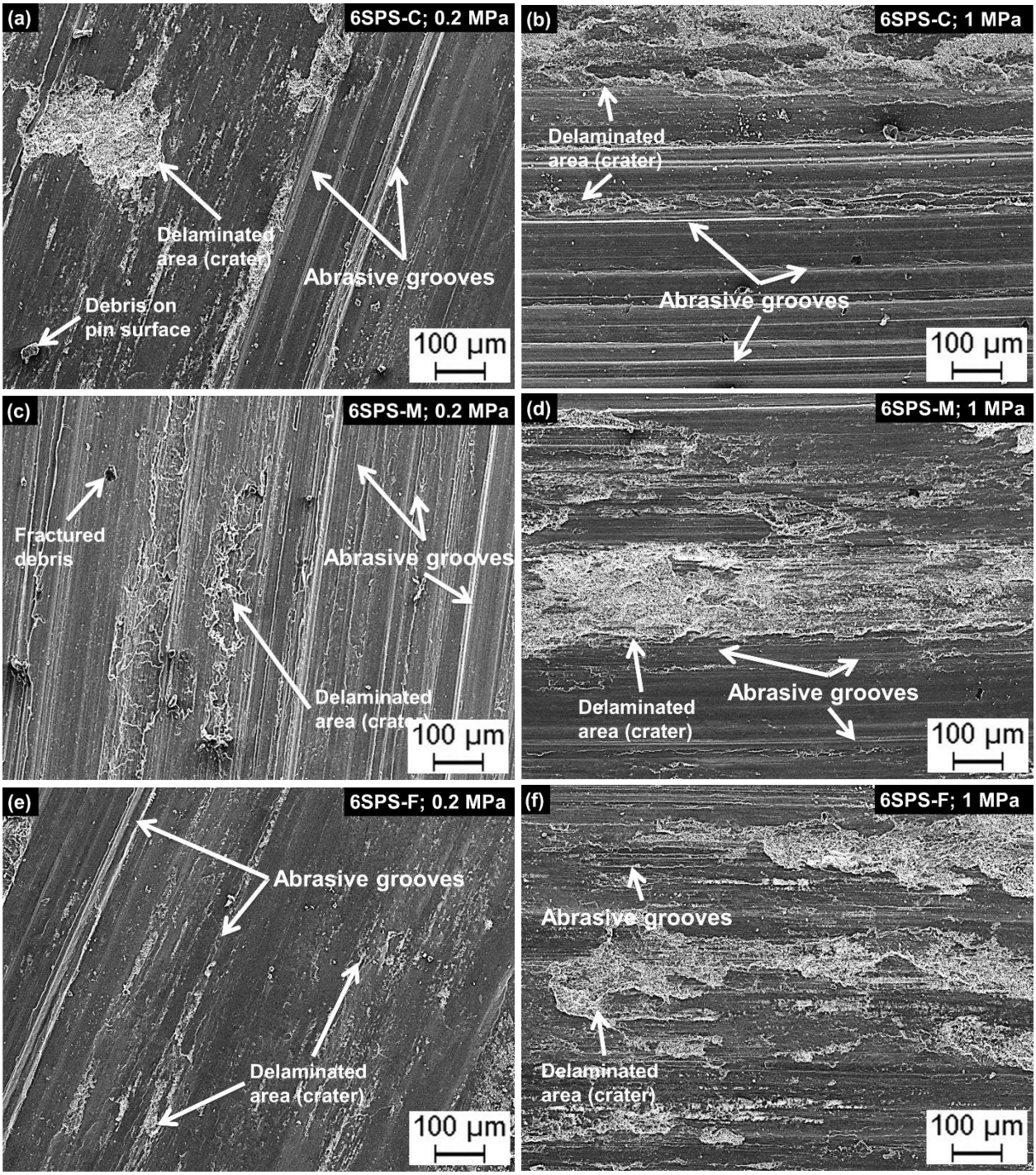
(a)
6SPS-C; 0.2 MPa
Delaminated area (crater)
Abrasive grooves
Debris on pin surface
100 µm
(b)
6SPS-C; 1 MPa
Delaminated area (crater)
Abrasive grooves
100 µm
(c)
6SPS-M; 0.2 MPa
Fractured debris
Abrasive grooves
Delaminated area (crater)
100 µm
(d)
6SPS-M; 1 MPa
Delaminated area (crater)
Abrasive grooves
100 µm
(e)
6SPS-F; 0.2 MPa
Abrasive grooves
Delaminated area (crater)
100 µm
(f)
6SPS-F; 1 MPa
Abrasive grooves
Delaminated area (crater)
100 µm

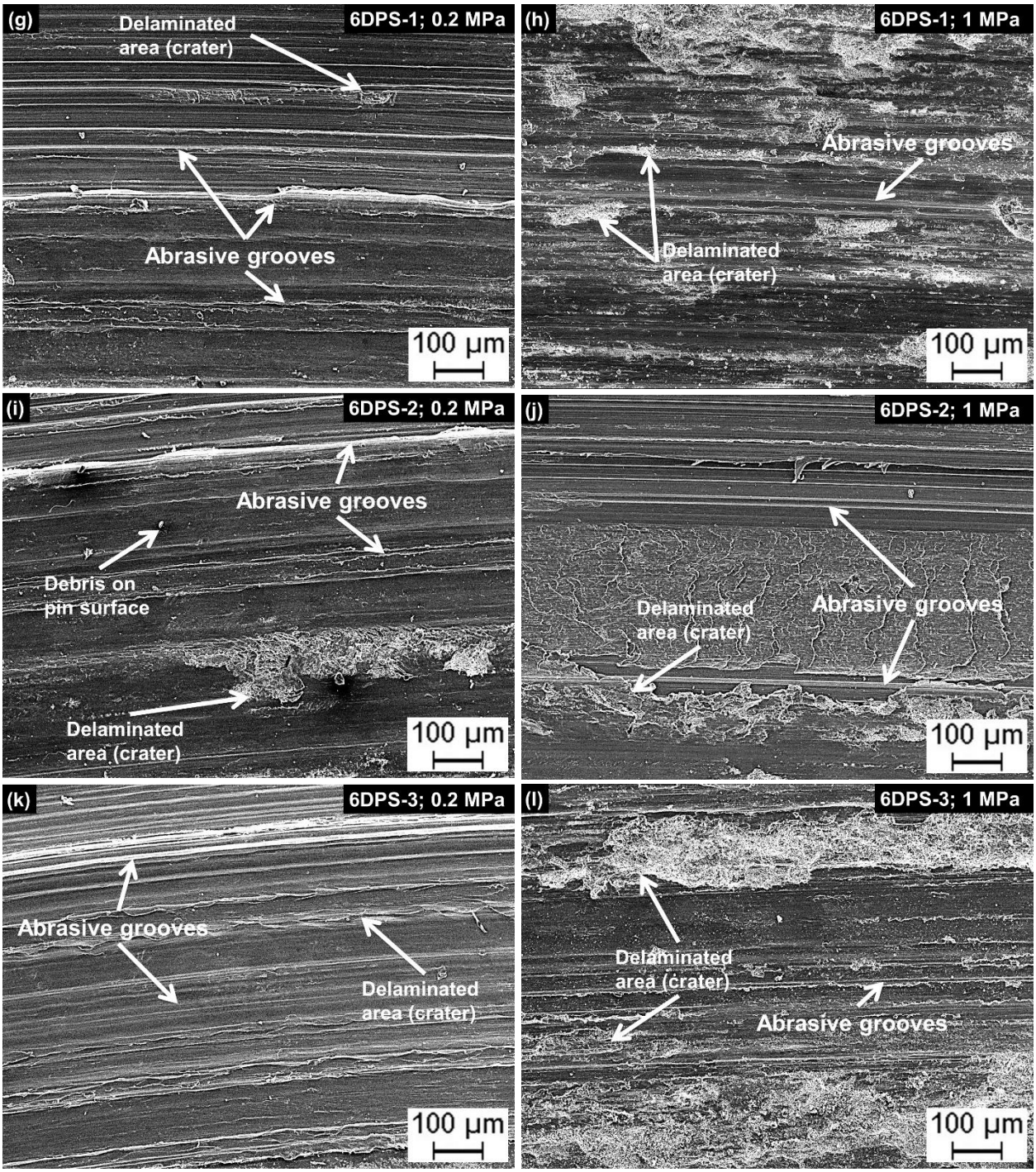

Figure 5.18 SEM micrographs of wear tracks of (a) 6SPS-C composite at 0.2 MPa, (b) 6SPS-C composite at 1 MPa, (c) 6SPS-M composite at 0.2 MPa, (d) 6SPS-M composite at 1 MPa, (e) 6SPS-F composite at 0.2 MPa, (f) 6SPS-F composite at 1 MPa, (g) 6DPS-1 composite at 0.2 MPa, (h) 6DPS-1 composite at 1 MPa, (i) 6DPS-2 composite at 0.2 MPa, (j) 6DPS-2 composite at 1 MPa, (k) 6DPS-3 composite at 0.2 MPa, and (l) 6DPS-3 composite at 1 MPa (all at the operating temperature of 200 ℃)

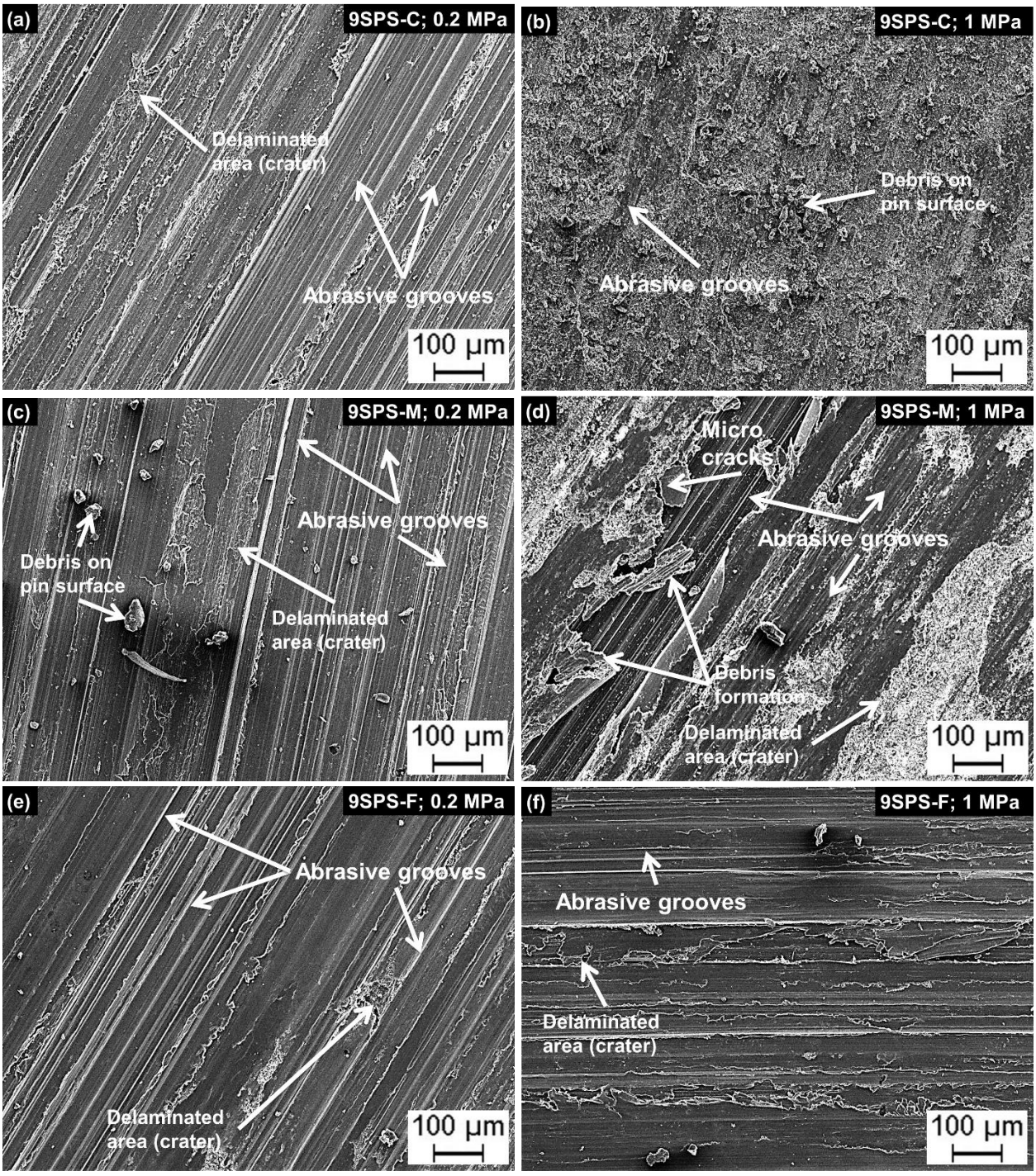
(a)
9SPS-C; 0.2 MPa
Delaminated area (crater)
Abrasive grooves
100 µm
(b)
9SPS-C; 1 MPa
Debris on pin surface
Abrasive grooves
100 µm
(c)
9SPS-M; 0.2 MPa
Abrasive grooves
Debris on pin surface
Delaminated area (crater)
100 µm
(d)
9SPS-M; 1 MPa
Micro cracks
Abrasive grooves
Debris formation
Delaminated area (crater)
100 µm
(e)
9SPS-F; 0.2 MPa
Abrasive grooves
Delaminated area (crater)
100 µm
(f)
9SPS-F; 1 MPa
Abrasive grooves
Delaminated area (crater)
100 µm

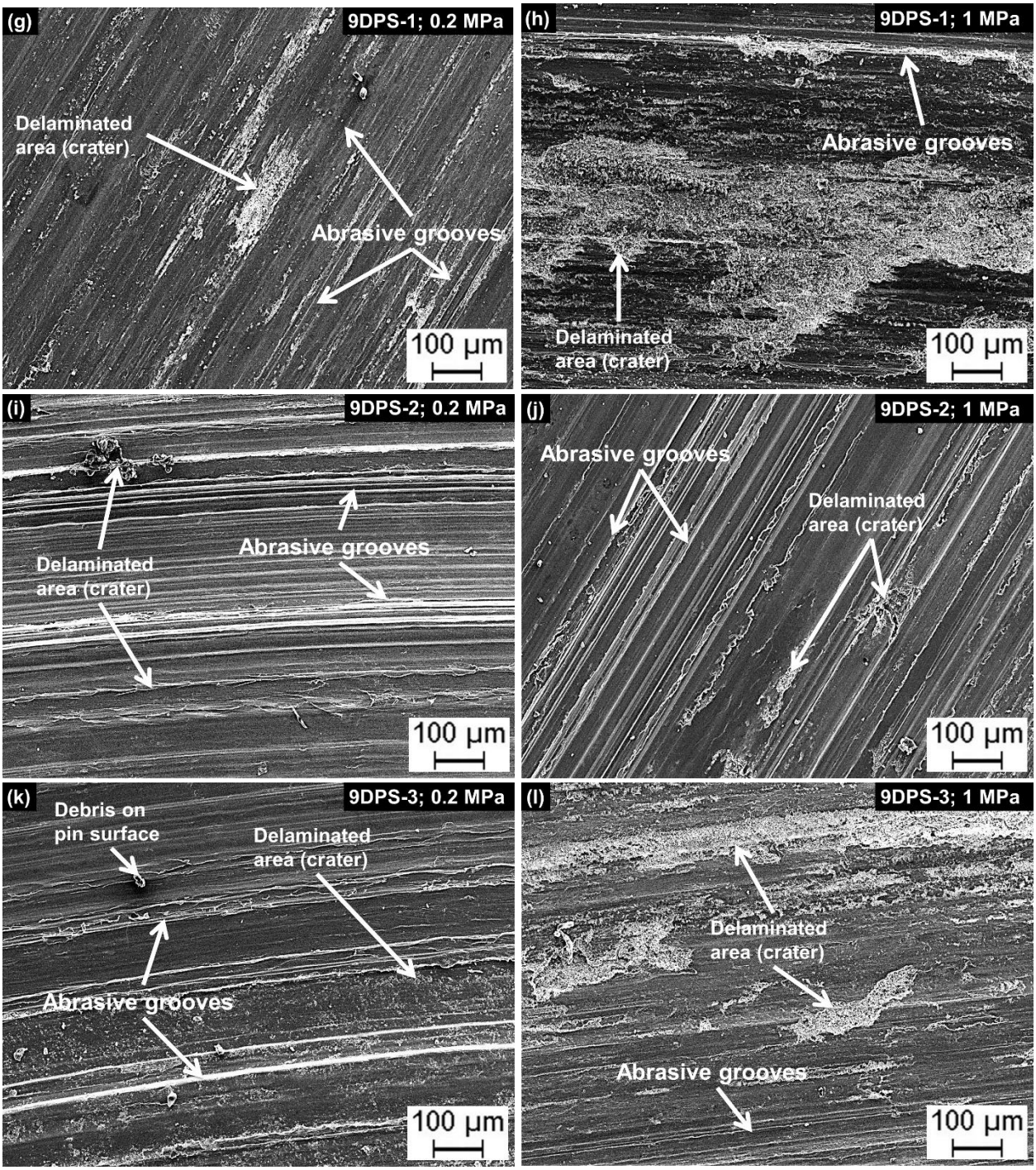

Figure 5.19 SEM micrographs of wear tracks of (a) 9SPS-C composite at 0.2 MPa, (b) 9SPS-C composite at 1 MPa, (c) 9SPS-M composite at 0.2 MPa, (d) 9SPS-M composite at 1 MPa, (e) 9SPS-F composite at 0.2 MPa, (f) 9SPS-F composite at 1 MPa, (g) 9DPS-1 composite at 0.2 MPa, (h) 9DPS-1 composite at 1 MPa, (i) 9DPS-2 composite at 0.2 MPa, (j) 9DPS-2 composite at 1 MPa, (k) 9DPS-3 composite at 0.2 MPa, and (l) 9DPS-3 composite at 1 MPa (all at the operating temperature of 200 ℃)

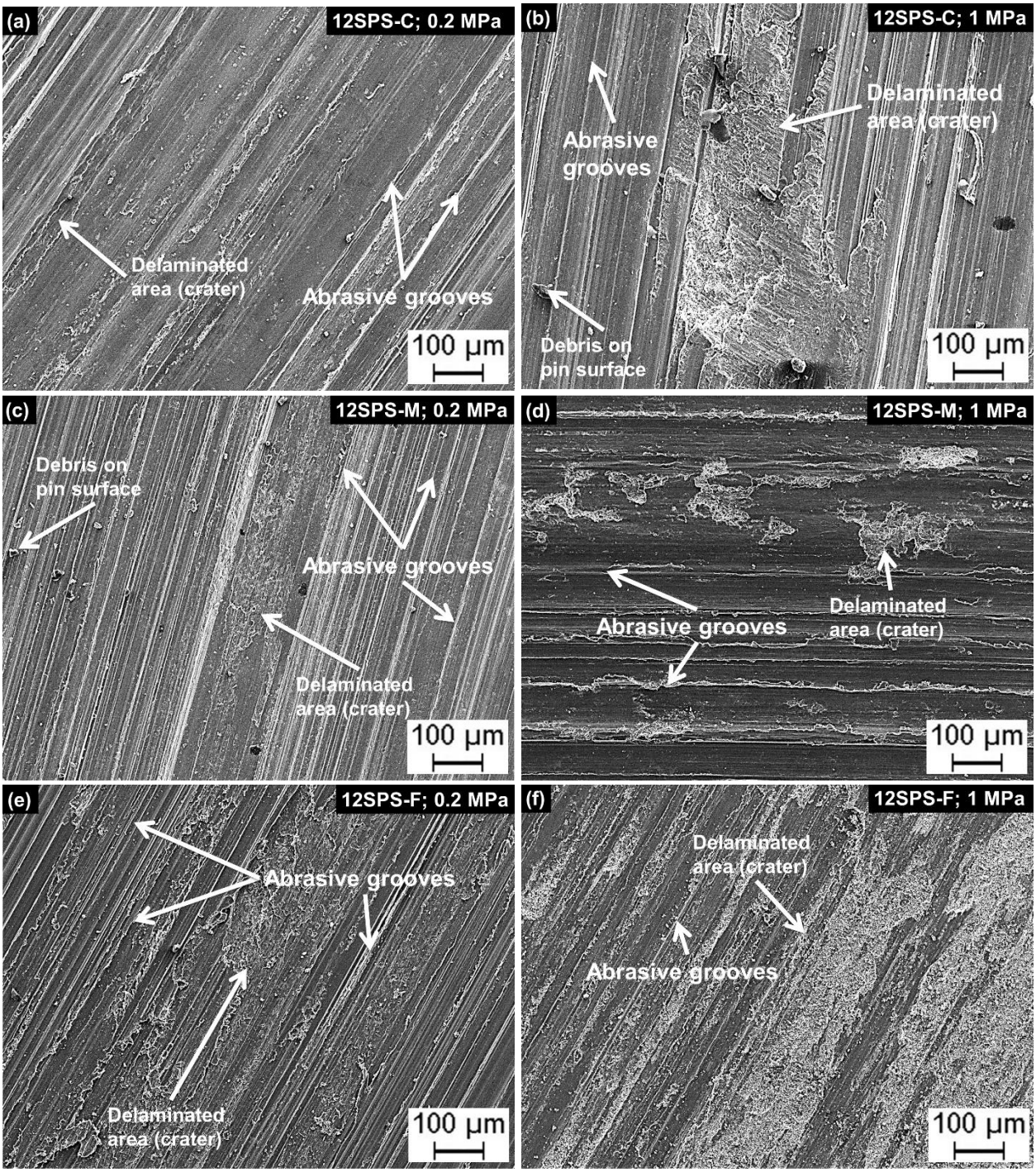
(a)
12SPS-C; 0.2 MPa
Delaminated area (crater)
Abrasive grooves
100 µm
(b)
12SPS-C; 1 MPa
Abrasive grooves
Delaminated area (crater)
Debris on pin surface
100 µm
(c)
12SPS-M; 0.2 MPa
Debris on pin surface
Abrasive grooves
Delaminated area (crater)
100 µm
(d)
12SPS-M; 1 MPa
Abrasive grooves
Delaminated area (crater)
100 µm
(e)
12SPS-F; 0.2 MPa
Abrasive grooves
Delaminated area (crater)
100 µm
(f)
12SPS-F; 1 MPa
Delaminated area (crater)
Abrasive grooves
100 µm

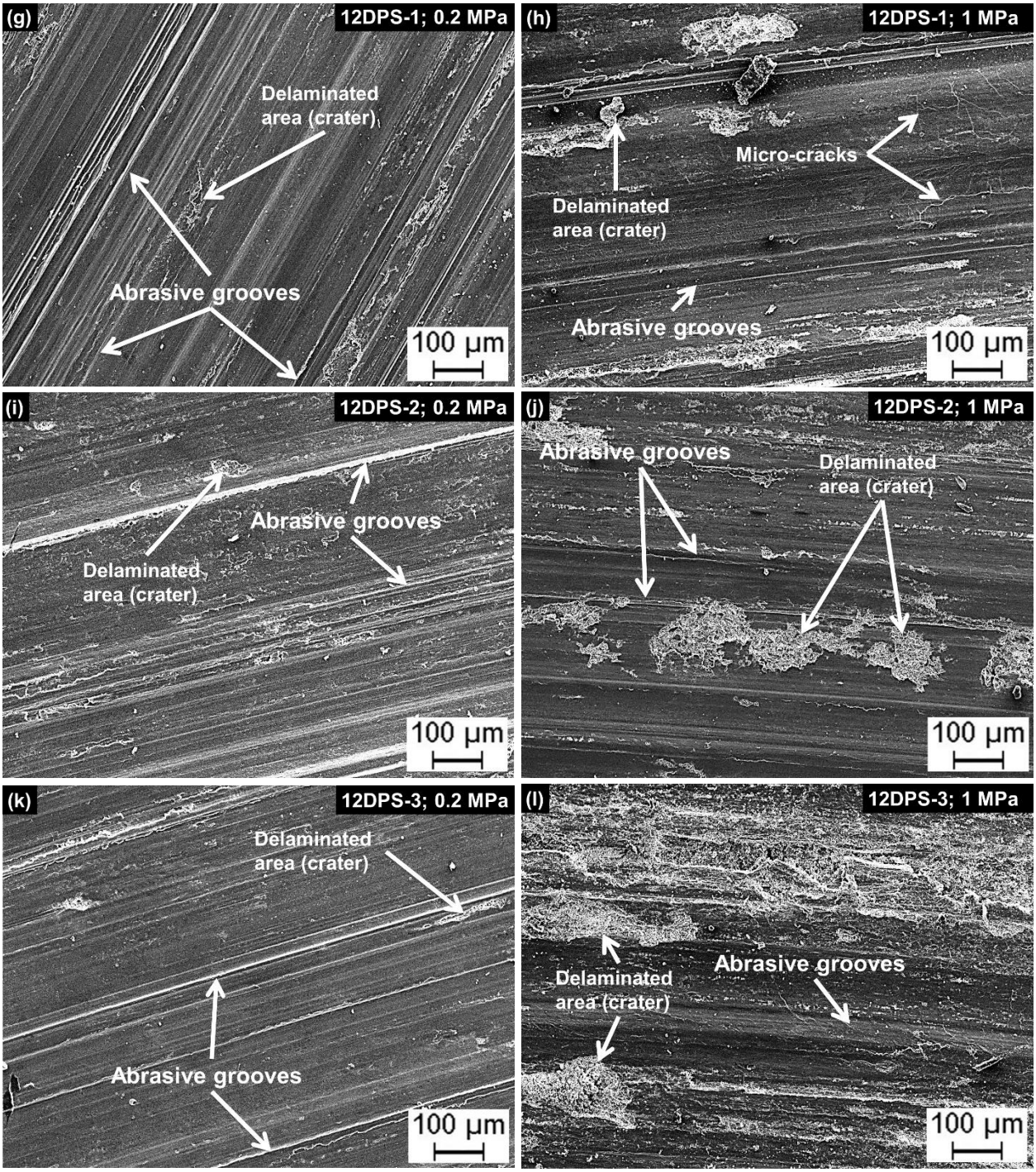

Figure 5.20 SEM micrographs of wear tracks of (a) 12SPS-C composite at 0.2 MPa, (b) 12SPS-C composite at 1 MPa, (c) 12SPS-M composite at 0.2 MPa, (d) 12SPS-M composite at 1 MPa, (e) 12SPS-F composite at 0.2 MPa, (f) 12SPS-F composite at 1 MPa, (g) 12DPS-1 composite at 0.2 MPa, (h) 12DPS-1 composite at 1 MPa, (i) 12DPS-2 composite at 0.2 MPa, (j) 12DPS-2 composite at 1 MPa, (k) 12DPS-3 composite at 0.2 MPa, and (l) 12DPS-3 composite at 1 MPa (all at the operating temperature of 200 ℃)

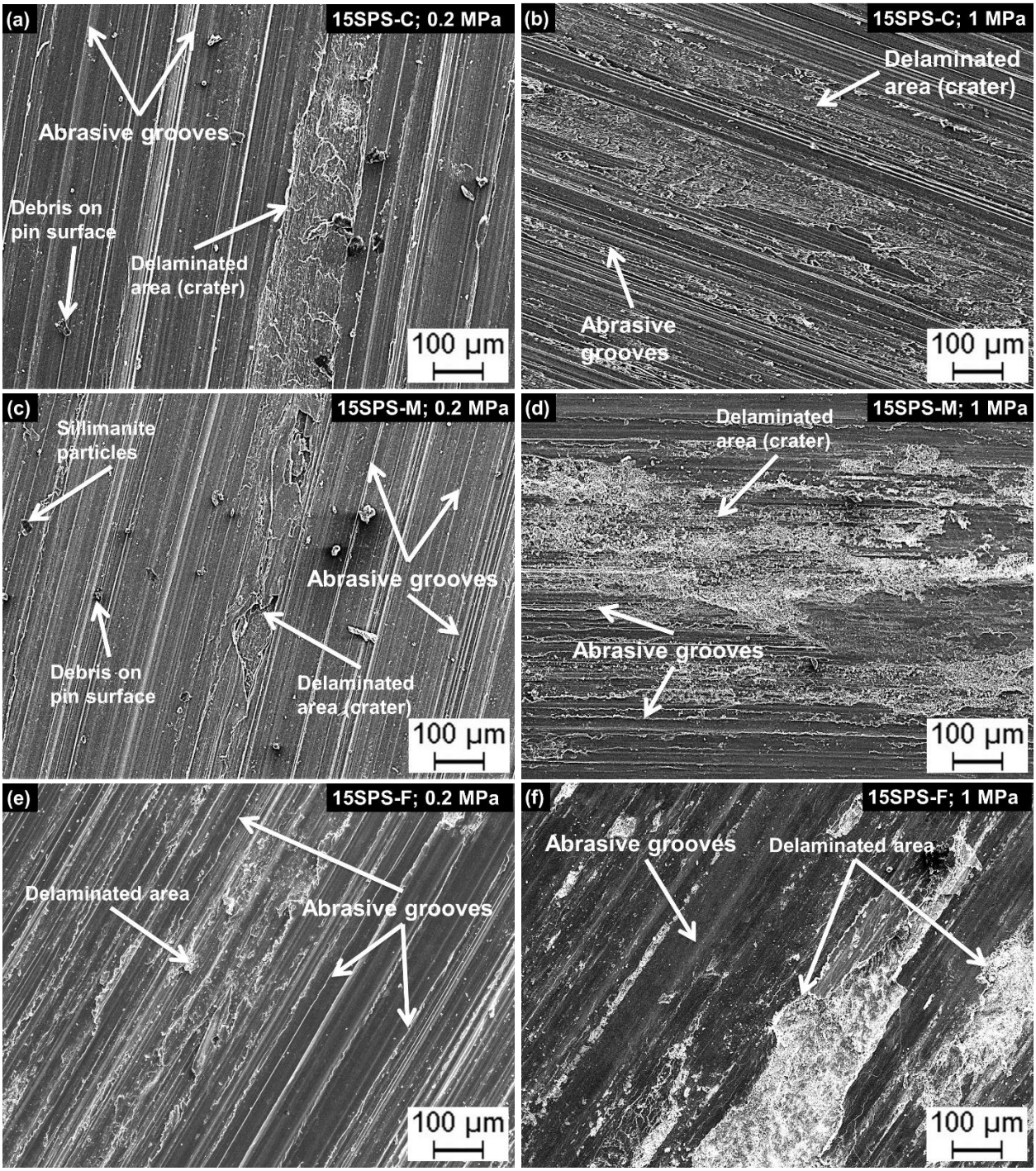
(a)
15SPS-C; 0.2 MPa
Abrasive grooves
Debris on pin surface
Delaminated area (crater)
100 µm
(b)
15SPS-C; 1 MPa
Delaminated area (crater)
Abrasive grooves
100 µm
(c)
15SPS-M; 0.2 MPa
Sillimanite particles
Abrasive grooves
Debris on pin surface
Delaminated area (crater)
100 µm
(d)
15SPS-M; 1 MPa
Delaminated area (crater)
Abrasive grooves
100 µm
(e)
15SPS-F; 0.2 MPa
Delaminated area
Abrasive grooves
100 µm
(f)
15SPS-F; 1 MPa
Abrasive grooves
Delaminated area
100 µm

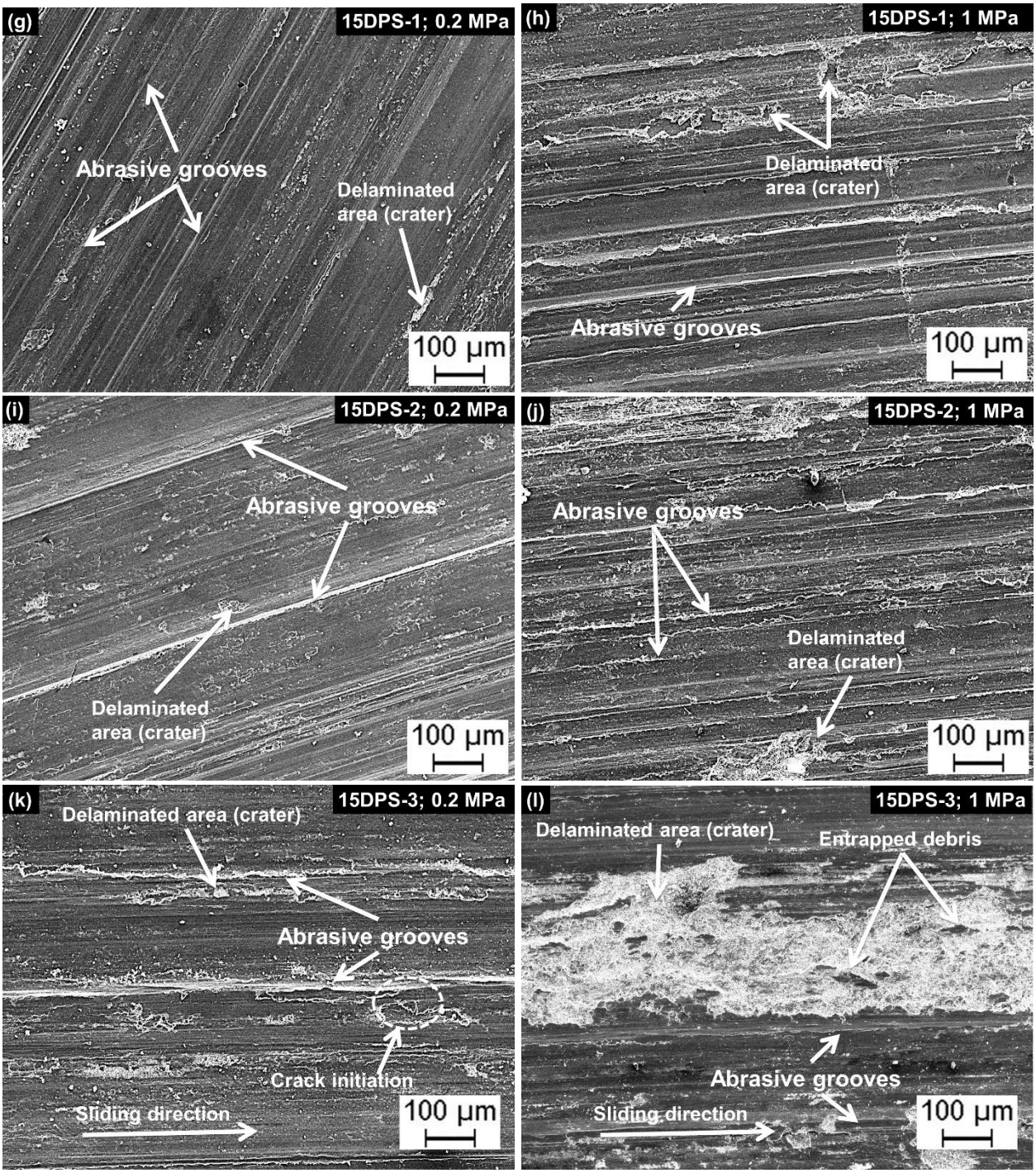

Figure 5.21 SEM micrographs of wear tracks of (a) 15SPS-C composite at 0.2 MPa, (b) 15SPS-C composite at 1 MPa, (c) 15SPS-M composite at 0.2 MPa, (d) 15SPS-M composite at 1 MPa, (e) 15SPS-F composite at 0.2 MPa, (f) 15SPS-F composite at 1 MPa, (g) 15DPS-1 composite at 0.2 MPa, (h) 15DPS-1 composite at 1 MPa, (i) 15DPS-2 composite at 0.2 MPa, (j) 15DPS-2 composite at 1 MPa, (k) 15DPS-3 composite at 0.2 MPa, and (l) 15DPS-3 composite at 1 MPa (all at the operating temperature of 200 ℃)

Figure 5.22 to 5.26 present the SEM micrographs of wear debris of 3 wt.%, 6 wt.%, 9 wt.%, 12 wt.%, and 15 wt.% sillimanite reinforced AMCs under the extreme contact pressure conditions of 0.2 MPa and 1 MPa at an operating temperature of 200 ℃. It was observed that majority of the debris were of flake type with grooves present on some of the debris (Figure 5.22 to 5.26). The grooves present on wear debris were due to the microploughing action and these indicated the abrasive nature of wear in initial stages [92]. Further, micro-cut debris were observed as shown in Figure 5.24(a, c, f) and Figure 5.25(b, f). Micro-cut debris appear because of microploughing action of asperities on the countersurfaces [173,174]. Several micro cracks were also visible on the wear debris. Micro cracks indicated the removal of material by delamination (Figure 5.22 to 5.26). Twisted and layered debris (corrugated structured debris) were also visible as shown in Figure 5.22(c, d), Figure 5.23(c, h, k, l), Figure 5.24(a, c, e, f, j, l), Figure 5.25(a, i, j, l), and Figure 5.26(b, c, f, i, j, l). Twisted and layered debris are indicative of repetitive nature of stress due to continuous rubbing action under contact pressure conditions [159,190]. Thread type debris were also observed. These indicated pullout of ductile material from pin surface as shown in Figure 5.22 to 5.26. Molten debris are shown in Figure 5.22h, Figure 5.23(b, j), Figure 5.24(a, d, h), Figure 5.25(b, d, h), and Figure 5.26(b, d). Molten debris signified that high rubbing action of counter surfaces during wear testing results in localized melting [92]. Fractured debris were also observed as shown in Figure 5.22(b, d, e, g, l), Figure 5.23(b, d, e, f, g, l), Figure 5.24(b, d, g, l), Figure 5.25(b, d, g, l), and Figure 5.26(b, d, f). Fracturing of debris occurred due to their entrapment between the countersurfaces [160].

Figure 5.26m–o present the high magnification SEM images of wear debris showing the crack pattern i.e. micro-crack initiation and propagation on the wear debris. Figure 5.26m–n show development of micro-cracks on the wear debris of AMCs. Crack initiation began in the sliding direction with most of the micro-cracks generally parallel to each other. As these micro-cracks propagated within the matrix of AMCs during testing, they were deflected/hindered by the reinforced sillimanite particles. As a result, the cracks started propagating in the transverse direction i.e. the cracks started to propagate in the direction perpendicular to their initial direction of travel). Thus, the micro-cracks started to propagate in different directions. These cracks met and formed ‘nodes’ (Figure 5.26o). A node is a point where different cracks meet and this results in removal of material in the form of delamination.

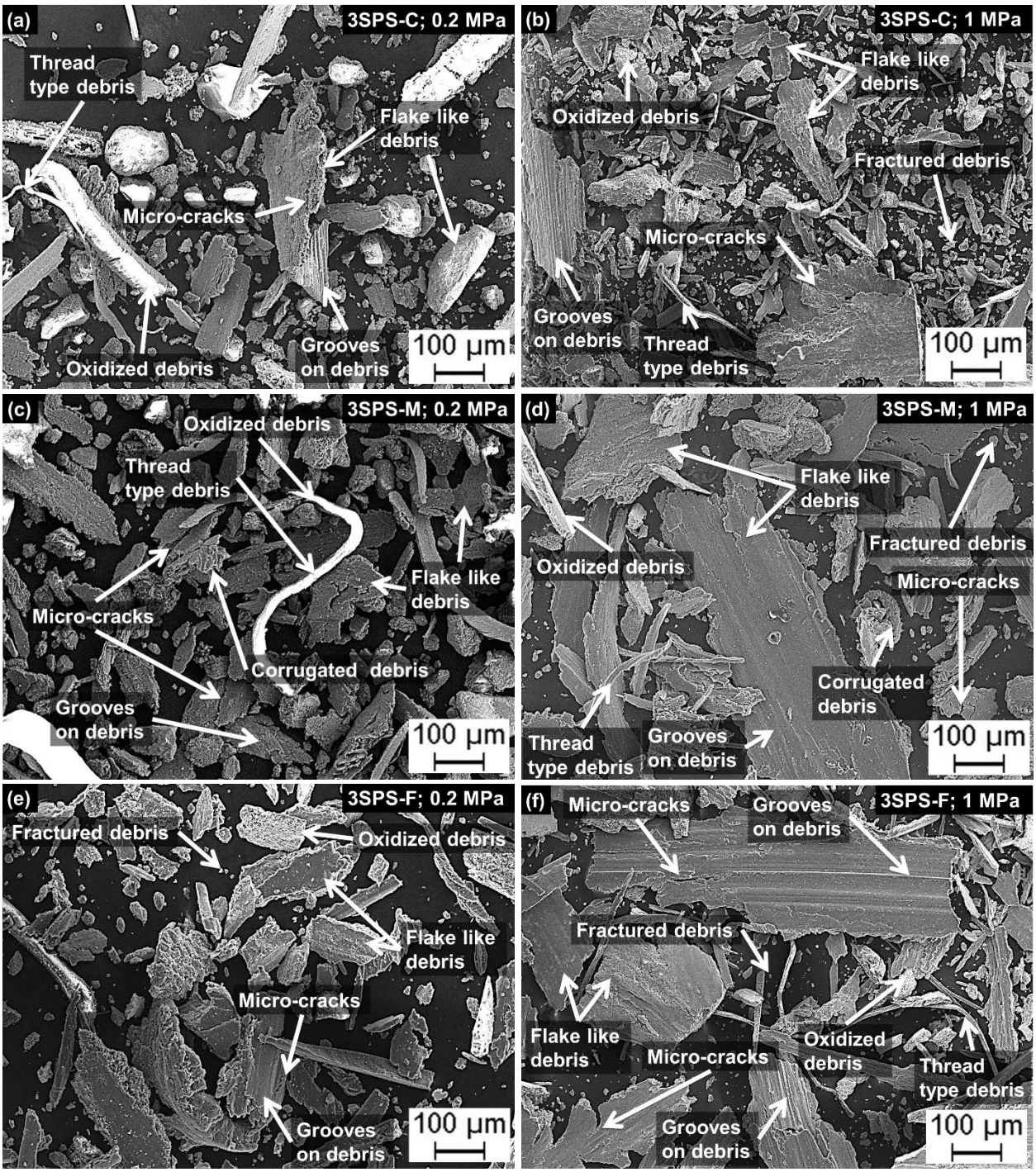
(a)
3SPS-C; 0.2 MPa
Thread type debris
Flake like debris
Micro-cracks
Oxidized debris
Grooves on debris
100 µm
(b)
3SPS-C; 1 MPa
Flake like debris
Oxidized debris
Fractured debris
Micro-cracks
Grooves on debris
Thread type debris
100 µm
(c)
3SPS-M; 0.2 MPa
Oxidized debris
Thread type debris
Flake like debris
Micro-cracks
Corrugated debris
Grooves on debris
100 µm
(d)
3SPS-M; 1 MPa
Flake like debris
Fractured debris
Oxidized debris
Micro-cracks
Corrugated debris
Thread type debris
Grooves on debris
100 µm
(e)
3SPS-F; 0.2 MPa
Fractured debris
Oxidized debris
Flake like debris
Micro-cracks
Grooves on debris
100 µm
(f)
3SPS-F; 1 MPa
Micro-cracks
Grooves on debris
Fractured debris
Flake like debris
Micro-cracks
Oxidized debris
Thread type debris
Grooves on debris
100 µm

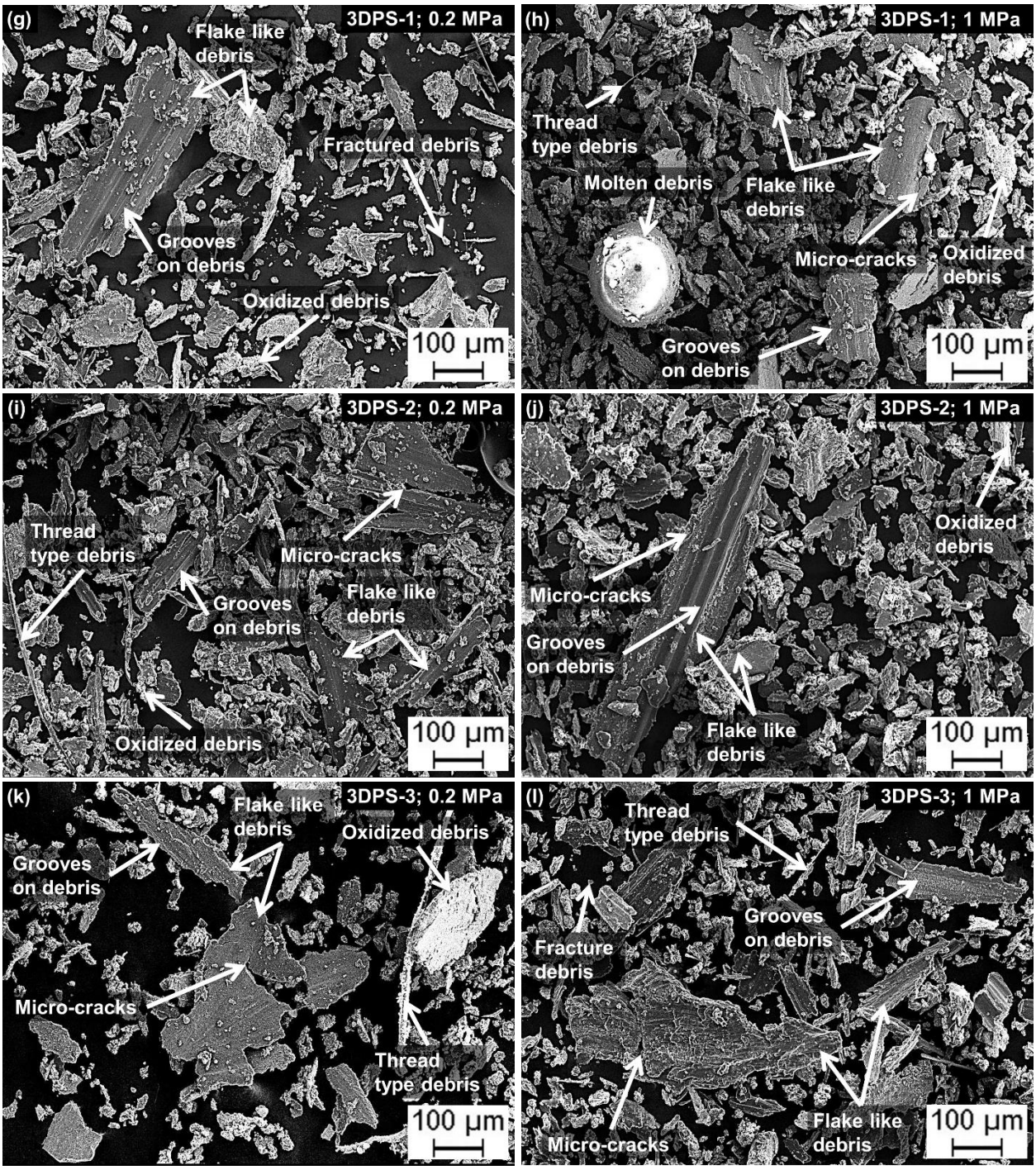

Figure 5.22 SEM micrographs of wear debris of (a) 3SPS-C at 0.2 MPa, (b) 3SPS-C composite at 1 MPa, (c) 3SPS-M composite at 0.2 MPa, (d) 3SPS-M composite at 1 MPa, (e) 3SPS-F composite at 0.2 MPa, (f) 3SPS-F composite at 1 MPa, (g) 3DPS-1 composite at 0.2 MPa, (h) 3DPS-1 composite at 1 MPa, (i) 3DPS-2 composite at 0.2 MPa, (j) 3DPS-2 composite at 1 MPa, (k) 3DPS-3 composite at 0.2 MPa, and (l) 3DPS-3 composite at 1 MPa (all at the operating temperature of 200 ℃)

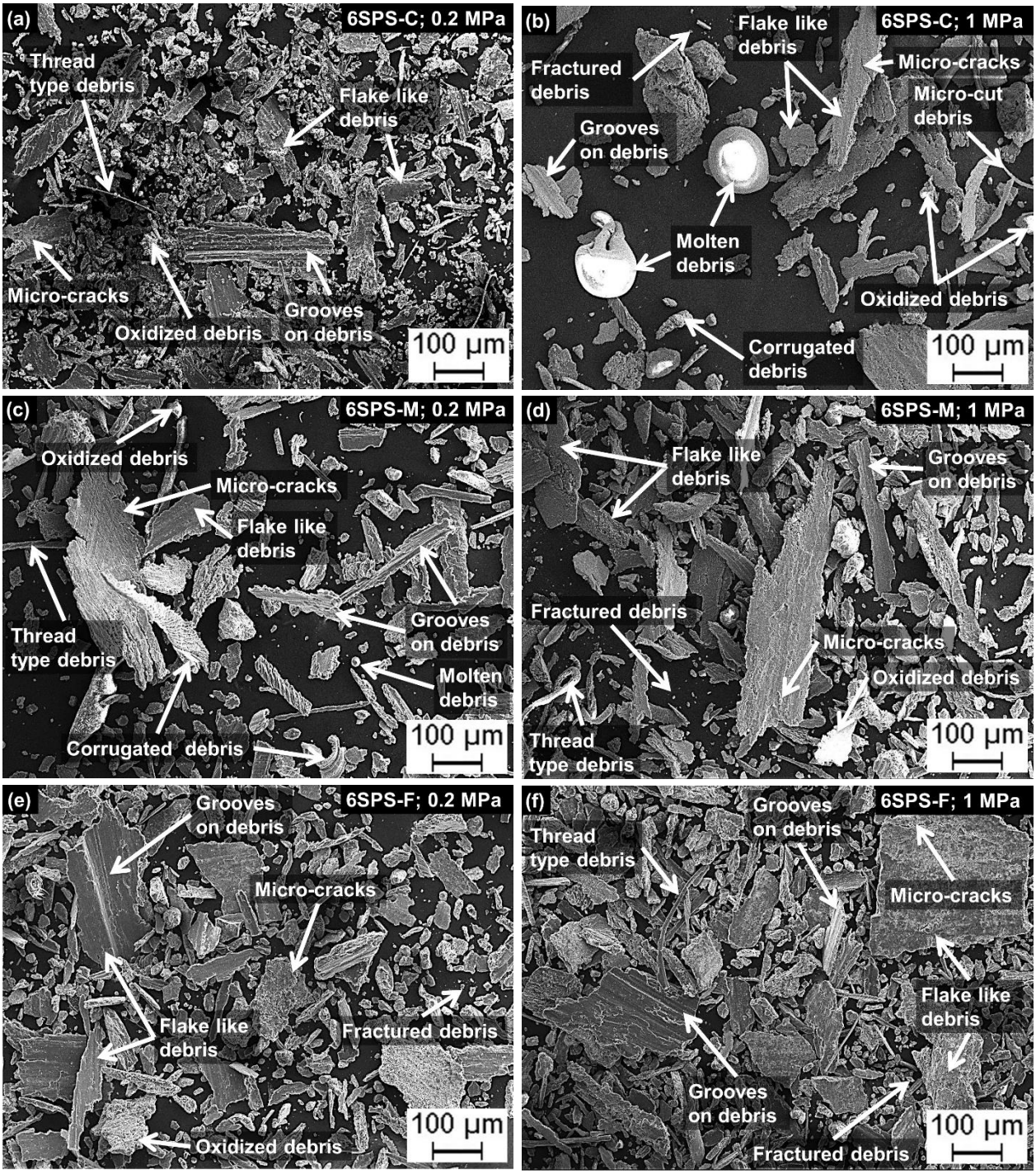
(a)
6SPS-C; 0.2 MPa
Thread type debris
Flake like debris
Micro-cracks
Oxidized debris
Grooves on debris
100 µm
(b)
6SPS-C; 1 MPa
Flake like debris
Fractured debris
Micro-cracks
Micro-cut debris
Grooves on debris
Molten debris
Oxidized debris
Corrugated debris
100 µm
(c)
6SPS-M; 0.2 MPa
Oxidized debris
Micro-cracks
Flake like debris
Thread type debris
Grooves on debris
Molten debris
Corrugated debris
100 µm
(d)
6SPS-M; 1 MPa
Flake like debris
Grooves on debris
Fractured debris
Micro-cracks
Oxidized debris
Thread type debris
100 µm
(e)
6SPS-F; 0.2 MPa
Grooves on debris
Micro-cracks
Flake like debris
Fractured debris
Oxidized debris
100 µm
(f)
6SPS-F; 1 MPa
Grooves on debris
Thread type debris
Micro-cracks
Flake like debris
Grooves on debris
Fractured debris
100 µm

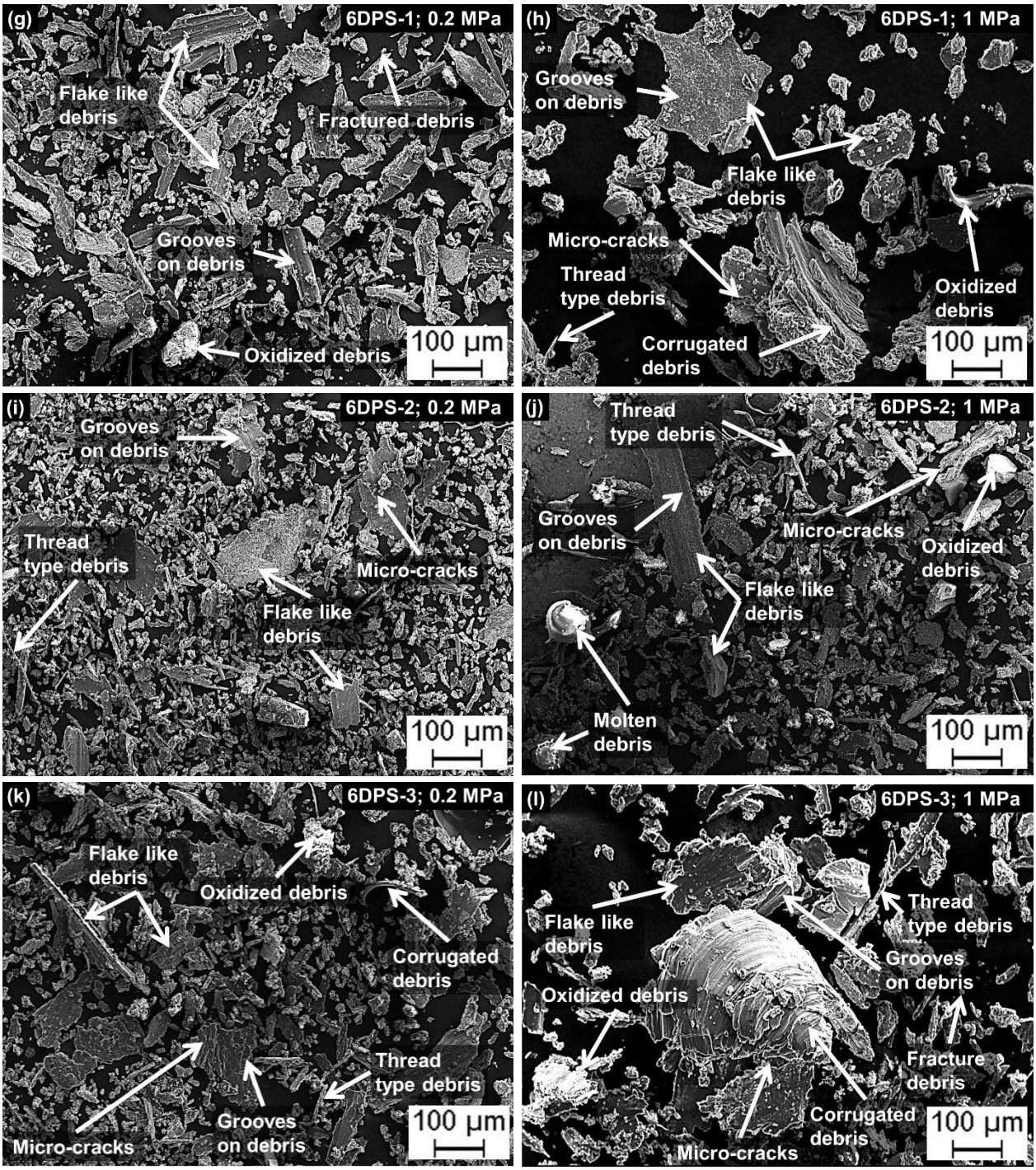

Figure 5.23 SEM micrographs of wear debris of (a) 6SPS-C composite at 0.2 MPa, (b) 6SPS-C composite at 1 MPa, (c) 6SPS-M composite at 0.2 MPa, (d) 6SPS-M composite at 1 MPa, (e) 6SPS-F composite at 0.2 MPa, (f) 6SPS-F composite at 1 MPa, (g) 6DPS-1 composite at 0.2 MPa, (h) 6DPS-1 composite at 1 MPa, (i) 6DPS-2 composite at 0.2 MPa, (j) 6DPS-2 composite at 1 MPa, (k) 6DPS-3 composite at 0.2 MPa, and (l) 6DPS-3 composite at 1 MPa (all at the operating temperature of 200 ℃)

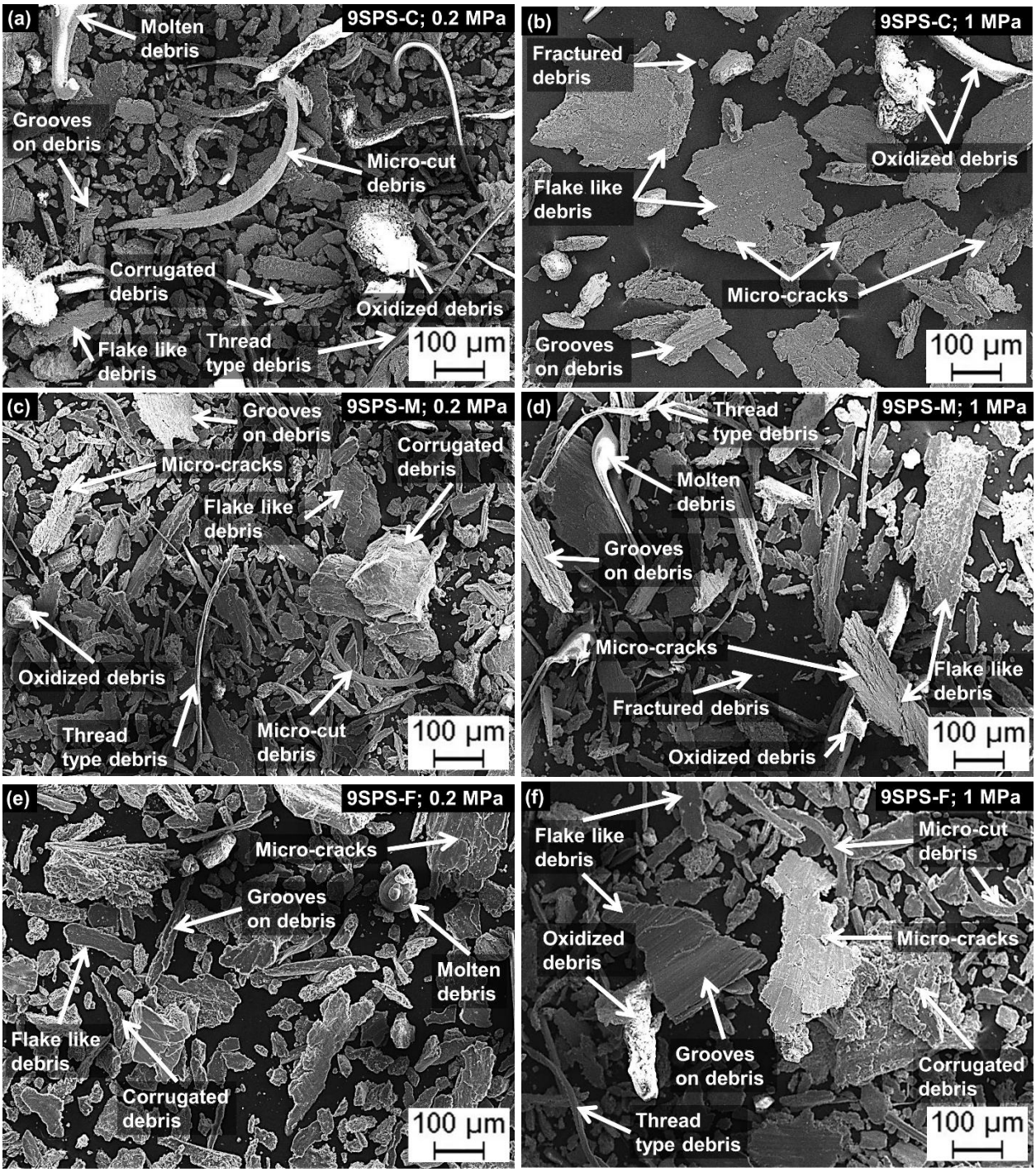
(a)
9SPS-C; 0.2 MPa
Molten debris
Grooves on debris
Micro-cut debris
Corrugated debris
Oxidized debris
Flake like debris
Thread type debris
100 µm
(b)
9SPS-C; 1 MPa
Fractured debris
Oxidized debris
Flake like debris
Micro-cracks
Grooves on debris
100 µm
(c)
9SPS-M; 0.2 MPa
Grooves on debris
Micro-cracks
Corrugated debris
Flake like debris
Oxidized debris
Thread type debris
Micro-cut debris
100 µm
(d)
9SPS-M; 1 MPa
Thread type debris
Molten debris
Grooves on debris
Micro-cracks
Flake like debris
Fractured debris
Oxidized debris
100 µm
(e)
9SPS-F; 0.2 MPa
Micro-cracks
Grooves on debris
Molten debris
Flake like debris
Corrugated debris
100 µm
(f)
9SPS-F; 1 MPa
Flake like debris
Micro-cut debris
Oxidized debris
Micro-cracks
Grooves on debris
Corrugated debris
Thread type debris
100 µm

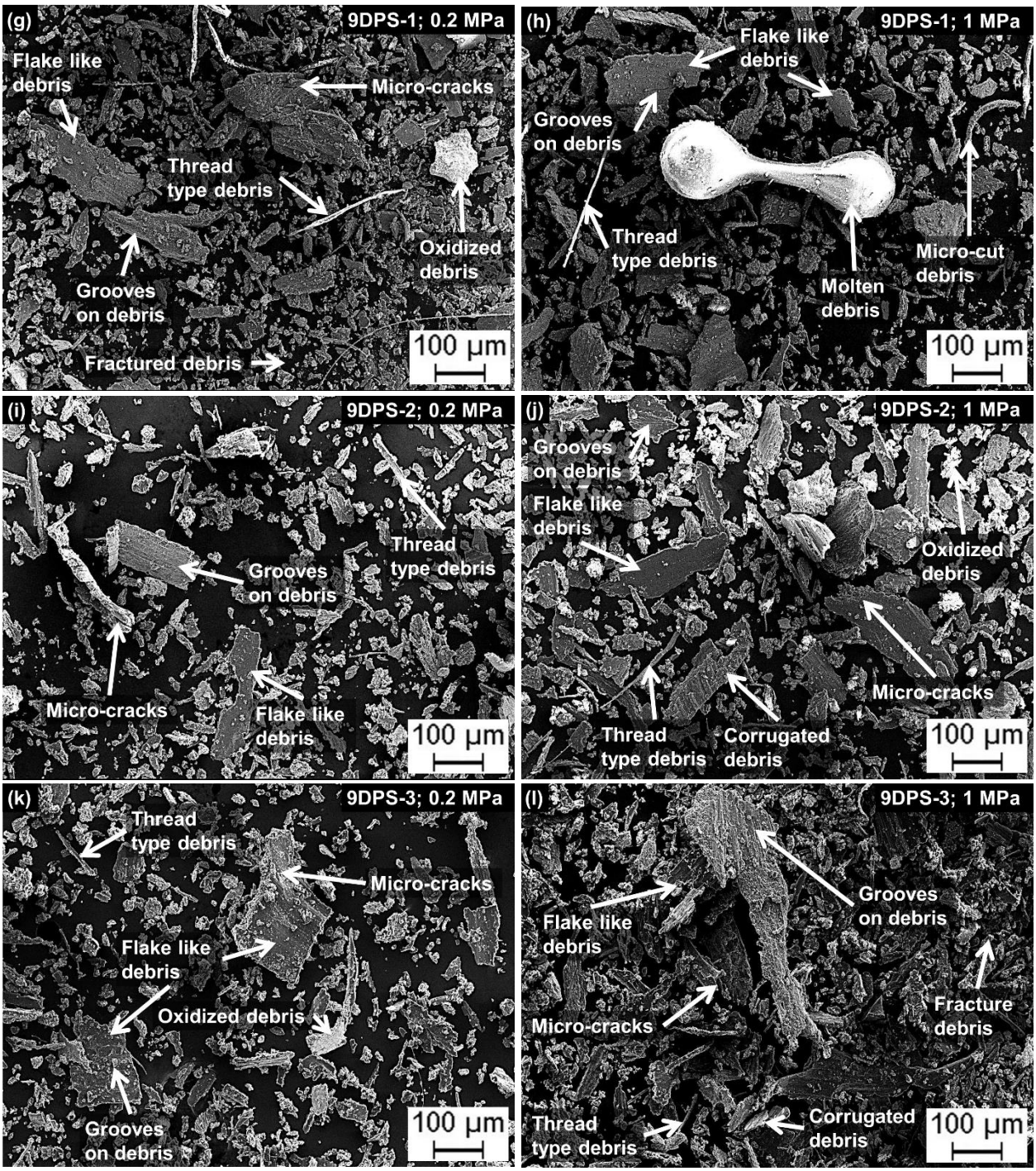

Figure 5.24 SEM micrographs of wear debris of (a) 9SPS-C composite at 0.2 MPa, (b) 9SPS-C composite at 1 MPa, (c) 9SPS-M composite at 0.2 MPa, (d) 9SPS-M composite at 1 MPa, (e) 9SPS-F composite at 0.2 MPa, (f) 9SPS-F composite at 1 MPa, (g) 9DPS-1 composite at 0.2 MPa, (h) 9DPS-1 composite at 1 MPa, (i) 9DPS-2 composite at 0.2 MPa, (j) 9DPS-2 composite at 1 MPa, (k) 9DPS-3 composite at 0.2 MPa, and (l) 9DPS-3 composite at 1 MPa (all at the operating temperature of 200 ℃)

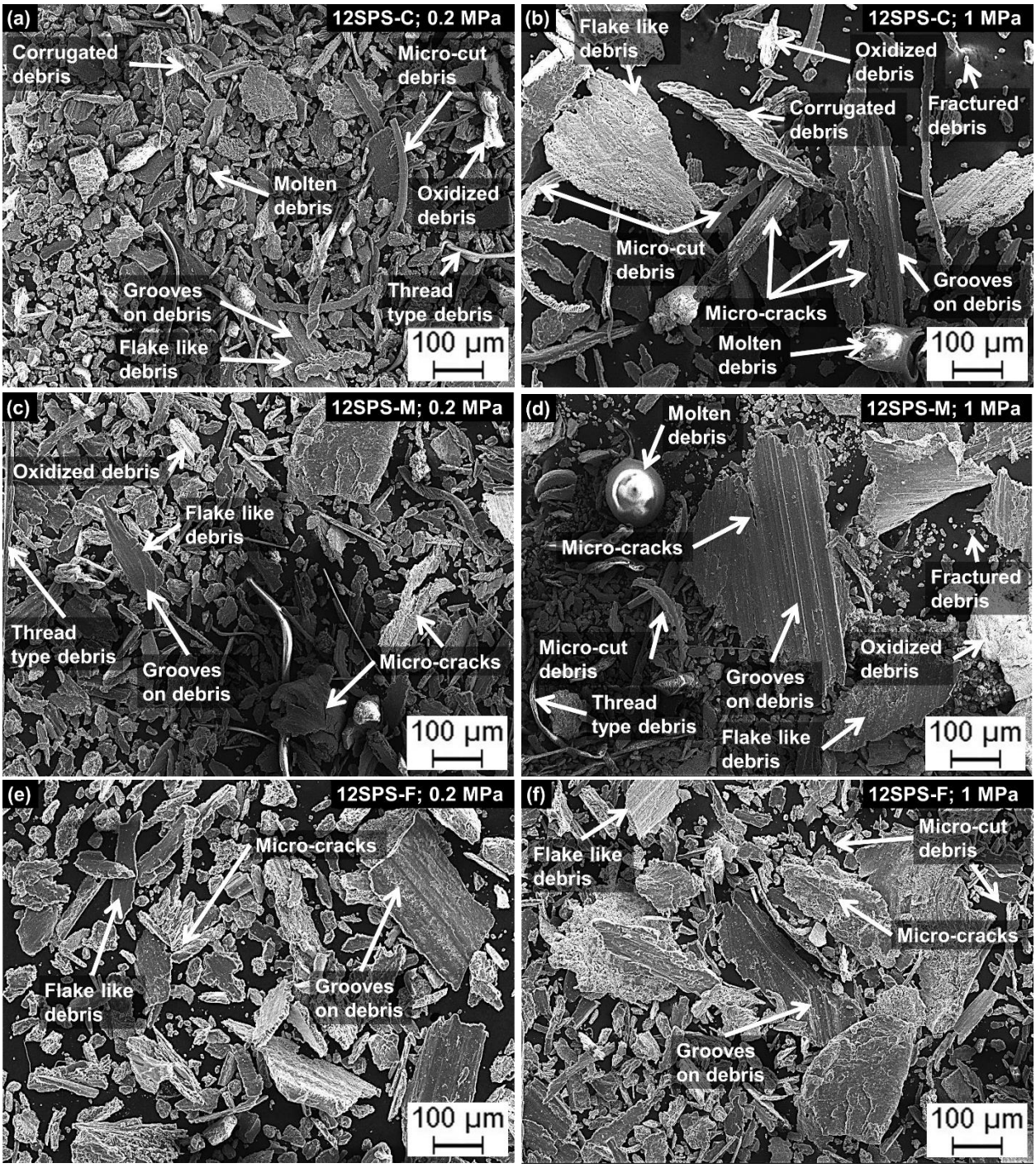
(a)
12SPS-C; 0.2 MPa
Corrugated debris
Micro-cut debris
Molten debris
Oxidized debris
Grooves on debris
Thread type debris
Flake like debris
100 µm
(b)
12SPS-C; 1 MPa
Flake like debris
Oxidized debris
Fractured debris
Corrugated debris
Micro-cut debris
Micro-cracks
Grooves on debris
Molten debris
100 µm
(c)
12SPS-M; 0.2 MPa
Oxidized debris
Flake like debris
Thread type debris
Grooves on debris
Micro-cracks
100 µm
(d)
12SPS-M; 1 MPa
Molten debris
Micro-cracks
Fractured debris
Micro-cut debris
Grooves on debris
Oxidized debris
Thread type debris
Flake like debris
100 µm
(e)
12SPS-F; 0.2 MPa
Micro-cracks
Flake like debris
Grooves on debris
100 µm
(f)
12SPS-F; 1 MPa
Flake like debris
Micro-cut debris
Micro-cracks
Grooves on debris
100 µm

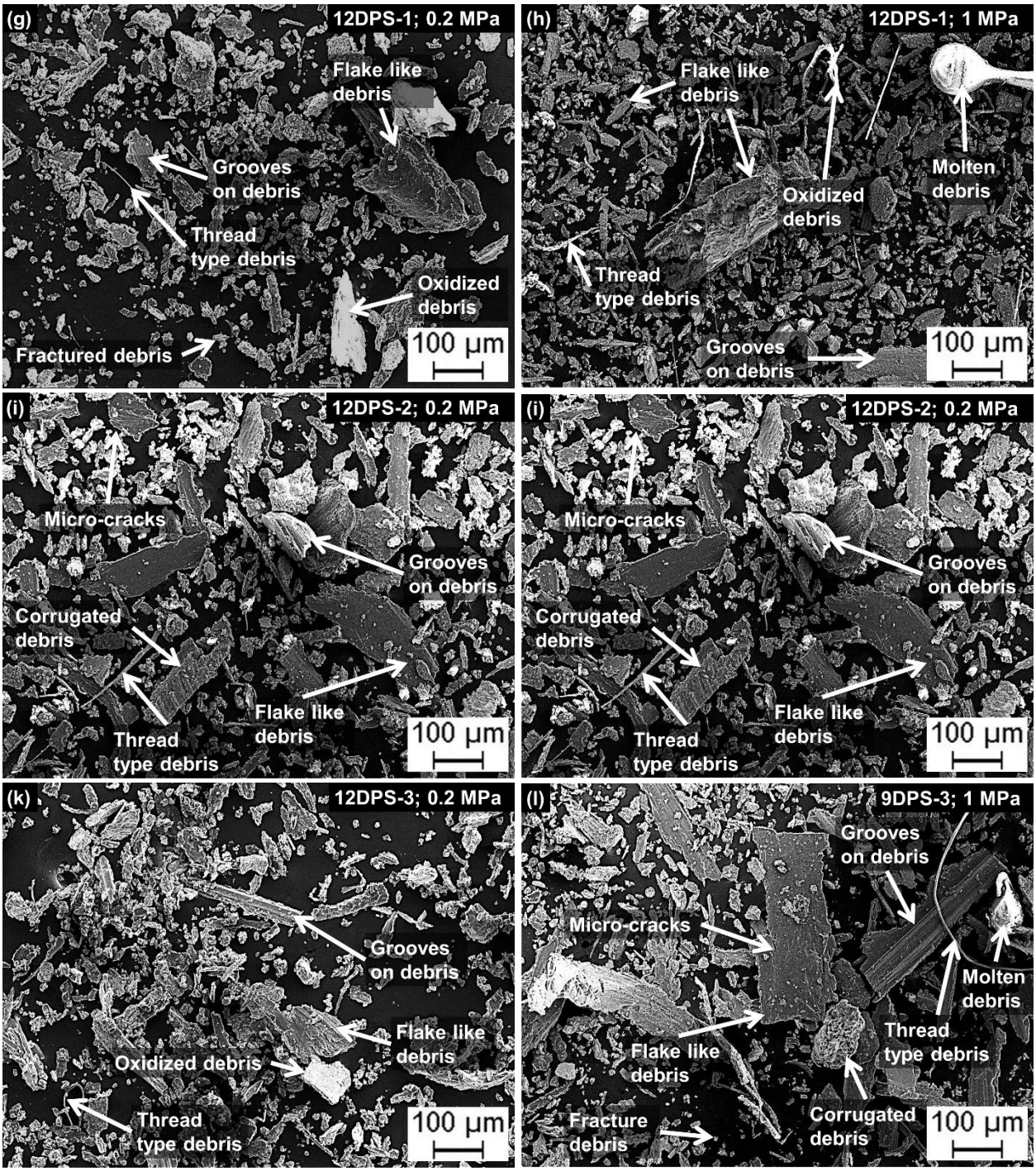

Figure 5.25 SEM micrographs of wear debris of (a) 12SPS-C composite at 0.2 MPa, (b) 12SPS-C composite at 1 MPa, (c) 12SPS-M composite at 0.2 MPa, (d) 12SPS-M composite at 1 MPa, (e) 12SPS-F composite at 0.2 MPa, (f) 12SPS-F composite at 1 MPa, (g) 12DPS-1 composite at 0.2 MPa, (h) 12DPS-1 composite at 1 MPa, (i) 12DPS-2 composite at 0.2 MPa, (j) 12DPS-2 composite at 1 MPa, (k) 12DPS-3 composite at 0.2 MPa, and (l) 12DPS-3 composite at 1 MPa (all at the operating temperature of 200 ℃)

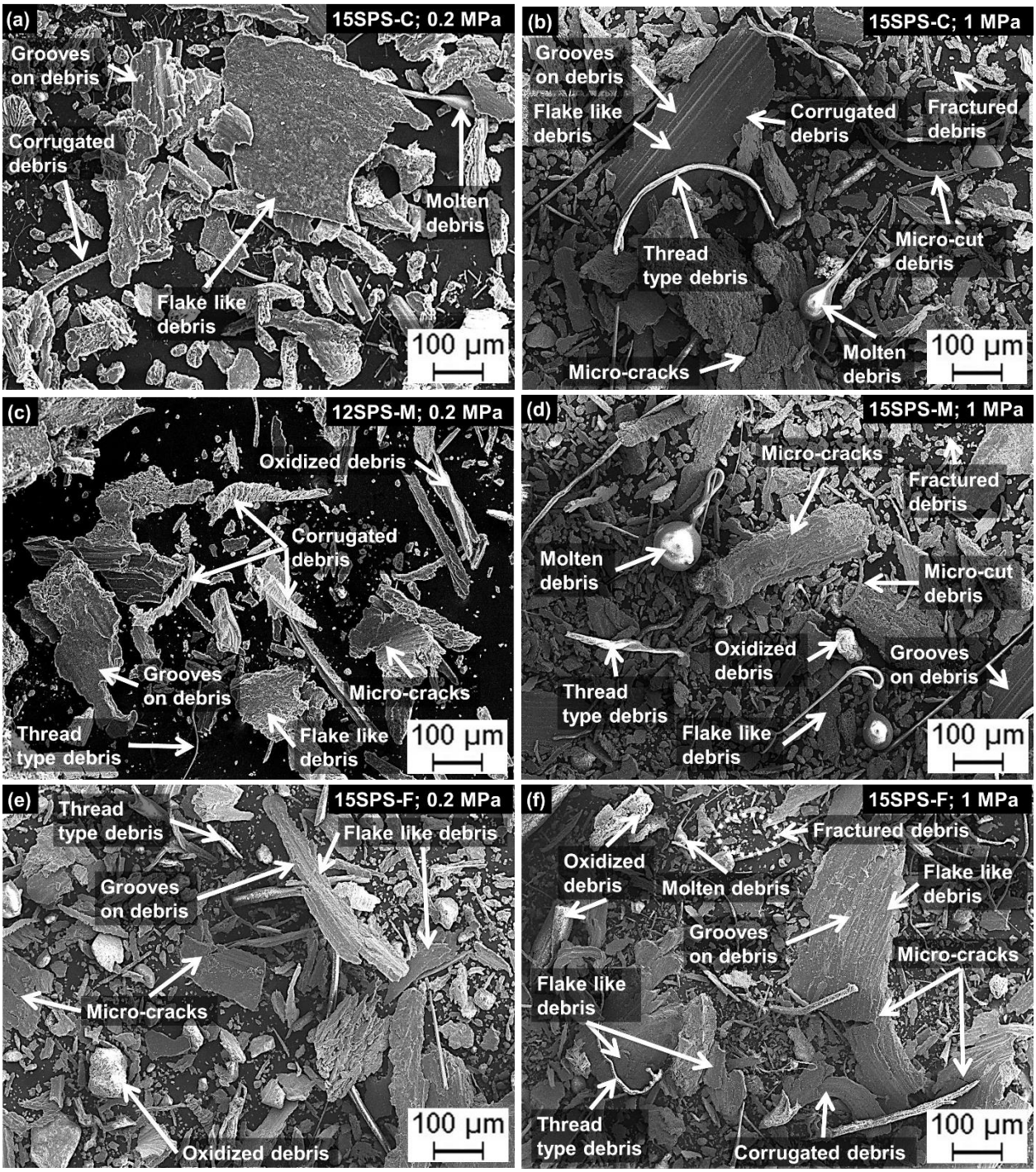
(a)
15SPS-C; 0.2 MPa
Grooves on debris
Corrugated debris
Molten debris
Flake like debris
100 µm
(b)
15SPS-C; 1 MPa
Grooves on debris
Flake like debris
Corrugated debris
Fractured debris
Thread type debris
Micro-cut debris
Micro-cracks
Molten debris
100 µm
(c)
12SPS-M; 0.2 MPa
Oxidized debris
Corrugated debris
Grooves on debris
Micro-cracks
Thread type debris
Flake like debris
100 µm
(d)
15SPS-M; 1 MPa
Micro-cracks
Fractured debris
Molten debris
Micro-cut debris
Oxidized debris
Grooves on debris
Thread type debris
Flake like debris
100 µm
(e)
15SPS-F; 0.2 MPa
Thread type debris
Flake like debris
Grooves on debris
Micro-cracks
Oxidized debris
100 µm
(f)
15SPS-F; 1 MPa
Fractured debris
Oxidized debris
Molten debris
Flake like debris
Grooves on debris
Micro-cracks
Flake like debris
Thread type debris
Corrugated debris
100 µm

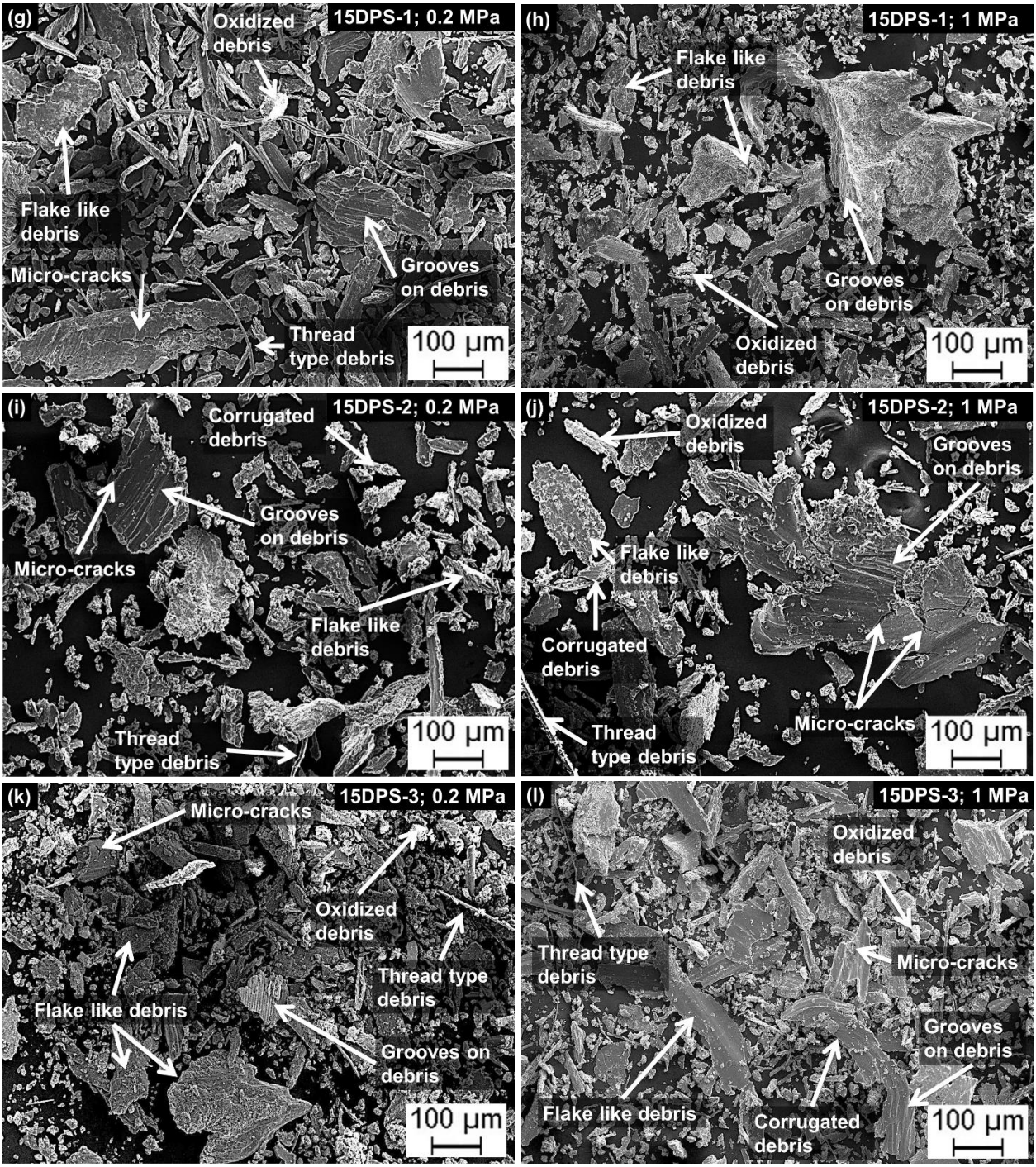
(g)
15DPS-1; 0.2 MPa
Oxidized debris
Flake like debris
Micro-cracks
Grooves on debris
Thread type debris
100 µm
(h)
15DPS-1; 1 MPa
Flake like debris
Grooves on debris
Oxidized debris
100 µm
(i)
15DPS-2; 0.2 MPa
Corrugated debris
Grooves on debris
Micro-cracks
Flake like debris
Thread type debris
100 µm
(j)
15DPS-2; 1 MPa
Oxidized debris
Grooves on debris
Flake like debris
Corrugated debris
Micro-cracks
Thread type debris
100 µm
(k)
15DPS-3; 0.2 MPa
Micro-cracks
Oxidized debris
Thread type debris
Flake like debris
Grooves on debris
100 µm
(l)
15DPS-3; 1 MPa
Oxidized debris
Thread type debris
Micro-cracks
Grooves on debris
Flake like debris
Corrugated debris
100 µm

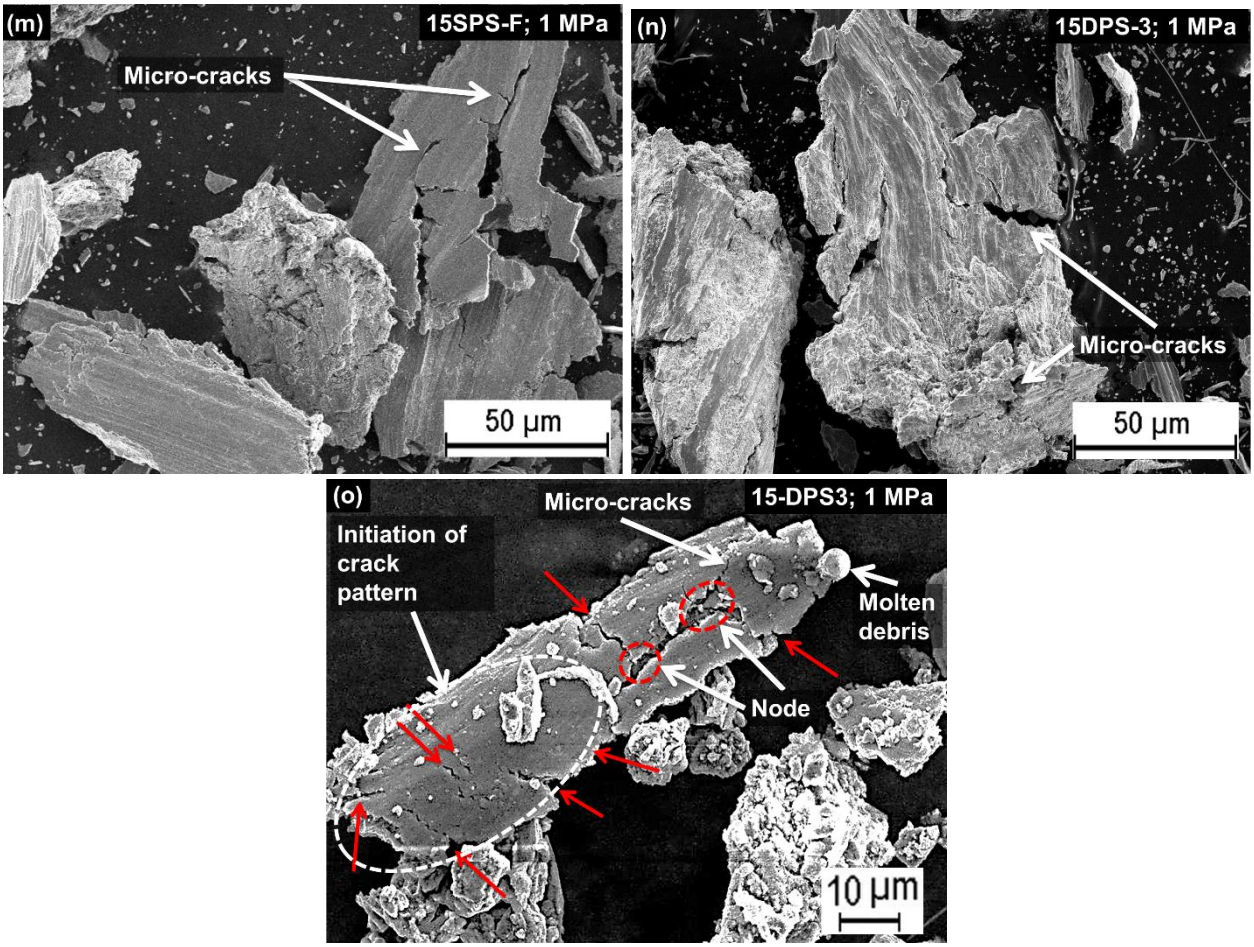

Figure 5.26 SEM micrographs of wear debris of (a) 15SPS-C composite at 0.2 MPa, (b) 15SPS-C composite at 1 MPa, (c) 15SPS-M composite at 0.2 MPa, (d) 15SPS-M composite at 1 MPa, (e) 15SPS-F composite at 0.2 MPa, (f) 15SPS-F composite at 1 MPa, (g) 15DPS-1 composite at 0.2 MPa, (h) 15DPS-1 composite at 1 MPa, (i) 15DPS-2 composite at 0.2 MPa, (j) 15DPS-2 composite at 1 MPa, (k) 15DPS-3 composite at 0.2 MPa, (l) 15DPS-3 composite at 1 MPa, and (m–o) high magnification images indicating the generation and propagation of the micro-cracks (all at the operating temperature of 200 ℃)

SEM analysis of wear tracks and wear debris indicated that at lower contact pressure (0.2 MPa), abrasive wear was predominant. This was evident from the SEM images of the wear tracks where narrow abrasive grooves were visible. The increase in particle addition led to the decrement in wear rate as was evident from the wear track analysis. For the contact pressure of 0.2 MPa, as the concentration of particles increased, the delamination areas on the wear tacks decreased. This indicated that for the contact pressure of 0.2 MPa, addition of sillimanite particles transformed the wear mechanism from abrasive/adhesive (for base alloy) to

predominantly abrasive type (for composites). Further, for the contact pressure of 1 MPa, a decrement in delaminated areas was observed. The wear mechanism of sillimanite reinforced composites transformed from predominantly adhesive wear regime (for base alloy) to a combination of abrasive and adhesive wear regime (for the composites). Next, for wear debris, the size of debris decreased with increase in sillimanite particle addition. Flake type debris are a result of adhesive wear mechanism. The reduction in size of flakes indicated the decrease in adhesive wear mechanism for composites.

Figure 5.27 presents the EDS analysis of wear track and wear debris of 15DPS-3 AMCs at low (0.2 MPa) and high contact pressure (1 MPa). At contact pressure of 0.2 MPa, the wear track of 15DPS-3 composite mainly consisted of aluminium, silicon, and oxygen indicating that the oxides were mainly of the pin surface (Figure 5.27a). However, at high contact pressure of 1 MPa, oxides of iron were also observed (Figure 5.27b). The source of iron was the countersurface EN32 steel disc. This indicated that at high contact pressure, wear of countersurface also occurs. Similar observations were also made from the EDS analysis of wear debris. For low contact pressure, EDS results of wear debris showed presence of oxides of mainly aluminium whereas at high contact pressure debris also contained oxides of iron (because of wear of countersurface steel disc).

Next, Figure 5.28 presents the area of wear tracks of 15DPS-3 composite tested at 0.2 MPa and 1 MPa at operating temperature of 200 ℃. The concentration of iron on the pin surface increased with increase in contact pressure (Figure 5.28a–b) which confirms the earlier reported results.

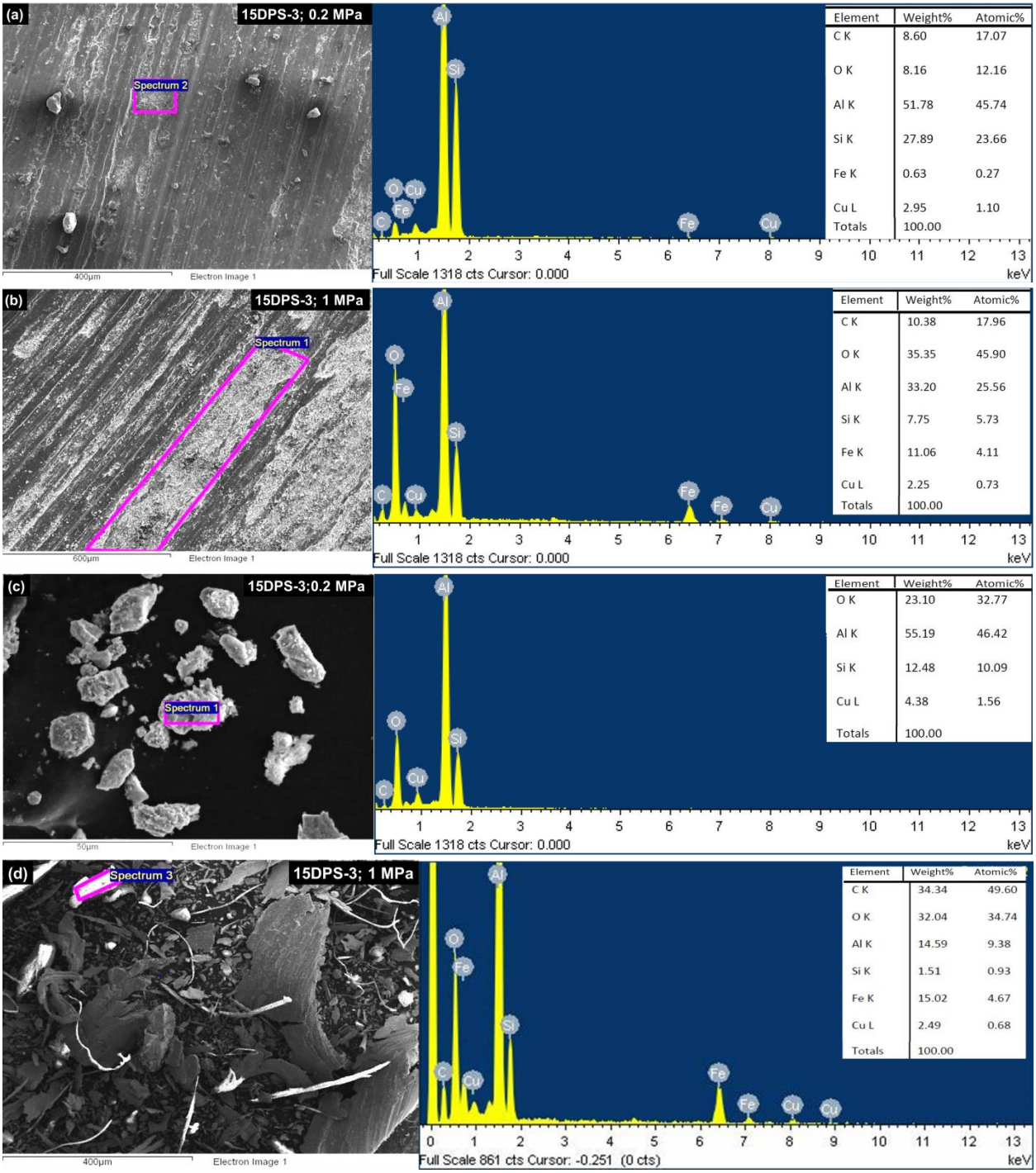

Figure 5.27 EDS analysis of 15DPS-3 composite for (a) wear tracks at 0.2 MPa, (b) wear tracks at 1 MPa, (c) wear debris at 0.2 MPa, and (d) wear debris at 1 MPa (all at operating temperature of 200 ℃)

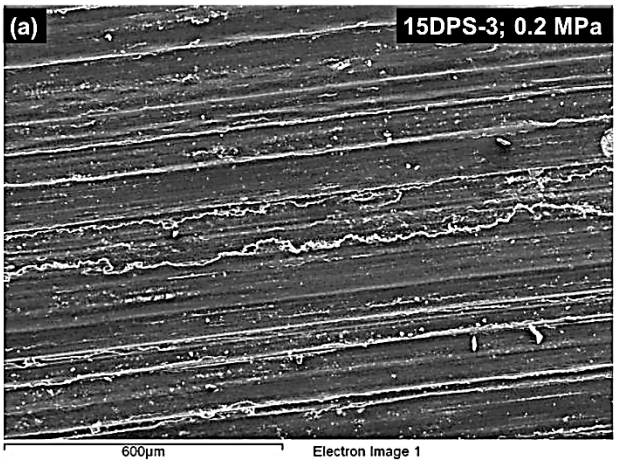

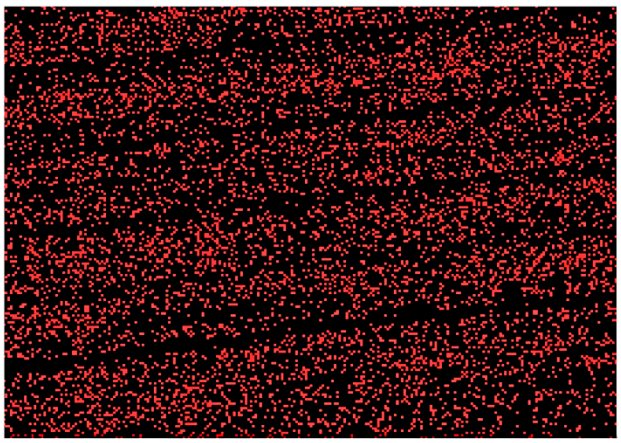

O Ka1

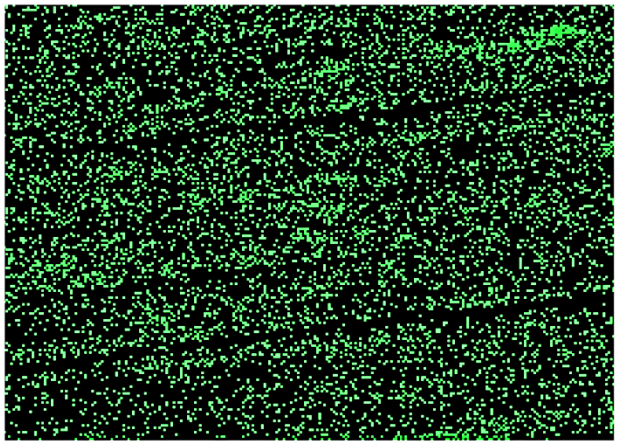

Si Ka1

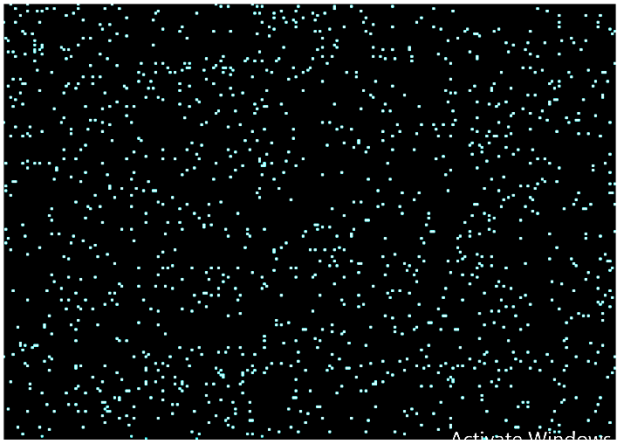

Fe Ka1

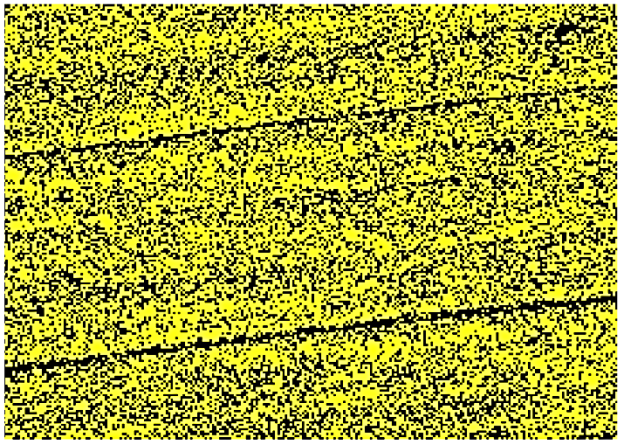

Al Ka1

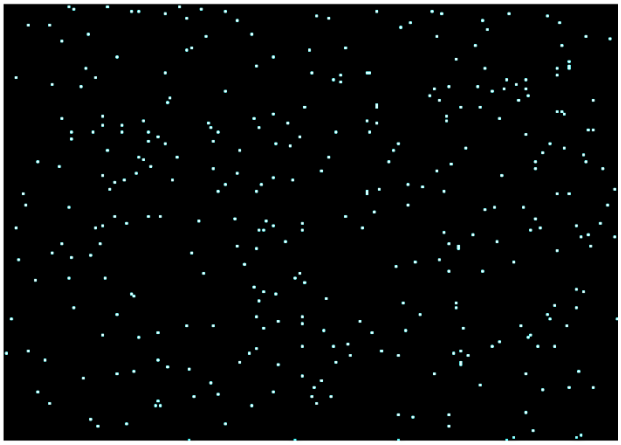

Cu Ka1

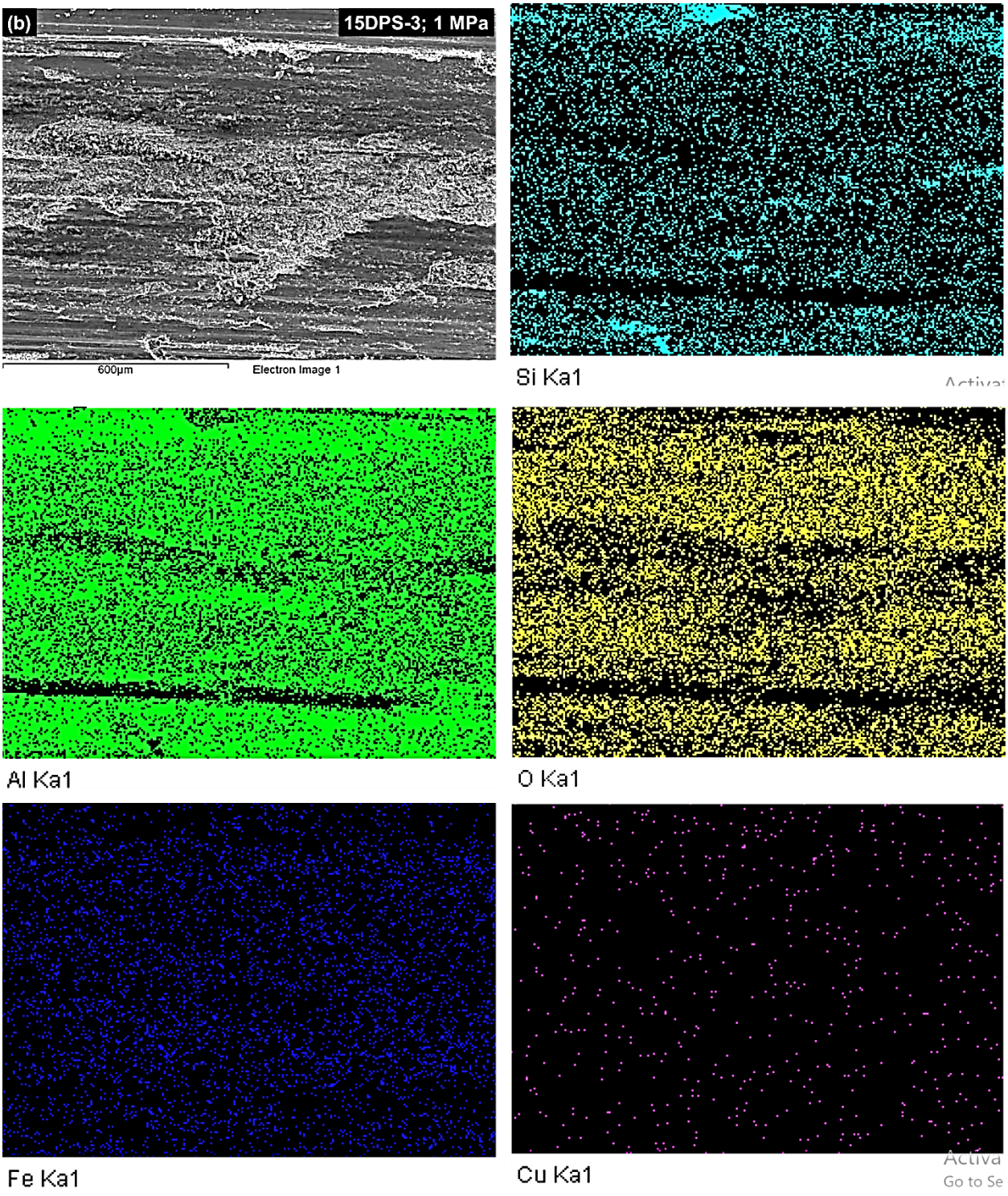

Figure 5.28 X-ray dot mapping of wear tracks of 15DPS-3 composite at (a) 0.2 MPa, and (b) 1 MPa (all at operating temperature of 200 ℃)

The next chapter presents the main conclusions drawn from the present research work.

CHAPTER 6
CONCLUSIONS

OVERVIEW

This chapter presents the major conclusions drawn from the present study. The composites containing different combination of reinforcement (wt.% and particle size) were tested at different operating conditions. The conclusions drawn from the room temperature and high temperature wear testing are presented in this chapter. The chapter also discusses the future scope of work.

6.1 ROOM TEMPERATURE STUDY

- EDS analysis of sillimanite particles indicated presence of aluminium, silicon, and oxygen as the constituents (shown as $SiAl_{1.8}O_{6.1}$), thus confirming the purity of sillimanite particles.
- XRD analysis of base alloy showed peaks of aluminium, silicon and aluminium-copper phases. In addition to this, for the AMCs, peaks of sillimanite particles and aluminium silicate ($Al_2Si_4O_{10}$) phases were also observed. Aluminium silicate was a product of interfacial reaction of matrix and sillimanite particles.
- Microstructure analysis of base alloy showed presence of aluminium-silicon eutectic mixture with large facets of primary silicon. X-ray line profile of base alloy clearly showed high concentration of copper in the proximity of primary silicon phase.
- Optical micrographs of AMCs revealed uniform distribution of sillimanite particles in the matrix till 15 wt.% reinforcement level without agglomeration. This indicated that methodology adopted was effective for processing the composites.
- X-ray line profile of AMCs indicated higher concentration of silicon phase in proximity of reinforced sillimanite particles. Further, X-ray dot mapping of AMCs revealed that sillimanite reinforcement refined the silicon morphology.
- High nanohardness values obtained at the particle-matrix interface of AMCs indicated that the methodology adopted for processing of AMCs was very effective. Brinell hardness of AMCs increased with increase in sillimanite reinforcement level and decrease in sillimanite particle size. Hardness of 15DPS-3 composites was superior to all other composite formulations. Hardness of this AMC was comparable (only 4.5% lower) to the commercial grade cast iron used in brake rotor applications.
- Sillimanite reinforced AMCs showed significantly reduced wear rate compared to base alloy throughout the entire spectrum of sliding distance at any given contact pressure condition.
- For any contact pressure condition, wear rate behaviour with respect to sliding distance was observed to be divided into two distinct zones of run-in-wear zone and steady-state-wear zone. Fragmentation of asperities, mechanical welding of pin-disc, compaction of wear debris, and formation of protective oxide film on the pin surface were the main reasons for change in wear rate during run-in-wear zone. Further, the formation and removal of transfer film (MML) at the same rate caused constant wear rate in the steady-state-wear zone.

- Wear rate of SPS and DPS composites deceased with increase in sillimanite reinforcement level till 15 wt.% i.e. till reinforcement level which did not cause agglomeration of reinforced particles. Further, for SPS composites, wear rate decreased with decrease in sillimanite particle size at a given reinforcement level. Thus, for SPS composites, the best wear rate behaviour was displayed by 15SPS-F composite with a reduction of 55% in wear rate over the base alloy. The overall best wear performance was shown by 15DPS-3 composite (59% reduction over base alloy). This showed that for maximum reduction in wear rate, a mix of fine and coarse sized particle reinforcement (with fine particles in larger proportion) to AMCs provides the best results.
- Mathematical predictions of wear rate showed good agreement with experimental results. Maximum reduction in wear rate of 15DPS-3 AMC (over base alloy) obtained experimentally was 59% and by mathematical modeling was 65%.
- The wear rate behaviour of the processed AMCs was close to that of the commercial grade cast iron used in brake rotor applications. The maximum wear rate of 15SPS-F and 15DPS-3 composite under 1 MPa condition was just 13% and 8% higher respectively compared to the commercial material.
- The processed AMCs showed significantly reduced COF values compared to base alloy throughout the entire spectrum of sliding distance at any given contact pressure condition. COF values of AMCs decreased with increase in reinforcement level and with decrease in particle size. Maximum reduction in COF value was observed for 15DPS-3 composite with a drop of 42% over the base alloy.
- The type of wear mechanism causing material loss during dry sliding wear of composites was mainly dependent on contact pressure and sliding distance. At low contact pressures and smaller sliding distances, abrasive wear was predominant. However, at higher contact pressures and larger sliding distances, adhesive wear was the main reason for materials loss. EDS analysis revealed presence of mechanically mixed layer (comprising of oxide of aluminium from pin surface and oxides of iron from steel disc surface).

6.2 HIGH TEMPERATURE STUDY

- DTG-TGA analysis revealed the thermal stability of sillimanite particles till 900 ℃. Addition of these particles to the base alloy decreased the CTE of composites. The CTE

value of 15SPS-F and 15DPS-3 AMCs was 25% and 28% lower than the base alloy, respectively. Experimental results and mathematical predictions with regard to CTE value of processed AMCs showed close agreement.

- The wear resistance of AMCs improved with an increase in particle reinforcement level and decrease in sillimanite particle size. However, increase in operating temperature and/or contact pressure resulted in decreased wear resistance, both for base alloy as well as AMCs.
- Sillimanite reinforcement increased the transition temperature (where wear behaviour changed from mild-to-severe wear) from 150 ℃ for the base alloy to 200 ℃ for the AMCs. For the contact pressure and operating temperature condition of 1 MPa and 200 ℃, the mean steady-state wear rate of 15SPS-F and 15DPS-3 composites was 78% and 80% lower than that of base alloy. Further, the mean steady-state wear rate of 15SPS-F and 15DPS-3 AMCs (at 1 MPa and 200 ℃) condition was comparable to that of the commercial material (15SPS-F showed 6.62% higher whereas 15DPS-3 showed 1.5% lower wear rate compared to the grey cast iron specimen).
- At any given contact pressure, COF value of composites was lower than those of base alloy. For the contact pressure and operating temperature condition of 1 MPa and 200 ℃, COF of 15SPS-F and 15DPS-3 composites was 52% and 54% lower than the base alloy, respectively. The COF values of 15SPS-F (0.42) and 15DPS-3 (0.41) composite were comparable to the COF value of the cast iron specimen (0.39).
- XRD analysis showed that at low contact pressure of 0.2 MPa, the wear tracks largely constituted of oxides of Al and Si viz. Al_2O_3 and SiO_2 whereas at high contact pressure of 1 MPa, the tracks also showed presence of oxides of iron. Further, XRD analysis of wear debris (under various contact pressures) of base alloy indicated presence of relatively large volumes of oxides compared to AMCs. This indicated the formation of stable oxide layer on the pin surface of AMCs. Also, the wear debris of AMCs showed a blend of various oxides (Al_2O_3, SiO_2, Fe_2O_3, FeO etc.), sillimanite particles, aluminium, and silicon particles which confirmed the formation of mechanically mixed layer (MML), also called tribolayer/transfer film.
- SEM micrographs of wear track and wear debris showed that at high operating temperatures, both abrasive and adhesive wear mechanisms were dominant. For the contact pressure and operating temperature condition of 0.2 MPa and 200 ℃, abrasive/adhesive wear behaviour

was predominant whereas, for 1 MPa and 200 ℃ condition, adhesive/delamination wear mechanism was the main material removal mechanism.

6.3 MAJOR CONCLUSIONS

- Attempts to process highly wear resistant LM30 alloy based AMCs reinforced with sillimanite through stir casting route were successful.
- Micrographs of AMCs showed uniform distribution of sillimanite particles till 15 wt.% beyond which agglomeration was noted. This indicated that the methodology adopted in the present work was effective in processing of composites.
- The hardness of the composites increased with an increase in sillimanite concentration and a decrease in particle size. The hardness of 15DPS-3 composites was superior to all the composite formulations.
- Wear resistance of 15DPS-3 composites was superior to all the other composite formulations both at room temperature as well as at elevated temperatures.
- A maximum reduction in COF value was observed for 15DPS-3 composites both at room temperature conditions and elevated temperature conditions.
- Overall the study revealed that the hardness, wear rate, and COF of 15DPS-3 composite was comparable to that of cast iron used in brake rotor applications. Thus, 15DPS-3 composites can act as a substitute material for brake rotors in light vehicles.

6.4 SCOPE OF FUTURE WORK

The present work discussed the dry sliding wear characteristics of processed composites both at room temperature and elevated temperature conditions. The scope of future work is presented below:

- Wear behaviour, COF values, nanohardness, and CTE of AMCs have been investigated. But in addition to this, for improved thermal resistance, the thermal properties like thermal conductivity, coefficient of linear expansion, etc. can also be investigated.
- The AMCs developed in the present work showed remarkable improvement in wear characteristics/ COF values etc. over the base alloy. The performance was even comparable to the commercially used cast iron material used for brake rotor applications. The developed

composites can be heat-treated through T4 and T6 standard routes to investigate further improvement in these properties.

- The composites developed in the present research work can also be investigated for corrosion/erosion studies under varied environments. This will widen the scope of these materials for marine applications.

REFERENCES

[1] Callister, W.D. (2013) Materials science and engineering: An introduction (9th edition). Willey sons. https://doi.org/10.1016/0261-3069(91)90101-9

[2] Shedbale, A.S., Singh, I. V. and Mishra, B.K. (2017) Heterogeneous and homogenized models for predicting the indentation response of particle reinforced metal matrix composites. *International Journal of Mechanics and Materials in Design*, Springer Netherlands. **13**, 531–52. https://doi.org/10.1007/s10999-016-9352-3

[3] Kumar, G.B.V., Rao, C.S.P. and Selvaraj, N. (2011) Mechanical and tribological behavior of particulate reinforced aluminum metal matrix composites- a review. *Journal of Minerals and Materials Characterization and Engineering*, **10**, 59–91. https://doi.org/10.4236/jmmce.2011.101005

[4] Prangnell, P.B., Barnes, S.J., Roberts, S.M. and Withers, P.J. (1996) The effect of particle distribution on damage formation in particulate reinforced metal matrix composites deformed in compression. *Materials Science and Engineering A*, **220**, 41–56. https://doi.org/10.1016/S0921-5093(96)10461-5

[5] Ibrahim, I.A., Mohamed, F.A. and Lavernia, E.J. (1991) Particulate reinforced metal matrix composites- a review. *Journal of Materials Science*, **26**, 1137–56. https://doi.org/10.1007/BF00544448

[6] Bui, T.Q., Nguyen, N.T., Lich, L. Van, Nguyen, M.N. and Truong, T.T. (2018) Analysis of transient dynamic fracture parameters of cracked functionally graded composites by improved meshfree methods. *Theoretical and Applied Fracture Mechanics*, **96**, 642–57. https://doi.org/10.1016/j.tafmec.2017.10.005

[7] Deuis, R.L.L., Subramanian, C. and Yellup, J.M.M. (1996) Abrasive wear of aluminium composites- a review. *Wear*, **201**, 132–44. https://doi.org/10.1016/S0043-1648(96)07228-6

[8] Kaushik, N.C. and Rao, R.N. (2016) The effect of wear parameters and heat treatment on two body abrasive wear of Al–SiC–Gr hybrid composites. *Tribology International*, **96**, 184–90. https://doi.org/10.1016/j.triboint.2015.12.045

[9] Thandalam, K.S., Ramanathan, S. and Sundarrajan, S. (2015) Synthesis, microstructural and mechanical properties of ex situ zircon particles ($ZrSiO_4$) reinforced metal matrix composites (MMCs): a review. *Journal of Materials Research and Technology*, **4**, 333–

47. https://doi.org/10.1016/j.jmrt.2015.03.003

[10] Das, S., Udhayabanu, V., Das, S. and Das, K. (2006) Synthesis and characterization of zircon sand/Al-4.5 wt% Cu composite produced by stir casting route. *Journal of Materials Science*, **41**, 4668–77. https://doi.org/10.1007/s10853-006-0056-1

[11] Hashim, J. (2001) The production of cast metal matrix composite by a modified stir casting method. *Jurnal Teknologi*, **35**, 9–20. https://doi.org/10.11113/jt.v35.588

[12] Hu, Q., Zhao, H. and Ge, J. (2016) Microstructure and mechanical properties of (B_4C+Al_3Ti)/Al hybrid composites fabricated by a two-step stir casting process. *Materials Science and Engineering: A*, **650**, 478–82. https://doi.org/10.1016/j.msea.2015.10.041

[13] Hashim, J., Looney, L. and Hashmi, M.S.J. (2001) The enhancement of wettability of SiC particles in cast aluminium matrix composites. *Journal of Materials Processing Technology*, **119**, 329–35. https://doi.org/10.1016/S0924-0136(01)00919-0

[14] Sozhamannan, G.G., Prabu, S.B. and Venkatagalapathy, V.S.K. (2012) Effect of processing paramters on metal matrix composites: stir casting process. *Journal of Surface Engineered Materials and Advanced Technology*, **02**, 11–5. https://doi.org/10.4236/jsemat.2012.21002

[15] Su, H., Gao, W., Zhang, H., Liu, H., Lu, J. and Lu, Z. (2010) Optimization of stirring parameters through numerical simulation for the preparation of aluminum matrix composite by stir casting process. *Journal of Manufacturing Science and Engineering*, **132**, 061007. https://doi.org/10.1115/1.4002851

[16] Zhou, W. and Xu, Z.M. (1997) Casting of SiC reinforced metal matrix composites. *Journal of Materials Processing Technology*, **63**, 358–63. https://doi.org/10.1016/S0924-0136(96)02647-7

[17] Prabu, S.B., Karunamoorthy, L., Kathiresan, S. and Mohan, B. (2006) Influence of stirring speed and stirring time on distribution of particles in cast metal matrix composite. *Journal of Materials Processing Technology*, **171**, 268–73. https://doi.org/10.1016/j.jmatprotec.2005.06.071

[18] Bhandare, R.G. and Sonawane, P.M. (2013) Preparation of Aluminium Matrix Composite by Using Stir Casting Method. *International Journal of Engineering and Advanced Technology (IJEAT)*, **3**, 61–5.

[19] Degischer, H.. (1997) Innovative light metals: metal matrix composites and foamed aluminium. *Materials & Design*, **18**, 221–6. https://doi.org/10.1016/S0261-3069(97)00054-X

[20] Hashim, J., Looney, L. and Hashmi, M.S.J. (1999) Metal matrix composites: production by the stir casting method. *Journal of Materials Processing Technology*, **92**–**93**, 1–7. https://doi.org/10.1016/S0924-0136(99)00118-1

[21] Kaftelen, H., Necip, U., Goller, G., Lutfi Oveoglu, M. and Henein, H. (2011) Comparative processing-structure-property studies of Al-Cu matrix composites reinforced with TiC particulates. *Composites Part A: Applied Science and Manufacturing*, **42**, 812–24. https://doi.org/10.1016/j.compositesa.2011.03.016

[22] Yigezu, B.S., Mahapatra, M.M. and Jha, P.K. (2013) Influence of reinforcement type on microstructure, hardness, and tensile properties of an aluminum alloy metal matrix composite. *Journal of Minerals and Materials Characterization and Engineering*, **1**, 124–30.

[23] Babu, K. V., Jappes, J.W., Rajan, T. and Uthayakumar, M. (2014) Dry sliding wear studies on SiC reinforced functionally graded aluminium matrix composites. *Proceedings of the Institution of Mechanical Engineers, Part L: Journal of Materials: Design and Applications*, 1–8. https://doi.org/10.1177/1464420714556665

[24] Kok, M. (2005) Production and mechanical properties of Al_2O_3 particle-reinforced 2024 aluminium alloy composites. *Journal of Materials Processing Technology*, **161**, 381–7. https://doi.org/10.1016/j.jmatprotec.2004.07.068

[25] Ghasali, E., Pakseresht, A., Rahbari, A., Eslami-shahed, H., Alizadeh, M. and Ebadzadeh, T. (2016) Mechanical properties and microstructure characterization of spark plasma and conventional sintering of Al-SiC-TiC composites. *Journal of Alloys and Compounds*, **666**, 366–71. https://doi.org/10.1016/j.jallcom.2016.01.118

[26] Samal, P., Vundavilli, P.R., Meher, A. and Mahapatra, M.M. (2020) Recent progress in aluminum metal matrix composites: A review on processing, mechanical and wear properties. *Journal of Manufacturing Processes*, **59**, 131–52. https://doi.org/10.1016/j.jmapro.2020.09.010

[27] Sagar, R. and Purohit, R. (2006) Fabrication and testing of Al-SiCp composite valve seat inserts. *The International Journal of Advanced Manufacturing Technology*, **29**, 922–8. https://doi.org/10.1007/s00170-005-2705-y

[28] Veeravalli, R.R., Nallu, R. and Mohammed Moulana Mohiuddin, S. (2016) Mechanical and tribological properties of AA7075-TiC metal matrix composites under heat treated (T6) and cast conditions. *Journal of Materials Research and Technology*, **5**, 377–83. https://doi.org/10.1016/j.jmrt.2016.03.011

[29] Pramanik, A. (2016) Effects of reinforcement on wear resistance of aluminum matrix

composites. *Transactions of Nonferrous Metals Society of China*, **26**, 348–58. https://doi.org/10.1016/S1003-6326(16)64125-0

[30] Kaushik, N.C. and Rao, R.N. (2016) Effect of grit size on two body abrasive wear of Al 6082 hybrid composites produced by stir casting method. *Tribology International*, **102**, 52–60. https://doi.org/10.1016/j.triboint.2016.05.015

[31] Sahin, Y. (2003) Preparation and some properties of SiC particle reinforced aluminium alloy composites. *Materials & Design*, **24**, 671–9. https://doi.org/10.1016/S0261-3069(03)00156-0

[32] Kaushik, N.C. and Rao, R.N. (2017) Influence of applied load on abrasive wear depth of hybrid Gr/SiC/Al-Mg-Si composites in two body condition. *Journal of Tribology*, **139**, 1–9. https://doi.org/10.1115/1.4035779

[33] Ramesh, C.S., Keshavamurthy, R., Pramod, S. and Koppad, P.G. (2011) Abrasive wear behavior of Ni–P coated Si_3N_4 reinforced Al6061 composites. *Journal of Materials Processing Techmology*, **211**, 1423–31. https://doi.org/10.1016/j.jmatprotec.2011.03.015

[34] Ramesh, C.S.Ã., Keshavamurthy, R., Channabasappa, B.H. and Pramod, S. (2010) Friction and wear behavior of Ni–P coated Si_3N_4 reinforced Al6061 composites. *Tribiology International*, **43**, 623–34. https://doi.org/10.1016/j.triboint.2009.09.011

[35] Radhika, N., Sasikumar, J., Sylesh, J.L. and Kishore, R. (2020) Dry reciprocating wear and frictional behaviour of B_4C reinforced functionally graded and homogenous aluminium matrix composites. *Journal of Materials Research and Technology*, **9**, 1578–92. https://doi.org/10.1016/j.jmrt.2019.11.084

[36] Baradeswaran, A. and Perumal, A.E. (2013) Influence of B_4C on the tribological and mechanical properties of Al 7075–B_4C composites. *Composites Part B*, **54**, 146–52. https://doi.org/10.1016/j.compositesb.2013.05.012

[37] Katkar, V.A., Gunasekaran, G., Rao, A.G. and Koli, P.M. (2011) Effect of the reinforced boron carbide particulate content of AA6061 alloy on formation of the passive film in seawater. *Corrosion Science*, **53**, 2700–12. https://doi.org/10.1016/j.corsci.2011.04.023

[38] Canakci, A. and Arslan, F. (2012) Abrasive wear behaviour of B_4C particle reinforced Al2024 MMCs. *The International Journal of Advanced Manufacturing Technology*, **63**, 785–95. https://doi.org/10.1007/s00170-012-3931-8

[39] Ray, A.K., Venkateswarlu, K., Chaudhury, S.K., Das, S.K., Kumar, B.R. and Pathak, L.C. (2002) Fabrication of TiN reinforced aluminium metal matrix composites through a powder metallurgical route. *Materials Science and Engineering A*, **338**, 160–5.

https://doi.org/10.1016/S0921-5093(02)00069-2

[40] Dobrzański, L.A., Kremzer, M. and Adamiak, M. (2008) Manufacturing of aluminium matrix composite materials reinforced by Al_2O_3 particles. *Journal of Achievements in Materials and Manufacturing Engineering*, **27**, 99–102.

[41] Baradeswaran, A. and Elaya Perumal, A. (2014) Study on mechanical and wear properties of Al7075/Al_2O_3/graphite hybrid composites. *Composites Part B: Engineering*, **56**, 464–71. https://doi.org/10.1016/j.compositesb.2013.08.013

[42] Yılmaz, O. and Buytoz, S. (2001) Abrasive wear of Al_2O_3-reinforced aluminium-based MMCs. *Composites Science and Technology*, **61**, 2381–92. https://doi.org/10.1016/S0266-3538(01)00131-2

[43] Singh, M., Mondal, D.P., Modi, O.P. and Jha, A.K. (2002) Two-body abrasive wear behaviour of aluminium alloy-sillimanite particle reinforced composite. *Wear*, **253**, 357–68. https://doi.org/10.1016/S0043-1648(02)00153-9

[44] Singh, M., Mondal, D.P., Jha, A.K. and Yegmeswaran, A.H. (2003) High stress abrasive wear behavior of sillimanite-reinforced Al-alloy matrix composite: A factorial design approach. *Journal of Materials Engineering and Performance*, **12**, 331–8. https://doi.org/10.1361/105994903770343196

[45] Singh, M., Mondal, D.P. and Das, S. (2006) Abrasive wear response of aluminium alloy-sillimanite particle reinforced composite under low stress condition. *Materials Science and Engineering A*, **419**, 59–68. https://doi.org/10.1016/j.msea.2005.11.056

[46] Prasad, M.G.A. and Bandekar, N. (2015) Study of microstructure and mechanical behavior of aluminum/garnet/carbon hybrid metal matrix composites (HMMCs) fabricated by chill casting method. *Journal of Materials Science and Chemical Engineering*, **3**, 1–8. https://dx.doi.org/10.4236/msce.2015.33001

[47] Sivakumar, S., Padmanaban, K.P. and Uthayakumar, M. (2014) Wear behavior of the Al (LM24)–garnet particulate composites under dry sliding conditions. *Proceedings of the Institution of Mechanical Engineers, Part J : Journal of Engineering Tribology*, **228**, 1410–20. https://doi.org/10.1177/1350650114541107

[48] Patel, S.K., Singh, V.P., Kumar, N., Kuriachen, B. and Nateriya, R. (2020) Wear Behaviour of Al-Silicon (LM13) Alloy Composite Reinforcement with TiC and ZrSiO4 Particles. *Silicon*, **12**, 211–21. https://doi.org/10.1007/s12633-019-00114-8

[49] Mazahery, A. and Shabani, M.O. (2012) Study on microstructure and abrasive wear behavior of sintered Al matrix composites. *Ceramics International*, Elsevier Ltd and

Techna Group S.r.l. **38**, 4263–9. https://doi.org/10.1016/j.ceramint.2012.02.008

[50] Das, S., Das, S. and Das, K. (2006) Ageing behavior of Al–4.5 wt% Cu matrix alloy reinforced with Al_2O_3 and $ZrSiO_4$ particulate varying particle size. *Journal of Materials Science*, **41**, 5402–6. https://doi.org/10.1007/s10853-006-0243-0

[51] Kumar, C.A.V. and Rajadurai, J.S. (2016) Influence of rutile (TiO_2) content on wear and microhardness characteristics of aluminium-based hybrid composites synthesized by powder metallurgy. *Transactions of Nonferrous Metals Society of China*, **26**, 63–73. https://doi.org/10.1016/S1003-6326(16)64089-X

[52] Arora, R., Kumar, S., Singh, G. and Pandey, O.P. (2015) Role of Different Range of Particle Size on Wear Characteristics of Al–Rutile Composites. *Particulate Science and Technology*, **33**, 229–33. https://doi.org/10.1080/02726351.2014.953648

[53] Das, S., Mondal, D.P. and Dixit, G. (2001) Correlation of abrasive wear with microstructure and mechanical properties of pressure die-cast aluminum hard-particle composite. *Metallurgical and Materials Transactions A*, **32A**, 633–42. https://doi.org/10.1007/s11661-001-0080-3

[54] Surappa, M.K. (2003) Aluminium matrix composites: Challenges and opportunities. *Sadhana*, **28**, 319–34. https://doi.org/10.1007/BF02717141

[55] Rohatgi, P. (1991) Cast aluminum-matrix composites for automotive applications. *Journal of Metals*, **43**, 10–5. https://doi.org/10.1007/BF03220538

[56] Banerji, A., Prasad, S. V., Surappa, M.K. and Rohatgi, P.K. (1982) Abrasive wear of cast aluminium alloy-zircon particle composites. *Wear*, **82**, 141–51. https://doi.org/10.1016/0043-1648(82)90288-5

[57] Clarke, J. and Sarkar, A.D. (1979) Wear characteristics of as-cast binary aluminium-silicon alloys. *Wear*, **54**, 7–16. https://doi.org/10.1016/0043-1648(79)90044-9

[58] Prasad, S. V and Asthana, R. (2004) Aluminum metal – matrix composites for automotive applications : tribological considerations. *Tribology Letters*, **17**, 445–53. https://doi.org/10.1023/B:TRIL.0000044492.91991.f3

[59] Allison, E.J. and Cole, G.S. (1993) Metal matrix composites in the automotive industry : opportunities and challenges. *The Journal of The Minerals, Metals and Materials Society*, **45**, 19–24. https://doi.org/10.1007/BF03223361

[60] Cole, G.S. and Sherman, A.M. (1995) Lightweight Materials for Automotive Applications. *Materials Characterization*, **35**, 3–9. https://doi.org/10.1016/1044-

5803(95)00063-1

[61] Deuis, R.L., Subramanian, C. and Yellupb, J.M. (1997) Dry sliding wear of aluminium composites- a review. *Composites Science and Technology*, **57**, 415–35. https://doi.org/10.1016/S0266-3538(96)00167-4

[62] Arslan, E., Totik, Y., Demirci, E.E., Vangolu, Y., Alsaran, A. and Efeoglu, I. (2009) High temperature wear behavior of aluminum oxide layers produced by AC micro arc oxidation. *Surface and Coatings Technology*, **204**, 829–33. https://doi.org/10.1016/j.surfcoat.2009.09.057

[63] Lasa, L. and Rodriguez-Ibabe, J.M.M. (2003) Wear behaviour of eutectic and hypereutectic Al-Si-Cu-Mg casting alloys tested against a composite brake pad. *Materials Science and Engineering A*, **363**, 193–202. https://doi.org/10.1016/S0921-5093(03)00633-6

[64] Kori, S.A. and Chandrashekharaiah, T.M. (2007) Studies on the dry sliding wear behaviour of hypoeutectic and eutectic Al-Si alloys. *Wear*, **263**, 745–55. https://doi.org/10.1016/j.wear.2006.11.026

[65] Surappa, M.K. (1997) Microstructure evolution during solidification of DRMMCs (discontinuously reinforced metal matrix composites): State of art. *Journal of Materials Processing Technology*, **63**, 325–33. https://doi.org/10.1016/S0924-0136(96)02643-X

[66] Srivatsan, T.S., Ibrahim, I.A., Mohamed, F.A. and Lavernia, E.J. (1991) Processing Techniques for Particulate-Reinforced Metal Aluminum Matrix Composites. *Journal of Materials Science*, **26**, 5965–78. https://doi.org/10.1007/BF01113872

[67] Kennedy, A.R. and Wyatt, S.M. (2001) Characterizing particle-matrix interfacial bonding in particulate Al-TiC MMCs produced by different methods. *Composites Part A: Applied Science and Manufacturing*, **32**, 555–9. https://doi.org/10.1016/S1359-835X(00)00052-X

[68] Thakur, S.K. and Dhindaw, B.K. (2001) The influence of interfacial characteristics between SiCp and Mg/Al metal matrix on wear, coefficient of friction and microhardness. *Wear*, **247**, 191–201. https://doi.org/10.1016/S0043-1648(00)00536-6

[69] Aqida, S.N., Ghazali, M.I. and Hashim, J. (2004) Effects of porosity on mechanical properties of metal matrix composite: an overview. *Jurnal Teknologi*, **40**, 17–32. https://doi.org/10.11113/jt.v40.395

[70] Rohatgi, P.K., Ray, S. and Liu, Y. (1992) Tribological properties of metal matrix-graphite particle composites. *International Materials Reviews*, **37**, 129–52. https://doi.org/10.1179/imr.1992.37.1.129

[71] Hashim, J., Looney, L. and Hashmi, M.S.J. (2002) Particle distribution in cast metal matrix composites - Part II. *Journal of Materials Processing Technology*, **123**, 258–63. https://doi.org/10.1016/S0924-0136(02)00099-7

[72] Ahmad, K.R., Jamaludin, S.B., Hussain, L.B. and Ahmad, Z.A. (2005) The influence of alumina particle size on sintered density and hardness of discontinuous reinforced aluminum metal matrix composite. *Jurnal Teknologi*, **42**, 49–57. https://doi.org/10.11113/jt.v42.732

[73] Miranda, G., Buciumeanu, M., Madeira, S., Carvalho, O., Soares, D. and Silva, F.S. (2015) Hybrid composites Metallic and ceramic reinforcements influence on mechanical and wear behavior. *Composites Part B: Engineering*, **74**, 153–65. https://doi.org/10.1016/j.compositesb.2015.01.007

[74] Bains, P.S. Sidhu, S.S. and Payal, H.S. (2015) Fabrication and machining of metal matrix composites: a review. *Materials and Manufacturing Processes*, **31**, 553–73. https://doi.org/10.1080/10426914.2015.1025976

[75] Saravanani, C., Subramanian, K., Sivakumari, D.B., Sathyanandhani, M. and Narayanani, R.S. (2015) Fabrication of aluminium metal matrix composite- a review. *Journal of Chemical and Pharmaceutical Sciences*, 82–7.

[76] Dash, K., Sukumaran, S. and Ray, B.C. (2014) The behaviour of aluminium matrix composites under thermal stresses. *Science and Engineering of Composite Materials*, **23**, 1–20. https://doi.org/10.1515/secm-2013-0185

[77] Saravanan, C., Subramanian, K., Krishnan, V.A. and Narayanan, R.S. (2015) Effect of particulate reinforced aluminium metal matrix composite- a review. *Mechanics and Mechanical Engineering*, **19**, 23–30.

[78] Cooke, K.O. (2012) A study of the effect of nanosized particles on transient liquid phase diffusion bonding Al6061 metal-matrix composite (MMC) using Ni/Al_2O_3 Nanocomposite Interlayer. *Metallurgical and Materials Transactions B*, **43**, 627–34. https://doi.org/10.1007/s11663-012-9643-5

[79] Wang, X.R., Yang, Y.Q., Luo, X., Zhang, W., Zhao, G.M. and Huang, B. (2013) An investigation of Ti-43Al-9V/Ti-6Al-4V interface by diffusion bonding. *Intermetallics*, **36**, 127–32. https://doi.org/10.1016/j.intermet.2012.12.018

[80] Babalola, P.O., Bolu, C.A., Inegbenebor, A.O. and Odunfa, K.M. (2014) Development of aluminium matrix composites: A review. *International Journal of Engineering and Technology Research*, **2**, 1–11.

[81] Srivastava, V.C., Mandal, R.K. and Ojha, S.N. (2001) Microstructure and mechanical properties of Al–Si alloys produced by spray forming process. *Materials Science and Engineering: A*, **304**–**306**, 555–8. https://doi.org/10.1016/S0921-5093(00)01514-8

[82] Pramod, S.L., Bakshi, S.R. and Murty, B.S. (2015) Aluminum-based cast in-situ composites: A review. *Journal of Materials Engineering and Performance*, **24**, 2185–207. https://doi.org/10.1007/s11665-015-1424-2

[83] Naik, S.K., Sanjay, S.J., Math, V.B. and Matti, R.S. (2015) Connecting rod made using particulate reinforced aluminum metal matrix composite - a review. *Journal of Emerging Technologies and Innovative Research*, **2**, 228–33.

[84] Umasankar, V., Xavior, M.A. and Karthikeyan, S. (2014) Experimental evaluation of the influence of processing parameters on the mechanical properties of SiC particle reinforced AA6061 aluminium alloy matrix composite by powder processing. *Journal of Alloys and Compounds Journal*, **582**, 380–6. https://doi.org/10.1016/j.jallcom.2013.07.129

[85] Behera, P. (2003) Heavy minerals in beach sands of Gopalpur and Paradeep along Orissa coastline, east cost of India. *Indian Journal of Marine Sciences*, **32**, 172–4.

[86] Jayaraju, N. (2004) Controls on formation and distribution of heavy minerals along southern tip of India. *J Ind Geophys Union*, **8**, 191–4.

[87] Panigrahi, S.P. (2013) Critical review of beach sand mining in india-with particular reference to chhatrapur sand complex (oscom) in Odisha-A case study. National Institute of Technology, Rourkela.

[88] Ihlen, P.M. (2000) Utilisation of sillimanite minerals, their geology, and potential occurrences in Norway- an overview. *NGU-Bulliten*, **436**, 113–28.

[89] Singh, M., Mondal, D.P., Jha, A.K., Das, S. and Yegneswaran, A.H. (2001) Preparation and properties of cast aluminium alloy-sillimanite particle composite. *Composites - Part A: Applied Science and Manufacturing*, **32**, 787–95. https://doi.org/10.1016/S1359-835X(00)00187-1

[90] Singh, M., Mondal, D.P., Dasgupta, R., Prasad, B.K., Jha, A.K. and Yegneswaran, A.H. (2003) Effect of sillimanite particle reinforcement on dry sliding wear behaviour of aluminium alloy composite. *Materials Science and Technology*, **19**, 303–12. https://doi.org/10.1179/026708303225009355

[91] Yang, D., Qiu, F., Zhao, Q., Wang, L. and Jiang, Q. (2017) The abrasive wear behavior of Al2014 composites reinforced with Ti5Si3-coated SiC. *Tribology international*, **112**, 33-41. https://doi.org/10.1016/j.triboint.2017.03.022

[92] Kumar, S., Sharma, V., Panwar, R.S. and Pandey, O.P. (2012) Wear behavior of dual particle size (dps) zircon sand reinforced aluminum alloy. *Tribology Letters*, **47**, 231–51. https://doi.org/10.1007/s11249-012-9983-y

[93] Alshmri, F., Atkinson, H. V., Hainsworth, S. V., Haidon, C. and Lawes, S.D.A. (2014) Dry sliding wear of aluminium-high silicon hypereutectic alloys. *Wear*, **313**, 106–16. https://doi.org/10.1016/j.wear.2014.02.010

[94] Lozano, D.E., Mercado-Solis, R.D., Perez, A.J., Talamantes, J., Morales, F. and Hernandez-Rodriguez, M.A.L. (2009) Tribological behaviour of cast hypereutectic Al-Si-Cu alloy subjected to sliding wear. *Wear*, **267**, 545–9. https://doi.org/10.1016/j.wear.2008.12.112

[95] Vijeesh, V., Prabhu, K.N. and Prabhu, V.V.K.N. (2014) Review of microstructure evolution in hypereutectic Al-Si alloys and its effect on wear properties. *Transactions of the Indian Institute of Metals*, **67**, 1–18. https://doi.org/10.1007/s12666-013-0327-x

[96] Aravind, M., Yu, P., Yau, M.Y. and Ng, D.H.L. (2004) Formation of Al2Cu and AlCu intermetallics in Al(Cu) alloy matrix composites by reaction sintering. *Materials Science and Engineering A*, **380**, 384–93. https://doi.org/10.1016/j.msea.2004.04.013

[97] Włodarczyk-Fligier, A., Dobrzański, L.A. and Adamiak, M. (2008) Wear resistance of PM composite materials reinforced with the Ti(C, N) ceramic particles. *Journal of Achievements in Materials and Manufacturing Engineering*, **30**, 147–50.

[98] Asghar, G., Peng, L., Fu, P., Yuan, L. and Liu, Y. (2020) Role of Mg2Si precipitates size in determining the ductility of A357 cast alloy. *Materials & Design*, **186**, 108280. https://doi.org/10.1016/j.matdes.2019.108280

[99] Lashgari, H.R., Zangeneh, S., Shahmir, H., Saghafi, M. and Emamy, M. (2010) Heat treatment effect on the microstructure, tensile properties and dry sliding wear behavior of A356-10%B4C cast composites. *Materials & Design*, **31**, 4414–22. https://doi.org/10.1016/j.matdes.2010.04.034

[100] Hernández-Méndez, F., Altamirano-Torres, A., Miranda-Hernández, J., Térres-Rojas, E. and Rocha-Rangel, E. (2011) Effect of nickel addition on microstructure and mechanical properties of aluminum-based alloys. *Materials Science Forum*, **691**, 10–4. https://doi.org/10.4028/www.scientific.net/MSF.691.10

[101] Rana, R.S., Purohit, R. and Das, S. (2012) Reviews on the influences of alloying elements on the microstructure and mechanical properties of aluminum alloys and aluminum alloy composites. *International Journal of Scientific and Research Publications*, **2**, 1–7.

[102] Nam, S.W. and Lee, D.H. (2000) The effect of Mn on the mechanical behavior of Al alloys. *Metals and Materials*, **6**, 13–6. https://doi.org/10.1007/BF03026339

[103] Şahin, Y. (2010) Abrasive wear behaviour of SiC/2014 aluminium composite. *Tribology International*, **43**, 939–43. https://doi.org/10.1016/j.triboint.2009.12.056

[104] Dwivedi, D.K. (2006) Wear behaviour of cast hypereutectic aluminium silicon alloys. *Materials & Design*, **27**, 610–6. https://doi.org/10.1016/j.matdes.2004.11.029

[105] Dwivedi, D.K., Arjun, T.S., Thakur, P., Vaidya, H. and Singh, K. (2004) Sliding wear and friction behaviour of Al-18% Si-0.5% Mg alloy. *Journal of Materials Processing Technology*, **152**, 323–8. https://doi.org/10.1016/j.jmatprotec.2004.04.379

[106] Dwivedi, D.K. (2010) Adhesive wear behaviour of cast aluminium–silicon alloys: Overview. *Materials & Design*, **31**, 2517–31. https://doi.org/10.1016/j.matdes.2009.11.038

[107] Vijeesh, V. and Prabhu, K.N. (2014) Review of microstructure evolution in hypereutectic Al–Si alloys and its effect on wear properties. *Transactions of the Indian Institute of Metals*, **67**, 1–18. https://doi.org/10.1007/s12666-013-0327-x

[108] Wang, R. and Lu, W. (2016) Hypereutectic Al-Si alloy with completely nodular eutectic silicon: microstructure and process. *International Journal of Materials Science and Applications*, **5**, 277–83. https://doi.org/10.11648/j.ijmsa.20160506.17

[109] Dai, H.S. and Liu, X.F. (2009) Optimal holding temperatures and phosphorus additions for primary silicon refinement in Al–high Si alloys. *Materials Science and Technology*, **25**, 1183–8. https://doi.org/10.1179/174328408X382235

[110] Wang, R. and Lu, W. (2012) Microstructural characteristic and mechanical behavior of nodular silicon hypereutectic Al-Si alloys. *The Journal of The Minerals, Metals & Materials Society*, **64**, 330–6. https://doi.org/10.1007/s11837-012-0251-2

[111] Zhang, H., Duan, H., Shao, G., Xu, L., Yin, J. and Yan, B., (2006) Modification mechanism of cerium on the Al-18Si alloy. *Rare Metals*, **25**, 11–5. https://doi.org/10.1016/S1001-0521(06)60006-5

[112] Sharma, S.C. (2001) The sliding wear behavior of Al6061-garnet particulate composites. *Wear*, **249**, 1036–45. https://doi.org/10.1016/S0043-1648(01)00810-9

[113] Ranganath, G., Sharma, S.C. and Krishna, M. (2001) Dry sliding wear of garnet reinforced zinc/aluminium metal matrix composites. *Wear*, **251**, 1408–13. https://doi.org/10.1016/S0043-1648(01)00781-5

[114] Lee, G.Y., Dharan, C.K.H. and Ritchie, R.O. (2002) A physically-based abrasive wear model for composite materials. *Wear*, **252**, 322–31. https://doi.org/10.1016/S0043-1648(01)00896-1

[115] Velasco, F., da Costa, C.E. and Torralba, J.M. (2002) Mechanical properties and wear behaviour of PM aluminium composite reinforced with (Fe_3Al) particles. *Powder Metallurgy*, **45**, 247–50. https://doi.org/10.1179/003258902225006952

[116] Shorowordi, K.M., Laoui, T., Haseeb, A.S.M.A., Celis, J.P. and Froyen, L. (2003) Microstructure and interface characteristics of B_4C, SiC and Al_2O_3 reinforced Al matrix composites: a comparative study. *Journal of Materials Processing Technology*, **142**, 738–43. https://doi.org/10.1016/S0924-0136(03)00815-X

[117] Korkut, M.H. (2004) Effect of particulate reinforcement on wear behaviour of aluminium matrix composites. *Materials Science and Technology*, **20**, 73–81. https://doi.org/10.1179/174328413X13789824293542

[118] Basavarajappa, S. and Chandramohan, G. (2005) Dry sliding wear behaviour of hybrid metal matrix composites. *Materials Science (Medžiagotyra)*, **11**, 253–7.

[119] Kumar, M.P., Sadashivappa, K., Prabhukumar, G.P. and Basavarajappa, S. (2006) Dry sliding wear behaviour of garnet particles reinforced zinc-aluminium alloy metal matrix composites. *Materials Science (Medžiagotyra)*, **12**, 209–13.

[120] Shorowordi, K.M., Haseeb, A.S.M.A. and Celis, J.P. (2006) Tribo-surface characteristics of Al–B_4C and Al–SiC composites worn under different contact pressures. *Wear*, **261**, 634–41. https://doi.org/10.1016/j.wear.2006.01.023

[121] Aigbodion, V.S. and Hassan, S.B. (2007) Effects of silicon carbide reinforcement on microstructure and properties of cast Al-Si-Fe/SiC particulate composites. *Materials Science and Engineering: A*, **447**, 355–60. https://doi.org/10.1016/j.msea.2006.11.030

[122] Basavarajappa, S., Chandramohan, G., Mahadevan, A., Thangavelu, M., Subramanian, R. and Gopalakrishnan, P. (2007) Influence of sliding speed on the dry sliding wear behaviour and the subsurface deformation on hybrid metal matrix composite. *Wear*, **262**, 1007–12. https://doi.org/10.1016/j.wear.2006.10.016

[123] Abdizadeh, H., Baharvandi, H.R. and Moghaddam, K.S. (2008) Comparing the effect of processing temperature on microstructure and mechanical behavior of ($ZrSiO_4$ or TiB_2)/aluminum composites. *Materials Science and Engineering: A*, **498**, 53–8. https://doi.org/10.1016/j.msea.2008.07.009

[124] Singla, M., Singh, L. and Chawla, V. (2009) Study of wear properties of Al-SiC

composites. *Journal of Minerals & Materials Characterization & Engineering*, **8**, 813–9.

[125] Hassan, A.M., Alrashdan, A., Hayajneh, M.T. and Mayyas, A.T. (2009) Wear behavior of Al-Mg-Cu-based composites containing SiC particles. *Tribology International*, **42**, 1230–8. https://doi.org/10.1016/j.triboint.2009.04.030

[126] Kumar, G.B.V., Rao, C.S.P., Selvaraj, N. and Bhagyashekar, M.S. (2010) Studies on Al6061-SiC and Al7075-Al_2O_3 metal matrix composites. *Journal of Minerals and Materials Characterization and Engineering*, **09**, 43–55. https://doi.org/10.4236/jmmce.2010.91004

[127] Rao, R.N. and Das, S. (2010) Effect of matrix alloy and influence of SiC particle on the sliding wear characteristics of aluminium alloy composites. *Materials & Design*, **31**, 1200–7. https://doi.org/10.1016/j.matdes.2009.09.032

[128] Rao, R.N. and Das, S. (2011) Effect of sliding distance on the wear and friction behavior of as cast and heat-treated Al-SiCp composites. *Materials & Design*, **32**, 3051–8. https://doi.org/10.1016/j.matdes.2011.01.033

[129] Kumar, S., Panwar, R.S. and Pandey, O.P. (2012) Tribological characteristics of aluminium tri-reinforced particles (Al-TRP) composites developed by liquid metallurgy route. *Advanced Materials Research*, **585**, 574–8. https://doi.org/10.4028/www.scientific.net/AMR.585.574

[130] Sharma, V., Kumar, S.and Pandey, O.P. (2012) Correlation of reinforced ceramic particle's nature and size with microstructure and wear behavior of Al-Si alloy composite. *Advanced Materials Research*, **585**, 564–8. https://doi.org/10.4028/www.scientific.net/AMR.585.564

[131] Rasidhar, L., Krishna, A.R. and Rao, C. (2013) Fabrication and investigation on properties of ilmenite ($FeTiO_3$) based Al-nanocomposite by stir casting process. *International Journal of Bio-Science and Bio-Technology*, **5**, 193–200.

[132] Umanath, K., Palanikumar, K. and Selvamani, S.T. (2013) Analysis of dry sliding wear behaviour of Al6061/SiC/Al_2O_3 hybrid metal matrix composites. *Composites Part B: Engineering*, **53**, 159–68. https://doi.org/10.1016/j.compositesb.2013.04.051

[133] Arora, R., Kumar, S., Singh, G. and Pandey, O.P. (2014) Influence of particle size and temperature on the wear properties of rutile-reinforced aluminium metal matrix composite. *Journal of Composite Materials*, **49**, 843–52. https://doi.org/10.1177/0021998314526079

[134] Arora, R., Sharma, A., Kumar, S., Singh, G. and Pandey, O.P. (2014) Study of the

oxidative wear of the aluminum rutile composites at higher contact pressure. *International Journal of Research in Mechanical Engineering & Technology*, **4**, 218–21.

[135] Viswanatha, B.M., Kumar, M.P., Basavarajappa, S. and Kiran, T.S. (2016) Study of the microstructure, hardness and tribological behavior of hypoeutectic Al-7Si hybrid composites. *Industrial Lubrication and Tribology*, **68**, 233–41. https://doi.org/10.1108/ILT-06-2015-0080

[136] Ghasali, E., Yazdani-rad, R., Asadian, K. and Ebadzadeh, T. (2017) Production of Al-SiC-TiC hybrid composites using pure and 1056 aluminum powders prepared through microwave and conventional heating methods. *Journal of Alloys and Compounds*, **690**, 512–8. https://doi.org/10.1016/j.jallcom.2016.08.145

[137] Daniel, S.A.A., Sakthivel, M., Gopal, P.M. and Sudhagar, S. (2018) Study on tribological behaviour of Al/SiC/MoS_2 hybrid metal matrix composites in high temperature environmental condition. *Silicon*, **10**, 2129–39. https://doi.org/10.1007/s12633-017-9739-2

[138] Kurapati, V.B., Kommineni, R. and Sundarrajan, S. (2018) Statistical analysis and mathematical modeling of dry sliding wear parameters of 2024 aluminium hybrid composites reinforced with fly ash and SiC particles. *Transactions of the Indian Institute of Metals*, **71**, 1809–25. https://doi.org/10.1007/s12666-018-1322-z

[139] Pethuraj, M., Uthayakumar, M., Rajakarunakaran, S. and Rajesh, S. (2018) Solid particle erosive behaviour of sillimanite reinforced aluminium metal matrix composites. *Materials Research Express*, **5**, 066514. https://doi.org/10.1088/2053-1591/aac8ba

[140] Vadghule, A.Y. and Kale, P.V.C. (2018) Tribological evaluation of LM26 Aluminum Metal Matrix Composites. *International Research Journal of Engineering and Technology (IRJET)*, **5**, 2553–8.

[141] Balakumar, S., Selvam, M.D. and Nelson, A.J.R. (2018) Wear and friction characteristics of aluminium matrix composites reinforced with flyash/Cu/Gr particles. *International Journal of ChemTech Research*, **11**, 121–33.

[142] Vinod, B., Ramanathan, S., Ananthi, V. and Selvakumar, N. (2019) Fabrication and characterization of organic and in-organic reinforced A356 aluminium matrix hybrid composite by improved double-stir casting. *Silicon*, **11**, 817–29. https://doi.org/10.1007/s12633-018-9881-5

[143] Mishra, S., Patnaik, A. and Kumar, S.R. (2019) Comparative analysis of wear behavior of garnet and fly ash reinforced Al7075 hybrid composite. *Materialwissenschaft Und Werkstofftechnik*, **50**, 86–96. https://doi.org/10.1002/mawe.201800121

[144] Çelik, Y.H. and Kilickap, E. (2019) Hardness and wear behaviours of Al matrix composites and hybrid composites reinforced with B_4C and SiC. *Powder Metallurgy and Metal Ceramics*, **57**, 613–22. https://doi.org/10.1007/s11106-019-00023-w

[145] Lakshmikanthan, A., Bontha, S., Krishna, M., Koppad, P.G. and Ramprabhu, T. (2019) Microstructure, mechanical and wear properties of the A357 composites reinforced with dual sized SiC particles. *Journal of Alloys and Compounds*, **786**, 570–80. https://doi.org/10.1016/j.jallcom.2019.01.382

[146] Gecu, R. and Karaaslan, A. (2020) Casting temperature dependent wear and corrosion behavior of 304 stainless steel reinforced A356 aluminium matrix bimetal composites fabricated by vacuum-assisted melt infiltration casting. *Wear*, **446**–**447**, 203183. https://doi.org/10.1016/j.wear.2020.203183

[147] Yadav, P.K., Dixit, G., Kuriachen, B., Verma, M.K., Patel, S.K. and Singh, R.K. (2020) Effect of reinforcements and abrasive size on high-stress tribological behaviour of aluminium piston matrix composites. *Journal of Bio- and Tribo-Corrosion*, **6**, 1–14. https://doi.org/10.1007/s40735-019-0317-6

[148] Girish, B.M., Shivakumar, B.P., Hanamantraygouda, M.B. and Satish, B.M. (2020) Wear behaviour of hot forged SiC reinforced aluminium 6061Composite materials. *Australian Journal of Mechanical Engineering*, 1–8. https://doi.org/10.1080/14484846.2020.1714353

[149] Degnan, C.C., Shipway, P.H. and Wood, J.V. (2001) Elevated temperature sliding wear behaviour of TiC-reinforced steel matrix composites. *Wear*, **251**, 1444–51. https://doi.org/10.1016/s0043-1648(01)00772-4

[150] Muratoğlu, M. and Aksoy, M. (2006) Abrasive wear of 2124Al-SiC composites in the temperature range 20-200 °C. *Journal of Materials Processing Technology*, **174**, 272–6. https://doi.org/10.1016/j.jmatprotec.2006.01.010

[151] Gong, K., He-li, L., Di, F. and Chang-hai, L. (2007) Ni_3Al-based intermetallic alloys as a new type of high-temperature and wear-resistant materials. *Journal of Iron and Steel Research, International*, **14**, 21–5. https://doi.org/10.1016/S1006-706X(08)60045-X

[152] Lee, J.M., Kang, S.B. and Han, J. (2008) Dry sliding wear of MAO-coated A356/20 vol.% SiCp composites in the temperature range 25-180 °C. *Wear*, **264**, 75–85. https://doi.org/10.1016/j.wear.2007.01.044

[153] Natarajan, S., Narayanasamy, R., Babu, S.P.K., Dinesh, G., Kumar, B.A. and Sivaprasad, K. (2009) Sliding wear behaviour of Al 6063/TiB_2 in situ composites at elevated temperatures. *Materials & Design*, **30**, 2521–31. https://doi.org/10.1016/j.matdes.2008.09.037

[154] Kumar, S., Sarma, V.S. and Murty, B.S. (2010) High temperature wear behavior of Al-4Cu-TiB_2 in situ composites. *Wear*, **268**, 1266–74. https://doi.org/10.1016/j.wear.2010.01.022

[155] Jerome, S., Ravisankar, B., Mahato, P.K. and Natarajan, S. (2010) Synthesis and evaluation of mechanical and high temperature tribological properties of in-situ Al-TiC composites. *Tribology International*, **43**, 2029–36. https://doi.org/10.1016/j.triboint.2010.05.007

[156] Rajaram, G., Kumaran, S., Rao, T.S. and Kamaraj, M. (2010) Studies on high temperature wear and its mechanism of Al-Si/graphite composite under dry sliding conditions. *Tribology International*, **43**, 2152–8. https://doi.org/10.1016/j.triboint.2010.06.004

[157] Zhu, H., Jar, C., Song, J., Zhao, J., Li, J. and Xie, Z. (2012) High temperature dry sliding friction and wear behavior of aluminum matrix composites (Al_3Zr+α-Al_2O_3)/Al. *Tribology International*, **48**, 78–86. https://doi.org/10.1016/j.triboint.2011.11.011

[158] Zhu, H., Jia, C., Li, J., Zhao, J., Song, J., Yao, Y. et al. (2012) Microstructure and high temperature wear of the aluminum matrix composites fabricated by reaction from Al-ZrO_2-B elemental powders. *Powder Technology*, **217**, 401–8. https://doi.org/10.1016/j.powtec.2011.10.056

[159] Kumar, S., Pandey, R., Panwar, R.S. and Pandey, O.P. (2013) Effect of particle size on wear of particulate reinforced aluminum alloy composites at elevated temperatures. *Journal of Materials Engineering and Performance*, **22**, 3550–60. https://doi.org/10.1007/s11665-013-0642-8

[160] Kumar, S., Panwar, R.S. and Pandey, O.P. (2013) Effect of dual reinforced ceramic particles on high temperature tribological properties of aluminum composites. *Ceramics International*, **39**, 6333–42. https://doi.org/10.1016/j.ceramint.2013.01.059

[161] Michael, H.B.R., Ramabalan, S., Dinaharan, I. and Vijay, S.J. (2014) Effect of TiB_2 content and temperature on sliding wear behavior of AA7075/TiB_2 in situ aluminum cast composites. *Archives of Civil and Mechanical Engineering*, **14**, 72–9. https://doi.org/10.1016/j.acme.2013.05.005

[162] Arora, R., Kumar, S., Singh, G. and Pandey, O.P. (2015) Effect of applied pressure on the tribological behaviour of dual particle size rutile reinforced LM13 alloy composites. *Characterization of Minerals, Metals, and Materials*, 755–62. https://doi.org/10.1007/978-3-319-48191-3_95

[163] Kumar N. Mathan, Senthil Kumaran, S. and Kumaraswamidhas, L.A. (2016) Wear behaviour of Al 2618 alloy reinforced with Si_3N_4, AlN and ZrB_2 in situ composites at

elevated temperatures. *Alexandria Engineering Journal*, **55**, 19–36. https://doi.org/10.1016/j.aej.2016.01.017

[164] Nemati, N., Emamy, M., Penkov, O. V., Kim, J. and Kim, D.E. (2016) Mechanical and high temperature wear properties of extruded Al composite reinforced with $Al_{13}Fe_4$ CMA nanoparticles. *Materials & Design*, **90**, 532–44. https://doi.org/10.1016/j.matdes.2015.11.001

[165] Raju, R.S.S., Panigrahi, M.K., Ganguly, R.I. and Srinivasa, G.R. (2019) Tribological behaviour of Al-1100-coconut shell ash (CSA) composite at elevated temperature. *Tribology International*, **129**, 55–66. https://doi.org/10.1016/j.triboint.2018.08.011

[166] ASTM. (2010) G 99: Standard Test Method for Wear Testing with a Pin-on-Disk Apparatus. *ASTM Standards,*. https://doi.org/10.1520/G0099-05R10.2

[167] Jorstad, J. and Apelian, D. (2009) Hypereutectic Al-Si alloys: Practical casting considerations. *International Journal of Metalcasting*, **3**, 13–36. https://doi.org/10.1007/BF03355450

[168] Rohatgi, P. and Asthana, R. (1991) The solidification of metal-matrix particulate composites. *The Journal of The Minerals, Metals & Materials Society*, **43**, 35–41. https://doi.org/10.1007/BF03220566

[169] Rohatgi, P.K., Kumar, P.A., Chelliah, N.M. and Rajan, T.P.D. (2020) Solidification processing of cast metal matrix composites over the last 50 years and opportunities for the future. *The Journal of The Minerals, Metals & Materials Society*, **72**, 2912–26. https://doi.org/10.1007/s11837-020-04253-x

[170] Kumar, G.S.P., Koppad, P.G., Keshavamurthy, R. and Alipour, M. (2017) Microstructure and mechanical behaviour of in situ fabricated AA6061–TiC metal matrix composites. *Archives of Civil and Mechanical Engineering*, **17**, 535–44. https://doi.org/10.1016/j.acme.2016.12.006

[171] Panwar, R.S. and Pandey, O.P. (2013) Analysis of wear track and debris of stir cast LM13/Zr composite at elevated temperatures. *Materials Characterization*, **75**, 200–13. https://doi.org/10.1016/j.matchar.2012.11.003

[172] Wang, W., Ajersch, F. and Löfvander, J.P.A. (1994) Si phase nucleation on SiC particulate reinforcement in hypereutectic A1-Si alloy matrix. *Materials Science and Engineering: A*, **187**, 65–75. https://doi.org/10.1016/0921-5093(94)90332-8

[173] Haque, M.M. and Sharif, A. (2001) Study on wear properties of aluminium-silicon piston alloy. *Journal of Materials Processing Technology*, **118**, 69–73.

https://doi.org/10.1016/S0924-0136(01)00869-X

[174] Show, B.K., Mondal, D.K. and Maity, J. (2014) Dry sliding wear behavior of aluminum-based metal matrix composites with single (Al_2O_3) and hybrid (Al_2O3+SiC) reinforcements. *Metallography, Microstructure, and Analysis*, **3**, 11–29. https://doi.org/10.1007/s13632-013-0113-5

[175] Mondal, D.P., Das, S., Rao, R.N. and Singh, M. (2005) Effect of SiC addition and running-in-wear on the sliding wear behaviour of Al–Zn–Mg aluminium alloy. *Materials Science and Engineering: A*, **402**, 307–https://doi.org/10.1016/j.msea.2005.05.023

[176] Chaudhury, S.K., Singh, A. K., Sivaramakrishnan, C.S. and Panigrahi, S.C. (2005) Wear and friction behavior of spray formed and stir cast Al–2Mg–11TiO_2 composites. *Wear*, **258**, 759–67. https://doi.org/10.1016/j.wear.2004.09.007

[177] Sharma, A., Kumar, S., Singh, G. and Pandey, O.P. (2015) Effect of particle size on wear behavior of Al-garnet composites. *Particulate Science and Technology*, **33**, 234–9. https://doi.org/10.1080/02726351.2014.954686

[178] Rajeev, V.R., Dwivedi, D.K. and Jain, S.C. (2010) Effect of load and reciprocating velocity on the transition from mild to severe wear behavior of Al-Si-SiCp composites in reciprocating conditions. *Materials & Design*, **31**, 4951–9. https://doi.org/10.1016/j.matdes.2010.05.010

[179] Sharma, A., Kumar, S., Singh, G. and Pandey, O.P. (2014) Evaluation of sliding wear behavior of garnet particle-containing LM13 alloy composites. *Procedia Materials Science*, **5**, 953–61. https://doi.org/10.1016/j.mspro.2014.07.383

[180] Rajmohan, T., Palanikumar, K. and Ranganathan, S. (2013) Evaluation of mechanical and wear properties of hybrid aluminium matrix composites. *Transactions of Nonferrous Metals Society of China*, **23**, 2509–17. https://doi.org/10.1016/S1003-6326(13)62762-4

[181] Singh, J. and Chauhan, A. (2016) Overview of wear performance of aluminium matrix composites reinforced with ceramic materials under the influence of controllable variables. *Ceramics International*, **42**, 56–81. https://doi.org/10.1016/j.ceramint.2015.08.150

[182] Rao, R.N., Das, S., Mondal, D.P., Dixit, G. and Devi, S.L.T. (2013) Dry sliding wear maps for AA7010 (Al–Zn–Mg–Cu) aluminium matrix composite. *Tribiology International*, **60**, 77–82. https://doi.org/10.1016/j.triboint.2012.10.007

[183] Yigezu, B.S., Jha, P.K. and Mahapatra, M.M. (2013) Effect of sliding distance, applied load, and weight percentage of reinforcement on the abrasive wear properties of in situ

synthesized Al–12%Si/TiC composites. *Tribology Transactions*, **56**, 546–54. https://doi.org/10.1080/10402004.2013.767401

[184] Bindumadhavan, P.N., Wah, H.K., and Prabhakar, O. (2001) Dual particle size (DPS) composites: Effect on wear and mechanical properties of particulate metal matrix composites. *Wear*, **248**, 112–20. https://doi.org/10.1016/S0043-1648(00)00546-9

[185] Flodin, A. and Andersson, S. (1997) Simulation of mild wear in spur gears. *Wear*, **207**, 16–23. https://doi.org/10.1016/S0043-1648(96)07467-4

[186] Long, T.T., Nishimura, T., Aisaka, T. and Morita, M. (1991) Wear resistance of Al-Si alloys and aluminium matrix composites. *Materials Transactions*, **32**, 181–8. https://doi.org/10.2320/matertrans1989.32.181

[187] Walczak, M., Pieniak, D. and Zwierzchowski, M. (2015) The tribological characteristics of SiC particle reinforced aluminium composites. *Archives of Civil and Mechanical Engineering*, **15**, 116–23. https://doi.org/10.1016/j.acme.2014.05.003

[188] Panwar, R.S., Kumar, S., Pandey, R. and Pandey, O.P. (2014) Study of non-lubricated wear of the Al-Si alloy composite reinforced with different ratios of coarse and fine size zircon sand particles at different ambient temperatures. *Tribology Letters*, **55**, 83–92. https://doi.org/10.1007/s11249-014-0335-y

[189] Chelliah, N.M., Kumar, R., Singh, H. and Surappa, M.K. (2017) Microstructural evolution of die-cast and homogenized AZ91 Mg-alloys during dry sliding condition. *Journal of Magnesium and Alloys*, **5**, 35–40. https://doi.org/10.1016/j.jma.2017.02.001

[190] Panwar, R.S. and Pandey, O.P. (2013) Study of wear behavior of zircon sand-reinforced LM13 alloy composites at elevated temperatures. *Journal of Materials Engineering and Performance*, **22**, 1765–75. https://doi.org/10.1007/s11665-012-0383-0

[191] Basavarajappa, S., Chandramohan, G., Mukund, K., Ashwin, M. and Prabu, M. (2006) Dry sliding wear behavior of Al 2219/SiC_p-Gr hybrid metal matrix composites. *Journal of Materials Engineering and Performance*, **15**, 668–74. https://doi.org/10.1361/105994906X150803

[192] Venkataraman, B. and Sundararajan, G. (2000) Correlation between the characteristics of the mechanically mixed layer and wear behaviour of aluminium , Al-7075 alloy and Al-MMCs. *Wear*, **245**, 22–38. https://doi.org/10.1016/S0043-1648(00)00463-4

[193] Hu, X., Liu, X., He, Q., Wang, H., Qin, S., Ren, L. et al. (2011) Thermal expansion of andalusite and sillimanite at ambient pressure: a powder X-ray diffraction study up to 1000°C. *Mineralogical Magazine*, **75**, 363–74.

https://doi.org/10.1180/minmag.2011.075.2.363

[194] Deng, C.F., Ma, Y.X., Zhang, P., Zhang, X.X. and Wang, D.Z. (2008) Thermal expansion behaviors of aluminum composite reinforced with carbon nanotubes. *Materials Letters*, **62**, 2301–3. https://doi.org/10.1016/j.matlet.2007.11.086

[195] Lu, T.W., Chen, W.P., Wang, P., Mao, M.D., Liu, Y.X. and Fu, Z.Q. (2018) Enhanced mechanical properties and thermo-physical properties of 7075Al hybrid composites reinforced by the mixture of Cr particles and SiC_p. *Journal of Alloys and Compounds*, **735**, 1137–44. https://doi.org/10.1016/j.jallcom.2017.11.227

[196] Hsieh, C.L. and Tuan, W.H. (2007) Thermal expansion behavior of a model ceramic-metal composite. *Materials Science and Engineering: A*, **460**–**461**, 453–8. https://doi.org/10.1016/j.msea.2007.01.109

[197] Yang, H., Hazen, R.M., Finger, L.W., Prewitt, C.T. and Downs, R.T. (1997) Compressibility and crystal structure of sillimanite, Al_2SiO_5, at high pressure. *Physics and Chemistry of Minerals*, **25**, 39–47. https://doi.org/10.1007/s002690050084

[198] Pabst, W., Gregorová, E., Uhlířová, T. and Musilová, A. (2013) Elastic properties of mullite and mullite-containing ceramics – Part 1: Theoretical aspects and review of monocrystal data. *Ceramics - Silikaty*, **57**, 265–74.

[199] Tan, H., Cheng, J., Wang, S., Zhu, S., Yu, Y., Qiao, Z. et al. (2018) Tribological behavior of Al–20Si–5Fe–2Ni alloy at elevated temperatures under dry sliding. *Journal of Tribology*, **140**, 031609. https://doi.org/10.1115/1.4038438

[200] Tan, H., Luo, Z., Li, Y., Yan, F., Duan, R. and Huang, Y. (2015) Effect of strengthening particles on the dry sliding wear behavior of Al_2O_3-M_7C_3/Fe metal matrix composite coatings produced by laser cladding. *Wear*, **324**–**325**, 36–44. https://doi.org/10.1016/j.wear.2014.11.023

Ceramics International 44 (2018) 104–114

Contents lists available at ScienceDirect

Ceramics International

journal homepage: www.elsevier.com/locate/ceramint

Effect of particle size on dry sliding wear behaviour of sillimanite reinforced aluminium matrix composites

Sandeep Sharma[a], Tarun Nanda[a], O.P. Pandey[b,*]

[a] Mechanical Engineering Department, Thapar University, Patiala 147004, Punjab, India
[b] School of Physics and Materials Science, Thapar University, Patiala 147004, Punjab, India

ARTICLE INFO

Keywords:
LM30 aluminium alloy
Wear resistance
Sillimanite
Reinforcement

ABSTRACT

Present work describes the development of Al-Si/sillimanite reinforced composites via stir casting route. Sillimanite is abundant mineral available in coastal regions of India and has not been explored much as reinforced mineral for the development of composites. In the present work, dry sliding wear behaviour of LM30 aluminium alloy reinforced with sillimanite has been investigated. Composites reinforced with sillimanite in different weight percentage (3–18 wt percentage) and particle size range (fine: 1–20 μm, medium: 32–50 μm, and coarse: 75–106 μm) were prepared. Microstructural studies revealed uniform distribution of sillimanite particles in the matrix of composites. Nanoindentation taken at different phases indicated good bonding between reinforced particles and matrix. Fine particles (1–20 μm) reinforced composites containing 15 wt% sillimanite exhibited higher wear resistance which is 55% more compared to base LM30 alloy. Beyond this reinforcement level, wear resistance deteriorated because of agglomeration of the fine particles. Analysis of wear track and debris revealed that at low applied loads, abrasive wear was predominant whereas at higher applied loads, adhesive wear was dominating factor.

1. Introduction

Aluminium matrix composites (AMCs) reinforced with ceramic particles have drawn considerable attention in automobile, defence, aerospace, and other structural applications as fuel efficient advanced materials for different tribological applications [1–3]. These composites provide greater flexibility in tailoring the desired mechanical properties for different engineering applications [4,5]. Aluminium and its alloys act as a good matrix material for the development of particulate reinforced composites as they possess low density, high specific strength, high corrosion resistance and ease of fabrication with low cost [6–8]. Reinforcement of hard ceramic particles in the matrix of aluminium is done to improve the tribological properties [9,10]. AMCs can be used as wear-resistant material in various parts of automobiles (viz. brake drums, pistons, cylinder heads, and liners etc.) and pump bodies [11–17]. Several studies on reinforcement of pure ceramic particles viz. silicon carbide [16–18], silicon nitride [19,20], boron carbide [21–23], and alumina [24–26] to improve the wear characteristics are reported. In these studies the addition of pure single particle size ceramic powders to improve the wear resistance/mechanical properties (hardness, strength etc.) of AMCs has been done. However, pure ceramics being expensive leads to enhancement in the cost of the fabricated AMCs which is not desirable for large scale applications of the composites. To reduce the cost, reinforcement of minerals like sillimanite [11–15], garnet [27–29], zircon [17,30–32], and rutile [33–36] has been tried where the improvement in wear properties has been reported.

Reinforcement of sillimanite to improve the wear characteristics in aluminium matrix (LM6) has also been done [11–15]. However, in these work only one particle size range (50–150 μm) has been studied. Considering the fact that sillimanite has high hardness, high modulus, high corrosion resistance, low coefficient of thermal expansion, high resistance to creep deformation, high thermal shock resistance, and excellent thermal stability, a detail study on reinforcement of sillimanite has been planned. Moreover, sillimanite being an ore of aluminium will develop better wettability with aluminium matrix.

In the present work, LM30 aluminium alloy was used as the matrix material. LM30 is a piston grade alloy which finds applications in brake drums, pistons, cylinder heads, and liners in automobile sector and pump bodies. Such parts are in a state of constant wear and thus wear analysis is an important aspect which affects their performance. The present work reports on development of LM30/sillimanite composites and wear characteristics of these developed composites. In this study three different particle size range of sillimanite (1–20 μm, 32–50 μm, and 75–106 μm) has been selected. Finally, wear tracks and wear debris

* Corresponding author.
E-mail address: oppandey@thapar.edu (O.P. Pandey).

http://dx.doi.org/10.1016/j.ceramint.2017.09.132
Received 27 June 2017; Received in revised form 4 September 2017; Accepted 16 September 2017
Available online 19 September 2017
0272-8842/ © 2017 Elsevier Ltd and Techna Group S.r.l. All rights reserved.

Tribology International 123 (2018) 142–154

Contents lists available at ScienceDirect

Tribology International

journal homepage: www.elsevier.com/locate/triboint

Effect of dual particle size (DPS) on dry sliding wear behaviour of LM30/sillimanite composites

Sandeep Sharma [a], Tarun Nanda [a], O.P. Pandey [b,*]

[a] Mechanical Engineering Department, Thapar Institute of Engineering and Technology, Patiala, 147004, Punjab, India
[b] School of Physics and Materials Science, Thapar Institute of Engineering and Technology, Patiala, 147004, Punjab, India

ARTICLE INFO

Keywords:
Sillimanite
Wear resistance
LM30 alloy
AMCs
Dual particle size

ABSTRACT

The effect of dual particle size (DPS) reinforcement (fine:coarse in weight ratios of 1:3, 1:1, and 3:1) on wear behaviour of LM30/sillimanite composites is reported. Optical micrographs revealed uniform distribution of particles in the matrix. $Al_2Si_4O_{10}$ phase was observed using XRD owing to the interfacial reactions of particle with matrix. Further, high nanohardness values of interface revealed sound particle-matrix bonding. The wear resistance of 15 wt.% DPS composites with weight ratio 3:1 improved by 59% over base alloy. In-addition, the results were comparable with the mathematical model and with cast iron used in brake drum applications. SEM-EDS analysis revealed that at low contact pressure, abrasive/adhesive wear mechanism was dominant, whereas at higher contact pressure delamination wear was dominant.

1. Introduction

Al-Si alloys are widely used in a variety of engineering applications as they possess low density, good castability, and high resistance to corrosion [1,2]. Aluminium alloys have proved their importance in the development of synthetic foams and composites. Aluminium synthetic foam finds its application in the area of high energy absorption and shock absorption [3–6]. Whereas, aluminium composites find their application in automobile sector, structural applications, and general engineering [7–13]. Hypereutectic Al-Si alloy having silicon content higher than 13 wt.% offer excellent wear resistance, lower density, and superior high temperature stability, thus enabling them to be used as wear resistant parts in the fabrication of automotive components (brake drum, connecting rods, cylinder liners, pistons, engine blocks), wear resistant parts in military, and components in general engineering applications (air conditioner compressors, multifunctional electronic packaging, mirror substrates, and support structures in optical systems) [9–11,14–16]. A hypereutectic Al-Si alloy specializes in astonishing wear resistance properties. The distribution of primary silicon phase in the matrix plays a crucial role in improving the wear resistance of hypereutectic Al-Si alloy [16,17]. Further, the wear behaviour of the hypereutectic Al-Si alloys is influenced by a variety of factors (i) the shape, size, and distribution of primary silicon phase in the matrix, (ii) the composition, distribution, and geometry of micro constituents in the matrix, and (iii) the external factors viz. applied load, sliding speed, working temperature, counter surface hardness, and operating environment etc. [15,18,19]. The growth of primary silicon depends upon the nucleation and cooling rate of hypereutectic Al-Si alloy [12]. The wear resistance decreases due to the presence of coarse and heterogeneous distribution of primary silicon [11]. Thus, for improved wear properties a refined and uniform distribution of primary silicon is desirable [11]. The primary silicon structure can be refined by (i) chemical method (addition of elements like Na, P, S etc.), (ii) physical method (using overheating electromagnetic stirring), and (iii) combined method (using elemental/mineral addition followed by overheating and stirring) [11,20–22].

Composites reinforced with single particle size (SPS) [23–25] and dual particle size (DPS) [26–28] with aluminium matrix using stir casting process has been widely studied. However, most of the studies on aluminium matrix composites (AMCs) have been conducted on pure ceramic particles viz. silicon carbide [29–31], silicon nitride [32,33], boron carbide [34–36], and alumina [37–39]. The pure ceramics are expensive and lead to the increase in cost of the fabricated AMCs which is not desirable for large scale engineering applications of the AMCs. To reduce the cost, reinforcement of minerals like sillimanite [40–42], garnet [43,44], zircon [24,45], and rutile [46,47] has been tried where the improvement in wear properties has been reported. India has a large coastline, and is gifted with valuable resources of beach sand minerals. The coastal lines of Kerela, Tamil Nadu, Odisha, and Andhra Pradesh has

* Corresponding author.
E-mail address: oppandey@thapar.edu (O.P. Pandey).

https://doi.org/10.1016/j.triboint.2017.12.031
Received 21 November 2017; Received in revised form 16 December 2017; Accepted 21 December 2017
Available online 22 December 2017
0301-679X/© 2017 Published by Elsevier Ltd.

Article

JOURNAL OF COMPOSITE MATERIALS

Journal of Composite Materials
2019, Vol. 53(11) 1521–1539
© The Author(s) 2018
Article reuse guidelines:
sagepub.com/journals-permissions
DOI: 10.1177/0021998318805203
journals.sagepub.com/home/jcm
SAGE

Effect of elevated temperatures and applied pressure on the tribological properties of LM30/sillimanite aluminium alloy composites

Sandeep Sharma[1], Tarun Nanda[1] and OP Pandey[2]

Abstract

The present study focuses on the development of low-cost, lightweight and highly wear resistant composites for brake rotor applications. Sillimanite mineral reinforced aluminum matrix composites were stir cast using three distinct reinforcement particle sizes. Reinforcement level was varied in the range of 3–15 wt%. The influence of operating temperature (50°C–300°C) and applied pressure (0.2–1.0 MPa) on the wear/friction behaviour of composites was observed. Optical micrographs showed homogenous particle distribution throughout the matrix. The high nanohardness obtained for interface regions signifies good particle–matrix bonding of processed composites. Dilatometry studies showed that the increase in sillimanite content decreased the coefficient of thermal expansion of the composites. Maximum improvement of 33% in coefficient of thermal expansion (over base alloy) was observed for 15 wt% fine composites. Wear analysis revealed that the developed composites provided adequate wear resistance till an operating temperature of 200°C, beyond which wear rate increased significantly. For the high operating temperature of 200°C, the steady-state wear of composites was comparable (only 6.62% higher) to the commercial cast iron alloy used in brake rotor applications. The aluminium-based composites developed in the present research are low cost (sillimanite is a naturally occurring mineral sand) and lightweight (60% lighter than cast iron) and can be used as an alternate material for brake rotors in light vehicles. Finally, SEM of worn out surfaces divulged the dominance of adhesive wear for material removal.

Keywords

Sillimanite, elevated temperatures, wear and friction, coefficient of thermal expansion

Introduction

Aluminium silicon (Al-Si) alloys are largely known for its superior combination of mechanical, chemical and physical properties.[1–4] These alloys find their applications in the variety of engineering fields like defence, aerospace and automobile sector.[5–8] Hypereutectic Al-Si alloys (Si >12.7%) exhibit better wear resistance than the eutectic (Si = 12.7%) or hypoeutectic (Si < 12.7%) alloys. The proeutectic Si in the hypereutectic Al-Si alloys enhances the wear resistance. Therefore, Al-Si alloys (Si >12.7%) are a favourable material for automotive components like brake rotor.[9,10] These components are subjected to varying applied pressures, at different ambient temperatures. In addition, aluminium matrix composites (AMCs) find their applications in automotive sector.[6,8,11–13] These components frequently operate at a high (near critical) temperature 0.4–0.6 T_m (T_m is melting temperature of Al-Si alloy in Kelvin).[14,15] This near critical temperature of components leads to thermal softening of aluminium alloys. This leads to the complete failure of the material.[16–18] Thus, there is a need to augment the high temperature tribological properties of hypereutectic Al alloys. To amplify the tribological properties, Al-Si alloys are reinforced with hard and thermally stable ceramic particles. Numerous authors have reported that the

[1]Mechanical Engineering Department, Thapar Institute of Engineering and Technology, India
[2]School of Physics and Materials Science, Thapar Institute of Engineering and Technology, India

Corresponding author:
OP Pandey, School of Physics and Materials Science, Thapar Institute of Engineering and Technology, Patiala 147004, Punjab, India.
Email: oppandey@thapar.edu

Materials Chemistry and Physics 258 (2021) 123988

Contents lists available at ScienceDirect

Materials Chemistry and Physics

journal homepage: www.elsevier.com/locate/matchemphys

Influence of two different range of sillimanite particle reinforcement on tribological characteristics of LM30 based composites under elevated temperature conditions

Sandeep Sharma [a], Rahul Gupta [a], Tarun Nanda [a], O.P. Pandey [b,*]

[a] Mechanical Engineering Department (MED), Thapar Institute of Engineering and Technology (TIET), Patiala 147004, Punjab, India
[b] School of Physics and Materials Science (SPMS), TIET, Patiala, 147004, Punjab, India

HIGHLIGHTS

- 15-DPS3 composite showed minimum grain size and globular shape for proeutectic Si.
- CTE, COF, and wear rate of 15-DPS3 composite was relatively lower than LM30 alloy.
- Lower CTE value by composites signifies the formation of strong interfacial bonding.
- For 15-DPS composite, the transition temperature of LM30 alloy got improved by 50 °C
- Properties shown by 15-DPS3 composite are comparable to brake rotor material (GCI).

ARTICLE INFO

Keywords:
Sillimanite
Wear rate
Friction coefficient
Thermal expansion

ABSTRACT

In this work, high temperature wear-resistant LM30/sillimanite composites for automotive applications have been fabricated. Dual particle size composites reinforced with naturally occurring sillimanite mineral were processed and investigated for operating temperatures in the range of 50–300 °C. Sillimanite particles with size range of 1–20 μm (fine) and 75–106 μm (coarse) were mixed in weight ratio of 3:1, 1:1, and 1:3 to be reinforced to the LM30 alloy. SEM micrographs and area mapping/line mapping profile results showed presence of different phases and revealed that sillimanite inclusion changed the morphology of proeutectic silicon to globular and refined its grain size. Particles were well distributed in LM30 matrix. Increase in reinforcement level of particles led to continuous improvement in properties. As such, the best properties were obtained in composite containing 15 wt% sillimanite with proportion of fine: coarse particles as 3:1 (15-DPS3 composite). The transition temperature of wear mode increased from 150 °C for base alloy to 200 °C for composites. For the temperature-pressure condition of 200–1 MPa, 15-DPS3 composite showed 15% higher hardness, 80% lower wear rate, 48% lower friction coefficient, and 28% lower thermal expansion coefficient than base alloy. These wear characteristics of composites were comparable to the commercially used grey cast iron material. XRD of wear track/debris confirmed the formation of tribolayer. SEM analysis of wear track/debris identified the wear mechanisms causing materials loss under different contact pressures. Light-weight and economical composites developed in this research can act as a good substitute for the heavy cast iron components used in industry.

1. Introduction

Hypereutectic Al–Si alloys of near eutectic composition (silicon> 12.8 wt%) are promising candidates for automotive components like brake rotors, pistons, cylinder heads etc. [1,2]. Such alloys mainly comprise of proeutectic silicon (Si) phase and Al–Si eutectic phase mixture. Proeutectic Si behaves like load-bearing member and provides relatively superior wear resistance compared to hypoeutectic or eutectic Al–Si alloys. However, a major problem in hypereutectic alloys is the segregation of primary Si which results in degradation of wear characteristics of Al–Si alloys [3]. Wear characteristics of these alloys can be improved by refining primary Si in terms of shape, size, and distribution

* Corresponding author. SPMS, TIET, Patiala, 147004, Punjab, India.
E-mail address: oppandey@thapar.edu (O.P. Pandey).

https://doi.org/10.1016/j.matchemphys.2020.123988
Received 8 August 2020; Received in revised form 18 October 2020; Accepted 24 October 2020
Available online 28 October 2020
0254-0584/© 2020 Elsevier B.V. All rights reserved.

IOP Publishing Mater. Res. Express 6 (2019) 056535 https://doi.org/10.1088/2053-1591/ab04ba

Materials Research Express

RECEIVED
1 December 2018

REVISED
10 January 2019

ACCEPTED FOR PUBLICATION
6 February 2019

PUBLISHED
15 February 2019

PAPER

Effect of heat treatment on the wear behavior of zircon reinforced aluminium matrix composites

Sandeep Sharma[1], **Suresh Kumar**[2], **Tarun Nanda**[1] **and O P Pandey**[3]

[1] Mechanical Engineering Department, Thapar Institute of Engineering and Technology, Patiala 147004, Punjab, India
[2] Terminal Ballistics Research Laboratory (TBRL), DRDO, Chandigarh 160003, India
[3] School of Physics and Materials Science, Thapar Institute of Engineering and Technology, Patiala 147004, Punjab, India

E-mail: oppandey@thapar.edu

Keywords: heat-treatment, LM13 aluminium alloy composites, zircon, T4 and T6

Abstract

Effect of heat treatment on the wear behavior of LM13/zircon reinforced composites have been studied. Stir casting process was used for the fabrication of composites with 10 wt% fine and coarse zircon particles. Further, T4 and T6 heat-treatment were carried out on the composite specimens. The hardness of the fine particle sized composites was superior in comparison to coarse particle sized composites. For T4 heat-treatment, maximum hardness of 201 BHN was obtained after natural aging of 20 days, beyond which the hardness value remained near-about constant. For T6 heat-treatment, maximum hardness of 212 BHN was observed for the artificial aging at 180 °C for 4 h. Maximum improvement in hardness (over the non-heat treated composites) observed for T6 a fine and T6 coarse composite was 15% and 13% respectively. Further, heat-treatment decreased the wear rate of the composites. Best results were obtained for T6 heat-treated composites. A maximum reduction of 25% and 27% (over the non-heat treated composites were obtained for T6 heat-treated coarse and fine samples respectively. Finally, SEM analysis revealed that abrasive wear mechanism was dominant for lower contact pressures (0.2 MPa). Whereas, for high contact pressure (1 MPa) adhesive wear mechanism was dominant.

1. Introduction

Aluminium silicon (Al–Si) alloys have found their applications in a variety of engineering applications viz. automobile, aerospace, and defense sector [1–4]. Different ceramic minerals (both natural and synthetic) have been added to the Al–Si alloys to enhance their mechanical as well as tribological properties. Various authors have reported that the addition of synthetic minerals like SiC [5, 6], B_4C [7, 8], Al_2O_3 [8, 9] etc and also the natural minerals like rutile [10], sillimanite [1, 11] etc led to the improvement in the wear resistance of Al–Si alloys. These studies indicate that aluminium matrix composites (AMCs) show better wear resistance as compared to Al–Si alloys. To further improve the wear resistance, AMCs are subjected to different heat treatment. To perform heat treatment, the Al–Si alloys are usually alloyed with copper and magnesium [12–14]. Mg/Cu reacts with Si/Al to form intermetallic compounds which have high hardness, therefore, improve the wear resistance of the composites [12, 15]. Silicon morphology also plays an important role in the enhancement of wear resistance of the aluminium silicon alloys. A fine and uniform distribution of silicon in the aluminium matrix will have superior wear resistance as compared to coarse/segregated silicon distribution. Silicon morphology can be further refined by the addition of hard ceramic reinforcement into the Al–Si alloy to form AMCs [1].

The vast literature available on AMCs revealed that the wear rate of the composites largely depends upon the size, shape, distribution, and weight percentage of reinforced ceramic particles in the Al–Si alloy [16–18]. Further, a few authors have reported the effect of heat treatment on the wear properties of the AMCs. Chen *et al* [19] revealed that T6 heat treatment of A356-SiC improved the fretting wear resistance of the composites. Lashgari *et al* [12] revealed that the T6 heat treatment of A356-B_4C composites improved the hardness and wear

© 2019 IOP Publishing Ltd

Wear 426–427 (2019) 27–36

Contents lists available at ScienceDirect

Wear

journal homepage: www.elsevier.com/locate/wear

Investigation of T4 and T6 heat treatment on the wear properties of sillimanite reinforced LM30 aluminium alloy composites

Sandeep Sharma[a], Tarun Nanda[a], O.P. Pandey[b,*]

[a] Mechanical Engineering Department, Thapar Institute of Engineering and Technology, Patiala 147004, Punjab, India
[b] School of Physics and materials Science, Thapar Institute of Engineering and Technology, Patiala 147004, Punjab, India

ARTICLE INFO

Keywords:
Heat-treatment
LM30 aluminium composites
Sillimanite
T4 and T6

ABSTRACT

In the present work, an attempt has been made to study the effects of heat treatment on the dry sliding wear properties of sillimanite reinforced LM30 aluminium matrix composites. Stir casting process was used for the processing of the composites. Composites with two different particle sizes (fine 1–20 μm and coarse 75–106 μm) and different weight ratio (3–15 wt% in the step size of 3 wt%) were fabricated. Further, the fabricated composites were subjected to the heat treatment as per T4 and T6 process. The composites were heated (at 540 °C), held at that temperature for 0.5–2 h and quenched in water. For T4, the composites were subjected to natural aging of 10–30 days at room temperature and for T6, composites were artificially aged by reheating to a temperature of 150–250 °C, holding there for 1–5 h, followed by air cooling. Hardness testing revealed that the composites subjected to T6 heat treatment exhibited superior hardness in comparison to normal composites and T4 heat treated composites. Further, wear analysis revealed that heat treatment of the composites affected the wear properties of the composites. Maximum improvement in the wear rate was observed for T6 heat treated composites. Also, the coefficient of friction of T6 heat treated composites was lower than other composites. Finally, SEM analysis revealed that the surface damage observed for T6 composites was lesser in comparison to other. In the initial period of wear abrasive wear was dominant and with increase in the sliding distance adhesive/delamination wear mechanism was dominant. Therefore, T6 composites revealed a superior combination of wear properties, and found to be in close comparison to grey cast iron used in the brake drum applications. Hence, 15 wt% reinforced T6 composites can be used as an alternate material for brake drum applications.

1. Introduction

Aluminium silicon alloys are widely used in the applications of automobile, aerospace and defense sector [1–4]. For heat treatment applications, Al-Si alloys are usually alloyed with copper and magnesium [5–7]. Heat treatment leads to the increase in the hardness of the Al-Si alloys. This increase in hardness of the alloys takes place due to the process of ageing or termed as age hardening. Age hardening is responsible for the improvement in the hardness of the composites. The mechanism responsible for the improved hardness is based upon the reactions of Mg/Cu with Si/Al. Mg and Si combine to form Mg_2Si precipitates and Al and Cu combine to form Al_2Cu precipitates. These precipitates are responsible for the strengthening of the alloy [5,8]. The precipitation of phase during the aging process takes place in the following ways: (i) Firstly, the atoms of the precipitating phase in the crystal lattice rearrange and the particles of the precipitate phase are formed. With passage of time clusters and Guinier-Preston zones are formed. The hardness increases due to the development of micro strains in the lattice. (ii) The Guinier-Preston zones gets transformed (from GP I to GP II zones) and intermediate phases. The formation of GP II zone leads to the maximum strengthening of the alloy. (iii) Next, from the transition phase a stable phase is formed. (iv) Lastly, the precipitate particles grow and larger particles are formed. These larger particles are formed at an expense of neighboring smaller particles. At higher ageing temperatures, these larger particles reduce the stress on the adjoining matrix and leads to a decrease in the hardness the alloy and composite [9].

The wear properties of the Al-Si-Cu-Mg alloys can be significantly improved via heat treatment. The silicon morphology plays an important role in the enhancement of wear resistance of the aluminium silicon alloys. The silicon morphology can be tailored by following methods (i) by the addition of chemical modifier (Na, Sr etc. called as chemical modification) and or (ii) by heat treatment (called as thermal modification) [1,7,10]. Apart from these two methods a third method to

* Corresponding author.
E-mail address: oppandey@thapar.edu (O.P. Pandey).

https://doi.org/10.1016/j.wear.2018.12.065
Received 3 September 2018; Received in revised form 28 November 2018; Accepted 21 December 2018
0043-1648/ © 2018 Elsevier B.V. All rights reserved.

IOP Publishing Mater. Res. Express 7 (2020) 016540 https://doi.org/10.1088/2053-1591/ab61a2

Materials Research Express

PAPER

A comparative study of dry sliding wear behaviour of sillimanite and rutile reinforced LM27 aluminium alloy composites

Rahul Gupta[1], **Sandeep Sharma**[1], **Tarun Nanda**[1] **and O P Pandey**[2]

[1] Mechanical Engineering Department, Thapar Institute of Engineering and Technology, Patiala 147004, Punjab, India
[2] School of Physics and Materials Science, Thapar Institute of Engineering and Technology, Patiala 147004, Punjab, India

E-mail: oppandey@gmail.com **and** oppandey@thapar.edu

Keywords: minerals, particles, nano-hardness, wear test, coefficient of friction, aluminium matrix composites

OPEN ACCESS

RECEIVED
19 October 2019

REVISED
29 November 2019

ACCEPTED FOR PUBLICATION
12 December 2019

PUBLISHED
6 January 2020

Original content from this work may be used under the terms of the Creative Commons Attribution 4.0 licence.

Any further distribution of this work must maintain attribution to the author(s) and the title of the work, journal citation and DOI.

Abstract

The present work compares the dry sliding wear characteristics of sillimanite reinforced and rutile reinforced LM27 aluminium alloy based composites prepared by stir casting process. Particles in the size range of 1–32 μm were added in 5, 10, and 15 wt%. Microstructure, nanohardness, coefficient of friction, and wear rate characteristics were evaluated. Optical microscopy revealed uniform distribution of both sillimanite and rutile particles in the matrix. The hardness of sillimanite reinforced composites was higher than rutile reinforced composites. Further, the wear resistance of sillimanite reinforced composites was superior to rutile reinforced composites. However, coefficient of friction values of sillimanite particle reinforced composites were higher than the rutile particle reinforced composites. SEM-EDS analysis of wear track and wear debris revealed that abrasive wear and adhesion/delamination mechanisms were responsible for the wear of composites at low and high applied load conditions respectively.

1. Introduction

Aluminium alloys have exceptional strength to weight ratio but lack in tribological properties. In order to enhance the tribological characteristics and mechanical properties of these alloys, aluminium matrix composites (AMCs) have been developed. AMCs exhibit high strength, low density, high toughness, high corrosion resistance, high wear resistance, low thermal expansion and high thermal conductivity [1–6]. Because of these properties, AMCs find use in a variety of engineering applications viz. aviation, automobile, and defence [1, 3, 4, 7]. Some auto-components like pistons, cylinder liners, brake discs, brake drums etc are processed using AMCs [2, 8, 9]. AMCs are generally stir cast with ceramic particle reinforcements of SiC, TiC, B_4C, Al_2O_3, TiB_2 etc [6, 7, 10]. Most of the research to improve the wear characteristics of AMCs has concentrated on reinforcing the aluminium matrix with synthetic ceramic particles like SiC, TiC, B_4C, Al_2O_3, TiB_2 etc [2–4, 6, 7, 10]. However, synthetic ceramics are costly and increase the overall cost of processing of AMCs. To decrease the processing cost, aluminium matrix is reinforced with natural ceramic minerals like sillimanite, rutile, zircon, garnet etc. These minerals are cheap and abundantly available in the coastal areas of India. Natural minerals when reinforced in aluminium matrix help in improving the wear properties of AMCs [11–16]. Each natural mineral has unique characteristics viz. chemical composition, physical properties, thermal properties, and mechanical properties. Sillimanite (Al_2SiO_5) is an ore of aluminium, and hence, sillimanite particles tend to form good interfacial bonding with Al-Si matrix. In addition to this, sillimanite particles have low density, high hardness, and low coefficient of thermal expansion. Thus, during wear testing, AMCs reinforced with sillimanite particles will show a lower rise in temperature with reduced wear rate and coefficient of friction (COF) values [12, 17]. On the other hand, rutile has high thermal stability, high hardness, and is considered as a low friction material. Rutile particle reinforcement in AMCs leads to increase in load-bearing capacity of composites and results in high yield strength, low wear rate, and low COF values. Rutile reacts chemically with aluminium matrix at the interface. This helps in improving the wetting of matrix and reinforcement [11, 18]. Each specific mineral reinforcement improves the tribological properties of AMCs in a unique manner. Therefore, it was

© 2020 The Author(s). Published by IOP Publishing Ltd

Ceramics International 46 (2020) 16849–16859

Contents lists available at ScienceDirect

Ceramics International

journal homepage: www.elsevier.com/locate/ceramint

Wear studies of hybrid AMCs reinforced with naturally occurring sillimanite and rutile ceramic particles for brake-rotor applications

Rahul Gupta[a], Sandeep Sharma[a], Tarun Nanda[a], O.P. Pandey[b,*]

[a] Mechanical Engineering Department, Thapar Institute of Engineering and Technology, Patiala, 147004, Punjab, India
[b] School of Physics and Materials Science, Thapar Institute of Engineering and Technology, Patiala, 147004, Punjab, India

ARTICLE INFO

Keywords:
Hybrid AMC
Wear and friction test
Thermal properties
Mineral reinforcement

ABSTRACT

Light weight hybrid aluminium matrix composites (AMCs) were developed for brake rotor applications and their wear behaviour was compared with commercial grade material under dry-sliding wear conditions. LM27 Al-alloy was reinforced with sillimanite/rutile particles (size: 1–32 μm; loading: 0–15 wt%.). Uniform distribution of reinforcement was achieved till 15 wt% level. High nano-hardness and high thermal conductivity at particle-matrix interface indicated good interfacial-bonding. Hybrid AMCs containing 15 wt% reinforcement showed 52% decrease in wear rate over base alloy and was comparable to commercial grade material used in industries. Hybrid AMCs displayed superior thermal conductivity over commercial material. Each reinforcement played a diverse but significant role. Sillimanite improved interfacial-bonding between matrix-reinforcement whereas rutile provided increased lubricity/grain refinement of the composites.

1. Introduction

Aluminium matrix composites (AMCs) containing ceramic particle reinforcement find use in various sectors including automotive, aeronautical, and military applications [1–4]. These composites are mainly used for manufacturing of auto-components like cylinder heads/blocks, pistons, connecting rods, brake/disc rotors etc. as they possess good specific strength, thermal characteristics, low coefficient of friction, and superior wear properties [5–8]. Ceramics have high strength, hardness, and are chemically stable. AMCs containing ceramic particles are used for different other engineering applications also [2,9]. A large group of researchers have worked on AMCs reinforced with synthetic ceramic materials like silicon carbide [10,11], silicon nitride [12,13], boron carbide [2,14], titanium carbide [15] and alumina [16,17] etc. for enhancing mechanical properties and wear resistance. However, synthetic ceramics are very expensive in comparison to naturally occurring ceramics, and thus, increase the cost of resulting composites [18]. To overcome this problem, composites containing naturally occurring mineral particles like sillimanite [19–21], garnet [22,23], zircon [24–26], and rutile [27,28] have been processed by a few researchers. The addition of minerals into AMCs is an effective and economical way of improving the properties of composites. In most of the reported work on mineral reinforced AMCs, only one type of mineral is reinforced in the AMCs (i.e. single reinforced particles). Though, hybrid composites containing two different ceramic particles have been studied by some authors but reinforcement of two or more minerals to enhance the properties are limited [14,16,17,28,29].

In the present research, hybrid composites were processed using automobile grade LM27 alloy as matrix and naturally occurring mineral particles of sillimanite (Al_2SiO_5) and rutile (TiO_2) as reinforcements. The main objective was to develop hybrid AMCs with improved wear characteristics which could act as an economical substitute for commercial materials used for brake rotor applications. Sillimanite and rutile are naturally occurring minerals that are abundantly found in the coastal areas of Kerala, Odisha, and Tamil Nadu of India [21]. These ceramic particles are very cheap (price of these minerals is less than even one-tenth of the price of synthetic ceramics like SiC), possess high hardness, high resistance to thermal shock, and good thermal stability along with the low coefficient of thermal expansion (CTE) [19,21]. Literature reports that rutile and sillimanite minerals perform specific functions when present as reinforcement in AMCs [30]. Rutile particle as reinforcement results in refinement of silicon phase present in Al–Si base alloy and also acts as a solid lubricant [27,30]. Sillimanite particles form strong interfacial bonding with the matrix material and provide high hardness to the resulting AMC [20,30]. Thus, in the present research, both reinforcements were used so that both properties of minerals can be explored for the preparation of a high wear resistant composite system.

* Corresponding author.
E-mail address: oppandey@thapar.edu (O.P. Pandey).

https://doi.org/10.1016/j.ceramint.2020.03.262
Received 13 January 2020; Received in revised form 26 March 2020; Accepted 27 March 2020
Available online 03 April 2020
0272-8842/ © 2020 Elsevier Ltd and Techna Group S.r.l. All rights reserved.